**Lipopeptidomimetics are Selective and Modifiable
Coactivator Protein–Protein Interaction Inhibitors**

by

Estefanía Martínez Valdivia

A dissertation submitted in partial fulfillment
of the requirements for the degree of
Doctor of Philosophy
(Chemical Biology)
in the University of Michigan
2024

Doctoral Committee:

      Professor Anna K. Mapp, Chair
      Assistant Professor Timothy Cernak
      Associate Professor Alison R.H. Narayan
      Professor Janet L. Smith

Estefanía Martínez Valdivia

estefmv@umich.edu

ORCID iD: 0000-0003-0791-8327

Dedication

A mi familia, a mis maestros, y a la curiosidad de mi niña interna.

Acknowledgments

Reflecting on my time at the University of Michigan, I can't help but feel an overwhelming sense of gratitude. This journey has shaped and pushed me in ways that I could not have predicted, but I am so happy to know that through the happiest of moments and the toughest of times, there was always a community of people rooting for me. I truly would not have gotten to this point without being propped up by this amazing support system, so to you all, thank you.

I would first like to thank my research advisor, Prof. Anna Mapp. I am immensely grateful to have been part of your group in the last five years. Through all of the challenges that took place over that timeframe, including a pandemic, scientific difficulties, life changes, and my personal growth, having you as a resource and support, has had an immeasurable value on my journey. I have been so fortunate to learn from your leadership and example in so many ways that extend beyond your vast scientific knowledge. Thank you for your encouragement, your trust, your kindness, and for pushing me to take on new challenges and responsibilities. Your guidance has shaped me in ways that I will carry with me into the future, so thank you.

Thank you as well to my committee members, Professors Janet Smith, Alison Narayan, Tim Cernak, and previously Joshi Alumkal. I have truly appreciated your feedback, suggestions, and the discussions we have had on my research progress. Meeting every year with you all has been a milestone I have looked forward to and an

occasion that was always motivating after the fact. Thank you for being part of my graduate school journey.

I also have to thank all of my mentors during my time as an undergraduate. A very special thank you to my undergraduate research advisor, Prof. Joan Schellinger at the University of San Diego. You were the first person to introduce me not only to academic research but also to doctoral programs as a path after graduation. You were instrumental in my participation in research activities that ultimately ensured I had a spot in graduate school, and most importantly, you helped me see that I was capable of getting admitted and succeeding in a graduate program. As one of my first scientific mentors ever, I am so grateful to have learned from you, especially about how to make a peptide! I also have to thank all of the wonderful professors in the Chemistry & Biochemistry department at USD, your devotion to teaching, and your commitment to students, played a huge role in my pursuit of research and science as a career. Additionally, I would like to thank Prof. Kiessling and her whole group for welcoming me in 2018 during my summer research experience in her lab. My time there helped solidify my decision to pursue a graduate degree, and I continue to be inspired by all the amazing science that you all do.

A big thank you to all of the Mapp lab members, past and present, whom I have had the huge pleasure of working with and learning from. The culture we have all built in the lab is one that made graduate school so much more enjoyable. As my last year at Michigan has progressed, I have had to take a step back at times and take in how lucky I am to be surrounded by such wonderful people and appreciate the last moments of getting to work alongside you all. I would especially like to thank Dr. Olivia Pattelli, first, for being a wonderful mentor during my rotation and my first years in the lab, especially

through the isolating times of the pandemic. Most importantly, thank you for being a wonderful friend, I count myself lucky to have shared so many of the most important moments of my time in Michigan with you, and I am so grateful to count on your support and advice from peptide synthesis questions to big life decision matters, and everything in between. Thank you as well to Dr. Stephen Joy, Dr. Yejun Liu, and Dr. Samantha De Salle, who taught me so much in my early graduate school years, you all are such inspirational lab mates, and I am happy I got to work with you. To Dr. Monica Rivas, Mary Villarreal, and Jael Rodriguez, thank you for being such wonderful cheerleaders, you have all uplifted me when I needed it most, and I will forever be grateful to you. To my mentees, Katherine, Marius, and Hannah, thank you so much for working with me in these years, you have each made unique contributions to different aspects of these projects, and I have learned so much from you. Also, a special shout out to the Mapp lab neighbors in the Wang lab, I have enjoyed having you all nearby in the past years.

To all of the friends I have made in Michigan, thank you for being a part of my life, for however long we overlapped. The community I found in Ann Arbor is one that carried me through the toughest times of graduate school, and I could not have done it without you all. From the members in my cohort in my earlier years, to my pod during COVID-19, friends from SACNAS, and neighbors, I enjoyed spending holidays, birthdays, summer days, and winter storms with you all. Thanks for being a family away from home. A very special note of appreciation for Vishal, getting to share my journey with you, and getting to see myself and my work through your eyes, has been a huge source of motivation in the most testing of times. Thank you for reminding me that I can do even the most difficult parts and that anything challenging is worth doing. Thank you as well to all of the friends

that were present from far away, and who were always so willing to provide their support even when I didn't know how to ask for it. I am so lucky to have you all in my life.

Finally, a big thank you to my family. To my lovely siblings, Isabel, Angel, and Arianna, I am so fortunate to share life with you, and you have been some of the biggest and most important constants in the last five years. I truly would not have made it here, all in one piece, if it wasn't because of how caring you have been. Thank you for your visits, which were always so well-timed for when I needed to see family the most. I love you all so much. To my parents, there are not enough ways that I can say thank you. This accomplishment is also yours, because it is also the culmination of all of your efforts, over so many years. Thank you for your endless love and support, and for showing me through example, that there are so many things within reach through resilience and hard work. I hope to continue to make you proud, and from the bottom of my heart, thank you!

Table of Contents

List of Tables

List of Figures

List of Appendices

List of Abbreviations

ABD	Activator binding domain
AcID	Activator interacting domain
ACTR	Activator for thyroid hormone and retinoid receptors
ARC105	Activator-recruited factor subunit 105 kDa
ATF6α	Activating transcription factor 6α
BME	β-mercaptoethanol
BSA	Buried surface area
CBP	CREB binding protein
CD	Circular dichroism
COVID-19	Coronavirus disease 2019
Cryo-EM	Cryogenic electron microscopy
CPP	Cell-penetrating peptide
CREB	cAMP response element-binding protein
CSP	Chemical shift perturbation
DBD	DNA binding domain
DCM	Dichloromethane
DIC	Diisopropylcarbodiimide
DIPEA	N,N-diisopropylethylamine
DMF	N,N-dimethylformamide
DMSO	Dimethyl sulfoxide
DNA	Deoxyribonucleic acid
DSF	Differential scanning fluorimetry
DTT	Dithiothreitol
EFP	Estrogen-responsive finger protein
ER	Endoplasmic reticulum

ETV	Ets translocation variant
FITC	Fluorescein isothiocyanate
Fmoc	Fluorenylmethyloxycarbonyl
FP	Fluorescence polarization
FPLC	Fast protein liquid chromatography
HIF-1α	Hypoxia-inducible factor 1 α
HBTU	Hexafluorophosphate benzotriazole tetramethyl uronium
HOBt	Hydroxybenzotriazole
HPLC	High-performance liquid chromatography
HSQC	Heteronuclear single quantum coherence
IBiD	IRF-3 binding domain
IC_{50}	Half-maximal inhibitory concentration
IDP	Intrinsically disordered protein
IDR	Intrinsically disordered region
IPTG	Isopropyl β-D-1thiogalactopyranoside
K_d	Dissociation constant
K_i	Inhibitory constant
KIX	Kinase-inducible domain (KID) interacting domain
LC-MS	Liquid-chromatography mass spectrometry
LPPM	Lipopeptidomimetic
Med15	Mediator subunit 15
Med25	Mediator subunit 25
MLL	Multi-lineage leukemia
MOA	Mechanism of action
mRNA	Messenger RNA
MW	Molecular Weight
Ni-NTA	Nickel-Nitrilotriacetic Acid
NMR	Nuclear magnetic resonance spectroscopy
NRD	Nuclear receptor domain
PDB	Protein Data Bank
PEA3	Polyoma enhancer activator 3

pKID	Phosphorylated kinase inducible domain
PIC	Preinitiation complex
POI	Protein of interest
PPI	Protein–protein interaction
PROTAC	Protein targeting chimera
PTM	Posttranslational modification
QTOF-MS	Quadrople time-of-flight mass spectrometry
RFU	Relative fluorescence units
RNA	Ribonucleic acid
RNA Pol II	RNA Polymerase II
RPM	Revolutions per minute
S protein	Spike protein
S/N	Signal-to-noise
SA	Surface area
SARS	Severe acute respiratory syndrome (Co-V-2)
SDS-PAGE	Sodium dodecyl sulphate–polyacrylamide gel electrophoresis
TAD	Transcriptional activation domain
TAZ1	Transcriptional adaptor zinc-binding 1
TBP	TATA box binding protein
TF	Transcription factor
TFA	Trifluoroacetic acid
TFE	2,2,2-Trifluoroethanol
TEA	Triethylamine
TEAD	Transcriptional enhanced associate domain
TIPS	Triisopropylsilane
Tm	Melting temperature
UV/VIS	Ultraviolet/visible spectroscopy
VP16	Herpes simplex virus protein 16
VWA	Von Willebrand factor type A
WT	Wild type
YAP	Yes-associated protein

Abstract

The protein-protein interactions (PPIs) of transcriptional coactivators are key to the synergistic activation of gene expression. The dysregulation of these PPI networks, particularly in the interactions between coactivator and activator proteins, is present in several forms of disease. Inhibition of coactivator PPIs is thereby a strategy to dissect the functional role of the interactions between transcriptional components in dysregulated contexts. Coactivator PPIs occur through intricate mechanisms of recognition, which involve dynamic complex formation, an undefined surface topology, and multiple binding partners. The functional disruption of these interactions with synthetic molecules has historically been challenging, considering that these factors limit the structural information available for developing inhibitors using rational-design or structure-based approaches. Here we propose that short peptides derived from the sequences within the interaction surfaces of coactivator-activator PPIs, have the potential to be developed into potent and selective inhibitors of these complexes. We demonstrate that peptide lipidation is a powerful form of modification to enhance the inhibitory activity of short activator-like peptides against coactivator complexes.

This dissertation presents the development and evaluation of lipopeptidomimetics (LPPMs) as inhibitors of the PPIs of coactivators. In our initial assessment of this strategy, we used a peptide with an amino acid sequence that shares characteristics with the composition of transcriptional activation domains (TAD) of activators, against the PPIs of

coactivator Med25. This protein, a subunit of Mediator, regulates the expression of genes implicated in various types of cancer. We demonstrate that the incorporation of a medium-chain, branched fatty acid to a heptameric peptide, LPPM-8, increases the compound's inhibitory activity by over 20-fold, rendering it a selective inhibitor of Med25 PPIs. Structure-activity relationship studies, combined with biophysical analyses, revealed that the lipid structure, specific amino acid residues, and the C-terminal moiety of the molecule each contribute to LPPM-8's effectiveness and the structural propensity as an inhibitor. We determined that this molecule acts primarily as an orthosteric inhibitor of Med25 PPIs, and we observed its biological activity in a cellular context.

Next, aiming to determine whether this strategy could be applied to multiple coactivator targets, we tested it against the PPIs of the KIX domain of coactivator CBP. We found that specific sequence modifications in LPPMs lead to altered selectivity for different coactivator targets. In particular, changing a single amino acid from aspartic acid to alanine (LPPM-8-D2A) resulted in a 10-fold selectivity switch towards the inhibition of CBP KIX compared to Med25 PPIs. This selectivity switch was validated by evaluating the LPPM-8-D2A multiple contexts, revealing its allosteric inhibition of KIX PPIs. These findings suggest that LPPMs are tunable scaffolds with potential as a generalizable strategy for inhibiting coactivator PPIs. Chapter 4 outlines the potential steps necessary to refine LPPM design into a high-throughput approach for the development of inhibitors and explores the application of this method to other coactivator and intrinsically disordered protein systems.

Chapter 1 Lipidation as a Strategy for the Development of Coactivator Protein–Protein Interaction Modulators

1.1 Abstract

Coactivators are complex proteins that play a central role in transcription, the process by which organisms execute gene expression to respond to environmental signals and maintain a homeostatic state. Specifically, at the onset of transcription and through protein–protein interactions (PPIs), coactivators act as informational bridges across the transcriptional machinery and thereby play a crucial role in the regulation and precise activation of particular gene programs. Provided the centrality of coactivator function, dysregulation in their PPI networks is a feature present in a multitude of diseases. Modulation of coactivator PPIs is thereby a strategy to both determine their intrinsic mechanisms of function and assess their role in the development of disease. Nonetheless, coactivators are structurally and functionally intricate targets, and they necessitate novel approaches for the development of inhibitors of their PPIs.

This introductory chapter summarizes the relevance and challenges of coactivator PPIs as targets for modulation and critically surveys previous approaches for inhibitor design. Furthermore, by referencing examples of bioactive natural products and the intrinsic interaction mechanisms of coactivators, the chapter proposes the use of lipid-peptide conjugates, as lipopeptidomimetics (LPPMs), as scaffolds that address several of the challenges in the development of coactivator PPI inhibitors.

1.2 Modulating Coactivator Protein–Protein Interactions

1.2.1 Coactivator•activator PPIs in transcription

Coactivators are essential components of the cellular apparatus, and their function within transcription spans chromatin remodeling, modulation of transcriptional activation, histone modification and mediation of the assembly of the preinitiation complex (PIC). [1,2] These different aspects of coactivator function have been reconciled over time into multiple models of their roles, for instance, as informational bridges between genomic enhancer and promoter regions. Early model proposals focused on the role of coactivators in mediating the assembly of the transcriptional machinery from a structural perspective, forming a stable, physical bridge between the promoter and enhancer regions of the genome.[3,4] Recent advances in the understanding of the dynamics of coactivators in multiprotein complexes, have led to models that incorporate indirect communication between promoters and enhancers, mediated by phase separation and progressive changes in the location of coactivators during transcriptional initiation. These include the proximity diffusion model, which suggests that enhancers enrich for transcription factors that then activate nearby promoters through diffusion. Alternatively, the transcription factor (TF) activity gradient (TAG) model posits that coactivators are held stable at enhancers through interactions with DNA-bound activators, and additional TFs acetylated at this site then diffuse towards the promoter to increase transcriptional output.[5-9] (Figure 1.1) Despite the open questions about the mechanism of the succession between different coactivator roles, present in all these models is the significance of coactivator protein–protein interaction networks for enacting their function.

Stable P-E Contact Model   **Proximity/Diffusion Model**   **TF Activity Gradient (TAG) Model**
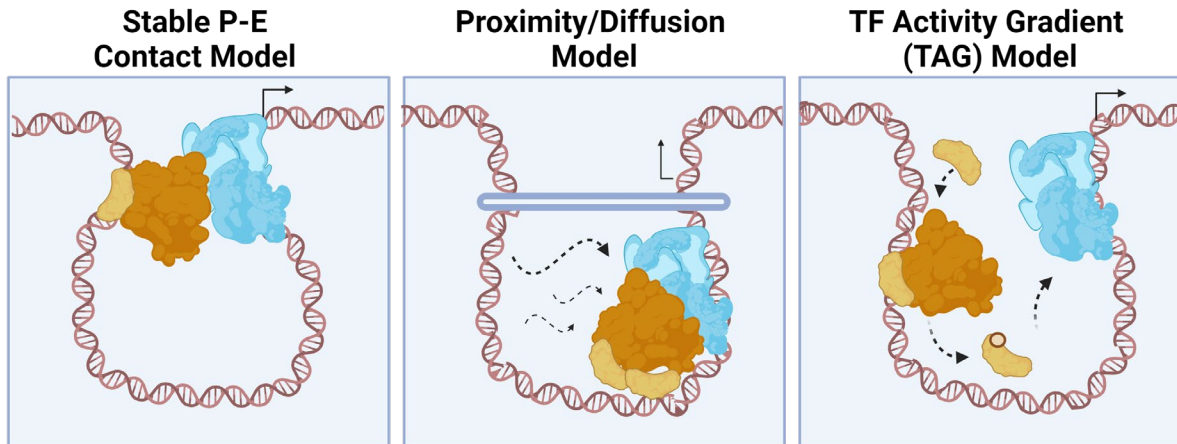
Figure 1.1 Models of enhancer-promoter communication. (Left) A cis-regulatory element is formed by a stable promoter-enhancer complex of TFs (yellow), coactivators (orange), and the GTF/ RNA Pol II (blue).[5] (Middle) TFs bind to the enhancer and diffuse to the promoter region to elicit Mediator-Pol II activation.[1] (Right) TFs are acetylated by enhancer bound coactivators, recruited by TFs, and diffuse to the promoter to activate transcription.[10] Figure created with BioRender.com.

Generally, in transcriptional activation, coactivators, through their activator binding domains (ABDs), directly interact with trans-activation domains (TADs) of transcription factors, or activators, bound at enhancer regions of DNA through their DNA-binding domains (DBDs), as illustrated in Figure 1.2.[11, 12] The interplay between these components recruits additional proteins in the transcriptional machinery, stimulating PIC formation.[13, 14] Through this process, coactivator•activator PPIs contribute to the modulation of gene expression. In this capacity, coactivators are known to be involved in development, cell growth and differentiation, and stem cell maintenance pathways.[15-17]
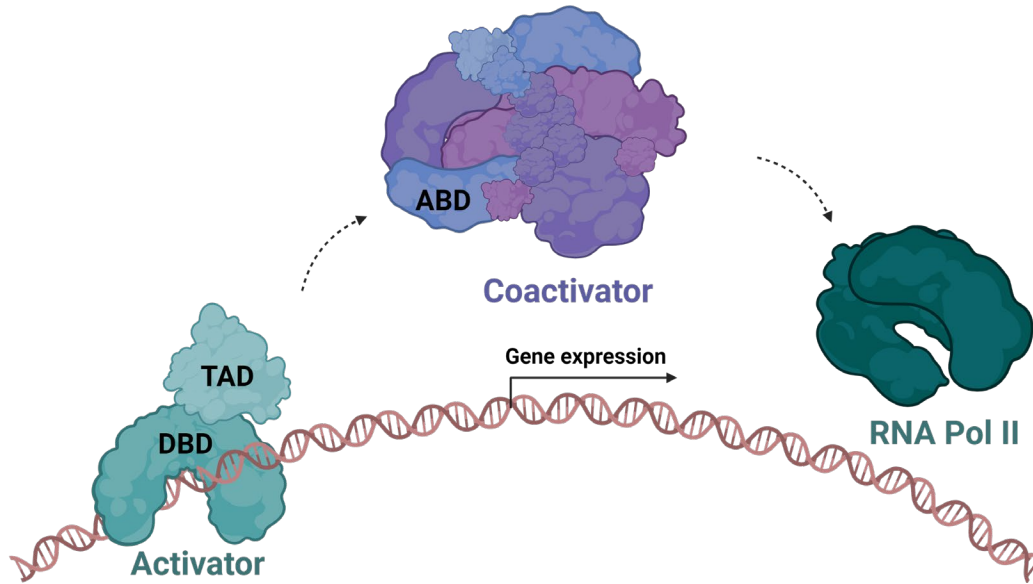
Figure 1.2. Protein–protein interactions mediate transcriptional activation. Transcriptional activators (blue) bind at the enhancer regions of genes through their DNA-binding domain (DBD). The transactivation domains (TADs) of activators bind to the activator binding domains (ABDs) of coactivators (purple). Coactivators modulate the recruitment of RNA polymerase II and the general transcription machinery. Figure created with BioRender.com.

1.2.2 Coactivator•activator PPIs are therapeutically relevant

Coactivators and activators are implicated in processes significant for cell growth and differentiation, so disruptions in their regulatory patterns are often present in various forms of disease. Misregulation of coactivator function has been characterized in autoimmune and neurological disorders, developmental syndromes, cardiovascular and metabolic diseases, and multiple kinds of cancer.[15-18] In cancer, for instance, changes in the function of TFs involved in specific pathways are known to be important markers of disease. These include processes for organizing cell identity, proliferative control, and signaling cascades that contribute to the response of cells to extracellular cues.[19] As described, coactivators, through their PPIs with activators, are involved in the expression of genes that span all of these categories, highlighting their potential widespread contribution to the development of malignant states. Thus, their notable therapeutic

relevance as a class of proteins has long been acknowledged, as evidenced by the targets in Table 1.1. [20-23] The subsequent section describes the unique features and therapeutic relevance of two coactivator target ABDs that will be highlighted in this dissertation, Med25 AcID and CBP KIX. This includes a summary of the diversity between the two with respect to their interactions, structure, biological function, and the characterization of their role in disease.

Table 1.1 Coactivator PPI dysregulation as targets in human disease

PPI Target	Types of Cancer	Impact in Disease Development	References
CBP KIX•Myb	Leukemia, breast, colon, pancreatic, glioblastomas, melanomas, esophageal	Activation of pro-proliferative, differentiative and survival enhancing gene programs	[24, 25]
CBP KIX•CREB	Prostate, breast, non-small-cell lung cancer and acute leukemia	Activation of cell differentiation, survival in the nervous system, apoptotic escape, metastasis	[26, 27]
BAF complex	Ewing sarcoma, pediatric malignant rhabdoid tumor, epithelioid sarcomas, carcinomas. meningiomas	Expression of pluripotency programs, impaired differentiation, and tumorigenesis.	[28-31]
CBP TAZ1•HIF1α	Breast, endothelial cancers	Activation of the hippo signaling pathway, cell cycle control and hypoxia resistance	[17, 32]
β-catenin•BCL9	Colorectal cancer, pancreatic, hepatocellular carcinomas	Activation of cell proliferation, migration, invasion, and tumor metastatic potential	[16]

| YAP•TEAD | Malignant pleural mesothelioma, lung cancer, breast cancer, glioblastomas, epithelial | Activation of pro-proliferative and survival enhancing gene programs | 18, 33 |

1.2.2.1 Med25 AcID is an emerging therapeutic target

Med25 is a subunit of the Mediator, an evolutionarily conserved, multi-subunit complex that serves as both a functional and architectural bridge in transcription.[34] As Mediator's tail module, Med25 is a variably present component that is engaged in the expression of non-basal level genes, modulating developmental and cellular differentiation processes.[11] The context-dependence of this function makes Med25 an ideal candidate for synthetic modulation. In addition, several lines of evidence suggest that Med25 plays an important role in disease-relevant contexts. For instance, Med25 is implicated in the dysregulated expression of genes contributing to metastasis and apoptotic evasion in breast and pancreatic cancer phenotypes.[35, 36]

Specifically, Med25 engages with activators involved in these apoptotic pathways through PPIs between its Activator Interacting Domain (AcID) and the TADs of members of the ETV/PEA3 family and ATF6α.[37, 38] AcID interacts with multiple activators through large and dynamic interaction surfaces, defined by the two faces, the H1 and H2 face, of a seven-stranded beta-barrel core that is flanked by alpha helices connected through dynamic loops (Figure 1.3). The structure of Med25 AcID, specifically the β-barrel core, is unique among ABDs of coactivators, and mechanistic studies in our group point to the presence of an allosteric network in AcID that connects the two binding interfaces H1 and H2. These studies also suggest a model of binding specificity within the protein domain

that is modulated by dynamic loops and alpha helices.[39] Advancements in our understanding of the recognition mechanisms that mediate Med25's protein network lay the groundwork for developing inhibitors that target Med25 PPIs and position Med25 as an attractive target for investigating its functional role in disease.
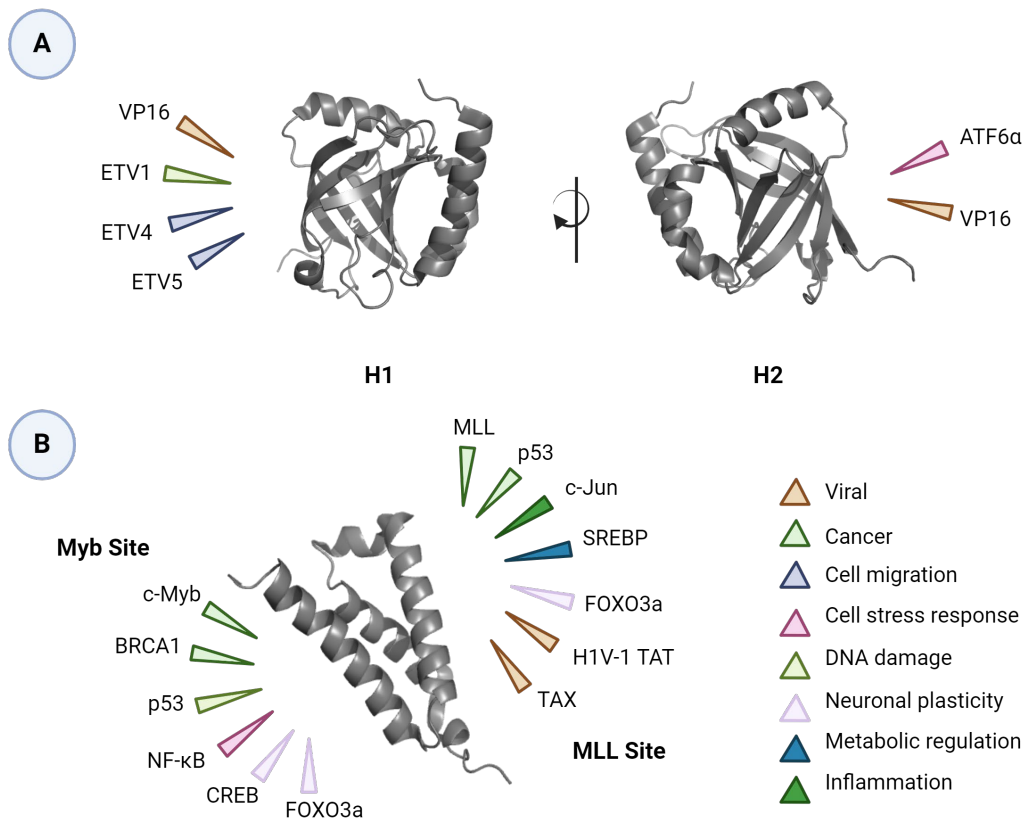
Figure 1.3. Activator PPIs of the ABDs of Med25 AcID and CBP KIX. Figure created with BioRender.com.

1.2.2.2 CBP/p300 KIX is a validated coactivator target in disease

CREB binding protein (CBP) and p300 are paralog proteins that act as master coactivators of transcription.[40] CBP/p300 are involved in important signaling pathways that when dysregulated have implications in the development of neurodegenerative diseases and cancer.[41, 42] CBP/p300 have various functions in transcription, such as chromatin remodeling, TF acetylation, and mediation of transcriptional activation through PPIs, all of which are attributable to their multi-domain structure. [42] (Figure 1.4) CBP/p300

serve as interaction hubs in gene regulatory networks, and through their multiple ABDs (including KIX, TAZ1, IBiD, TAZ2) they engage with over 100 activators.[43] Given this centrality in transcriptional PPI networks, and its interactions with oncogenic transcription factors, CBP/p300 have long been recognized as significant targets for pharmacological intervention, and several of the PPIs they engage in have been identified as validated disease targets (See Table 1.1).[16]
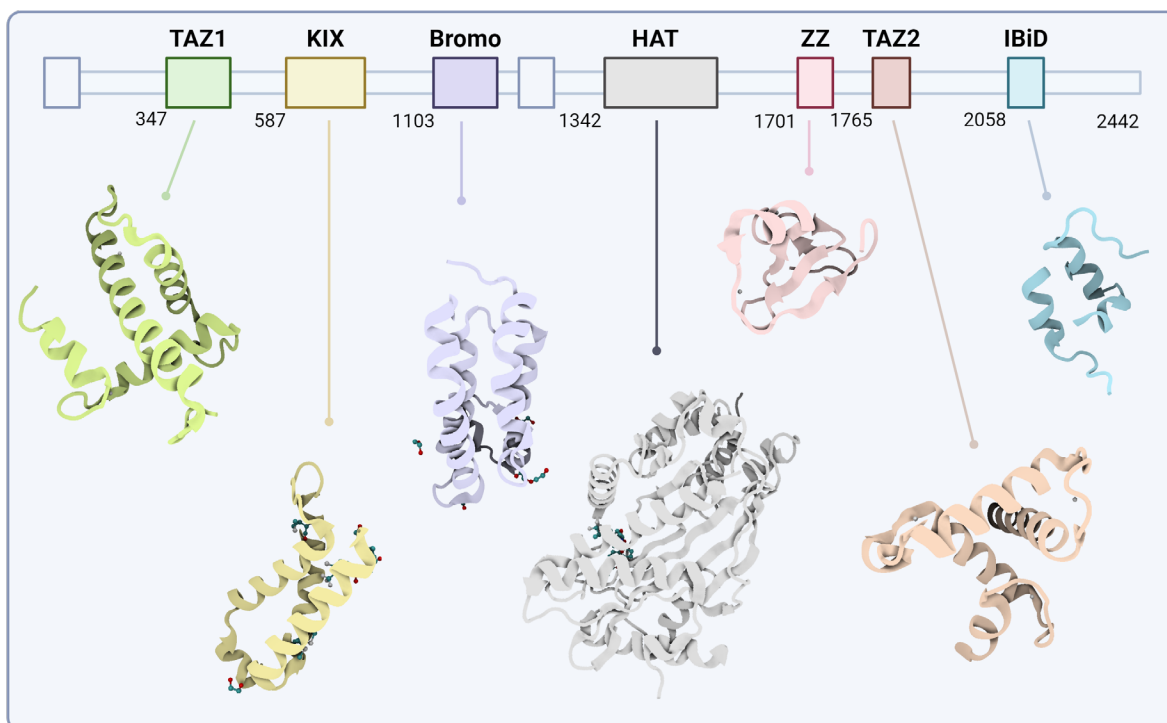
Figure 1.4. Structure and organization of the domains of CBP. PDB IDs: 1U2N, 419O, 4OUF, 5KJ2, 1TOT, 1F81, 1JJS. Figure adapted from Mapp et al. 2018.[44] Figure created with BioRender.com.

The KIX domain of CBP/p300 interacts with over 15 activator TADs using two distinct binding surfaces, which are allosterically connected through the hydrophobic core of the three alpha helices that comprise its structure.[45] A broad range of dysregulation in the PPIs of the KIX domain has been identified in diseases, including leukemia, colorectal and breast cancers. In this realm, a multitude of strategies have been employed to inhibit its activity, such as the use of natural products, small molecules, tethering approaches,

8

and peptide-based tools.[44, 46-48] As such, CBP KIX is not only an important target in its own right but can also serve as a model for validating novel strategies for developing coactivator PPI inhibitors, given the extensive characterization of its dynamic structure and biological function.

1.2.3 Challenges and opportunities of targeting coactivator•activator PPIs

An approach to target the function of dysregulated transcription factors in disease is to inhibit the protein–protein interactions in which they engage at various stages of transcription. This strategy was first introduced over two decades ago when many aspects of TF function were still not fully understood.[18, 49, 50] Such a strategy has demonstrated tractability, with some TF PPI inhibitors currently being evaluated as therapeutic agents in clinical trials. These include inhibitors of the PPI between activator p53 and transcriptional regulator ubiquitin E3 ligase MDM2, for the treatment of carcinomas and acute leukemia.[15, 17, 51] Notably, the p53•MDM2 PPI has high affinity, a small and well-defined binding surface (<1800 Å^2), and a validated oncogenic role. These characteristics are conductive to inhibitor development but do not represent all therapeutically relevant TF PPIs, including those with coactivators.[52] For instance, numerous coactivator•activator PPIs have been characterized as having a binding surface area between 2000–5000 Å^2.[53] Incorporating strategies that account for the unique features of coactivators in inhibitor design represents the next step toward probing coactivator•activator PPIs with potential for therapeutic intervention.[54-56] This section outlines these unique features and the specific challenges they present for inhibitor development.

1.2.3.1 Coactivator systems are structurally and dynamically complex

9

Within the interactome, coactivators exist as hub proteins, meaning they are highly connected through interactions with multiple binding partners, and they functionally link various PPI network modules.[57-59] The basis for their ability to interact with several transcription factors rests largely in the existence of intrinsically-disordered regions (IDRs) within their structures.[60-65] Depending on the particular TF, these IDRs can range in length and may exist as tails, linkers, loop substructures or intrinsically disordered proteins (IDPs) with transient secondary structures.[38, 66] In coactivator•activator PPIs, for instance, these IDRs may be present as loops and linkers in coactivator ABD units, as is the case of Med25 AcID, whereas activator TADs may present as IDPs and exhibit coupled folding-upon-binding to a cognate ABD.[67] IDRs enable a higher degree of flexibility and malleability in transcriptional proteins, endowing them with tunable molecular recognition and enabling them to adapt and bind to multiple partners, often with context-dependent selectivity.[68]

IDRs are known to exist as ensembles, compilations of rapidly exchanging conformations that represent the accessible structures of the domain[69]. Functionally, conformations within an ensemble may be related to selectivity of binding, as in the case of the PPIs between coactivator Med25 AcID and a subset of proteins in the ETV/PEA3 family of activators. In this case, it was identified that ETV4 binds to Med25 in a unique conformation in comparison to ETV1/5, despite having high sequence similarity. [70] Considering the unique gene programs each of these activators is engaged in,[71] their structural flexibility as IDRs, and the ability of coactivator Med25 to discern between them and functionally respond in an specific manner, the dynamic potential of these systems is exponentially higher, contrasting with one-to-one systems of interaction.

The sequence composition of IDRs in transcriptional proteins consists mainly of amino acids with short nonpolar side chains and a high degree of charge, comparatively deficient in large hydrophobic amino acids, when compared to globular proteins[64, 71-73]. The features that these amino acids confer onto coactivators and activators, and their presentation as IDRs, led to an initial model of interaction between coactivator•activator domains that suggested that the PPIs between them largely occurred in a non-specific manner, driven mainly by electrostatic and hydrophobic interactions.[64] More recent models suggest a more specific relationship between sequence and the molecular recognition capabilities of IDRs. These models are based on recent studies which determined that the number and relative location of charges within a TAD sequence can significantly affect the ensemble composition of an activator IDR.[74, 75] This notion contrasts earlier assessments that suggested sequence-independence in the recognition mechanism of TAD PPIs, as seen in studies of Gcn4p[76] and EFP.[77] Current models of the mechanism of these PPIs reconcile this data, suggesting that while coactivator•activator PPIs may not exhibit the same geometric complementarity as other classes of PPIs, the overall composition of the interacting surfaces have specific property profiles. These profiles, based on TAD sequences, showcase a degree of permissibility among functionally similar sequences while maintaining specificity in the PPIs. This view also addresses the frequently observed low sequence conservation among related TADs.[78-81]

In the context of protein–protein interactions, IDRs within coactivators and activators result in a mechanism of binding termed "fuzzy", which relates to the presence of a finite number of structurally distinct bound configurations in the complex, in constant

exchange.[78, 82] In certain cases, the PPIs of fuzzy coactivator•activator complexes are initiated by a limited number of residues that contribute strongly to binding, known as anchor residues. Surrounding sequences contribute additional, albeit transient, contacts to the binding.[58, 83] For example, coactivator•activator pair GAL11•GCN4 exhibits this phenomenon, with two residues, Phe124 and Trp120 in the TAD of GNC4, acting as anchor residues.[84] The dynamic nature of coactivator PPIs, as a result of the fuzzy binding and the presence of IDRs in interacting surfaces, leads to higher versatility and adaptability in the protein complexes, adding a layer of complexity in the regulation of these PPIs.[85] One example is the negative regulatory domain (NRD) of the TAD of FoxM1. The dynamics of this activator are regulated by phosphorylation of its NRD sequence, which leads to the de-sequestration of its TAD from a structured to a disordered state. This transition then allows for the formation of a fuzzy complex with either the TAZ2 or KIX ABDs of CBP.[50] Although IDRs and fuzziness offer advantages in the intrinsic function of coactivator•activator PPIs, they also result in challenges when attempting to obtain detailed structural information of the same PPI complexes. Consequently, this presents certain challenges for the development of PPI inhibitors in dysregulated contexts. The subsequent section will discuss the impact of fuzziness on inhibitor discovery, along with the current progress in the field and underexplored avenues to address this challenge.

1.2.3.2 Challenges in the development of coactivator PPI inhibitors

While IDRs offer a suite of functional advantages to coactivators in their interactions with activators, studies have also demonstrated that IDRs can be drivers of disease, especially within transcriptional proteins.[86] Dysregulated states of TF PPIs may

be present as overexpression, chromosomal translocation, or deregulated functional interactions.[39] Furthermore, a characteristic of PPIs mediated at least in part by IDRs is transience, a state of binding that lasts a brief period of time, often characterized by moderate binding affinities.[87] These factors result in PPI complexes that are challenging to inhibit, as identifying and designing molecules with significantly higher potency than those of their cognate binding partners is difficult.[88] Moreover, large, shallow surface areas and the absence of hot spot residues, as in the case of the Med25 AcID•ATF6α PPI, further complicate the identification of molecules that can bind specifically and with a competitive affinity to inhibit a functional PPI. [83, 85, 86]

Although the features signifying a challenge in discovering transcriptional inhibitors underscore the reasons these proteins have been coined "undruggable", it is also true that significant strides have been made to uncover appropriate strategies to inhibit these PPIs.[89] Recognizing which approaches have shown promise and which have necessitated redirection is beneficial for identifying additional paths forward. For instance, while efforts have been directed towards identifying small molecule modulators of coactivator PPIs, the potential of success with this approach is contingent upon the characteristics of the protein of interest (POI). One study searching for suitable small molecule inhibitor scaffolds for various targets found that PPIs with buried surface area (BSA) values exceeding 2000 Å^2 may be difficult to inhibit using small molecule modalities.[90]

In fact, many of the small molecules highlighted in recent reviews as successful inhibitors of TF activity predominantly fall into one of two categories: 1) their mechanism of action (MOA) is alternative to PPI inhibition of the POI, or 2) the inhibitors are natural

product (NPs) or NP derivatives.[46, 91, 92] In the first case, these small molecules may target the kinase activity of transcriptional proteins or act as proteolysis-targeting chimeras (PROTACs), amenable approaches with their own sets of challenges[93, 94]. In the second case, although NPs show promise in potency and biological activity, their complex architecture hinders synthesis and derivatization, limiting their potential as generalizable scaffolds for coactivator PPI inhibition. However, two recently identified inhibitors in this class have highlighted the benefit of targeting specific areas within an ABD. (Figure 1.5) These include non-canonical binding sites, such as the third binding site of KIX targeted by garcinolic acid,[95] and dynamic substructures, like the Med25 AcID scaffolding helix binding site targeted by norstictic acid.[96] It has been suggested that these non-canonical binding sites are crucial for developing selective coactivator PPI inhibitors, a significant aspect of these studies, especially compared to previously reported NP inhibitors of CBP KIX.[97] Nonetheless, covalent approaches, such as the mechanism of binding of norstictic acid, pose potential issues for downstream development in treating dysregulated transcription due to susceptibility to treatment resistance from high mutation rates in cancer.[86, 98] In contrast, synthetic small molecules that act as orthosteric or allosteric inhibitors of PPIs often lack the required potency to serve as chemical probes or to be effective biologically.[99-101] Given these considerations, an outstanding contribution to the field would be the development of a strategy for creating modifiable, synthetically accessible, and functional coactivator PPI inhibitors. The next section, guided by the framework presented in Ran and Gestwicki,[102] examines peptides as the foundational modality for inhibiting coactivator PPIs with these accumulated challenges.
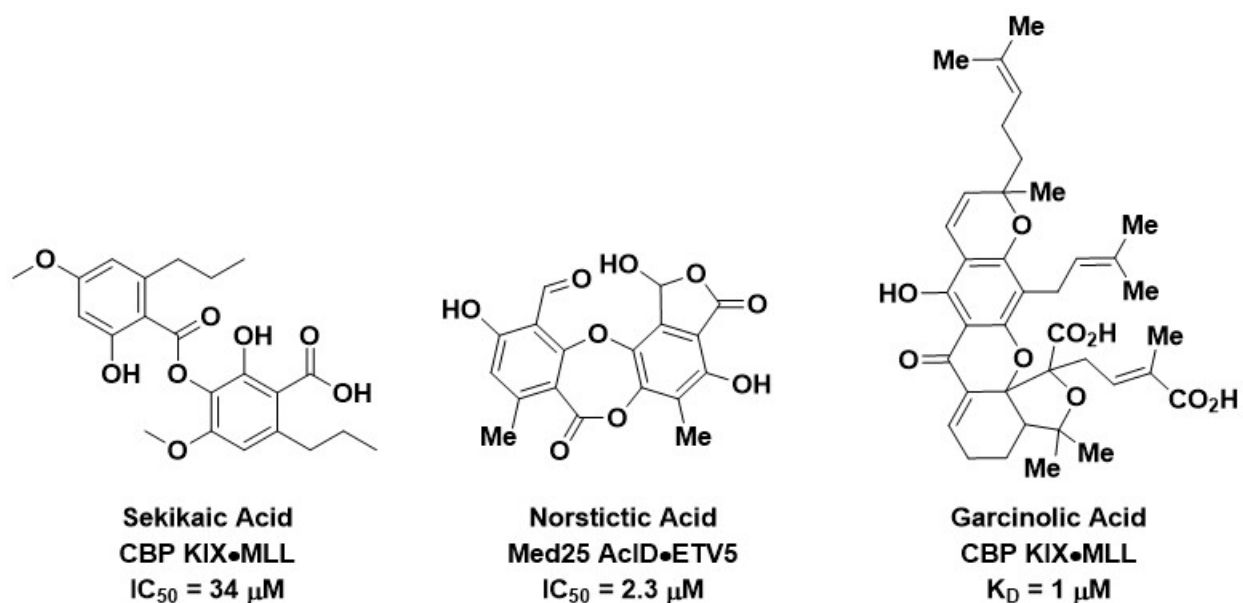
Figure 1.5. Natural product inhibitors of coactivator PPIs.[46, 91, 103]

1.3 Development of peptide-based coactivator inhibitors

1.3.1 Peptide inhibitors of protein–protein interactions

Peptides are an alternative to small molecules in the pursuit of inhibiting large PPI complexes, particularly those with the same structural and dynamic challenges as coactivator proteins.[104] PPI surfaces feature increasing levels of complexity, partly determined by the type of epitopes displayed at their interfaces, these being primary, secondary or tertiary structures (Figure 1.6).[100] Compared to synthetic small molecules, peptides can exhibit high levels of chemical diversity, partly owing to their ability to adopt various conformations in solution and when bound to a target.[47] Depending on their length, peptides can also establish multiple contacts with protein surfaces displaying a higher level of structural epitopes.[104-106] Recent examples of dual-site inhibitors of CBP KIX demonstrate the potential of high-molecular weight peptide scaffolds to achieve high potency and selectivity in modulating these challenging PPIs.[107, 108] However, the size of

these molecules poses specific challenges regarding intra-cellular transport and proteolytic stability. In terms of smaller peptide scaffolds, one area that has seen significant progress is the development of peptidomimetics that are chemically stabilized to mimic the secondary structure motifs, such as α-helices, present on PPI surfaces.[34, 50, 64, 109] Proteins with helices at their interaction surfaces comprise about 60% of multiprotein complexes, therefore, these advances underscore the value of adapting inhibitor design strategies to match the known characteristics of the intended targets.
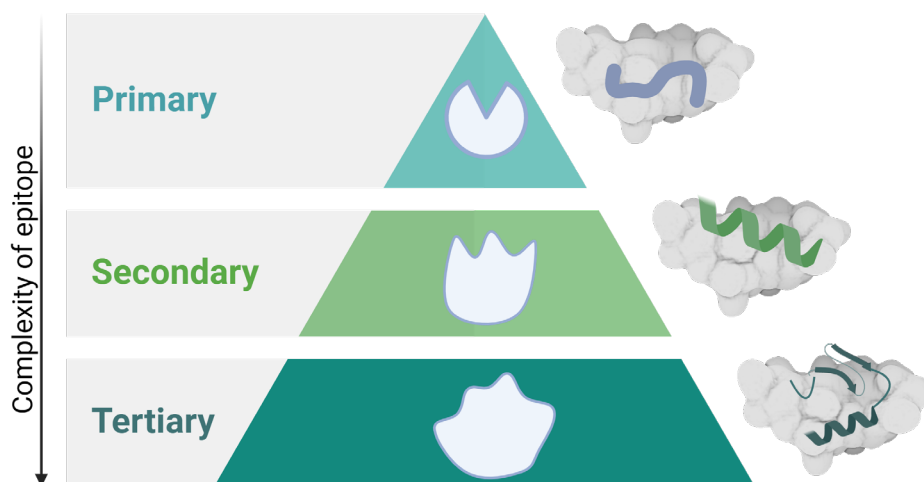
Figure 1.6. Epitope complexity of PPI surfaces. PPIs can be classified based on the structure at the binding surface of one of the binding partners. The complexity increases from a primary linear sequence, single secondary structures, or a combination of multiple types of secondary structures, including loops, β-sheets, and helices. Adapted from: Arkin *et al.* Chemistry & Biology 2014[100]. Figure created with BioRender.com.

Only about 0.01% of PPIs within the interactome have been targeted with an inhibitor.[110] Therefore, it is crucial to devise additional strategies for inhibitor design, especially to target protein surfaces with tertiary binding epitopes. A significant portion of coactivator surfaces can be described as having such epitopes, considering the topography and surface area over which their PPIs occur.[111] Furthermore, the interacting sequences on these surfaces have evolved to engage in transient interactions and exhibit a degree of permissibility with regards to recognition and binding.[112] In fact, coactivators

often rely on regulatory mechanisms outside of their interacting surfaces, as well as on contextual clues, to engage with their binding partners seletively.[113, 114] Given this context, it is apparent that the structure of binding surfaces on coactivators is not uniform across binding partners, nor readily discernible when complexed.[115] Additionally, due to their dynamic nature, the native sequences on activator interacting surfaces, absent of the full-length protein scaffold, are likely not optimized for potency or selectivity.[70] Thus, when designing short peptide-based inhibitors to target tertiary-epitopes on coactivator surfaces, simply mimicking the conformation of the interacting surface on either binding partner, as done by structure-based design for secondary epitopes, may be less viable. Such a strategy might not yield inhibitors with affinity or selectivity comparable to that of their cognate binding partners. This necessitates the exploration of novel forms of structural modification in the design of short peptide inhibitors that go beyond exact mimicry of the interacting surfaces they target.

1.3.2 TADs: A starting point for peptide-based inhibitors

TADs contain short sequences that mediate binding to coactivators and are required for activating transcription. For certain activators, these regions have been delineated through mutational and truncation studies.[116, 117] These minimal binding sequences are often between 7-15 amino acids long and are amphipathic, containing both negatively charged and small non-polar residues.[118-120] The nine amino acid transactivation domain, or 9aaTAD, for example, is a family of over 40 eukaryotic activators that can activate transcription as small peptides, sharing common features such as size, variable sequence patterns, and amphipathic nature.[121] The discovery of these minimal recognition motifs has partly contributed to the design of synthetic

transcriptional activators, composed of either TAD-derived peptides or small molecules conjugated to DNA-binding domains. These have demonstrated the ability to activate transcription in various systems.[122-124] Such studies have been paramount in advancing the understanding of artificially modulating gene expression and have underscored the capability of short TAD sequences to retain binding recognition while also enacting a biological response.

However, these short peptides, without additional chemical modifications, rarely function as inhibitors of transcription due to their low potency and selectivity. For instance, Henchey and coworkers identified a decapeptide within the TAD of the Hypoxia Inducible Factor 1, (HIF-1α), that, when constrained to form an α-helix, binds to p300 CH1 with twice the affinity compared to the unconstrained, albeit identical, peptide.[125] An additional challenge in dynamic surfaces is that these proteins may exhibit a level of permissibility in the diversity of backbone modifications they interact with, and certain forms of modification may not enhance the affinity or inhibitory activity of a peptidomimetic for a particular coactivator. Rowe *et al* 's study illustrates this challenge: modifications to the structures of natural and artificial TAD peptides, in the form of D-, β-, and peptoid mimetics, maintained but did not significantly enhance their affinity for CBP KIX.[126]

In other cases, modifications can endow peptides with other characteristics, such as proteolytic stability and bioactivity, without necessarily improving their binding affinity for a protein target. Ramaswamy and colleagues designed a retro-inverso form of a 17-mer within Myb, illustrating this scenario in a biological setting. Although their molecule, MYBMIM, conserves binding to CBP KIX and induces a biological response in an acute myeloid leukemia (AML) model, it binds to KIX with approximately five times weaker

affinity than the unmodified construct.[127] Taken together, these examples suggest that a valuable contribution to the field would be a peptide modification strategy that not only transcends structure at interaction surfaces, but also enhances both binding affinity and conferral of properties essential for biological activity, and does so with the ultimate goal of modulating transcription. Given what has been learned from peptide-based artificial activators and inhibitors, sequences that share the characteristics of minimal binding regions of TAD peptides, especially in terms of size, charge, and sequence composition, therefore stand as promising candidates for testing such modification strategies.

1.4 Lipidation as a strategy for developing peptide inhibitors

1.4.1 Lipidation in nature and its biological function

The conjugation of lipids to macromolecules is a common form of post-translational modification that regulates their function in biological systems. Lipidation is a powerful modulator of protein function as it can affect changes in the ability of a particular protein to interact with membranes and other proteins, as well as altering its intracellular stability, hydrophobicity, conformation, and in some cases, enzymatic activity. [127, 128] Similarly, lipopeptides are a class of natural products produced as secondary metabolites by a diversity of fungi and bacteria, with known biological activity that stem from the combination of their peptide and lipid moieties. The amphipathicity of lipopeptides modifies their physical properties and conformations in a way that can enable their activity as antimicrobials, antifungal and surfactants.[128, 129]

The therapeutic relevance of this class of natural products is exemplified by the number of lipopeptide agents entering clinical use. For example, daptomycin was the first cyclic lipopeptide antibiotic approved by the FDA in 2006 for the treatment of skin

infections caused by Gram-positive bacteria.[130] Continued research in this area has led to the identification of polymyxins B and E as gram-negative targeting agents for the treatment of several antibiotic-resistant bacteria.[131] Table 1.2 lists several lipopeptide drugs that are approved treatments for different forms of infections.

Table 1.2. FDA-approved lipopeptide drugs

Drug	Type of agent	Mechanism of action	Ref.
Daptomycin	GP antibiotic	Inhibition of cell wall synthesis	[132]
Polymyxin B	GN antibiotic	Membrane destabilization	[133]
Caspofungin	Antifungal	Inhibition of fungal cell wall synthesis	[134]
Micafungin	Antifungal	Inhibition of fungal cell wall synthesis	[135]
Colistin	GN antibiotic	Membrane destabilization	[136]
Colistimethate	GN antibiotic	Membrane destabilization	[137]
Rezafungin	Antifungal	Inhibition of fungal cell wall synthesis	[98]

The mechanisms of action of the drugs listed are all related to the disruption of different aspects of the cell wall or membrane. In a similar manner, Surfactin, a cyclic lipopeptide that has been studied for its antiproliferative activity in a variety of cancer cell lines, acts by selectively destabilizing the cytosolic membranes of cancer cells. [138] Although these agents all share a similar mechanism of action, lipidation confers a wide variety of functionalities to the peptides wo which they are appended, often dependent on the characteristics of the lipid itself. For this reason, the distinctive characteristics of lipopeptide natural products have positioned the conjugation of peptides with lipids as an attractive strategy in the design of biologically active molecules for a wide variety of applications.

1.4.2 Lipidation in the development of probes and therapeutics

Peptide lipidation can modify the physicochemical and pharmacological properties of peptides to enhance their bioactivity. Studies show that lipidation can modulate a peptide's hydrophobicity, secondary structure and self-assembling propensities while maintaining or improving their ability to bind to their targets.[135, 136, 139] At a molecular level, these features are promising in the development of chemical probes that can be utilized to study the function or biological relevance of a particular target.[138] For example, in the development of glucagon peptides that bind to the glucagon-like peptide 1 receptor, a study found that lipidation of a glucagon analog directly enhanced the affinity of the peptide for the receptor by stabilizing its structure and thermodynamic profile.[135] In fact, structure-activity relationship studies of the lipidated peptides showed that their functionality were dependent on the structure of the lipid and the site of attachment to the peptide. Another example, the development of the synthetic antimicrobial lipopeptide WL-C$_6$, demonstrates that lipidation can lead to the acquisition of bioactivity from an otherwise functionally inert peptide sequence.[138] These examples suggest that lipidation is a modification that goes beyond prolonging the pharmacokinetic parameters of molecules; it is in fact a potent tool to optimize the structure-function relationship of peptides for their protein targets.[140-142]

Furthermore, given the roles of lipid metabolism and function in biological systems, lipidation can be designed to also improve a molecule's half-life, metabolic stability, and bioavailability in complex biological settings, which demonstrates the potential of this type of synthetic modification for downstream therapeutic development.[135, 138, 143] A recent study, demonstrated this fact in the context of treatment of COVID-19. The authors tested

changes in the biological activity of a lipidated and hydrocarbon-stapled peptide that binds to a segment of the protein 6HB, part of the viral mechanism for cell entry. Their results showed that lipidation and hydrocarbon stapling of the peptide, leads to improvements in the stability, solubility, potency and overall antiviral activity of the constructs against SARS-CoV-2.[136] These conclusions are in accordance with previous findings, which also highlighted prolongation of systemic circulation, proteolytic stability, and membrane permeability of lipidated peptides in metabolic models.[144] A common thread among the above-mentioned studies is that lipidation has the potential to enhance the function of a peptide, but that this activity is contingent upon the composition, length, substitution, and location of the lipid.[5, 145, 146] Ultimately, lipidation of peptide sequences has widespread potential to increase their efficacy in a biological context. Considering the breath of biological functions that can result from lipidation, these modified peptide scaffolds can have important applications in challenging systems. Lipidation is a strategy that has so far gone unexplored in the development of coactivator•activator PPI inhibitors but warrants evaluation.

1.5 Dissertation Summary

The biological relevance of dysregulated coactivator PPI networks, and the challenges that exist in modulating them, call for novel approaches in designing inhibitors of their interactions. Considering the structural and dynamic features of coactivators, molecular scaffolds that may act as successful inhibitors must have the following starting characteristics: intrinsic recognition for coactivator surfaces, competitive selectivity over other coactivator domains, and a modifiable structure for the dissection of structure-activity relationships, and also for broader application against multiple targets. The work

22

in this dissertation posits that conjugation of lipids to peptides with TAD-like characteristics is a strategy to yield such selective and modifiable scaffolds. Here, these scaffolds are termed lipopeptidomimetics (LPPMs).

In Chapter 2, the results of testing this hypothesis against the PPIs of the coactivator Med25 AcID as proof-of-concept, are presented. Biophysical and biochemical assessments identify the determinants of activity within the structure of the lipopeptidomimetic, and an initial exploration into the activity of a lead LPPM in a cellular model highlights the potential of this approach. Furthermore, the discussion on this chapter identifies points of expansion to our knowledge about coactivator PPIs, based on the trends observed in the roles of the lipid and peptide structure for activity.

In Chapter 3, the modifiability of the selectivity of the LPPM scaffold is evaluated by testing a library of LPPM analogs against the PPIs of a second coactivator, CBP KIX, which differs significantly from Med25. An analog with better selectivity for KIX is identified, and multiple biophysical tests are utilized to verify and characterize the observed switch in selectivity. Lastly, Chapter 4 offers an outlook into the potential applications of this strategy in other coactivator and intrinsically disordered systems, and outlines the steps required to advance LPPM development into a high-throughput approach for developing inhibitors.

1.6 References

References

(1) El Khattabi, L.; Zhao, H.; Kalchschmidt, J.; Young, N.; Jung, S.; Van Blerkom, P.; Kieffer-Kwon, P.; Kieffer-Kwon, K. R.; Park, S.; Wang, X.; et al. A Pliable Mediator Acts as a Functional Rather Than an Architectural Bridge between Promoters and Enhancers. *Cell* **2019**, *178*, 1145–1158.e1120. DOI: 10.1016/j.cell.2019.07.011

(2) Richter, W. F.; Nayak, S.; Iwasa, J.; Taatjes, D. J. The Mediator complex as a master regulator of transcription by RNA polymerase II. *Nature Reviews Molecular Cell Biology* **2022**, *23*, 732–749. DOI: 10.1038/s41580-022-00498-3

(3) Ferrie, J. J.; Karr, J. P.; Graham, T. G. W.; Dailey, G. M.; Zhang, G.; Tjian, R.; Darzacq, X. p300 is an obligate integrator of combinatorial transcription factor inputs. *Mol Cell* **2023**. DOI: 10.1016/j.molcel.2023.12.004

(4) Boija, A.; Klein, I. A.; Sabari, B. R.; Dall'Agnese, A.; Coffey, E. L.; Zamudio, A. V.; Li, C. H.; Shrinivas, K.; Manteiga, J. C.; Hannett, N. M.; et al. Transcription Factors Activate Genes through the Phase-Separation Capacity of Their Activation Domains. *Cell* **2018**, *175*, 1842–1855.e1816. DOI: 10.1016/j.cell.2018.10.042

(5) Ptashne, M.; Gann, A. Transcriptional activation by recruitment. *Nature* **1997**, *386*, 569–577. DOI: 10.1038/386569a0

(6) Ma, J. Transcriptional activators and activation mechanisms. *Protein & Cell* **2011**, *2*, 879–888. DOI: 10.1007/s13238-011-1101-7

(7) Soutourina, J. Transcription regulation by the Mediator complex. *Nature Reviews Molecular Cell Biology* **2018**, *19*, 262–274. DOI: 10.1038/nrm.2017.115

(8) Rengachari, S.; Schilbach, S.; Aibara, S.; Dienemann, C.; Cramer, P. Structure of the human Mediator-RNA polymerase II pre-initiation complex. *Nature* **2021**, *594*, 129–133. DOI: 10.1038/s41586-021-03555-7

(9) Fong, Y. W.; Cattoglio, C.; Yamaguchi, T.; Tjian, R. Transcriptional regulation by coactivators in embryonic stem cells. *Trends Cell Biol* **2012**, *22*, 292–298. DOI: 10.1016/j.tcb.2012.04.002

(10) Karr, J. P.; Ferrie, J. J.; Tjian, R.; Darzacq, X. The transcription factor activity gradient (TAG) model: contemplating a contact-independent mechanism for enhancer–promoter communication. *Genes & Development* **2022**, *36*, 7–16. DOI: 10.1101/gad.349160.121

(11) Jaeger, M. G.; Schwalb, B.; Mackowiak, S. D.; Velychko, T.; Hanzl, A.; Imrichova, H.; Brand, M.; Agerer, B.; Chorn, S.; Nabet, B.; et al. Selective Mediator dependence of cell-type-specifying transcription. *Nature Genetics* **2020**, *52*, 719–727. DOI: 10.1038/s41588-020-0635-0

(12) Larke, M. S. C.; Schwessinger, R.; Nojima, T.; Telenius, J.; Beagrie, R. A.; Downes, D. J.; Oudelaar, A. M.; Truch, J.; Graham, B.; Bender, M. A.; et al. Enhancers predominantly regulate gene expression during differentiation via transcription initiation. *Molecular Cell* **2021**, *81*, 983–997.e987. DOI: 10.1016/j.molcel.2021.01.002

(13) Lee, Tong I.; Young, Richard A. Transcriptional Regulation and Its Misregulation in Disease. *Cell* **2013**, *152*, 1237–1251. DOI: https://doi.org/10.1016/j.cell.2013.02.014

(14) Santos-Terra, J.; Deckmann, I.; Fontes-Dutra, M.; Schwingel, G. B.; Bambini-Junior, V.; Gottfried, C. Transcription factors in neurodevelopmental and associated psychiatric disorders: A potential convergence for genetic and environmental risk factors. *Int J Dev Neurosci* **2021**, *81*, 545–578. DOI: 10.1002/jdn.10141

(15) Lambert, M.; Jambon, S.; Depauw, S.; David-Cordonnier, M. H. Targeting Transcription Factors for Cancer Treatment. *Molecules* **2018**, *23*. DOI: 10.3390/molecules23061479

(16) Darnell, J. E., Jr. Transcription factors as targets for cancer therapy. *Nat Rev Cancer* **2002**, *2*, 740–749. DOI: 10.1038/nrc906

(17) Bradner, J. E.; Hnisz, D.; Young, R. A. Transcriptional Addiction in Cancer. *Cell* **2017**, *168*, 629–643. DOI: 10.1016/j.cell.2016.12.013

(18) Bushweller, J. H. Targeting transcription factors in cancer - from undruggable to reality. *Nat Rev Cancer* **2019**, *19*, 611–624. DOI: 10.1038/s41568-019-0196-7

(19) Fry, E. A.; Inoue, K. c-MYB and DMTF1 in Cancer. *Cancer Invest* **2019**, *37*, 46-65. DOI: 10.1080/07357907.2018.1550090

(20) Cicirò, Y.; Sala, A. MYB oncoproteins: emerging players and potential therapeutic targets in human cancer. *Oncogenesis* **2021**, *10*, 19. DOI: 10.1038/s41389-021-00309-y

(21) Hooglugt, A.; van der Stoel, M. M.; Boon, R. A.; Huveneers, S. Endothelial YAP/TAZ Signaling in Angiogenesis and Tumor Vasculature. *Front Oncol* **2020**, *10*, 612802. DOI: 10.3389/fonc.2020.612802

(22) Xiang, L.; Gilkes, D. M.; Hu, H.; Luo, W.; Bullen, J. W.; Liang, H.; Semenza, G. L. HIF-1α and TAZ serve as reciprocal co-activators in human breast cancer cells. *Oncotarget* **2015**, *6*, 11768-11778. DOI: 10.18632/oncotarget.4190

(23) Muñoz, L.; Nomdedéu, J. F.; Villamor, N.; Guardia, R.; Colomer, D.; Ribera, J. M.; Torres, J. P.; Berlanga, J. J.; Fernández, C.; Llorente, A.; et al. Acute myeloid leukemia with MLL rearrangements: clinicobiological features, prognostic impact and value of flow cytometry in the detection of residual leukemic cells. *Leukemia* **2003**, *17*, 76-82. DOI: 10.1038/sj.leu.2402708

(24) White, B. D.; Chien, A. J.; Dawson, D. W. Dysregulation of Wnt/β-catenin signaling in gastrointestinal cancers. *Gastroenterology* **2012**, *142*, 219–232. DOI: 10.1053/j.gastro.2011.12.001

(25) Tang, T. T.; Konradi, A. W.; Feng, Y.; Peng, X.; Ma, M.; Li, J.; Yu, F. X.; Guan, K. L.; Post, L. Small Molecule Inhibitors of TEAD Auto-palmitoylation Selectively Inhibit Proliferation and Tumor Growth of NF2-deficient Mesothelioma. *Mol Cancer Ther* **2021**, *20*, 986–998. DOI: 10.1158/1535-7163.Mct-20-0717

(26) Xiao, X.; Li, B. X.; Mitton, B.; Ikeda, A.; Sakamoto, K. M. Targeting CREB for cancer therapy: friend or foe. *Curr Cancer Drug Targets* **2010**, *10*, 384–391. DOI: 10.2174/156800910791208535

(27) Sapio, L.; Salzillo, A.; Ragone, A.; Illiano, M.; Spina, A.; Naviglio, S. Targeting CREB in Cancer Therapy: A Key Candidate or One of Many? An Update. *Cancers* **2020**, *12*, 3166. DOI: 10.3390/cancers12113166

(28) Alfert, A.; Moreno, N.; Kerl, K. The BAF complex in development and disease. *Epigenetics & Chromatin* **2019**, *12*. DOI: 10.1186/s13072-019-0264-y

(29) St Pierre, R.; Kadoch, C. Mammalian SWI/SNF complexes in cancer: emerging therapeutic opportunities. *Curr Opin Genet Dev* **2017**, *42*, 56–67. DOI: 10.1016/j.gde.2017.02.004

(30) Lu, C.; Allis, C. D. SWI/SNF complex in cancer. *Nature Genetics* **2017**, *49*, 178–179. DOI: 10.1038/ng.3779

(31) El Hadidy, N.; Uversky, V. N. Intrinsic Disorder of the BAF Complex: Roles in Chromatin Remodeling and Disease Development. *Int J Mol Sci* **2019**, *20*. DOI: 10.3390/ijms20215260

(32) Cunningham, R.; Hansen, C. G. The Hippo pathway in cancer: YAP/TAZ and TEAD as therapeutic targets in cancer. *Clin Sci (Lond)* **2022**, *136*, 197–222. DOI: 10.1042/cs20201474

(33) Ding, Q.; Zhang, Z.; Liu, J.-J.; Jiang, N.; Zhang, J.; Ross, T. M.; Chu, X.-J.; Bartkovitz, D.; Podlaski, F.; Janson, C.; et al. Discovery of RG7388, a Potent and Selective p53–MDM2 Inhibitor in Clinical Development. *Journal of Medicinal Chemistry* **2013**, *56*, 5979–5983. DOI: 10.1021/jm400487c

(34) Harper, T. M.; Taatjes, D. J. The complex structure and function of Mediator. *J Biol Chem* **2018**, *293*, 13778–13785. DOI: 10.1074/jbc.R117.794438

(35) Pellecchia, A.; Pescucci, C.; De Lorenzo, E.; Luceri, C.; Passaro, N.; Sica, M.; Notaro, R.; De Angioletti, M. Overexpression of ETV4 is oncogenic in prostate cells through promotion of both cell proliferation and epithelial to mesenchymal transition. *Oncogenesis* **2012**, *1*, e20. DOI: 10.1038/oncsis.2012.20

(36) Landrieu, I.; Verger, A.; Baert, J. L.; Rucktooa, P.; Cantrelle, F. X.; Dewitte, F.; Ferreira, E.; Lens, Z.; Villeret, V.; Monté, D. Characterization of ERM transactivation domain binding to the ACID/PTOV domain of the Mediator subunit MED25. *Nucleic Acids Res* **2015**, *43*, 7110-7121. DOI: 10.1093/nar/gkv650

(37) Sela, D.; Conkright, J. J.; Chen, L.; Gilmore, J.; Washburn, M. P.; Florens, L.; Conaway, R. C.; Conaway, J. W. Role for human mediator subunit MED25 in recruitment of mediator to promoters by endoplasmic reticulum stress-responsive transcription factor ATF6α. *J Biol Chem* **2013**, *288*, 26179-26187. DOI: 10.1074/jbc.M113.496968

(38) Qi, T.; Qu, Q.; Li, G.; Wang, J.; Zhu, H.; Yang, Z.; Sun, Y.; Lu, Q.; Qu, J. Function and regulation of the PEA3 subfamily of ETS transcription factors in cancer. *Am J Cancer Res* **2020**, *10*, 3083-3105.

(39) Henderson, A. R.; Henley, M. J.; Foster, N. J.; Peiffer, A. L.; Beyersdorf, M. S.; Stanford, K. D.; Sturlis, S. M.; Linhares, B. M.; Hill, Z. B.; Wells, J. A.; et al. Conservation of coactivator engagement mechanism enables small-molecule allosteric modulators. *Proceedings of the National Academy of Sciences* **2018**, *115*, 8960-8965. DOI: 10.1073/pnas.1806202115

(40) Breen, M. E.; Mapp, A. K. Modulating the masters: chemical tools to dissect CBP and p300 function. *Curr Opin Chem Biol* **2018**, *45*, 195–203. DOI: 10.1016/j.cbpa.2018.06.005

(41) Valor, L. M.; Viosca, J.; Lopez-Atalaya, J. P.; Barco, A. Lysine acetyltransferases CBP and p300 as therapeutic targets in cognitive and neurodegenerative disorders. *Curr Pharm Des* **2013**, *19*, 5051–5064. DOI: 10.2174/13816128113199990382

(42) Wang, F.; Marshall, C. B.; Ikura, M. Transcriptional/epigenetic regulator CBP/p300 in tumorigenesis: structural and functional versatility in target recognition. *Cell Mol Life Sci* **2013**, *70*, 3989–4008. DOI: 10.1007/s00018-012-1254-4

(43) Bedford, D. C.; Kasper, L. H.; Fukuyama, T.; Brindle, P. K. Target gene context influences the transcriptional requirement for the KAT3 family of CBP and p300 histone acetyltransferases. *Epigenetics* **2010**, *5*, 9–15. DOI: 10.4161/epi.5.1.10449

(44) Breen, M. E.; Mapp, A. K. Modulating the masters: chemical tools to dissect CBP and p300 function. *Current Opinion in Chemical Biology* **2018**, *45*, 195–203. DOI: https://doi.org/10.1016/j.cbpa.2018.06.005

(45) Brüschweiler, S.; Konrat, R.; Tollinger, M. Allosteric Communication in the KIX Domain Proceeds through Dynamic Repacking of the Hydrophobic Core. *ACS Chemical Biology* **2013**, *8*, 1600-1610. DOI: 10.1021/cb4002188

(46) Breen, M. E.; Joy, S. T.; Baruti, O. J.; Beyersdorf, M. S.; Henley, M. J.; De Salle, S. N.; Ycas, P. D.; Croskey, A.; Cierpicki, T.; Pomerantz, W. C. K.; et al. Garcinolic Acid Distinguishes Between GACKIX Domains and Modulates Interaction Networks. *ChemBioChem* **2023**, *24*. DOI: 10.1002/cbic.202300439

(47) Liu, Y.; Joy, S. T.; Henley, M. J.; Croskey, A.; Yates, J. A.; Merajver, S. D.; Mapp, A. K. Inhibition of CREB Binding and Function with a Dual-Targeting Ligand. *Biochemistry* **2024**, *63*, 1–8. DOI: 10.1021/acs.biochem.3c00469

(48) Joy, S. T.; Henley, M. J.; De Salle, S. N.; Beyersdorf, M. S.; Vock, I. W.; Huldin, A. J. L.; Mapp, A. K. A Dual-Site Inhibitor of CBP/p300 KIX is a Selective and Effective Modulator of Myb. *Journal of the American Chemical Society* **2021**, *143*, 15056-15062. DOI: 10.1021/jacs.1c04432

(49) Stein, E. M.; DeAngelo, D. J.; Chromik, J.; Chatterjee, M.; Bauer, S.; Lin, C. C.; Suarez, C.; de Vos, F.; Steeghs, N.; Cassier, P. A.; et al. Results from a First-in-Human Phase I Study of Siremadlin (HDM201) in Patients with Advanced Wild-Type TP53 Solid Tumors and Acute Leukemia. *Clin Cancer Res* **2022**, *28*, 870–881. DOI: 10.1158/1078-0432.Ccr-21-1295

(50) Cesa, L. C.; Mapp, A. K.; Gestwicki, J. E. Direct and Propagated Effects of Small Molecules on Protein-Protein Interaction Networks. *Front Bioeng Biotechnol* **2015**, *3*, 119. DOI: 10.3389/fbioe.2015.00119

(51) Khan, S. H.; Ahmad, F.; Ahmad, N.; Flynn, D. C.; Kumar, R. Protein-protein interactions: principles, techniques, and their potential role in new drug development. *J Biomol Struct Dyn* **2011**, *28*, 929-938. DOI: 10.1080/07391102.2011.10508619

(52) Hu, G.; Wu, Z.; Uversky, V.; Kurgan, L. Functional Analysis of Human Hub Proteins and Their Interactors Involved in the Intrinsic Disorder-Enriched Interactions. *International Journal of Molecular Sciences* **2017**, *18*, 2761. DOI: 10.3390/ijms18122761

(53) Shammas, S. L. Mechanistic roles of protein disorder within transcription. *Curr Opin Struct Biol* **2017**, *42*, 155–161. DOI: 10.1016/j.sbi.2017.02.003

(54) Bertolazzi, P.; Bock, M. E.; Guerra, C. On the functional and structural characterization of hubs in protein–protein interaction networks. *Biotechnology Advances* **2013**, *31*, 274–286. DOI: https://doi.org/10.1016/j.biotechadv.2012.12.002

(55) Göös, H.; Kinnunen, M.; Salokas, K.; Tan, Z.; Liu, X.; Yadav, L.; Zhang, Q.; Wei, G.-H.; Varjosalo, M. Human transcription factor protein interaction networks. *Nature Communications* **2022**, *13*, 766. DOI: 10.1038/s41467-022-28341-5

(56) Lambert, S. A.; Jolma, A.; Campitelli, L. F.; Das, P. K.; Yin, Y.; Albu, M.; Chen, X.; Taipale, J.; Hughes, T. R.; Weirauch, M. T. The Human Transcription Factors. *Cell* **2018**, *172*, 650–665. DOI: 10.1016/j.cell.2018.01.029

(57) Chen, H.; Pugh, B. F. What do Transcription Factors Interact With? *J Mol Biol* **2021**, *433*, 166883. DOI: 10.1016/j.jmb.2021.166883

(58) Uversky, V. N.; Oldfield, C. J.; Dunker, A. K. Intrinsically disordered proteins in human diseases: introducing the D2 concept. *Annu Rev Biophys* **2008**, *37*, 215–246. DOI: 10.1146/annurev.biophys.37.032807.125924

(59) Singh, G. P.; Ganapathi, M.; Dash, D. Role of intrinsic disorder in transient interactions of hub proteins. *Proteins* **2007**, *66*, 761-765. DOI: 10.1002/prot.21281

(60) Dunker, A. K.; Lawson, J. D.; Brown, C. J.; Williams, R. M.; Romero, P.; Oh, J. S.; Oldfield, C. J.; Campen, A. M.; Ratliff, C. M.; Hipps, K. W.; et al. Intrinsically disordered protein. *J Mol Graph Model* **2001**, *19*, 26–59. DOI: 10.1016/s1093-3263(00)00138-8

(61) Millard, P. S.; Bugge, K.; Marabini, R.; Boomsma, W.; Burow, M.; Kragelund, B. B. IDDomainSpotter: Compositional bias reveals domains in long disordered protein regions-Insights from transcription factors. *Protein Sci* **2020**, *29*, 169–183. DOI: 10.1002/pro.3754

(62) Davey, N. E. The functional importance of structure in unstructured protein regions. *Current Opinion in Structural Biology* **2019**, *56*, 155–163. DOI: https://doi.org/10.1016/j.sbi.2019.03.009

(63) Robustelli, P.; Piana, S.; Shaw, D. E. Mechanism of Coupled Folding-upon-Binding of an Intrinsically Disordered Protein. *Journal of the American Chemical Society* **2020**, *142*, 11092–11101. DOI: 10.1021/jacs.0c03217

(64) Holehouse, A. S.; Kragelund, B. B. The molecular basis for cellular function of intrinsically disordered protein regions. *Nature Reviews Molecular Cell Biology* **2023**. DOI: 10.1038/s41580-023-00673-0

(65) Wright, P. E.; Dyson, H. J. Intrinsically unstructured proteins: re-assessing the protein structure-function paradigm. *J Mol Biol* **1999**, *293*, 321–331. DOI: 10.1006/jmbi.1999.3110

(66) Henley, M. J.; Linhares, B. M.; Morgan, B. S.; Cierpicki, T.; Fierke, C. A.; Mapp, A. K. Unexpected specificity within dynamic transcriptional protein–protein complexes. *Proceedings of the National Academy of Sciences* **2020**, *117*, 27346-27353. DOI: 10.1073/pnas.2013244117

(67) Müller-Späth, S.; Soranno, A.; Hirschfeld, V.; Hofmann, H.; Rüegger, S.; Reymond, L.; Nettels, D.; Schuler, B. Charge interactions can dominate the dimensions of intrinsically disordered proteins. *Proceedings of the National Academy of Sciences* **2010**, *107*, 14609–14614. DOI: 10.1073/pnas.1001743107

(68) Marsh, J. A.; Forman-Kay, J. D. Sequence determinants of compaction in intrinsically disordered proteins. *Biophys J* **2010**, *98*, 2383–2390. DOI: 10.1016/j.bpj.2010.02.006

(69) Staller, M. V.; Ramirez, E.; Kotha, S. R.; Holehouse, A. S.; Pappu, R. V.; Cohen, B. A. Directed mutational scanning reveals a balance between acidic and hydrophobic residues in strong human activation domains. *Cell Systems* **2022**, *13*, 334–345.e335. DOI: https://doi.org/10.1016/j.cels.2022.01.002

(70) Ravarani, C. N.; Erkina, T. Y.; De Baets, G.; Dudman, D. C.; Erkine, A. M.; Babu, M. M. High-throughput discovery of functional disordered regions: investigation of transactivation domains. *Mol Syst Biol* **2018**, *14*, e8190. DOI: 10.15252/msb.20188190

(71) Sigler, P. B. Acid blobs and negative noodles. *Nature* **1988**, *333*, 210–212. DOI: 10.1038/333210a0

(72) Das, R. K.; Pappu, R. V. Conformations of intrinsically disordered proteins are influenced by linear sequence distributions of oppositely charged residues. *Proceedings of the National Academy of Sciences* **2013**, *110*, 13392–13397. DOI: 10.1073/pnas.1304749110

(73) Ng, K. P.; Potikyan, G.; Savene, R. O.; Denny, C. T.; Uversky, V. N.; Lee, K. A. Multiple aromatic side chains within a disordered structure are critical for transcription and transforming activity of EWS family oncoproteins. *Proc Natl Acad Sci U S A* **2007**, *104*, 479–484. DOI: 10.1073/pnas.0607007104

(74) Zarin, T.; Strome, B.; Nguyen Ba, A. N.; Alberti, S.; Forman-Kay, J. D.; Moses, A. M. Proteome-wide signatures of function in highly diverged intrinsically disordered regions. *eLife* **2019**, *8*, e46883. DOI: 10.7554/eLife.46883

(75) Brown, C. J.; Johnson, A. K.; Dunker, A. K.; Daughdrill, G. W. Evolution and disorder. *Current Opinion in Structural Biology* **2011**, *21*, 441–446. DOI: https://doi.org/10.1016/j.sbi.2011.02.005

(76) Warfield, L.; Tuttle, L. M.; Pacheco, D.; Klevit, R. E.; Hahn, S. A sequence-specific transcription activator motif and powerful synthetic variants that bind Mediator using a fuzzy protein interface. *Proceedings of the National Academy of Sciences* **2014**, *111*, E3506–E3513. DOI: 10.1073/pnas.1412088111

(77) Olsen, J. G.; Teilum, K.; Kragelund, B. B. Behaviour of intrinsically disordered proteins in protein-protein complexes with an emphasis on fuzziness. *Cell Mol Life Sci* **2017**, *74*, 3175–3183. DOI: 10.1007/s00018-017-2560-7

(78) Tompa, P.; Fuxreiter, M. Fuzzy complexes: polymorphism and structural disorder in protein-protein interactions. *Trends Biochem Sci* **2008**, *33*, 2–8. DOI: 10.1016/j.tibs.2007.10.003

(79) Merritt, H. I.; Sawyer, N.; Watkins, A. M.; Arora, P. S. Anchor Residues Govern Binding and Folding of an Intrinsically Disordered Domain. *ACS Chemical Biology* **2022**, *17*, 2723–2727. DOI: 10.1021/acschembio.2c00619

(80) Rajamani, D.; Thiel, S.; Vajda, S.; Camacho, C. J. Anchor residues in protein-protein interactions. *Proc Natl Acad Sci U S A* **2004**, *101*, 11287–11292. DOI: 10.1073/pnas.0401942101

(81) Scholes, N. S.; Weinzierl, R. O. Molecular Dynamics of "Fuzzy" Transcriptional Activator-Coactivator Interactions. *PLoS Comput Biol* **2016**, *12*, e1004935. DOI: 10.1371/journal.pcbi.1004935

(82) Marceau, A. H.; Brison, C. M.; Nerli, S.; Arsenault, H. E.; McShan, A. C.; Chen, E.; Lee, H. W.; Benanti, J. A.; Sgourakis, N. G.; Rubin, S. M. An order-to-disorder structural switch activates the FoxM1 transcription factor. *Elife* **2019**, *8*. DOI: 10.7554/eLife.46131

(83) Tsafou, K.; Tiwari, P. B.; Forman-Kay, J. D.; Metallo, S. J.; Toretsky, J. A. Targeting Intrinsically Disordered Transcription Factors: Changing the Paradigm. *J Mol Biol* **2018**, *430*, 2321–2341. DOI: 10.1016/j.jmb.2018.04.008

(84) Krishnamurthy, M.; Dugan, A.; Nwokoye, A.; Fung, Y. H.; Lancia, J. K.; Majmudar, C. Y.; Mapp, A. K. Caught in the act: covalent cross-linking captures activator-coactivator interactions in vivo. *ACS Chem Biol* **2011**, *6*, 1321–1326. DOI: 10.1021/cb200308e

(85) Henley, M. J.; Koehler, A. N. Advances in targeting 'undruggable' transcription factors with small molecules. *Nature Reviews Drug Discovery* **2021**, *20*, 669–688. DOI: 10.1038/s41573-021-00199-0

(86) Ran, X.; Gestwicki, J. E. Inhibitors of protein-protein interactions (PPIs): an analysis of scaffold choices and buried surface area. *Curr Opin Chem Biol* **2018**, *44*, 75-86. DOI: 10.1016/j.cbpa.2018.06.004

(87) Chen, A.; Koehler, A. N. Transcription Factor Inhibition: Lessons Learned and Emerging Targets. *Trends Mol Med* **2020**, *26*, 508–518. DOI: 10.1016/j.molmed.2020.01.004

(88) Xie, X.; Yu, T.; Li, X.; Zhang, N.; Foster, L. J.; Peng, C.; Huang, W.; He, G. Recent advances in targeting the "undruggable" proteins: from drug discovery to clinical trials. *Signal Transduction and Targeted Therapy* **2023**, *8*, 335. DOI: 10.1038/s41392-023-01589-z

(89) Gao, H.; Sun, X.; Rao, Y. PROTAC Technology: Opportunities and Challenges. *ACS Medicinal Chemistry Letters* **2020**, *11*, 237–240. DOI: 10.1021/acsmedchemlett.9b00597

(90) Jeon, J. Y.; Sparreboom, A.; Baker, S. D. Kinase Inhibitors: The Reality Behind the Success. *Clin Pharmacol Ther* **2017**, *102*, 726–730. DOI: 10.1002/cpt.815

(91) Garlick, J. M.; Sturlis, S. M.; Bruno, P. A.; Yates, J. A.; Peiffer, A. L.; Liu, Y.; Goo, L.; Bao, L.; De Salle, S. N.; Tamayo-Castillo, G.; et al. Norstictic Acid Is a Selective Allosteric Transcriptional Regulator. *Journal of the American Chemical Society* **2021**, *143*, 9297-9302. DOI: 10.1021/jacs.1c03258

(92) Majmudar, C. Y.; Højfeldt, J. W.; Arevang, C. J.; Pomerantz, W. C.; Gagnon, J. K.; Schultz, P. J.; Cesa, L. C.; Doss, C. H.; Rowe, S. P.; Vásquez, V.; et al. Sekikaic acid and lobaric acid target a dynamic interface of the coactivator CBP/p300. *Angew Chem Int Ed Engl* **2012**, *51*, 11258-11262. DOI: 10.1002/anie.201206815

(93) Boike, L.; Henning, N. J.; Nomura, D. K. Advances in covalent drug discovery. *Nature Reviews Drug Discovery* **2022**, *21*, 881–898. DOI: 10.1038/s41573-022-00542-z

(94) Vasan, N.; Baselga, J.; Hyman, D. M. A view on drug resistance in cancer. *Nature* **2019**, *575*, 299–309. DOI: 10.1038/s41586-019-1730-1

(95) Noël, R.; Shin, Y.; Song, X.; He, Y.; Koenig, M.; Chen, W.; Ling, Y. Y.; Lin, L.; Ruiz, C. H.; LoGrasso, P.; et al. Synthesis and SAR of 4-(pyrazol-3-yl)-pyridines as novel c-jun N-terminal kinase inhibitors. *Bioorg Med Chem Lett* **2011**, *21*, 2732–2735. DOI: 10.1016/j.bmcl.2010.11.104

(96) Ihnen, M.; zu Eulenburg, C.; Kolarova, T.; Qi, J. W.; Manivong, K.; Chalukya, M.; Dering, J.; Anderson, L.; Ginther, C.; Meuter, A.; et al. Therapeutic potential of the poly(ADP-ribose) polymerase inhibitor rucaparib for the treatment of sporadic human ovarian cancer. *Mol Cancer Ther* **2013**, *12*, 1002–1015. DOI: 10.1158/1535-7163.Mct-12-0813

(97) Best, J. L.; Amezcua, C. A.; Mayr, B.; Flechner, L.; Murawsky, C. M.; Emerson, B.; Zor, T.; Gardner, K. H.; Montminy, M. Identification of small-molecule antagonists that inhibit an activator:coactivator interaction. *Proceedings of the National Academy of Sciences* **2004**, *101*, 17622–17627. DOI: 10.1073/pnas.0406374101

(98) Frye, S. V. The art of the chemical probe. *Nat Chem Biol* **2010**, *6*, 159–161. DOI: 10.1038/nchembio.296

(99) Lu, H.; Zhou, Q.; He, J.; Jiang, Z.; Peng, C.; Tong, R.; Shi, J. Recent advances in the development of protein–protein interactions modulators: mechanisms and clinical trials. *Signal Transduction and Targeted Therapy* **2020**, *5*, 213. DOI: 10.1038/s41392-020-00315-3

(100) Arkin, M. R.; Tang, Y.; Wells, J. A. Small-molecule inhibitors of protein-protein interactions: progressing toward the reality. *Chem Biol* **2014**, *21*, 1102–1114. DOI: 10.1016/j.chembiol.2014.09.001

(101) Cunningham, A. D.; Qvit, N.; Mochly-Rosen, D. Peptides and peptidomimetics as regulators of protein–protein interactions. *Current Opinion in Structural Biology* **2017**, *44*, 59–66. DOI: https://doi.org/10.1016/j.sbi.2016.12.009

(102) Azzarito, V.; Long, K.; Murphy, N. S.; Wilson, A. J. Inhibition of α-helix-mediated protein–protein interactions using designed molecules. *Nature Chemistry* **2013**, *5*, 161–173. DOI: 10.1038/nchem.1568

(103) Majmudar, C. Y.; Højfeldt, J. W.; Arevang, C. J.; Pomerantz, W. C.; Gagnon, J. K.; Schultz, P. J.; Cesa, L. C.; Doss, C. H.; Rowe, S. P.; Vásquez, V.; et al. Sekikaic Acid and Lobaric Acid Target a Dynamic Interface of the Coactivator CBP/p300. *Angewandte Chemie International Edition* **2012**, *51*, 11258-11262. DOI: 10.1002/anie.201206815

(104) Araghi, R. R.; Keating, A. E. Designing helical peptide inhibitors of protein–protein interactions. *Current opinion in structural biology* **2016**, *39*, 27–38.

(105) Modell, A. E.; Blosser, S. L.; Arora, P. S. Systematic Targeting of Protein–Protein Interactions. *Trends in Pharmacological Sciences* **2016**, *37*, 702–713. DOI: 10.1016/j.tips.2016.05.008

(106) Pelay-Gimeno, M.; Glas, A.; Koch, O.; Grossmann, T. N. Structure-Based Design of Inhibitors of Protein-Protein Interactions: Mimicking Peptide Binding Epitopes. *Angewandte Chemie International Edition* **2015**, *54*, 8896–8927. DOI: 10.1002/anie.201412070

(107) Sawyer, N.; Watkins, A. M.; Arora, P. S. Protein Domain Mimics as Modulators of Protein–Protein Interactions. *Accounts of Chemical Research* **2017**, *50*, 1313–1322. DOI: 10.1021/acs.accounts.7b00130

(108) Watkins, A. M.; Arora, P. S. Structure-based inhibition of protein–protein interactions. *European Journal of Medicinal Chemistry* **2015**, *94*, 480–488. DOI: https://doi.org/10.1016/j.ejmech.2014.09.047

(109) Thompson, A. D.; Dugan, A.; Gestwicki, J. E.; Mapp, A. K. Fine-tuning multiprotein complexes using small molecules. *ACS Chem Biol* **2012**, *7*, 1311–1320. DOI: 10.1021/cb300255p

(110) Pricer, R.; Gestwicki, J. E.; Mapp, A. K. From Fuzzy to Function: The New Frontier of Protein-Protein Interactions. *Acc Chem Res* **2017**, *50*, 584–589. DOI: 10.1021/acs.accounts.6b00565

(111) Wuo, M. G.; Arora, P. S. Engineered protein scaffolds as leads for synthetic inhibitors of protein–protein interactions. *Current Opinion in Chemical Biology* **2018**, *44*, 16–22. DOI: https://doi.org/10.1016/j.cbpa.2018.05.013

(112) Thuerauf, D. J.; Morrison, L. E.; Hoover, H.; Glembotski, C. C. Coordination of ATF6-mediated transcription and ATF6 degradation by a domain that is shared with the viral transcription factor, VP16. *J Biol Chem* **2002**, *277*, 20734–20739. DOI: 10.1074/jbc.M201749200

(113) Friedman, J. S.; Khanna, H.; Swain, P. K.; DeNicola, R.; Cheng, H.; Mitton, K. P.; Weber, C. H.; Hicks, D.; Swaroop, A. The Minimal Transactivation Domain of the Basic Motif-Leucine Zipper Transcription Factor NRL Interacts with TATA-binding Protein*. *Journal of Biological Chemistry* **2004**, *279*, 47233–47241. DOI: https://doi.org/10.1074/jbc.M408298200

(114) Giniger, E.; Ptashne, M. Transcription in yeast activated by a putative amphipathic α helix linked to a DNA binding unit. *Nature* **1987**, *330*, 670–672. DOI: 10.1038/330670a0

(115) Ma, J.; Ptashne, M. A new class of yeast transcriptional activators. *Cell* **1987**, *51*, 113–119. DOI: 10.1016/0092-8674(87)90015-8

(116) Piskacek, M.; Havelka, M.; Rezacova, M.; Knight, A. The 9aaTAD Transactivation Domains: From Gal4 to p53. *PLoS One* **2016**, *11*, e0162842. DOI: 10.1371/journal.pone.0162842

(117) Kuznetsova, S.; Ait-Si-Ali, S.; Nagibneva, I.; Troalen, F.; Le Villain, J. P.; Harel-Bellan, A.; Svinarchuk, F. Gene activation by triplex-forming oligonucleotide coupled to the activating domain of protein VP16. *Nucleic Acids Res* **1999**, *27*, 3995–4000. DOI: 10.1093/nar/27.20.3995

(118) Mapp, A. K.; Ansari, A. Z.; Ptashne, M.; Dervan, P. B. Activation of gene expression by small molecule transcription factors. *Proc Natl Acad Sci U S A* **2000**, *97*, 3930–3935. DOI: 10.1073/pnas.97.8.3930

(119) Stanojevic, D.; Young, R. A. A highly potent artificial transcription factor. *Biochemistry* **2002**, *41*, 7209–7216. DOI: 10.1021/bi015906b

(120) Henchey, L. K.; Kushal, S.; Dubey, R.; Chapman, R. N.; Olenyuk, B. Z.; Arora, P. S. Inhibition of Hypoxia Inducible Factor 1—Transcription Coactivator Interaction by a Hydrogen Bond Surrogate α-Helix. *Journal of the American Chemical Society* **2010**, *132*, 941–943. DOI: 10.1021/ja9082864

(121) Rowe, S. P.; Mapp, A. K. Assessing the permissiveness of transcriptional activator binding sites. *Biopolymers* **2008**, *89*, 578-581. DOI: 10.1002/bip.20946

(122) Ramaswamy, K.; Forbes, L.; Minuesa, G.; Gindin, T.; Brown, F.; Kharas, M. G.; Krivtsov, A. V.; Armstrong, S. A.; Still, E.; de Stanchina, E.; et al. Peptidomimetic blockade of MYB in acute myeloid leukemia. *Nature Communications* **2018**, *9*, 110. DOI: 10.1038/s41467-017-02618-6

(123) Jiang, H.; Zhang, X.; Chen, X.; Aramsangtienchai, P.; Tong, Z.; Lin, H. Protein Lipidation: Occurrence, Mechanisms, Biological Functions, and Enabling Technologies. *Chem Rev* **2018**, *118*, 919-988. DOI: 10.1021/acs.chemrev.6b00750

(124) Chen, B.; Sun, Y.; Niu, J.; Jarugumilli, G. K.; Wu, X. Protein Lipidation in Cell Signaling and Diseases: Function, Regulation, and Therapeutic Opportunities. *Cell Chemical Biology* **2018**, *25*, 817–831. DOI: https://doi.org/10.1016/j.chembiol.2018.05.003

(125) Meena, K. R.; Kanwar, S. S. Lipopeptides as the antifungal and antibacterial agents: applications in food safety and therapeutics. *Biomed Res Int* **2015**, *2015*, 473050. DOI: 10.1155/2015/473050

(126) Hamley, I. W. Lipopeptides: from self-assembly to bioactivity. *Chemical Communications* **2015**, *51*, 8574-8583. DOI: 10.1039/c5cc01535a

(127) Taylor, S. D.; Palmer, M. The action mechanism of daptomycin. *Bioorg Med Chem* **2016**, *24*, 6253-6268. DOI: 10.1016/j.bmc.2016.05.052

(128) Ledger, E. V. K.; Sabnis, A.; Edwards, A. M. Polymyxin and lipopeptide antibiotics: membrane-targeting drugs of last resort. *Microbiology (Reading)* **2022**, *168*. DOI: 10.1099/mic.0.001136

(129) Rybowicz, J.; Gurk-Turner, C. Caspofungin: the first agent available in the echinocandin class of antifungals. *Proc (Bayl Univ Med Cent)* **2002**, *15*, 97-99. DOI: 10.1080/08998280.2002.11927822

(130) de la Torre, P.; Reboli, A. C. Micafungin: an evidence-based review of its place in therapy. *Core Evid* **2014**, *9*, 27-39. DOI: 10.2147/ce.S36304

(131) Andrade, F. F.; Silva, D.; Rodrigues, A.; Pina-Vaz, C. Colistin Update on Its Mechanism of Action and Resistance, Present and Future Challenges. *Microorganisms* **2020**, *8*. DOI: 10.3390/microorganisms8111716

(132) de la Rosa-Carrillo, D.; Suárez-Cuartín, G.; Golpe, R.; Máiz Carro, L.; Martinez-Garcia, M. A. Inhaled Colistimethate Sodium in the Management of Patients with Bronchiectasis Infected by Pseudomonas aeruginosa: A Narrative Review of Current Evidence. *Infect Drug Resist* **2022**, *15*, 7271-7292. DOI: 10.2147/idr.S318173

(133) Garcia-Effron, G. Rezafungin-Mechanisms of Action, Susceptibility and Resistance: Similarities and Differences with the Other Echinocandins. *J Fungi (Basel)* **2020**, *6*. DOI: 10.3390/jof6040262

(134) Wu, Y. S.; Ngai, S. C.; Goh, B. H.; Chan, K. G.; Lee, L. H.; Chuah, L. H. Anticancer Activities of Surfactin and Potential Application of Nanotechnology Assisted Surfactin Delivery. *Front Pharmacol* **2017**, *8*, 761. DOI: 10.3389/fphar.2017.00761

(135) Zhang, L.; Bulaj, G. Converting peptides into drug leads by lipidation. *Curr Med Chem* **2012**, *19*, 1602–1618. DOI: 10.2174/092986712799945003

(136) Kowalczyk, R.; Harris, P. W. R.; Williams, G. M.; Yang, S. H.; Brimble, M. A. Peptide Lipidation - A Synthetic Strategy to Afford Peptide Based Therapeutics. *Adv Exp Med Biol* **2017**, *1030*, 185–227. DOI: 10.1007/978-3-319-66095-0_9

(137) Hutchinson, J. A.; Burholt, S.; Hamley, I. W. Peptide hormones and lipopeptides: from self-assembly to therapeutic applications. *Journal of Peptide Science* **2017**, *23*, 82–94. DOI: 10.1002/psc.2954

(138) Ward, B. P.; Ottaway, N. L.; Perez-Tilve, D.; Ma, D.; Gelfanov, V. M.; Tschöp, M. H.; DiMarchi, R. D. Peptide lipidation stabilizes structure to enhance biological function. *Molecular Metabolism* **2013**, *2*, 468–479. DOI: https://doi.org/10.1016/j.molmet.2013.08.008

(139) Lai, Z.; Chen, H.; Yuan, X.; Tian, J.; Dong, N.; Feng, X.; Shan, A. Designing double-site lipidated peptide amphiphiles as potent antimicrobial biomaterials to combat multidrug-resistant bacteria. *Frontiers in Microbiology* **2022**, *13*, Original Research. DOI: 10.3389/fmicb.2022.1074359

(140) Menacho-Melgar, R.; Decker, J. S.; Hennigan, J. N.; Lynch, M. D. A review of lipidation in the development of advanced protein and peptide therapeutics. *J Control Release* **2019**, *295*, 1–12. DOI: 10.1016/j.jconrel.2018.12.032

(141) Bird, G. H.; Patten, J. J.; Zavadoski, W.; Barucci, N.; Godes, M.; Moyer, B. M.; Owen, C. D.; DaSilva-Jardine, P.; Neuberg, D. S.; Bowen, R. A.; et al. A stapled lipopeptide platform for preventing and treating highly pathogenic viruses of pandemic potential. *Nature Communications* **2024**, *15*, 274. DOI: 10.1038/s41467-023-44361-1

(142) Trier, S.; Linderoth, L.; Bjerregaard, S.; Strauss, H. M.; Rahbek, U. L.; Andresen, T. L. Acylation of salmon calcitonin modulates in vitro intestinal peptide flux through membrane permeability enhancement. *European Journal of Pharmaceutics and Biopharmaceutics* **2015**, *96*, 329–337. DOI: https://doi.org/10.1016/j.ejpb.2015.09.001

(143) Rocco D, R. J., Murray P, Caccetta R. . Acyl lipidation of a peptide: effects on activity and epidermal permeability in vitro. . *Drug Des Devel Ther* **2016**, *10*, 2203–2209 DOI: https://doi.org/10.2147/DDDT.S104111

(144) Nikolovska-Coleska, Z.; Wang, R.; Fang, X.; Pan, H.; Tomita, Y.; Li, P.; Roller, P. P.; Krajewski, K.; Saito, N. G.; Stuckey, J. A.; et al. Development and optimization of a binding assay for the XIAP BIR3 domain using fluorescence polarization. *Anal Biochem* **2004**, *332*, 261-273. DOI: 10.1016/j.ab.2004.05.055

(145) Mapp, A. K.; Ansari, A. Z. A TAD further: exogenous control of gene activation. *ACS Chem Biol* **2007**, *2*, 62-75. DOI: 10.1021/cb600463w

(146) Brent, R.; Ptashne, M. A eukaryotic transcriptional activator bearing the DNA specificity of a prokaryotic repressor. *Cell* **1985**, *43*, 729-736. DOI: https://doi.org/10.1016/0092-8674(85)90246-6

Chapter 2 A Lipopeptidomimetic of Transcriptional Activation Domains Selectively Disrupts Med25 PPIs‡

2.1 Abstract

The transcriptional activation domains (TADs) of activators contain recognition sequences to bind to activator binding domains (ABDs) of coactivators. Short amphipathic peptides derived from TADs retain the ability to bind ABDs at the same surfaces as their respective full-length proteins, but they do so with low affinity and poor selectivity. Thus, they lack the necessary characteristics to be utilized as inhibitors of coactivator•activator PPIs. In this chapter, I describe a strategy encompassing the incorporation of a medium-length, branched fatty acid to the N-terminus of a TAD-derived heptameric peptide. This modification increases its affinity of the coactivator Med25 >>20-fold, (K_i >100 µM to 4 µM), yielding a lipopeptidomimetic (LPPM-8) that is an effective inhibitor of Med25 protein–protein interactions.

Through a structure-activity analysis, we found that the lipid, the peptide sequence, and the C-terminal functionalization, each contribute to the structure of the lead inhibitor LPPM-8 and its effectiveness as an inhibitor. LPPM-8 engages Med25 through interaction with the H2 face of its Activator Interaction Domain and in doing so stabilizes full-length protein in the cellular proteome. Further, genes regulated by Med25-activator PPIs are inhibited in a cell model of triple-negative breast cancer. Thus, LPPM-8 is a useful tool for studying Med25 and Mediator complex biology and the results indicate that lipopeptidomimetics may be a robust source of inhibitors for activator-coactivator complexes.

2.2 Introduction

2.2.1 Minimal TADs are ineffective inhibitors of coactivator PPIs

In transcriptional activation, coactivators are recruited to genomic loci through the protein–protein interactions (PPIs) formed with the transcriptional activation domains (TADs) of activators.[1-3] The interactions between these components mediates the assembly of the transcriptional machinery and the activation of particular gene programs, often in response to intracellular or environmental cues.[4] The sequence composition of TADs is largely composed of hydrophobic (L,V,F,W,M) and acidic (D,E) residues.[5-7] As a result, when unbound, these domains contain significant segments of intrinsic disordered regions (IDRs).[8] Many studies have demonstrated that peptides derived from sequences within TADs, often between 7-15 amino acids long, have the ability to act as synthetic transcriptional activators when attached to a DNA-binding domain.[9-14] These results suggest the existence of intrinsic recognition features in the sequences of TADs for

binding to coactivators, and propose a mechanism of interaction between coactivators and activators that is specific, albeit quite dynamic.[15-18]

Coactivator networks are dysregulated in many forms of diseases, and a strategy to better dissect their role, is the development of inhibitors targeting specific coactivators.[19, 20] Considering the activity of peptides derived from TAD sequences, these are attractive foundational structures for the development of inhibitors of coactivator•activator PPIs. However, in the absence of structural modifications, including the stabilization of structural epitopes for interacting with surfaces of higher structural order, these short peptides are often poor inhibitors.[21, 22] For instance, they do not exhibit a competitive affinity for inhibiting coactivator PPIs, nor are they selective in a biological setting for a specific target, limiting their use as chemical probes.[23, 24] Furthermore, a number of coactivator•activator complexes engage in fuzzier complexes than other coactivator complexes, limiting the availability of structural information to develop such stabilized peptide inhibitors, or eliminating the application of such a strategy in general.[25] For these reasons, an approach for designing coactivator•activator PPI inhibitors that harnesses the recognition capabilities of TADs, and does not depend on mimicking defined structural features of interaction surfaces, would be a significant milestone in studying these systems.

2.2.2 Lipidation of peptides confers biological function

The conjugation of a lipid to the N-terminus of peptides has been shown in different instances to diversify their function (Figure 2.1). For example, the structural features of the appended lipid may contribute to certain biochemical and biophysical characteristics of the peptide, including modified potency, and properties of assembly. Regarding the

modification of potency for a particular target, studies have been conducted to assess the relationship between acyl chain length and potency of lipidated GLP1 analogs and melanocortin ligands for their cognate receptors. These have determined that increasing lipid length results in higher potency but can oscillate or plateau after a length of C_{12} -C_{14} due to anchoring of the lipidated peptides into cell membranes.[26, 27] In relation to the structure assembly properties of lipopeptides, Poschner and Langosch demonstrated that acylation of Leu and Val-containing peptides leads to the increasing stabilization of their helix content as a function of acyl chain length.[28] This principle has been observed in the development of therapeutics, including in the development of GLP1 analogs for treatment of metabolic diseases. Acylation of these sequences with carbon chains ranging in length between C_8-$C_{16,}$ led to the elevation in their aqueous helical content, a property that was correlated with increased affinity of these peptides for their target receptors.[29] Potency and structural propensity, are all important characteristics of peptide-based molecules in chemical probe and therapeutic pipelines.

Properties of assembly & improved potency

Increased stability & modified immunogenicity

Membrane permeability & nuclear colocalization
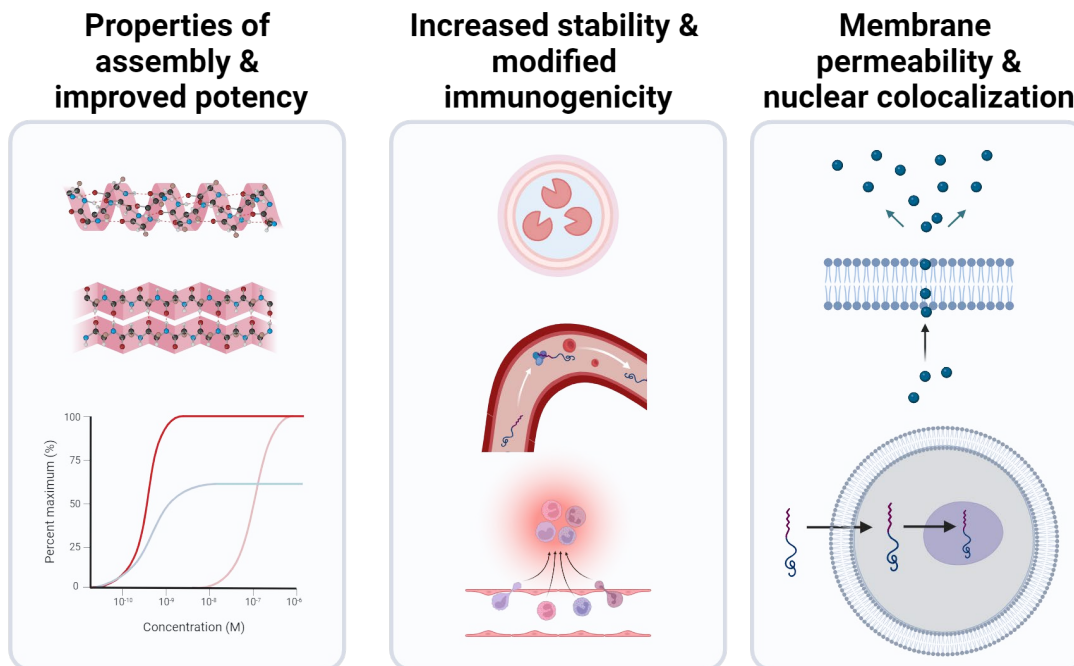
Figure 2.1. Characteristics of lipidated peptides related to improved biological function. Figure created with BioRender.com.

Lipidation of peptides can also lead to a higher compatibility within complex biological systems, including circulation stability and modified immunogenicity. In terms of stability, lipidated molecules exhibit significant improvements in half-life in serum and in vivo in comparison to their unmodified peptide counterparts. Improvements in half-life ranging between 10-fold and 100-fold for GLP1 analogs, for example, can be attributed to both the addition of a shield against proteolytic degradation, and to the binding of these peptides to circulating albumin, a protein responsible for transporting lipids and hydrophobic molecules in the bloodstream.[28, 30, 31]. Another factor that has been determined to be affected by lipidation, is the immunogenicity of peptides. Results from various studies on bioconjugates suggest a functional link between the type and length of the acyl chain appended to the peptide, and the immune response measured in a system. Bacteria-inspired lipid epitopes for example, may lead to the activation of the

immune response, whereas the linkage type between the lipid and the peptide may decrease this immunogenicity, amide linkers are less immunogenic than thioester linkers, for instance.[3, 4, 32, 33]

Lipidation can also improve a peptide's membrane permeability, a common obstacle in the development of peptide-based probes. A strategy that is often coopted, is the incorporation of cell penetrating peptides (CPPs) at various locations in the peptide sequence.[34] The density of positive charge and the size of typical CPPs, can be incompatible in some applications. In TAD derived peptides, for example, results from mechanistic studies suggest an important role of the negative charges for binding recognition and affinity to coactivators, so appending a CPP to these short peptides has the possibility of decreasing their inhibitory activity against coactivator•activator PPIs.[35, 36] Lipidation is an alternative to CPPs for endowing a molecule with membrane permeability. This property is also dependent on the length of the acyl chain, as data indicates that an appropriate length to provide permeability is between C_8 and C_{12}.[37, 38] The potential of this strategy for membrane permeability is illustrated by studies that demonstrate that lipidation of CPPs themselves can further facilitate membrane insertion and translocation of CPP cargo.[39] Considering that molecules targeting transcriptional components must get across two membranes, lipidation is a strategy with ample potential for designing short, stable and efficient coactivator PPI inhibitors. We opted to test this hypothesis with the coactivator Med25 and the interactions with its activator network.

2.2.3 Med25 is a model target for inhibition of coactivator PPIs

Med25 is a component of the Mediator complex, a master regulator and coactivator in the expression of most gene transcripts.[40, 41] As part of the tail module of Mediator,

Med25 is an exchangeable subunit with the primary role of interacting with transcription factors for transcriptional upregulation.[42-45] Specifically, Med25 activates the expression of genes through PPIs of its Activator Interaction Domain (AcID) with transcription factors of the ETV/PEA3 family, as well as ATF6α and VP16.[46-49] The activation of ETV/PEA3 regulated genes, leads to cell growth and cellular migration, and is implicated in tumor progression and metastasis.[50] ATF6α is a TF that in the context of cellular stress, activates genes in the unfolded protein response (UPR) pathways.[51] VP16 is implicated the expression of viral proteins upon infection of host cells.[52]

The biological relevance of these genetic programs suggests that Med25 has important functions to be further dissected. In fact, several lines of evidence suggest that dysregulation in the PPI network of Med25 contributes to the development of a number of cancers, positioning it as an emerging therapeutic target.[10] Med25 has also been identified as a protein with potential lipid-binding affinities, as it was identified to bind to arachidonic acid in a lipid-binding proteomics study.[53] To this date, This a unique feature among transcriptional coactivators, and also a feature with a biological role that has yet to be understood. Med25 is an appropriate representative of the structural and dynamic features of coactivators that make them challenging targets. This is exemplified by the fact that Med25 has only a single inhibitor reported thus far, Norstictic acid. This covalent natural product targets Lysine residues at a flanking α-helix of the H1 face of the protein, thereby inhibiting the Med25 AcID•ETV5 PPI.[49] Considering its role in disease, the pending questions about its PPI network, and the lack of useful chemical probes to dissect its function, Med25 is an apt target to test novel strategies in PPI inhibitor design. Here we investigate one such strategy and demonstrate that lipidation of a short amphipathic

peptide modifies the inhibitory activity of a weak binder of Med25 and leads to an effective inhibitor of Med25 PPIs. Ultimately, our results suggest that this approach has potential as a generalizable strategy for developing functional PPI inhibitors from transcription factor-derived sequences.

2.3 Results and Discussion

2.3.1 Acylation of a TAD-derived peptide leads to an LPPM with increased affinity for Med25 AcID

To test the hypothesis that acylation of a peptide increases its inhibitory activity against Med25 PPIs, we designed a sequence drawing from the composition of Med25-binding proteins. The initial peptide, EDLLLLV, contains a balance of hydrophobic and polar/acidic amino acids, much like the amphipathic sequences characteristic of the ETV and ATF6α TADs, and its length resembles that of minimal binding sequences of the same activators.[21, 49, 54] We first synthesized *N*-acetylated analogs of this sequence, including carboxy-terminal and carboxamide-terminal sequences, considering the C-terminal variations between natural and common synthetic peptide moieties. Furthermore, we included both D and L enantiomeric sequences, based on previous studies of TAD-coactivator interactions that suggest permissibility in the binding profile between D and L-TAD peptides, a common feature of fuzzy complexes with IDR interacting surfaces.[28, 55, 56] In advance of the incorporation of increasingly complex lipids to the base peptide sequence, members of the analog library were named lipopeptidomimetics, or LPPM-#, for short. The activity of these LPPMs was assessed in a competitive fluorescence polarization assay format, which measures the inhibition of the complex formed between Med25 AcID and the fluorescently labeled TAD of ATF6α,

a TF that interacts at the H2 face of AcID. As a secondary assessment of its engagement

with Med25 alone, the effect of these LPPMs on the melting temperature (T_m) of AcID

was measured using differential scanning fluorimetry (DSF).

Table 2.1. In-vitro activity assessment of LPPMs 2-5 as determined by competitive fluorescence polarization assays and differential scanning fluorimetry.

LPPM	D/L	R	K_i (µM)	$|\Delta T_m|$ (°C)
2	D	-OH	90 ± 9	2.8 ± 0.2
3	L	-OH	100 ± 20	0.2 ± 0.2
4	D	-NH$_2$	40 ± 2	4.3 ± 0.3
5	L	-NH$_2$	31 ± 3	0.3 ± 0.2

Inhibition of Med25 AcID•ATF6α (residues 38-75) by LPPMs 2-5 as determined by competitive FP assays. IC_{50} values were measured by titrating the lipopeptidomimetics with 20 nM FITC-ATF6α in complex with Med25 AcID (50% bound). The IC_{50} values were converted to K_i values using the apparent K_d from direct binding measurements of Med25 AcID•ATF6α and using a published K_i calculator.[57] Data shown is the average of three independent experiments performed in technical triplicate with the indicated error (SD). Change in the melting temperature (ΔTm) of 8 µM Med25 AcID in the presence of 5 eq of the indicated lipopeptidomimetic as determined by differential scanning fluorimetry. Temperature-dependent unfolding was monitored using Sypro Orange fluorescence. Values represent the change in melting temperature relative to unbound Med25 AcID control. The ΔTm values are the average of two independent experiments performed in technical triplicate with the indicated error (SD). FP experiments performed by O. Pattelli.

As summarized on Table 2.1, the acetylated LPPM-2 and LPPM-3 analogs are

poor inhibitors of the Med25 AcID•ATF6α PPI, with K_i values of 90 and 100 µM,

respectively. The C-terminal carboxamide analogs, LPPM-4, and LPPM-5, display a ~2-

fold enhanced activity by FP, but maintain a moderate affinity with values in the double

digit micromolar. The ΔT_m of Med25 AcID derived from DSF measurements, shows that

these LPPMs engage modestly with the protein. Comparison of these results grouped by

the C-terminal moiety of the LPPMs, suggests that the D- and L- peptides likely have

distinct binding modes in their interactions with the AcID domain, based on the ~10 fold

difference in the ΔTm inflicted by LPPM-2, LPPM-4, and LPPM-3, LPPM-5 . These data

confirm that these acetylated heptamers can interact with Med25 but do so with a weak

affinity and do not effectively inhibit the Med25•ATF6α PPI. Additionally, there is an observed permissibility in the backbone differences between the D- and L- versions of the LPPMs in relation to their interaction with AcID. Considering the intrinsic proteolytic stability of D-peptides in cellular contexts, the D-peptide sequences were carried forward for additional characterization. These results not only confirm the underlying assumptions of our proposed hypothesis but are also supported by previous mechanistic studies of amphipathic peptide binding and function in transcriptional fuzzy complexes.

Previous work has demonstrated a link between the acyl chain length and increasing affinity of lipidated peptides for binding to a particular protein target.[56-59] However, for lipopeptides assessed in cellular environments, an optimal length (C_8-C_{12}) has been identified that balances both potency and membrane permeability with membrane anchoring features resulting from lipidation.[60-62] For this reason, we assessed the impact of appending a medium-chain fatty acid (C_{11}) to LPPMs on both the inhibition of Med25•ATF6α and engagement to AcID (Table 2.2).
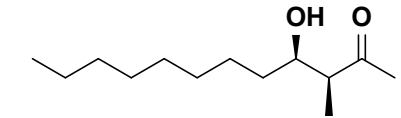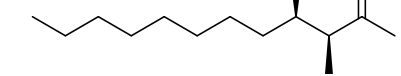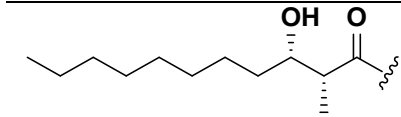
Table 2.2. In-vitro activity assessment of LPPMs 6-7 as determined by competitive fluorescence polarization assays and differential scanning fluorimetry.

LPPM	R_1	R	Ki (µM)	|ΔTm| (°C)
6		-OH	2.6 ± 0.2	18 ± 2
7		-NH$_2$	0.5 ± 0.2	2.3 ± 0.1

Inhibition of Med25 AcID•ATF6α (residues 38-75) by LPPMs 6-7 as determined by competitive FP assays. IC$_{50}$ values were measured by titrating the lipopeptidomimetics with 20 nM FITC-ATF6α in complex with Med25 AcID (50% bound). The IC$_{50}$ values were converted to K$_i$ values using the apparent K$_d$ from direct binding measurements of Med25 AcID•ATF6α and using a published K$_i$ calculator.[57] Data shown is the average of three independent experiments performed in technical triplicate with the indicated error (SD). Change in the melting temperature (ΔTm) of 8 µM Med25 AcID in the presence of 5 eq of the indicated lipopeptidomimetic as determined by differential scanning fluorimetry. Temperature-dependent unfolding was monitored using Sypro Orange fluorescence. Values represent the change in melting temperature relative to unbound Med25 AcID control. The ΔTm values are the average of two independent experiments performed in technical triplicate with the indicated error (SD).

As observed by the low micromolar K_is of both LPPM-6 and LPPM-7 for inhibiting the PPI between Med25•ATF6α, acylation with a longer carbon chain results in increased activity by comparison to the acetylated analogs. By DSF, LPPM-6 produced a 6-fold change in Med25 T_m relative to LPPM-2, while LPPM-7 maintained a similar profile to that of LPPM-4. This suggests that the undecanoic acid moiety and the carboxy C-terminus both contribute to a tighter binding to the protein. We recognized that appending a lipid to an amphipathic sequence could have an effect on the overall hydrophobicity of the molecules. Considering this in addition to the display of limited aqueous solubility of LPPM-6 and LPPM-7, we assessed their propensity to aggregate by measuring their K_i at increasing concentrations of detergent. As noted on Table 2.3 and Figures 2.2 and Appendix Figure B.3, the K_i of LPPM-7 exhibited a fold-change of >2 between detergent concentrations of 0.001% and 0.1%, suggesting that it may function in part as an aggregate.[63]

Table 2.3. In-vitro activity assessment of LPPMs 8-10 as determined by competitive fluorescence polarization assays and differential scanning fluorimetry.

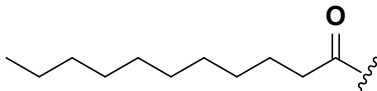| LPPM	R_1	R	Ki (µM)	$|\Delta Tm|$ (°C)
8		-OH	3.9 ± 0.8	12.2 ± 0.3
9		-NH₂	3 ± 2	1.7 ± 0.01
10		-OH	4.7 ± 0.4	14.4 v-± 0.6

Inhibition of Med25 AcID•ATF6α (residues 38-75) by LPPMs 8-10 as determined by competitive FP assays. IC_{50} values were measured by titrating the lipopeptidomimetics with 20 nM FITC-ATF6α in complex with Med25 AcID (50% bound). The IC_{50} values were converted to K_i values using the apparent K_d from direct binding measurements of Med25 AcID•ATF6α and using a published K_i calculator.[57] Data shown is the average of three independent experiments performed in technical triplicate with the indicated error (SD). Change in the melting temperature (ΔTm) of 8 µM Med25 AcID in the presence of 5 eq of the indicated lipopeptidomimetic as determined by differential scanning fluorimetry. Temperature-dependent unfolding was monitored using Sypro Orange fluorescence. Values represent the change in melting temperature

relative to unbound Med25 AcID control. The ΔTm values are the average of two independent experiments performed in technical triplicate with the indicated error (SD).

We reasoned that incorporation of functional groups on the lipid would increase solubility and could result in the decrease of aggregate formation. Noting that bacterial lipopeptides commonly feature a β-hydroxyl group and, less frequently, α-branching, we incorporated we incorporated (2S, 3R)-2-methyl-3-hydroxyundecanoate and (2R,3S)- 2-methyl-3-hydroxyundecanoate into analogs LPPM-8, -9, and -10.[64, 65]
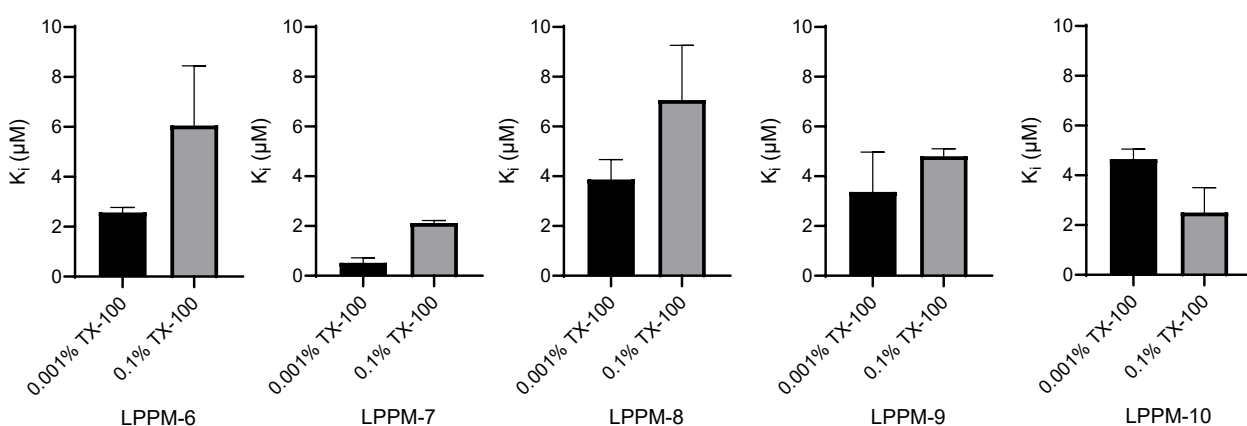
Figure 2.2 Inhibition of Med25 AcID•ATF6α by LPPM-6, LPPM-7, LPPM-8, LPPM-9 and LPPM-10 with different Triton X-100 concentrations as determined by competitive fluorescence polarization assays. Apparent IC_{50} values were determined through titration of compound for Med25 AcID•ATF6α PPI performed in experimental triplicate with the indicated error (SD). The IC_{50} values were converted to Ki values using the apparent K_D value based on the direct binding of Med25 AcID•ATF6α PPI using a Ki calculator. Data shown is the average of three independent experiments with the indicated error (SD). The analogs exhibited nearly identical activity in the competitive binding assay, with the stereochemistry of the lipid tail having no measurable impact (Table 2.3). Further, the Kis of these analogs were largely unaffected in an analogous detergent screen to the previously described. Importantly, incubation of Med25 AcID with LPPM-8, or -10 induced a significant change in T_m through DSF. This was not the case with LPPM-9, as only a minor change in Med25 T_m (1.7 °C) was observed, following the same trend as that of LPPM-7.Taken together, the data indicate that the seemingly minor change from a C-

terminal carboxylate versus C-terminal carboxamide, has a measurable effect on engagement of Med25 AcID by these molecules.

The binding of LPPM-8 and LPPM-9 to Med25 AcID was assessed using ^{1}H,^{15}N- and ^{1}H,^{13}C-HSQC spectroscopy. Given the dynamic backbone and substructures within the AcID domain, ^{1}H,^{13}C-HSQC is a well suited technique to identify direct contacts of the ligands to the protein relative to ^{1}H,^{15}N-HSQC.[66] This data demonstrates that LPPM-8 is a bona fide ligand of Med25, but LPPM-9 is not, in accordance with the differences in the T_m measured by the DSF experiments of Table 2.3.

Med25 AcID interacts with amphipathic activators through two binding surfaces that are allosterically connected.[67] Activator ATF6α interacts with the H2 face for instance, while members of the ETV/PEA3 family of activators engage at the H1 surface.[64, 67] Addition of 1.1 eq. of LPPM-8 led to several ^{1}H,^{15}N- and ^{1}H,^{13}C-HSQC chemical shift perturbations (CSPs) of residues mainly located on the H2 binding surface of Med25 AcID. Most of the residues perturbed in the ^{1}H,^{13}C-HSQC spectra are solvent exposed and located on the H2 face β-barrel and flanking α-helices (α1 and α2). (Figures 2.3-2.6)
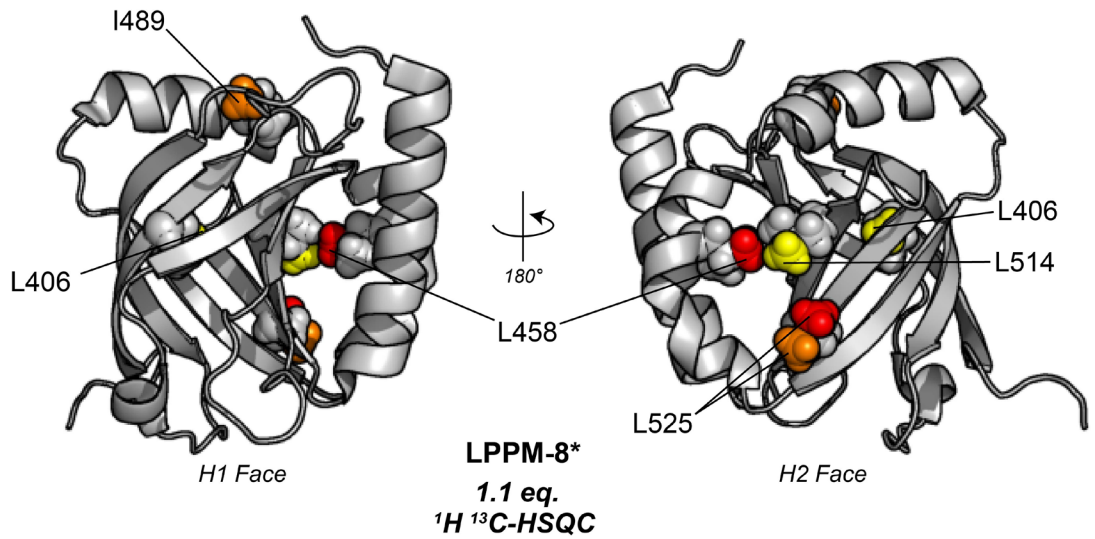
Figure 2.3. ^{1}H, ^{13}C-HSQC CSPs induced by binding of 1.1 eq of LPPM-8 mapped onto Med25 AcID (PDB ID 2XNF). Yellow = 0.02 ppm - 0.0249 ppm, orange = 0.025 ppm - 0.049 ppm, red ≥ 0.0491.
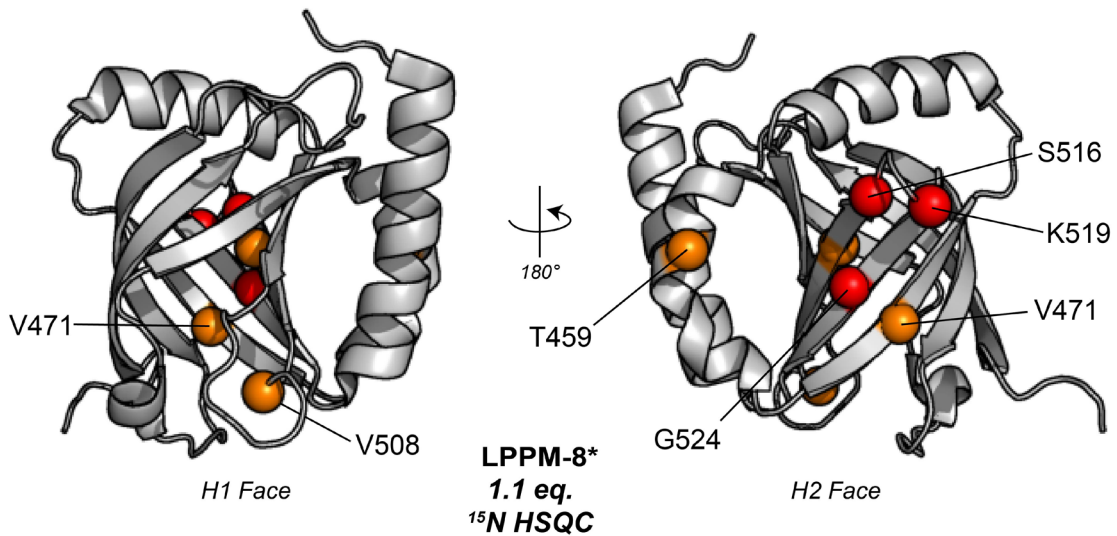
Figure 2.4 ^{1}H, ^{15}N-HSQC CSPs induced by binding of 1.1 eq of LPPM-8 mapped onto Med25 AcID (PDB ID 2XNF). Only residues with CSPs > 0.0851 ppm are labeled. Orange = 0.0851 ppm-0.14 ppm, red ≥ 0. 141. All perturbed residues above signal to noise ratio (≥ 0.02 ppm) found in Appendix Figure B.8.
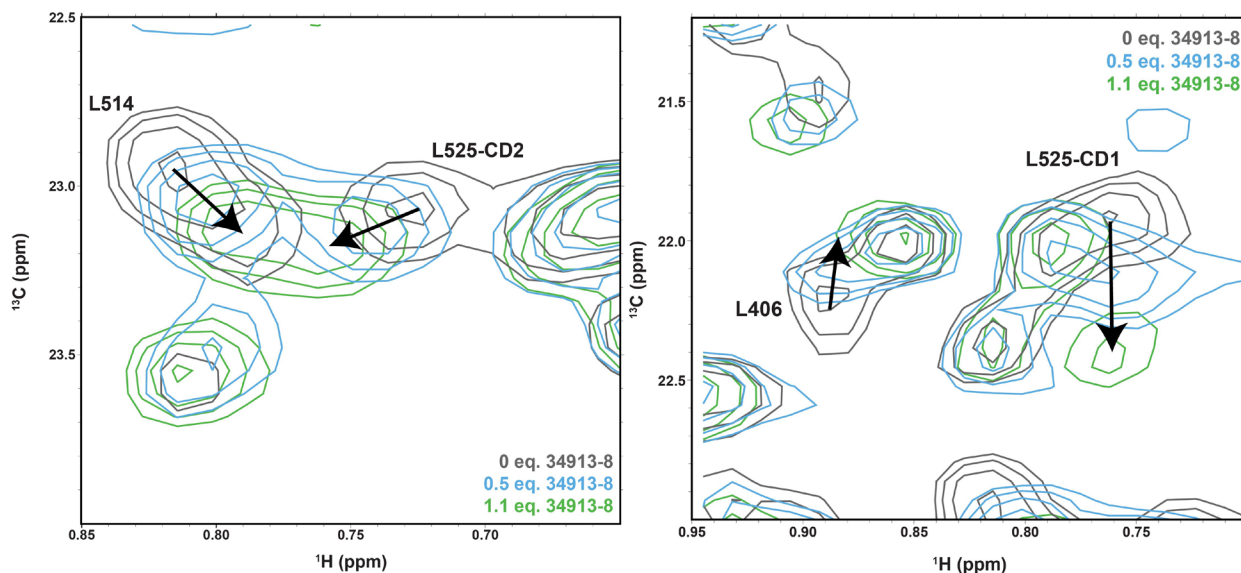
Figure 2.5. Overlay of ^{1}H, ^{13}C-HSQC CSPs of free Med25 (dark grey), 0.5 eq LPPM-8 (light blue) 1.1 eq of LPPM-8 (green) for Med25 residues L406, L514, and L525.

The concentration dependence and linear shifts of the methyl groups of L525 and L514 are uniquely relevant, as they suggest that LPPM-8 engages more than one substructure within the binding surface of Med25. Higher equivalents of LPPM-8 in relation to the protein concentration showed increased CSPs at both binding faces, though the H1 face lacked notable perturbations of solvent-exposed residues (Appendix Figure B.9). Taken together, these data suggest that LPPM-8 directly binds to the H2 face of Med25 AcID through the engagement with the β-barrel and the dynamic framing helices, and in doing so induces conformational changes in the protein domain. This demonstrates that LPPM-8 orthosterically inhibits the PPIs at the H2 of Med25, such as those with ATF6α, while PPIs at the H1 face are inhibited through an allosteric mechanism. Appendix Figure B.20 summarizes the inhibition constants of LPPM-8 against the PPIs between Med25 and the H1-binding ETV/PEA3 family of TADs (ETV1, ETV4, ETV5), all higher than its K_i against Med25•ATF6α.
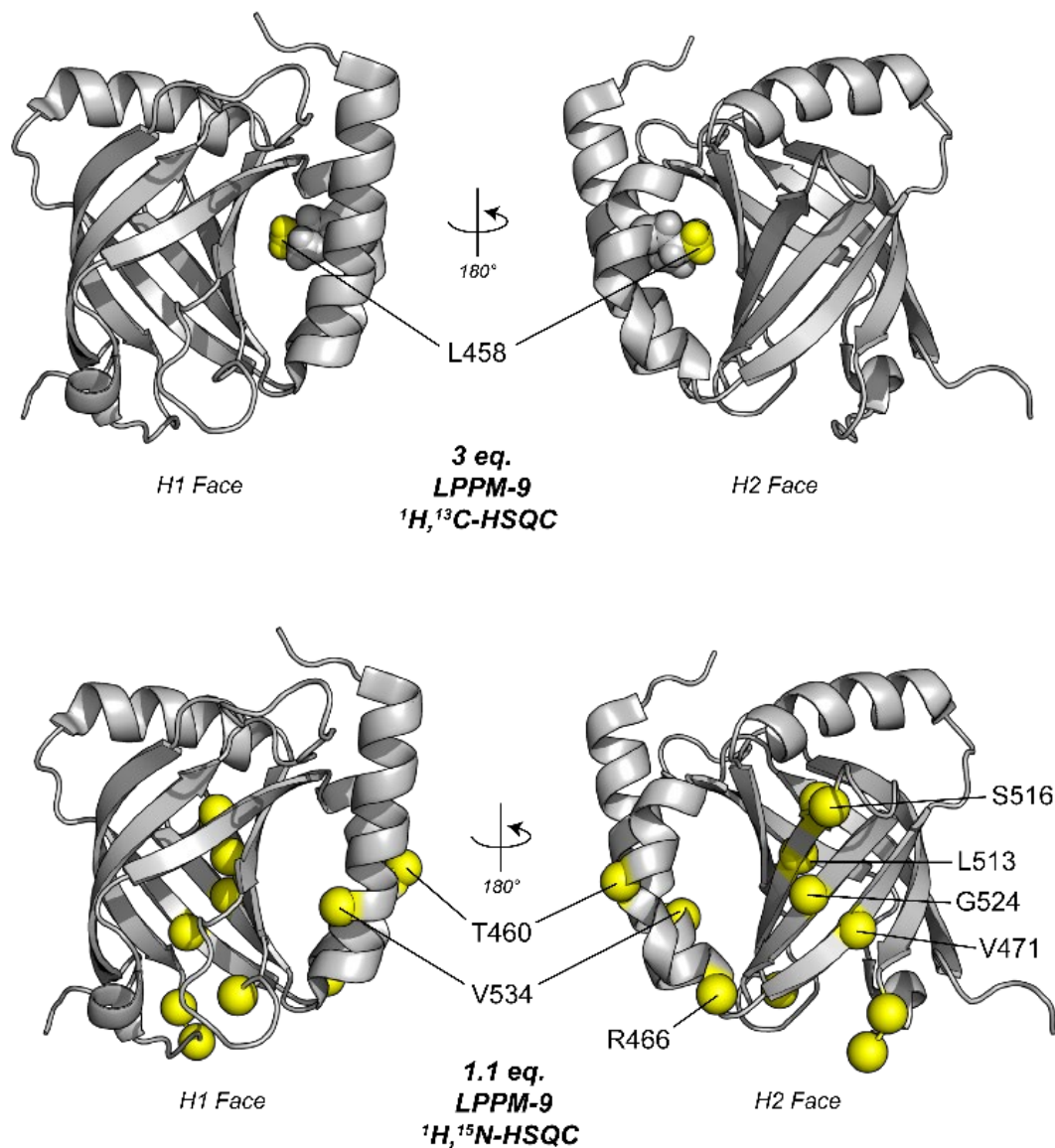
Figure 2.6. (Top) ^{1}H, ^{13}C-HSQC CSPs induced by binding of 3.0 eq of LPPM-9 mapped onto Med25 AcID (PDB ID 2XNF). Yellow = 0.02 ppm - 0.0249 ppm. (Bottom) ^{1}H, ^{15}N-HSQC CSPs induced by binding of 1.1 eq of LPPM-9 mapped onto Med25 AcID (PDB ID 2XNF) Yellow = 0.02 ppm - 0.085 ppm. All perturbed residues above signal to noise ratio (≥ 0.02 ppm) found in Appendix Figure B.18.

Contrastingly, superstoichiometric concentrations (3 equivalents) of LPPM-9 only result in minimal chemical shift perturbations of Med25 residues in ^{1}H,^{13}C-HSQC experiments, as evidenced by the single residue on Figure 2.6 to pass the established threshold of 0.02 ppm. Additionally, only mild perturbations (0.02 ppm - 0.085 ppm) are observed at 1.1 equivalents on ^{1}H,^{15}N-HSQC. The results from these structural

experiments indicate little to no specific binding to Med25 AcID by LPPM-9. In conjunction with the DSF data, it is apparent that the single-atom change at the C-terminus, from a carboxy to a carboxamide, is a structural modification that leads to the loss of inhibitory function in this LPPMs against Med25.

2.3.2 Structural propensity of LPPMs is determined by their C-terminus

A premise that arose from the observations in the differences in engagement between LPPM-8 and LPPM-9, is that the C-terminal atom and by default in the charge at that group, may contribute to structural features of the molecule which in turn are important for binding to Med25. To assess this idea, circular dichroism (CD) studies of the D-amino acid containing LPPMs were conducted. The CD spectra of LPPM-8 and LPPM-9 demonstrate that the C-terminal moiety corresponds with an important difference in the structural propensity that is likely responsible for the difference in Med25 engagement for the two LPPMs. As observed on Figure 2.7, LPPM-9 has measurable α-helical character, with maxima at 207 and 221 nm, consistent with the spectra of α-helices of D-amino acid sequences.[68] In contrast, LPPM-8 and LPPM-10 show strong absorbance at 204 nm, suggestive of polyproline helical character, which also appears to be independent of the chirality of the substituents of the lipid tails. This type of helix is distinguishable from D-amino acid unfolded or random coil structures, which are characterized by a maximum at around ~195 nm.[69, 70] This polyproline character is consistent with previous reports of short peptides containing small non-polar residues that also exhibit a structural propensity towards polyproline formation.[71-73]
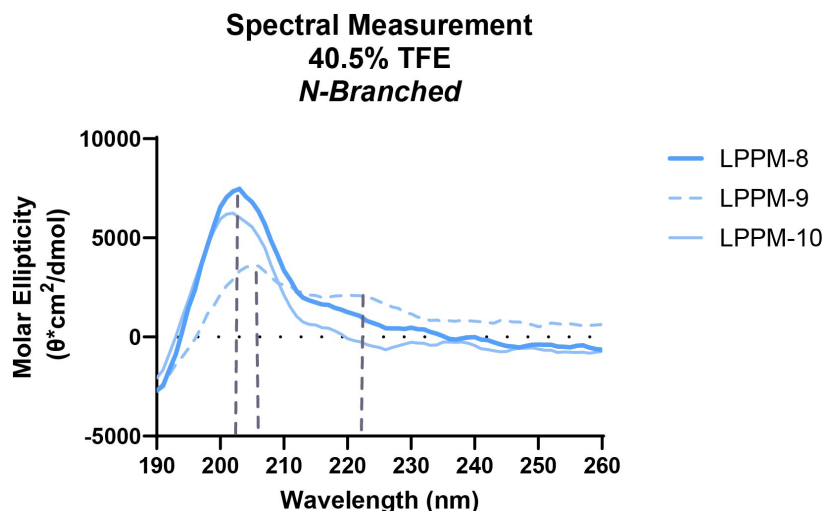
Figure 2.7. Circular dichroism spectra for *N*-branched LPPMs. The molar ellipticity of each sample was determined from the mean residue CD corrected for the number of amino acids and the concentration of sample using the Jasco Spectra Manager Software v.2.5[74]. CD spectra were obtained in 40% TFE/potassium phosphate buffer. Data is representative of experiments performed in duplicate.

We also assessed whether the identity of the *N*-acyl group has an impact on the propensity towards either polyproline or α-helical character by measuring the CD spectra of the remaining D-amino acid containing LPPMs. As presented on Figure 2.8, LPPM-2 and LPPM-6 showcase polyproline character, while LPPM-4 and LPPM-7 are α-helical. These results are consistent with the characteristics of LPPM-8 and LPPM-9, that is, that the C-terminus group of these LPPMs determines the type of helical character they display, independent of the simpler acyl groups in their structures. It is notable however, that the intensity of both types of helices decreases with the increasing length and complexity of the appended lipid. This suggests that the structural propensity is embedded in the peptide sequence, changes with the identity of the C-terminus.
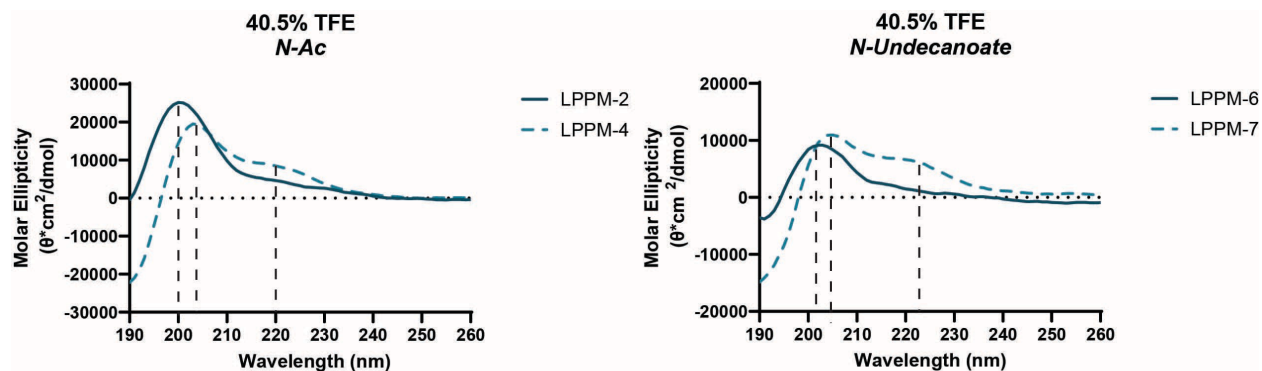
Figure 2.8. Circular dichroism spectra for *N*-Acetyl and *N*-undecanoate LPPMs. The molar ellipticity of each sample was determined from the mean residue CD corrected for the number of amino acids and the concentration of sample using the Jasco Spectra Manager Software v.2.5[74]. CD spectra were obtained in 40% TFE/potassium phosphate buffer. Data is representative of experiments performed in duplicate.

These measurements were also performed at a 10-fold lower salt concentration, (Appendix Figure B.22) to assess the dependence of the structural propensity of the LPPMs on the ionic strength of the aqueous environment. These measurements reveal a dependence of the α-helical propensity of C-terminal carboxamide LPPMs for the higher salt concentration, as seen by the decrease in the intensity of the peak maxima at 221 nm, whereas the polyproline character of C-terminal carboxy LPPMs is independent of salt changes. Differences in the spectra of LPPMs across TFE titrations were also assessed, to account for effects observed as a result of the helical-inducing characteristics of this solvent. Figure 2.9 below shows that the maxima of C-terminal carboxy LPPMs exhibit a slight right-shift at increasing TFE concentrations, suggesting that helical-inducing environments may promote the polyproline character over that of random-coil of these LPPMs. On the other hand, titrations of TFE with C-terminal carboxamide LPPMs do not lead to horizontal shifts on the spectra, but differences in signal intensity are observed instead, especially for LPPMS -7 and -9, suggesting a link between the longer acyl tails and the propensity of the molecules towards α-helicity (Appendix Figure B.23). Changes in the secondary structure of Med25 AcID incubated

53

with LPPM-8 and LPPM-9 were also assessed and are presented in Appendix Figure B.25. A comparable difference in the intensity of the secondary structure signal of the protein is observed with both LPPMs, perhaps as a function of the D-amino acid composition present in which has a subtractive effect on the intensity of the protein spectra. In addition, considering the direct contacts of LPPM-8 on the rigid surface of the AcID β-barrel core, it is possible that any conformational changes on the protein upon binding of LPPM-8 are not detected by CD.
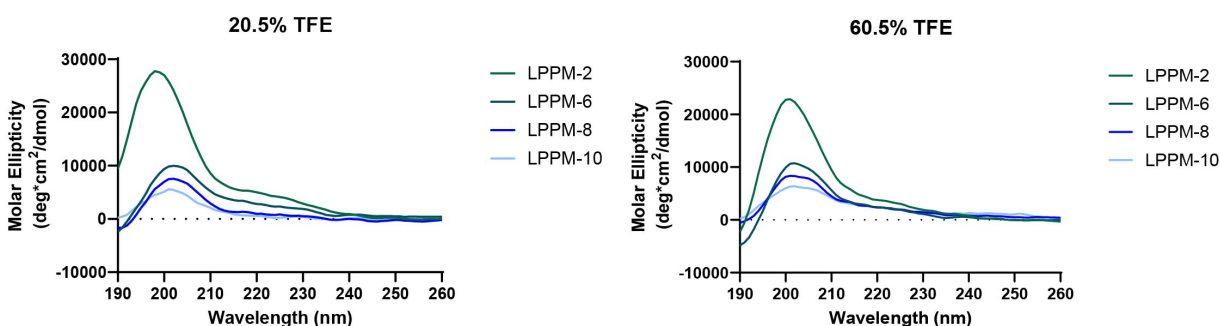
Figure 2.9. Circular dichroism spectra of C-terminal -OH LPPMs at increasing TFE%. The molar ellipticity of each sample was determined from the mean residue CD corrected for the number of amino acids and the concentration of sample using the Jasco Spectra Manager Software v.2.5. Data was obtained from 5 acquisitions.

This CD data, in conjunction with the *in-vitro* characterization of the previous section, reveals how the lipid tail and the C-terminal moiety of LPPMs contribute significantly to the engagement of the molecule with Med25. Additionally, the findings outlined in this section led to the hypothesis that the absence of specific binding of LPPM-9 to Med25 may stem from its potential interference with the helical ATF6α. A series of experiments were performed to characterize this potential interaction, and they are summarized in Appendix D of this dissertation. From these studies, a structural model arises for binding in which the C-terminal negative charge may act as an anchor for

binding to Med25, a specific interaction that is facilitated by the unique structural conformation of the carboxy LPPM as a polyproline helix.[75] This conformation may provide additional functionality to LPPM-8 in a biological system, as certain studies suggest that polyproline peptides can display a degree of membrane permeability and structural stability for interacting with their target macromolecules.[76, 77]

2.3.3 Inhibitory activity of LPPM-8 is sequence dependent

To identify the amino acid residues that contribute the most to inhibition of Med25, an alanine scan of LPPM-8 was carried out (Figure 2.10). The resulting library B was tested against the Med25•ATF6α complex using a competitive fluorescence polarization binding assay format; as well as DSF measurements with the AcID domain (Figure 2.11), and circular dichroism of the LPPMs (Figures 2.10).
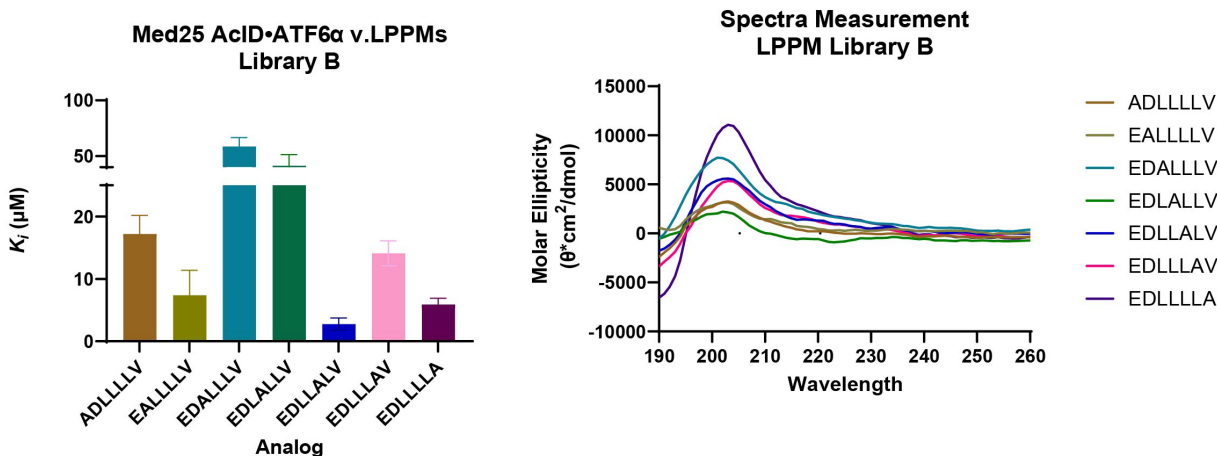
Figure 2.10.Inhibitory activity and structural propensity of LPPM library B.(Left) Inhibition binding curves of Med25 AcID•ATF6α by alanine scan of LPPM-8 as determined by competitive fluorescence polarization assays. Apparent IC_{50} values were determined through titration of compound for Med25 AcID•ATF6α in experimental triplicate with the indicated error (SD). The IC_{50} values were converted to K_i values using the apparent K_d value based on the direct binding of Med25 AcID•ATF6α. Data shown is the average of three independent experiments with the indicated error (SD). (Right) Circular dichroism spectra for Alanine Scan (Library B) of LPPM-8. The molar ellipticity of each sample was determined from the mean residue CD corrected for the number of amino acids and the concentration of sample using the Jasco Spectra Manager Software v.2.5[74]. CD spectra were obtained in 40% TFE/potassium phosphate buffer. Data is representative of experiments performed in duplicate.

Mutation at V7A had the least impact on inhibition, and both the CD spectra and ΔT_m of this analog were nearly identical to that of parent LPPM-8. In contrast, modification of two of the central leucine residues, L3A and L4A, leads to significant loss in activity and a change in the CD spectra. From these results it is clear that these residues play an important role for both inhibition and structure. However, mutants L5A and L6A have minimal effect on inhibition, but the extent to which the T_m of Med25 is affected upon incubation with these analogs decreases. Of the mutation at the two polar residues, E1A appears to be more important for Med25 binding than D2A (~4-fold change in K_i), although the DSF data suggests that the removal of the charge in D2A is more impactful in the engagement of the LPPM with AcID. Taken together, these data support a model in which the identity and location of individual amino acids within the sequence specifically contribute to the inhibitory activity of the LPPMs against Med25 PPIs and to the conformation of the peptides. These findings are also in accordance with previous reports of TAD-peptides with sequence-dependent activities, as well as with the identification of the relevant patterning and sequence composition of IDRs for activity.[5, 7]
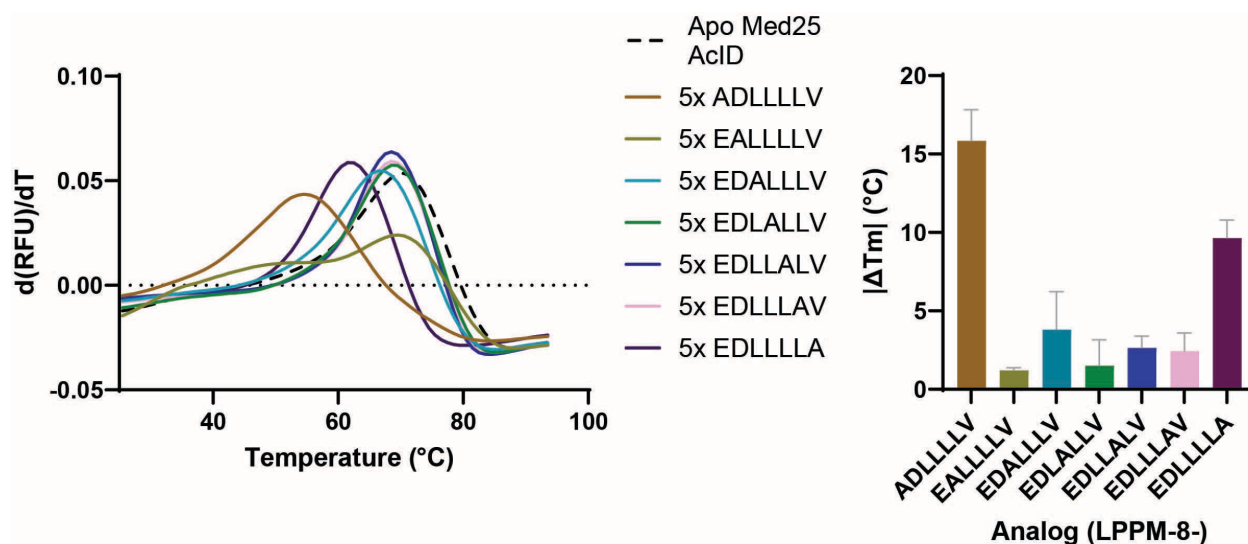
Figure 2.11. Engagement of LPPM library B with Med25 AcID. Left. DSF data for Alanine Scan of LPPM-8 (Library B). First derivative of the raw fluorescence units (RFU) traces of Med25 AcID with 5 equiv. of each

respective LPPM. Right. Change in the Tm of Med25 AcID upon incubation with Library B LPPMs. Melting temperatures were determined from raw fluorescence data using DSFworld. Data was obtained in technical triplicates with the indicated error (SD) and is representative of experiments performed in biological triplicates.

To obtain further insight into the way in which modifications to the peptide sequence can change the activity and engagement of the inhibitors to Med25, a third LPPM library was developed, a proline scan of the internal residues of the peptide sequence of LPPM-8 (Residues E1 through L6). This library was evaluated in a similar fashion to the previous ones, using competitive FP binding assays against Med25•ATF6α and DSF with the AcID domain. For most residues, the substitution of each residue to a proline led to a 4 to 5-fold decrease in affinity, except for E1P, and L4P, both of which exhibited a 2-fold increase in their K_i values (Figure 2.12). By contrast, the DSF assessment shows that engagement of the LPPMs to Med25 decreases below the threshold of what is considered a significant change in the T_m of the protein except for when either charged residue is modified to a P. Except for D2P, these results match the trend observed in the DSF measurements of the alanine scan library, suggesting that each residue contributes to the engagement of LPPM-8 to Med25. In the case of D2P, a significant change in the T_m of Med25 is observed with the proline substitution but not with alanine at this position. This may be due to the proline stabilizing a conformation that changes the charge at E to an analogous form as the charge at D. Overall, this data reaffirms the conclusion that the identity and placement of the amino acids within the sequence are important for specific inhibition of Med25 AcID PPIs.

Med25 AcID•ATF6α v.LPPMs Library C — K_i (μM) vs Analog (LPPM-8-): PDLLLLV, EPLLLLV, EDPLLLV, EDLPLLV, EDLLPLV, EDLLLPV

Engagement with Med25 AcID by DSF — $|\Delta Tm|$ (°C) vs Analog (LPPM-8-): PDLLLLV, EPLLLLV, EDPLLLV, EDLPLLV, EDLLPLV, EDLLLPV
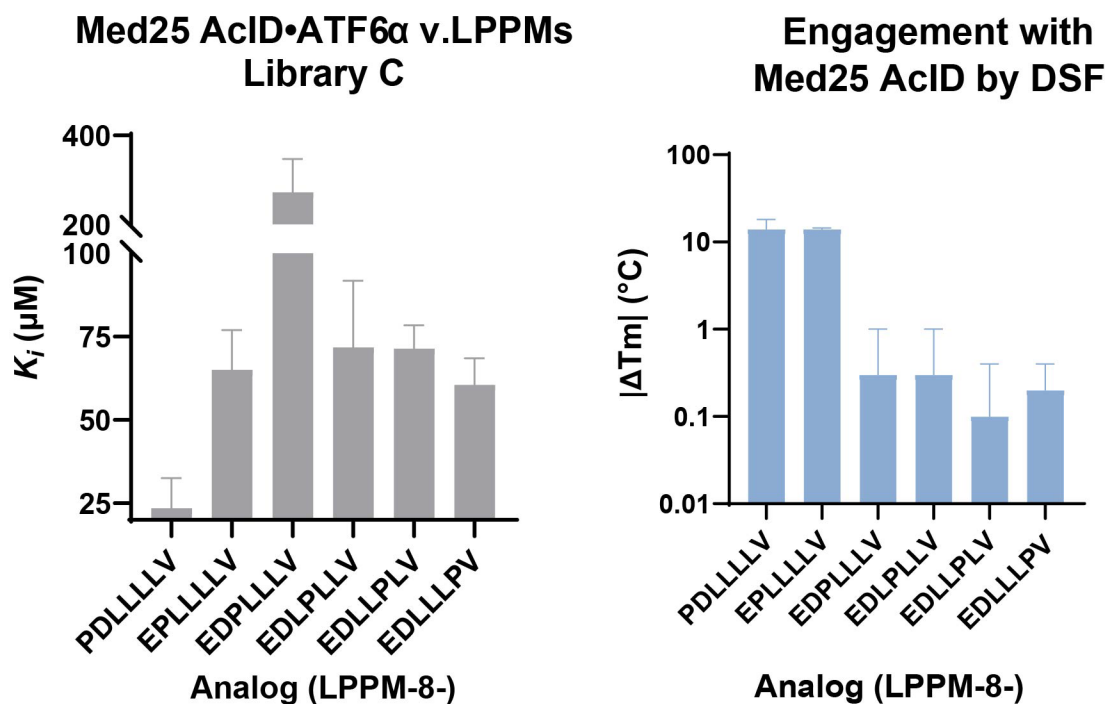
Figure 2.12 Inhibitory activity and engagement of LPPM library C with Med25 AcID.(Left) Inhibition binding curves of Med25 AcID•ATF6α by proline scan of LPPM-8 as determined by competitive fluorescence polarization assays. Apparent IC_{50} values were determined through titration of compound for Med25 AcID•ATF6α in experimental triplicate with the indicated error (SD). The IC_{50} values were converted to K_i values using the apparent K_d value based on the direct binding of Med25 AcID•ATF6α. Data shown is the average of three independent experiments with the indicated error (SD). (Right) DSF data for Proline Scan of LPPM-8 (Library C). Change in the Tm of Med25 AcID upon incubation with 5 equivalents of each LPPM from Library C. Melting temperatures were determined from raw fluorescence data using DSFworld. Data was obtained in technical triplicates with the indicated error (SD) and is representative of experiments performed in biological duplicates. First derivative of the melting curve of these data found in Appendix figure B.32.

Substitution with proline was selected to introduce a structurally disruptive effect by comparison to the substitutions with alanine. Considering the polyproline features of the C-terminal carboxy LPPMs, however, it is also possible that the introduction of proline residues may actually stabilize or increase that polyproline character, to assess this, CD measurements of selected LPPMs with proline substitutions were also conducted. As illustrated on Appendix Figure B.24, the proline substitution has different effects on the propensity of conformation of these analogs. For instance, LPPM-8-L6P, and LPPM-D2P, maintain the polyproline character of LPPM-8, whereas in LPPM-E1A and LPPM-8-L5A,

the maxima left-shifts near the area characteristic of random-coil structures. Though these changes don't clearly correlate to the inhibitory activity of the analogs, they suggest that the residues of this peptide sequence can also influence the structural properties of LPPMs.

As outlined previously, our work demonstrated that polar groups at the lipid of these LPPMs have an effect on the solubility and propensity of aggregation of the molecules in aqueous solutions. To assess the existence of similar differences in the solubility and aggregate formation as a result of the decrease in the overall charge of the molecule in the alanine mutants E1A and D2A, analogous detergent screens were conducted. These molecules were tested in FP binding assays against the Med25•ATF6α PPI, at increasing concentrations of Triton X-100. (Figure 2.13)
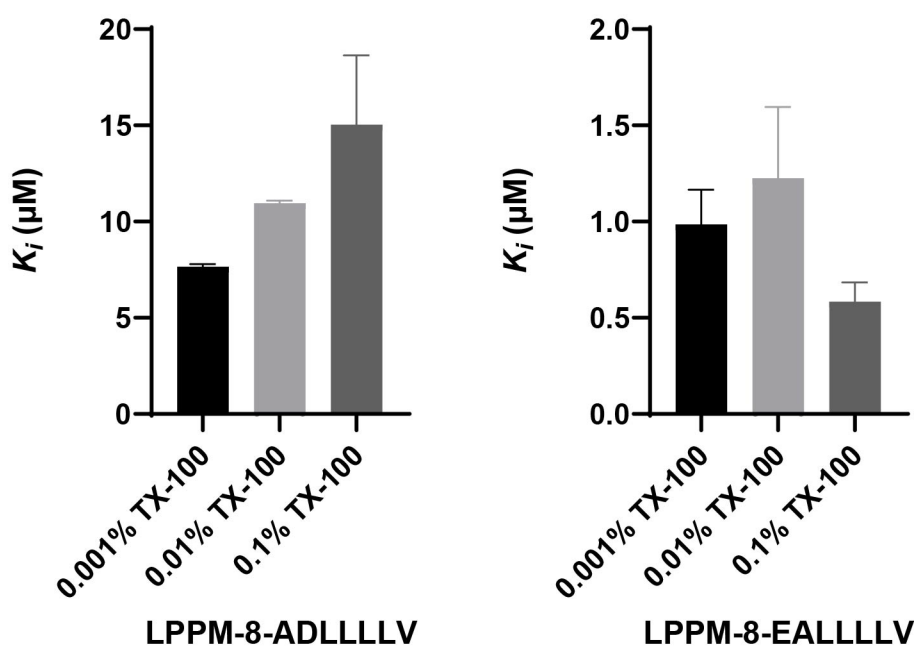
Figure 2.13. Inhibition of Med25 AcID•ATF6α by LPPM-8 alanine charged analogs with different Triton X-100 concentrations as determined by competitive fluorescence polarization assays. Apparent IC_{50} values were determined through titration of compound for Med25 AcID•ATF6α PPI performed in experimental triplicate with the indicated error (SD). The IC_{50} values were converted to Ki values using the apparent Kd value based on the direct binding of Med25 AcID•ATF6α PPI using a Ki calculator. Data shown is the average of two independent experiments with the indicated error (SD).

We observe that the removal of the negative charge at the E residue leads to a 2-fold increase in the *Ki* value of the LPPM across detergent concentrations of 0.001% and 0.1%, suggesting that it has a slight propensity towards aggregate formation. Contrastingly, removal of the negative charge at the D position shows the opposite trend when comparing the *Ki* values between detergent concentration of 0.001% and 0.1%, suggesting different activities of each of these charges as part of the LPPM-8 inhibitor. The same trends were observed when a different detergent, NP40, was used (Appendix Figure B.28). Overall, these analogs have a similar propensity of aggregation as those exhibited by LPPM-8,9 and 10, corroborating that polar groups at the lipid tail have a higher effect on the solubility of the molecules than the changes of a single negative charge within the peptide sequence. Furthermore, in the context of the differences in the activity these two analogs exhibited in the biochemical and biophysical assessments above, it can be concluded that the negatively charged groups, just as the other residues within the sequence, play unique roles in their contribution to the inhibitory activity of the LPPM against Med25 PPIs that also correlates to the location of the same within the peptide sequence.

2.3.4 LPPM-8 is a selective inhibitor of Med25 AcID PPIs

Selective engagement by an inhibitor for a particular coactivator is a significant challenge, and it is also observed in the PPIs of the TAD domains from native transcriptional activators. For instance, peptide sequences taken from the TAD of p53 can interact with the ABDs of CBP/P300 TAZ1, TAZ2, KIX and IBiD, and Med25 AcID.[78] For a previously reported inhibitor of Med25 PPIs, improvement of the molecule's selectivity for its cognate coactivator was achieved through the engagement of dynamic

substructures within the protein domain.[52] With the knowledge that LPPM-8 binds to Med25 in part by engaging the dynamic framing α-helices of AcID, we proceeded to evaluate the selectivity of this LPPM for Med25 relative to a broader range of coactivator-activator complexes in a series of competitive inhibition assays previously used for assessing coactivator inhibitor selectivity[52, 79]. The results, presented in Figure 2.14 below, demonstrate that LPPM-8 has very good selectivity in the context of transient, coactivator PPIs, with a >6-fold preference for Med25 across the complexes tested. This was also a feature unique to this LPPM, as LPPM-9 for example, does not display the same degree of selectivity for any complex within the coactivator panel tested. (Appendix Figure B.30)
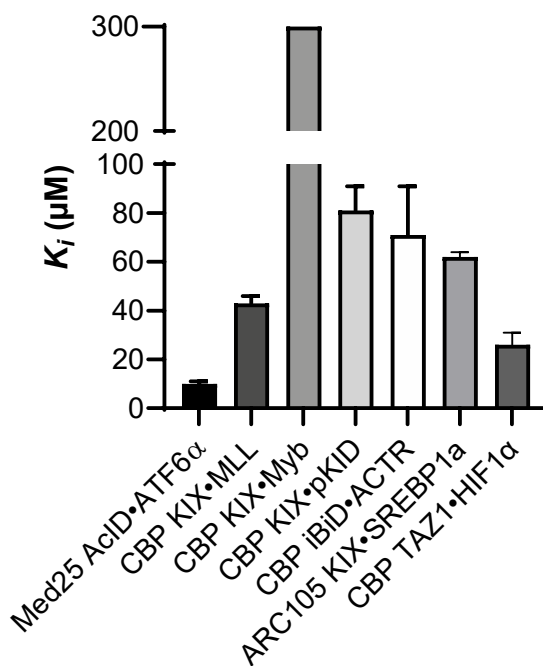
Figure 2.14. Selectivity of LPPM-8 for Med25 AcID as determined by the inhibition of related PPI networks using competitive fluorescence polarization assays. IC_{50} values using a suite of coactivators bound to FITC-activators at 20 nM (CBP KIX•MLL/Myb/pKID, CBP IBiD•ACTR). The IC_{50} values were converted to K_i values using a published K_i calculator [55] and the corresponding K_d value of each coactivator•activator direct binding measurement. Med25 AcID•ATF6α,CBP KIX•MLL/Myb, CBP KIX•pKID, CBP TAZ1• HIF1α data shown is the average of three independent experiments performed in technical triplicate with the indicated

61

error (SD). ARC105•SREBP1a and CBP IBiD•ACTR data shown is the average of two independent experiments performed in technical triplicate with the indicated error (SD). No error bars are shown for the K_i against CBP KIX•Myb because the IC_{50} was greater than the highest concentration of LPPM-8 tested (300 µM), and thus, we can accurately report the K_i only as > 300 µM.

With this demonstrated *in-vitro* selectivity, engagement of the full-length Med25 protein by LPPM-8 in a cellular context using the triple-negative breast cancer cell line VARIO68 was performed. This cell line exhibits upregulated expression of Med25 and of its ETV/PEA3 activator binding partners. Incubation of nuclear extracts with LPPM-8 led to stabilization of endogenous Med25 relative to DMSO-treated samples, consistent with LPPM-8 engagement of AcID in the context of endogenous, full-length Med25 (Appendix Figure B.32). In contrast, the addition of LPPM-9 has little effect on endogenous Med25 stability (Appendix Figure B.33). We further probed LPPM-8 engagement of Med25 by the testing its effect on a key Med25-dependent gene, MMP2, in VARI068 cells.[52] Treatment with LPPM-8 downregulated MMP2 gene expression, while treatment with negative control LPPM-9 did not (Appendix Figure B.32). These results suggest that LPPM-8 has the potential to be utilized to perform a broad examination of the specific effects of modulating the Med25 PPI network in cells and the related transcriptional changes.

2.4 Conclusions and Future Directions

Med25 serves as an interaction hub for a variety of amphipathic transcription factors; yet as is the case with other coactivators, peptides derived from the amphipathic sequences of the TADs of activator binding partners are not effective inhibitors of their PPIs. The data from this chapter demonstrates that incorporation of a branched fatty acid at the N-terminus of a short (7-residue) amphipathic peptide leads to >20-fold increase in potency against Med25•activator PPIs *in-vitro* and with very good selectivity. We dissect

the structure-activity relationship of various features within the LPPM structures, and find that the appended lipid, and the location and identity of the peptide sequences are critical defining the structure and affinity of these inhibitors for Med25. The lead inhibitor, LPPM-8, displays an orthosteric mechanism of inhibition against ATF6α PPIs, and preliminary data indicates activity of this molecule in cells. Given the role that lipid structure and amino acid sequence play in the function of the lipopeptidomimetics examined against Med25, we next assessed the potential of our LPPM libraries for targeting different coactivator PPI targets. Taken together, our data suggest that lipopeptidomimetics can be a valuable and thus-far unexplored tool for the molecular intervention of coactivators and their PPI networks.

2.5 Materials and Methods

Protein Expression and Purification

Med25 AcID

The Med25 expression plasmid pET21b-Med25(394-543)-His6 was generously provided by Professor Patrick Cramer of the Max Planck Institute for Biophysical Chemistry, Göttingen, Germany.[67] WT Med25 AcID was expressed as previously described with minor modifications.[64, 67] Plasmid was transformed via heat-shock into competent E. coli BL21 (DE3) cells. The cells were then plated on LB agar plates with selection antibiotic. A 5 mL overnight culture was prepared from plated colonies in LB, and it was used on inoculate a 1-L TB culture supplemented with 0.1 mg/mL of ampicillin. ^{13}C,^{15}N-labeled Med25 AcID was expressed as previously described with minor modifications. WT[67] Med25 AcID was expressed as previously described with minor modifications.[64, 80] Plasmid was transformed via heat-shock into competent E. coli BL21

(DE3) cells. The cells were then plated on LB agar plates with selection antibiotic. A 50 mL overnight culture was prepared from plated colonies in LB, and it was used on inoculate a 1L culture of M9 minimal media supplemented with 0.1 mg/mL of ampicillin, 1 g/L $^{15}NH_4Cl$, 2 g/L ^{13}C-D-glucose, and 0.5% $^{13}C,^{15}N$-labeled Bioexpress media (all labeled components were purchased from Cambridge Isotopes). Previous to inoculation, the overnight culture was pelleted, and media exchanged into the same M9 minimal media. The culture was grown at 37°C (250 rpm) until an OD_{600} of 0.6.-0.8 was reached. The culture was cooled to 21°C for 1 hour, and expression was induced with addition of isopropyl β-D-1-thiogalactopyranoside (IPTG, final concentration 0.1 mM). Cultures were grown overnight at 21°C (250 rpm), and the next morning the cells were pelleted by centrifugation at 6000 rpm at 4 °C for 30 minutes. Pellets were flash frozen in liquid N_2 and stored at -80°C until lysis.

Purification of both proteins was performed according to previously described methods using an AKTA Pure FPLC.[80, 81] Cell pellets were resuspended in ~35 mL lysis buffer (10 mM phosphate, 300 mM NaCl, 10 mM imidazole, pH 7.2), 40 µL β-mercaptoethanol, and a cOmplete protease inhibitor tablet (Roche). Cells were lysed by sonication and insoluble cellular material was pelleted by centrifugation at 9500 rpm for 20 min at 4ºC. The lysate filtered and loaded onto an AKTA Pure FPLC equipped with a 5 mL Ni HisTrap HP column (GE Healthcare) pre-equilibrated with wash buffer (10 mM phosphate, 300 mM NaCl, 10 mM imidazole, pH 7.2). Med25 AcID was then purified using a gradient of 10–600 mM imidazole (other buffer components were constant), and fractions containing CBP KIX were pooled and subjected to secondary purification using a HiTrap SP HP cation exchange column (GE Healthcare) using buffer (50 mM sodium

64

phosphate, 1 mM dithiothreitol (DTT), pH 7.2) with gradient of 0-1 M NaCl. Upon elution, Fractions containing protein were dialyzed into storage buffer (10 mM sodium phosphate, 100 mM NaCl, 10% glycerol, pH 6.8) or NMR buffer (20 mM sodium phosphate, 150 mM NaCl, pH 6.5). Concentration was determined via ultraviolet/visible (UV/Vis) spectroscopy on a NanoDrop instrument at 280 nm using an extinction coefficient of 22,460 $M^{-1}cm^{-1}$. Protein was aliquoted, flash frozen in liquid N_2 and stored at –80ºC until needed. Protein identity was confirmed by mass spectrometry (Agilent 6545 LC/Q-TOF) and purity was assessed via sodium dodecyl sulphate–polyacrylamide gel electrophoresis (SDS-PAGE) on a 4-20% tris-glycine (Biorad) gel stained using Quick Coomassie (Anatrace).

CBP KIX

CBP KIX (586-672) was expressed as previously described with minor modifications.[81] Plasmid was transformed via heat-shock into competent E. coli BL21 (DE3) cells. The cells were then plated on LB agar plates with selection antibiotic. A 5 mL overnight culture was prepared from plated colonies in LB, and it was used to inoculate a 1-L TB culture supplemented with 0.1 mg/mL of ampicillin. The culture was grown at 37°C (250 rpm) until an OD_{600} of 0.6.-0.8 was reached. The culture was cooled to 21°C for 1 hour, and expression was induced with addition of isopropyl β-D-1-thiogalactopyranoside (IPTG, final concentration 0.1 mM). Cultures were grown overnight at 21°C (250 rpm), and the next morning the cells were pelleted by centrifugation at 6000 rpm at 4 °C for 30 minutes. Pellets were flash frozen in liquid N_2 and stored at -80°C until lysis.

Protein purification was performed according to previously described methods using an AKTA Pure FPLC.[82, 83] Cell pellets were resuspended in ~35 mL lysis buffer (10 mM phosphate, 300 mM NaCl, 10 mM imidazole, pH 7.2), 40 µL β-mercaptoethanol, and

a cOmplete protease inhibitor tablet (Roche). Cells were lysed by sonication and insoluble cellular material was pelleted by centrifugation at 9500 rpm for 20 min at 4ºC. The lysate filtered and loaded onto an AKTA Pure FPLC equipped with a 5 mL Ni HisTrap HP column (GE Healthcare) pre-equilibrated with wash buffer (10 mM phosphate, 300 mM NaCl, 10 mM imidazole, pH 7.2). CBP KIX was then purified using a gradient of 10–600 mM imidazole (other buffer components were constant), and fractions containing CBP KIX were pooled and subjected to secondary purification using a HiTrap SP HP cation exchange column (GE Healthcare) using buffer (50 mM sodium phosphate, 1 mM dithiothreitol (DTT), pH 7.2) with gradient of 0-1 M NaCl. Previous to column loading, a secondary cOmplete protease inhibitor tablet (Roche) was dissolved into the pooled fractions. Upon elution, fractions containing pure protein were dialyzed into storage buffer (10 mM sodium phosphate, 100 mM NaCl, 10% glycerol, pH 6.8) or NMR buffer (20 mM sodium phosphate, 150 mM NaCl, pH 6.5) overnight at 4ºC. Concentration was determined via ultraviolet/visible (UV/Vis) spectroscopy on a NanoDrop instrument at 280 nm using an extinction coefficient of 12,950 $M^{-1}cm^{-1}$. Aliquots were flash frozen in liquid N2 and stored at –80 ºC until further use. Protein identity was confirmed by mass spectrometry (Agilent 6545 LC/Q-TOF) and purity was assessed via sodium dodecyl sulphate–polyacrylamide gel electrophoresis (SDS-PAGE) on a 4-20% tris-glycine (Biorad) gel stained using Quick Coomassie (Anatrace).

ARC105 KIX

ARC105 KIX (1-78) from plasmid pET-15B His6-ARC105(1-78) was expressed as previously described with minor modifications.[84] Plasmid was transformed via heat-shock into competent E. coli BL21 (DE3) cells. The cells were then plated on LB agar plates

with selection antibiotic. A 10 mL overnight culture was prepared from plated colonies in LB, and it was used to inoculate a 1-L TB culture supplemented with 0.1 mg/mL of ampicillin. The culture was grown at 37ºC (250 rpm) until an OD_{600} of 0.6.-0.8 was reached. The culture was cooled to 21ºC for 1 hour, and expression was induced with addition of isopropyl β-D-1-thiogalactopyranoside (IPTG, final concentration 0.1 mM). Cultures were grown overnight at 21ºC (250 rpm), and the next morning the cells were pelleted by centrifugation at 6000 rpm at 4 ºC for 30 minutes.

Pellets were flash frozen in liquid N_2 and stored at -80ºC until lysis. Cell pellets were resuspended in ~35 mL lysis buffer (10 mM phosphate, 300 mM NaCl, 10 mM imidazole, pH 7.2), 40 µL β-mercaptoethanol, and a cOmplete protease inhibitor tablet (Roche). Cells were lysed by sonication and insoluble cellular material was pelleted by centrifugation at 9500 rpm for 20 min at 4ºC. The lysate was filtered and loaded onto an AKTA Pure FPLC equipped with a 5 mL Ni HisTrap HP column (GE Healthcare) pre-equilibrated with wash buffer (10 mM phosphate, 300 mM NaCl, 10 mM imidazole, pH 7.2). Arc105 KIX was then purified using a gradient of 10–600 mM imidazole (other buffer components were constant), and fractions containing Arc105 KIX were pooled and subjected to secondary purification using a HiTrap SP HP cation exchange column (GE Healthcare) using buffer (50 mM sodium phosphate, 1 mM dithiothreitol (DTT), pH 7.2) with gradient of 0-1 M NaCl. Previous to column loading, a secondary cOmplete protease inhibitor tablet (Roche) was dissolved into the pooled fractions. Upon elution, fractions containing pure protein were dialyzed into storage buffer (10 mM sodium phosphate, 100 mM NaCl, 10% glycerol, pH 6.8) overnight at 4ºC. Concentration was determined via ultraviolet/visible (UV/Vis) spectroscopy on a NanoDrop instrument at 280 nm using an

extinction coefficient of 6,990 $M^{-1}cm^{-1}$. Aliquots were flash frozen in liquid N_2 and stored at –80ºC until further use. Protein identity was confirmed by mass spectrometry (Agilent 6545 LC/Q-TOF) and purity was assessed via sodium dodecyl sulphate–polyacrylamide gel electrophoresis (SDS-PAGE) on a 4-20% tris-glycine (Biorad) gel stained using Quick Coomassie (Anatrace).

CBP TAZ1

The expression plasmid for CBP TAZ1(324-423) was generously provided by Prof. Paramjit Arora.[79, 85] Protein was expressed in BL21 DE3 E. coli. Cells were grown in LB containing 0.1 mg/mL ampicillin and 1 mM $ZnCl_2$ to an optical density (OD 600 nm) of 0.8 (37°C, 250 rpm), cooled to 22°C and induced with 100 µM IPTC for 5 hours. Cells were harvested by centrifugation (20 min, 6500xg) and stored at -80°C. Cell pellets were lysed by sonication in lysis buffer (50 mM Tris, 150mM NaCl, pH 6.3) containing cOmplete protease inhibitor (Roche, 11873580001). The GST tagged protein was affinity purified using a GSTrap column (GE Healthcare). After initial binding of the protein to the column, elution was conducted using a buffer containing 10 mM reduced glutathione. An additional round of purification was completed using ion-exchange chromatography on a Source S column (GE Healthcare) in phosphate buffer (50 mM, 1 mM DTT, pH 7.2) by eluting with a NaCl gradient from 0 to 1M. Purified protein was buffer-exchanged by dialysis (overnight, 4°C) into 10 mM Tris, 100 mM NaH_2PO_4, 10% glycerol, 1mM DTT, 100 µM $ZnCl_2$, pH 6.8. Purity was determined by Coomassie stained polyacrylamide gel. Protein concentration was determined by UV-Vis spectroscopy using an extinction coefficient, ε= 49,110 $M^{-1}cm^{-1}$. Purified protein samples (>90% pure) were aliquoted and stored at -80°C.

Lipid tail synthesis

(2S,3R)-2-methyl-3-hydroxyundecanoic acid and (2R,3S)-2-methyl-3-hydroxy undecanoic acid were synthesized according to standard aldol reaction protocols and stored as solid, pure products.[86]

Solid phase synthesis and purification of activator peptides

Activator peptides were synthesized using rink amide resin (CEM) using standard Fmoc solid-phase peptide synthesis protocols as previously described.[79, 81, 86] The peptides were cleaved with 95% trifluoroacetic acid (TFA, Sigma Aldrich), 2.5% triisopropylsilane (TIPS, Sigma Aldrich), and 2.5% H2O solution for two hours, and subsequently precipitated with chilled diethyl ether. The products were purified to homogeneity using reverse-phase HPLC on a C18 column with a 10-40% solvent B gradient (A: 0.1% TFA in water, B: acetonitrile) and stored at -20°C as DMSO stock solutions. The identity of each peptide was confirmed by LC-MS (Agilent 6545 LC/Q-TOF). FITC-labeled peptides were quantified on a NanoDrop instrument at 495 nm using extinction coefficient 72,000 $M^{-1}cm^{-1}$. Acetylated IBiD was quantified at 280 nm using extinction coefficient 1,490 $M^{-1}cm^{-1}$.

Solid phase synthesis and purification of LPPMs

Peptide portion of LPPMs were synthesized using either rink amide resin (CEM) or Fmoc-D-Val-Tentagel S TRT resin (Rapp Polymere) and standard Fmoc solid-phase peptide synthesis protocols as previously described.[79, 86] LPPM-2-LPPM-5 were acetylated at the N-terminus using a cocktail of acetic anhydride and triethylamine (TEA, Fisher Scientific) in DCM for 30 min. Analogs LPPM-6 and LPPM-7 were coupled with undecanoic acid (5 equiv.) using 1:1:1 ratio of 0.5 M HBTU in DMF, 0.49 M HOBT in DMF,

and 1.0 M DPIEA in DMF for 15 hr. Analogs LPPM-8 and LPPM-9 were coupled to pure (2S, 3R)-2-methyl-3hydroxyundecanoic acid (5 equiv.) using 1:1:1 ratio 0.5 M HBTU in DMF, 0.49 M HOBT in DMF, and 1.0 M DIPEA in DMF for 16 hr. Analog LPPM-10 was coupled to pure (2R, 3S)-2-methyl-3-hydroxyundecanoic acid (2 equiv.) using 1:1:1 ratio 0.5 M HBTU in DMF, 0.49 M HOBT in DMF, and 1.0 M DIPEA in DMF for 16 hr.

The peptides were cleaved with 95% trifluoroacetic acid (TFA, Sigma Aldrich), 2.5% triisopropylsilane (TIPS, Sigma Aldrich), and 2.5% H_2O solution for two hours, and subsequently precipitated with chilled diethyl ether. The products were purified to homogeneity using reverse-phase HPLC on a C_{18} column with a 10-100% solvent B gradient (A: 0.1% TFA in water, B: acetonitrile) and stored at -20°C as DMSO stock solutions. The identity of each peptide was confirmed by LC-MS (Agilent 6545 LC/Q-TOF).

Direct binding assays

Dissociation constants (K_d) for fluorescein-labeled activator peptide tracers with respective coactivator ABDs were determined using fluorescence polarization as previously described.[55, 81] For each experiment, 20 nM tracer was incubated with varying concentrations of protein in binding buffer (10 mM $NaPO_4$, 100 mM NaCl, 10% glycerol, 0.001% NP-40, pH 6.8) and incubated in a black 384 well low volume plate (Corning) for 30 minutes. Fluorescence polarization was detected using a BioTek plate reader equipped with the Fl-FP module (485 nm/520 nm) and the dissociation constant was calculated using by fitting the formula below to the observed polarization values as a function of protein concentration. Data was analyzed using GraphPad Prism 10.

$$y = c + (b - c) \times \frac{(Kd + a + x) - \sqrt{(Kd + a + x)^2 - 4ax}}{2a}$$

Competition binding assays

Inhibition values (K_i, IC_{50}) for LPPMs were determined using a competitive fluorescence polarization assay format, as previously described.[81, 86] Assays were run in experimental triplicate with a final sample volume of 20 µL, in a low volume, black, 384-well plate (Corning) and read using a plate reader (BioTek) equipped with the FI-FP module (485/520 nm). Each experiment used a final tracer concentration of 20 nM of FITC-labelled peptide and a concentration of protein equivalent to 3x the K_d in binding buffer (10 mM $NaPO_4$, 100 mM NaCl, 10% glycerol, 0.001% NP-40, pH 6.8). Protein and tracer were precomplexed and incubated in the presence of serially diluted LPPM (50 nM to 400 µM) for 30 minutes. Polarization values were fit to a non-linear regression using the built-in equation "log(inhibitor) vs. response – variable slope (four parameters)" (shown below) in Prism 10 to derive IC_{50} values. The IC_{50} values were converted to K_i values using the apparent K_d value calculated from the direct binding experiments of each coactivator ABD•FITC-TAD complex using a K_i calculator.[87] Reported K_i values are the average of three biological replicates with the indicated error representing the standard deviation of the triplicates.

$$y = Bottom + (Top - Bottom)/(1 + 10^{(LogIC50-X)*HillSlope})$$

Differential Scanning Fluorimetry

Experiments were performed in technical triplicate of 20 µL sample volumes as previously described.[74, 87, 88] Assay buffer used was 10 mM sodium phosphate, 100 mM sodium chloride, 10% glycerol, 0.001% NP40, and pH 6.8. To determine T_m, 8 µM protein in the presence of 5X SYPRO orange dye (1:1000 dilution in buffer of purchased 5000X stock in DMSO; Invitrogen) was incubated alone or with ligands (2, 3, 5, 7, 10X) at RT for 30 minutes. An Applied Biosystems StepOnePlus qPCR instrument was used to obtain

melting curves by excitation at 488 nm and emission measured at 602 nm over a temperature gradient of 25–95°C with a 1 °C/min increase. Raw fluorescence data was imported into the online data analysis program, DSFworld, and Tm was calculated by determining the maximum of the first derivative (dRFU).[87, 88] For data visualization, raw fluorescence units and dRFU was plotted as a function of temperature using GraphPad Prism software. Change in melting temperature (ΔT_m) of each ligand was calculated as the difference between the Tm of the protein and the Tm of the protein + ligand. Reported values are the averages of biological duplicates and their indicated error representing the standard deviation of the duplicates.

Circular Dichroism

CD spectra were recorded on a JASCO J-1500 CD Spectrometer using 1 mm length quartz cuvettes, a scan speed of 50 nm/min, temperature 4°C, and range 190-260 nm. The spectra were averaged over 5 acquisitions with the baseline subtracted from analogous conditions to those of the samples. The samples were prepared in phosphate buffer (either 10 mM potassium phosphate, 100 mM NaF, pH 7, or 1 mM potassium phosphate, 10 mM NaF, pH 7, as indicated). To monitor effects of trifluoroethanol on helix conformation, titration experiments of trifluoroethanol between 20-60% were conducted. The molar ellipticity ($degcm^2dmol^{-1}$) of each sample was determined from the mean residue CD corrected for the number of amino acids and the concentration of sample using the Jasco Spectra Manager Software v.2.5[80]. Data represents the results of experiments performed in biological duplicate.

NMR Spectroscopy

NMR assignments of Med25 AcID (395-545) and CBP KIX (586-672) were determined from previous studies using ^{13}C,^{15}N-labeled protein. [Henderson, Henley, Pattelli, Breen] Constant time ^{1}H,^{15}N-HSQC and ^{1}H,^{13}C-HSQC experiments were performed using 75 μM ^{13}C,^{15}N-labeled Med25 in NMR buffer (20 mM sodium phosphate pH 6.5, 150 mM NaCl, 3 mM DTT, 10% D2O, and 2% DMSO) on a Bruker 600 MHz instrument equipped with a cryoprobe. Data processing and visualization was performed using NMRPipe[89] and NMRFAM-Sparky[90], respectively. Ligand-protein complexes were assessed at titration points of 0.2, 0.5, 0.8, 1.1, 2, and 3 equivalents of compound, relative to protein concentration. Control spectra were obtained with Med25 AcID or CBP KIX and DMSO only. Chemical shift perturbations (Δδ) were calculated from the proton (ΔδH) and carbon (ΔδC) chemical shifts by:

$$\Delta\delta = \sqrt{(\Delta\delta_H)^2 + (0.25 \times \Delta\delta_C)^2}$$

Mammalian Cell Culture

VARI068 cells are from a culture of a triple negative breast cancer patient-derived xenograft as previously described.[91,92] VARI068 cells were grown in Dulbecco's Modified Eagle Medium (Gibco, cat. #: 11965092) supplemented with 10% fetal bovine serum (FBS), 1x Antibiotic-Antimycotic and 10mg/mL gentamicin in a 37 ºC incubator with 5% carbon dioxide.

Cellular Thermal Shift Assays

VARI068 cells were harvested using standard protocols and pelleted (~4 million cells per pellet) in 1.5 mL microcentrifuge tubes at 1500 x g for 5 minutes at 4 ºC. Nuclear extracts were generated according to the manufacturer's protocols using NE-PER Nuclear and Cytoplasmic Extraction Reagents (Thermo Fisher Scientific, cat #: 78833).

Nuclear extracts were buffer exchanged into phosphate buffered saline (PBS) using Zeba Desalting Column, 7K MWCO (Thermo Fisher Scientific). Prepared nuclear extracts were evenly split into three samples. LPPM-8 and LPPM-9 (dissolved in DMSO) were added to two samples at the indicated concentration with equivalent volume of DMSO added to the final sample. Final concentration of DMSO was 0.1% v/v. Dosed nuclear extracts were incubated at room temperature for 30 mins. Following incubation, extracts were aliquoted into thin-walled PCR tubes (20 µL per tube, ~300,000 cells per tube).

A Labnet Multigene OPTIMAX PCR was used to heat samples for 3 minutes at six temperatures: 54 ºC, 58 ºC, 62 ºC, 66 ºC, 70 ºC, 74 ºC. Contents of PCR tubes were centrifuged at 17000 x g for 2 minutes at 4 ºC and transferred, leaving the precipitated protein pellet undisturbed. LDS loading dye was added to supernatant, boiled, loaded onto a 4-20% mini-PROTEAN TGX gel (BioRad), and run at 170V for 1 hour. Protein was transferred from gel to PDVF membrane using standard prootocls on a Bio-Rad Trans-Blot Turbo Transfer System. The membrane was blocked for 1 hour at RT with gentle shaking using SuperBlock™ Blocking Buffer in PBS (Thermo Scientific). Super Block was removed and Med25 antibody (Novus Biologicals, NBP2-55868) was added to membrane (1:500 dilution with 1:500 Tween 20 in SuperBlock™) and incubated overnight at 4 ºC with gentle shaking. The primary antibody was removed, and the membrane was washed three times with PBST. Secondary antibody (Santa Cruz, sc-2357, 1:1000 with 1:500 Tween 20 in SuperBlock™) was added to the membrane and incubated for 1 hour at RT with gentle shaking. Secondary antibody was removed, and membrane was washed three times with PBST. HRP substrate (Thermo Scientific) was added to the membrane and incubated for 1 minute at RT. Western blot was visualized using Chemiluminescence on

an Azure Biosystems c600 imager. Blots were analyzed using ImageJ software. Reported values are representative of one biological duplicate.

Quantitative Polymerase Chain Reaction

For endogenous gene expression analysis, VARI068 cells were seeded in a 24-well plate ($1x10^5$ cells/well) and allowed to adhere overnight at 37 ºC. Media was removed and replaced with fresh media containing vehicle or compound delivered in DMSO (0.2% v/v) at the indicated concentrations. After 3 hours, the media was removed, and total RNA was isolated using RNeasy Plus Mini Kits (Qiagen) following the manufacturer's protocol. Each RNA sample was used to synthesize cDNA using iScript Reverse Transcription Supermix (Bio-Rad). RT-qPCR samples were run in technical triplicate on an Applied Biosystems StepPlusOne instrument using the cDNA, GoTaq qPCR Master Mix (Promega).

Primers	Sequence (5'-3')
Human RPL19 Forward	ATGTATCACAGCCTGTACCTG
Human RPL19 Reverse	TTCTTGGTCTCTCTTCCTCCTTG
MMP2 Forward	CATTCCAGGCATCTGCGATGAG
MMP2 Reverse	AGCGAGTGGATGCCGCCTTTAA

RT-PCR analysis was performed using the comparative CT method (ΔΔCT Method) to estimate MMP2 mRNA transcript levels compared to control RPL19 mRNA transcript levels. Reported values are the averages of biological triplicates and their indicated error representing the standard deviation of the triplicates.

2.6 References

References

(1) Chen, H.; Pugh, B. F. What do Transcription Factors Interact With? *J Mol Biol* **2021**, *433*, 166883. DOI: 10.1016/j.jmb.2021.166883

(2) Gill, G.; Sadowski, I.; Ptashne, M. Mutations that increase the activity of a transcriptional activator in yeast and mammalian cells. *Proc Natl Acad Sci U S A* **1990**, *87*, 2127-2131. DOI: 10.1073/pnas.87.6.2127

(3) Hope, I. A.; Mahadevan, S.; Struhl, K. Structural and functional characterization of the short acidic transcriptional activation region of yeast GCN4 protein. *Nature* **1988**, *333*, 635-640. DOI: 10.1038/333635a0

(4) Ravarani, C. N.; Erkina, T. Y.; De Baets, G.; Dudman, D. C.; Erkine, A. M.; Babu, M. M. High-throughput discovery of functional disordered regions: investigation of transactivation domains. *Mol Syst Biol* **2018**, *14*, e8190. DOI: 10.15252/msb.20188190

(5) Holehouse, A. S.; Kragelund, B. B. The molecular basis for cellular function of intrinsically disordered protein regions. *Nature Reviews Molecular Cell Biology* **2023**. DOI: 10.1038/s41580-023-00673-0

(6) Sigler, P. B. Acid blobs and negative noodles. *Nature* **1988**, *333*, 210–212. DOI: 10.1038/333210a0

(7) Tompa, P.; Fuxreiter, M. Fuzzy complexes: polymorphism and structural disorder in protein-protein interactions. *Trends Biochem Sci* **2008**, *33*, 2–8. DOI: 10.1016/j.tibs.2007.10.003

(8) Pricer, R.; Gestwicki, J. E.; Mapp, A. K. From Fuzzy to Function: The New Frontier of Protein-Protein Interactions. *Acc Chem Res* **2017**, *50*, 584–589. DOI: 10.1021/acs.accounts.6b00565

(9) Sanborn, A. L.; Yeh, B. T.; Feigerle, J. T.; Hao, C. V.; Townshend, R. J.; Lieberman Aiden, E.; Dror, R. O.; Kornberg, R. D. Simple biochemical features underlie transcriptional activation domain diversity and dynamic, fuzzy binding to Mediator. *Elife* **2021**, *10*. DOI: 10.7554/eLife.68068

(10) Nyanguile, O.; Uesugi, M.; Austin, D. J.; Verdine, G. L. A nonnatural transcriptional coactivator. *Proc Natl Acad Sci U S A* **1997**, *94*, 13402–13406. DOI: 10.1073/pnas.94.25.13402

(11) Piskacek, M.; Vasku, A.; Hajek, R.; Knight, A. Shared structural features of the 9aaTAD family in complex with CBP. *Mol Biosyst* **2015**, *11*, 844-851. DOI: 10.1039/c4mb00672k

(12) Warfield, L.; Tuttle, L. M.; Pacheco, D.; Klevit, R. E.; Hahn, S. A sequence-specific transcription activator motif and powerful synthetic variants that bind Mediator using a fuzzy protein interface. *Proceedings of the National Academy of Sciences* **2014**, *111*, E3506–E3513. DOI: 10.1073/pnas.1412088111

(13) Su, B. G.; Henley, M. J. Drugging Fuzzy Complexes in Transcription. *Front Mol Biosci* **2021**, *8*, 795743. DOI: 10.3389/fmolb.2021.795743

(14) Scholes, N. S.; Weinzierl, R. O. Molecular Dynamics of "Fuzzy" Transcriptional Activator-Coactivator Interactions. *PLoS Comput Biol* **2016**, *12*, e1004935. DOI: 10.1371/journal.pcbi.1004935

(15) Perkins, J. R.; Diboun, I.; Dessailly, B. H.; Lees, J. G.; Orengo, C. Transient protein-protein interactions: structural, functional, and network properties. *Structure* **2010**, *18*, 1233–1243. DOI: 10.1016/j.str.2010.08.007

(16) Zhuang, J.-J.; Liu, Q.; Wu, D.-L.; Tie, L. Current strategies and progress for targeting the "undruggable" transcription factors. *Acta Pharmacologica Sinica* **2022**, *43*, 2474–2481. DOI: 10.1038/s41401-021-00852-9

(17) Talukdar, P. D.; Chatterji, U. Transcriptional co-activators: emerging roles in signaling pathways and potential therapeutic targets for diseases. *Signal Transduct Target Ther* **2023**, *8*, 427. DOI: 10.1038/s41392-023-01651-w

(18) Sawyer, N.; Watkins, A. M.; Arora, P. S. Protein Domain Mimics as Modulators of Protein-Protein Interactions. *Acc Chem Res* **2017**, *50*, 1313-1322. DOI: 10.1021/acs.accounts.7b00130

(19) Lao, B. B.; Drew, K.; Guarracino, D. A.; Brewer, T. F.; Heindel, D. W.; Bonneau, R.; Arora, P. S. Rational design of topographical helix mimics as potent inhibitors of protein-protein interactions. *J Am Chem Soc* **2014**, *136*, 7877-7888. DOI: 10.1021/ja502310r

(20) Ramaswamy, K.; Forbes, L.; Minuesa, G.; Gindin, T.; Brown, F.; Kharas, M. G.; Krivtsov, A. V.; Armstrong, S. A.; Still, E.; de Stanchina, E.; et al. Peptidomimetic blockade of MYB in acute myeloid leukemia. *Nature Communications* **2018**, *9*, 110. DOI: 10.1038/s41467-017-02618-6

(21) Rowe, S. P.; Mapp, A. K. Assessing the permissiveness of transcriptional activator binding sites. *Biopolymers* **2008**, *89*, 578-581. DOI: 10.1002/bip.20946

(22) Arkin, M. R.; Tang, Y.; Wells, J. A. Small-molecule inhibitors of protein-protein interactions: progressing toward the reality. *Chem Biol* **2014**, *21*, 1102–1114. DOI: 10.1016/j.chembiol.2014.09.001

(23) Lau, J.; Bloch, P.; Schäffer, L.; Pettersson, I.; Spetzler, J.; Kofoed, J.; Madsen, K.; Knudsen, L. B.; McGuire, J.; Steensgaard, D. B.; et al. Discovery of the Once-Weekly Glucagon-Like Peptide-1 (GLP-1) Analogue Semaglutide. *Journal of Medicinal Chemistry* **2015**, *58*, 7370-7380. DOI: 10.1021/acs.jmedchem.5b00726

(24) Todorovic, A.; Holder, J. R.; Bauzo, R. M.; Scott, J. W.; Kavanagh, R.; Abdel-Malek, Z.; Haskell-Luevano, C. N-Terminal Fatty Acylated His-dPhe-Arg-Trp-NH2 Tetrapeptides: Influence of Fatty Acid Chain Length on Potency and Selectivity at the Mouse Melanocortin Receptors and Human Melanocytes. *Journal of Medicinal Chemistry* **2005**, *48*, 3328-3336. DOI: 10.1021/jm0490843

(25) Poschner, B. C.; Langosch, D. Stabilization of conformationally dynamic helices by covalently attached acyl chains. *Protein Sci* **2009**, *18*, 1801-1805. DOI: 10.1002/pro.155

(26) Ward, B. P.; Ottaway, N. L.; Perez-Tilve, D.; Ma, D.; Gelfanov, V. M.; Tschöp, M. H.; DiMarchi, R. D. Peptide lipidation stabilizes structure to enhance biological function. *Molecular Metabolism* **2013**, *2*, 468–479. DOI: https://doi.org/10.1016/j.molmet.2013.08.008

(27) Jensen, L.; Helleberg, H.; Roffel, A.; van Lier, J. J.; Bjørnsdottir, I.; Pedersen, P. J.; Rowe, E.; Derving Karsbøl, J.; Pedersen, M. L. Absorption, metabolism and excretion of the GLP-1 analogue semaglutide in humans and nonclinical species. *European Journal*

of Pharmaceutical Sciences **2017**, *104*, 31–41. DOI: https://doi.org/10.1016/j.ejps.2017.03.020

(28) Menacho-Melgar, R.; Decker, J. S.; Hennigan, J. N.; Lynch, M. D. A review of lipidation in the development of advanced protein and peptide therapeutics. *J Control Release* **2019**, *295*, 1–12. DOI: 10.1016/j.jconrel.2018.12.032

(29) Quinlan, G. J.; Martin, G. S.; Evans, T. W. Albumin: Biochemical properties and therapeutic potential. *Hepatology* **2005**, *41*, 1211-1219. DOI: 10.1002/hep.20720

(30) Cloake, N. C.; Beaino, W.; Trifilieff, E.; Greer, J. M. Thiopalmitoylation of Altered Peptide Ligands Enhances Their Protective Effects in an Animal Model of Multiple Sclerosis. *The Journal of Immunology* **2014**, *192*, 2244-2251. DOI: 10.4049/jimmunol.1301871

(31) Nadège, P.; Erwann, G.; Judith, G. M.; Elisabeth, T. Solid-phase synthesis of a biotin-labelled thiopalmitoylated myelin proteolipid protein epitope and application in the study of uptake of antigen by macrophages. *International Journal of Peptide Research and Therapeutics* **2003**, *10*, 581-587. DOI: 10.1007/s10989-004-3534-9

(32) Schultz, H. S.; Østergaard, S.; Sidney, J.; Lamberth, K.; Sette, A. The effect of acylation with fatty acids and other modifications on HLA class II:peptide binding and T cell stimulation for three model peptides. *PLOS ONE* **2018**, *13*, e0197407. DOI: 10.1371/journal.pone.0197407

(33) Xie, J.; Bi, Y.; Zhang, H.; Dong, S.; Teng, L.; Lee, R. J.; Yang, Z. Cell-Penetrating Peptides in Diagnosis and Treatment of Human Diseases: From Preclinical Research to Clinical Application. *Front Pharmacol* **2020**, *11*, 697. DOI: 10.3389/fphar.2020.00697

(34) Yang, N. J.; Hinner, M. J. Getting across the cell membrane: an overview for small molecules, peptides, and proteins. *Methods Mol Biol* **2015**, *1266*, 29–53. DOI: 10.1007/978-1-4939-2272-7_3

(35) Johannessen, L.; Remsberg, J.; Gaponenko, V.; Adams, K. M.; Barchi, J. J., Jr.; Tarasov, S. G.; Jiang, S.; Tarasova, N. I. Peptide structure stabilization by membrane anchoring and its general applicability to the development of potent cell-permeable inhibitors. *Chembiochem* **2011**, *12*, 914–921. DOI: 10.1002/cbic.201000563

(36) Hedegaard, S. F.; Bruhn, D. S.; Khandelia, H.; Cárdenas, M.; Nielsen, H. M. Shuffled lipidation pattern and degree of lipidation determines the membrane interaction behavior of a linear cationic membrane-active peptide. *Journal of Colloid and Interface Science* **2020**, *578*, 584–597. DOI: https://doi.org/10.1016/j.jcis.2020.05.121

(37) Allen, B. L.; Taatjes, D. J. The Mediator complex: a central integrator of transcription. *Nature Reviews Molecular Cell Biology* **2015**, *16*, 155–166. DOI: 10.1038/nrm3951

(38) Richter, W. F.; Nayak, S.; Iwasa, J.; Taatjes, D. J. The Mediator complex as a master regulator of transcription by RNA polymerase II. *Nature Reviews Molecular Cell Biology* **2022**, *23*, 732–749. DOI: 10.1038/s41580-022-00498-3

(39) Soutourina, J. Transcription regulation by the Mediator complex. *Nature Reviews Molecular Cell Biology* **2018**, *19*, 262–274. DOI: 10.1038/nrm.2017.115

(40) El Khattabi, L.; Zhao, H.; Kalchschmidt, J.; Young, N.; Jung, S.; Van Blerkom, P.; Kieffer-Kwon, P.; Kieffer-Kwon, K. R.; Park, S.; Wang, X.; et al. A Pliable Mediator Acts as a Functional Rather Than an Architectural Bridge between Promoters and Enhancers. *Cell* **2019**, *178*, 1145–1158.e1120. DOI: 10.1016/j.cell.2019.07.011

(41) Zhao, H.; Young, N.; Kalchschmidt, J.; Lieberman, J.; El Khattabi, L.; Casellas, R.; Asturias, F. J. Structure of mammalian Mediator complex reveals Tail module architecture and interaction with a conserved core. *Nature Communications* **2021**, *12*, 1355. DOI: 10.1038/s41467-021-21601-w

(42) Jaeger, M. G.; Schwalb, B.; Mackowiak, S. D.; Velychko, T.; Hanzl, A.; Imrichova, H.; Brand, M.; Agerer, B.; Chorn, S.; Nabet, B.; et al. Selective Mediator dependence of cell-type-specifying transcription. *Nature Genetics* **2020**, *52*, 719–727. DOI: 10.1038/s41588-020-0635-0

(43) Verger, A.; Baert, J.-L.; Verreman, K.; Dewitte, F.; Ferreira, E.; Lens, Z.; de Launoit, Y.; Villeret, V.; Monté, D. The Mediator complex subunit MED25 is targeted by the N-terminal transactivation domain of the PEA3 group members. *Nucleic Acids Research* **2013**, *41*, 4847-4859. DOI: 10.1093/nar/gkt199

(44) Landrieu, I.; Verger, A.; Baert, J.-L.; Rucktooa, P.; Cantrelle, F.-X.; Dewitte, F.; Ferreira, E.; Lens, Z.; Villeret, V.; Monté, D. Characterization of ERM transactivation domain binding to the ACID/PTOV domain of the Mediator subunit MED25. *Nucleic Acids Research* **2015**, *43*, 7110-7121. DOI: 10.1093/nar/gkv650

(45) Sela, D.; Conkright, J. J.; Chen, L.; Gilmore, J.; Washburn, M. P.; Florens, L.; Conaway, R. C.; Conaway, J. W. Role for Human Mediator Subunit MED25 in Recruitment of Mediator to Promoters by Endoplasmic Reticulum Stress-responsive Transcription Factor ATF6β **. *Journal of Biological Chemistry* **2013**, *288*, 26179-26187. DOI: 10.1074/jbc.M113.496968

(46) Vojnic, E.; Mourão, A.; Seizl, M.; Simon, B.; Wenzeck, L.; Larivière, L.; Baumli, S.; Baumgart, K.; Meisterernst, M.; Sattler, M.; et al. Structure and VP16 binding of the Mediator Med25 activator interaction domain. *Nature Structural & Molecular Biology* **2011**, *18*, 404-409. DOI: 10.1038/nsmb.1997

(47) Qi, T.; Qu, Q.; Li, G.; Wang, J.; Zhu, H.; Yang, Z.; Sun, Y.; Lu, Q.; Qu, J. Function and regulation of the PEA3 subfamily of ETS transcription factors in cancer. *Am J Cancer Res* **2020**, *10*, 3083-3105.

(48) Oka, O. B. V.; Pierre, A. S.; Pringle, M. A.; Tungkum, W.; Cao, Z.; Fleming, B.; Bulleid, N. J. Activation of the UPR sensor ATF6α is regulated by its redox-dependent dimerization and ER retention by ERp18. *Proc Natl Acad Sci U S A* **2022**, *119*, e2122657119. DOI: 10.1073/pnas.2122657119

(49) Kuznetsova, S.; Ait-Si-Ali, S.; Nagibneva, I.; Troalen, F.; Le Villain, J. P.; Harel-Bellan, A.; Svinarchuk, F. Gene activation by triplex-forming oligonucleotide coupled to the activating domain of protein VP16. *Nucleic Acids Res* **1999**, *27*, 3995–4000. DOI: 10.1093/nar/27.20.3995

(50) Pellecchia, A.; Pescucci, C.; De Lorenzo, E.; Luceri, C.; Passaro, N.; Sica, M.; Notaro, R.; De Angioletti, M. Overexpression of ETV4 is oncogenic in prostate cells through promotion of both cell proliferation and epithelial to mesenchymal transition. *Oncogenesis* **2012**, *1*, e20-e20. DOI: 10.1038/oncsis.2012.20

(51) Niphakis, M. J.; Lum, K. M.; Cognetta, A. B., 3rd; Correia, B. E.; Ichu, T. A.; Olucha, J.; Brown, S. J.; Kundu, S.; Piscitelli, F.; Rosen, H.; et al. A Global Map of Lipid-Binding Proteins and Their Ligandability in Cells. *Cell* **2015**, *161*, 1668-1680. DOI: 10.1016/j.cell.2015.05.045

(52) Garlick, J. M.; Sturlis, S. M.; Bruno, P. A.; Yates, J. A.; Peiffer, A. L.; Liu, Y.; Goo, L.; Bao, L.; De Salle, S. N.; Tamayo-Castillo, G.; et al. Norstictic Acid Is a Selective

Allosteric Transcriptional Regulator. *J Am Chem Soc* **2021**, *143*, 9297-9302. DOI: 10.1021/jacs.1c03258

(53) Thuerauf, D. J.; Morrison, L. E.; Hoover, H.; Glembotski, C. C. Coordination of ATF6-mediated transcription and ATF6 degradation by a domain that is shared with the viral transcription factor, VP16. *J Biol Chem* **2002**, *277*, 20734–20739. DOI: 10.1074/jbc.M201749200

(54) Zarin, T.; Strome, B.; Nguyen Ba, A. N.; Alberti, S.; Forman-Kay, J. D.; Moses, A. M. Proteome-wide signatures of function in highly diverged intrinsically disordered regions. *eLife* **2019**, *8*, e46883. DOI: 10.7554/eLife.46883

(55) Nikolovska-Coleska, Z.; Wang, R.; Fang, X.; Pan, H.; Tomita, Y.; Li, P.; Roller, P. P.; Krajewski, K.; Saito, N. G.; Stuckey, J. A.; et al. Development and optimization of a binding assay for the XIAP BIR3 domain using fluorescence polarization. *Anal Biochem* **2004**, *332*, 261-273. DOI: 10.1016/j.ab.2004.05.055

(56) Kowalczyk, R.; Harris, P. W. R.; Williams, G. M.; Yang, S. H.; Brimble, M. A. Peptide Lipidation - A Synthetic Strategy to Afford Peptide Based Therapeutics. *Adv Exp Med Biol* **2017**, *1030*, 185–227. DOI: 10.1007/978-3-319-66095-0_9

(57) Rounds, T.; Straus, S. K. Lipidation of Antimicrobial Peptides as a Design Strategy for Future Alternatives to Antibiotics. *International Journal of Molecular Sciences* **2020**, *21*, 9692.

(58) Trier, S.; Linderoth, L.; Bjerregaard, S.; Strauss, H. M.; Rahbek, U. L.; Andresen, T. L. Acylation of salmon calcitonin modulates in vitro intestinal peptide flux through membrane permeability enhancement. *European Journal of Pharmaceutics and Biopharmaceutics* **2015**, *96*, 329–337. DOI: https://doi.org/10.1016/j.ejpb.2015.09.001

(59) Rocco D, R. J., Murray P, Caccetta R. . Acyl lipidation of a peptide: effects on activity and epidermal permeability in vitro. . *Drug Des Devel Ther* **2016**, *10*, 2203–2209 DOI: https://doi.org/10.2147/DDDT.S104111

(60) Feng, B. Y.; Shoichet, B. K. A detergent-based assay for the detection of promiscuous inhibitors. *Nature Protocols* **2006**, *1*, 550-553. DOI: 10.1038/nprot.2006.77

(61) Sukmarini, L. Marine Bacterial Ribosomal Peptides: Recent Genomics- and Synthetic Biology-Based Discoveries and Biosynthetic Studies. *Mar Drugs* **2022**, *20*. DOI: 10.3390/md20090544

(62) Tareq, F. S.; Lee, M. A.; Lee, H. S.; Lee, J. S.; Lee, Y. J.; Shin, H. J. Gageostatins A-C, antimicrobial linear lipopeptides from a marine Bacillus subtilis. *Mar Drugs* **2014**, *12*, 871-885. DOI: 10.3390/md12020871

(63) Cook, E. C.; Usher, G. A.; Showalter, S. A. The Use of (13)C Direct-Detect NMR to Characterize Flexible and Disordered Proteins. *Methods Enzymol* **2018**, *611*, 81-100. DOI: 10.1016/bs.mie.2018.08.025

(64) Henderson, A. R.; Henley, M. J.; Foster, N. J.; Peiffer, A. L.; Beyersdorf, M. S.; Stanford, K. D.; Sturlis, S. M.; Linhares, B. M.; Hill, Z. B.; Wells, J. A.; et al. Conservation of coactivator engagement mechanism enables small-molecule allosteric modulators. *Proceedings of the National Academy of Sciences* **2018**, *115*, 8960-8965. DOI: 10.1073/pnas.1806202115

(65) Verger, A.; Baert, J. L.; Verreman, K.; Dewitte, F.; Ferreira, E.; Lens, Z.; de Launoit, Y.; Villeret, V.; Monté, D. The Mediator complex subunit MED25 is targeted by the N-terminal transactivation domain of the PEA3 group members. *Nucleic Acids Res* **2013**, *41*, 4847-4859. DOI: 10.1093/nar/gkt199

(66) Sela, D.; Conkright, J. J.; Chen, L.; Gilmore, J.; Washburn, M. P.; Florens, L.; Conaway, R. C.; Conaway, J. W. Role for human mediator subunit MED25 in recruitment of mediator to promoters by endoplasmic reticulum stress-responsive transcription factor ATF6α. *J Biol Chem* **2013**, *288*, 26179-26187. DOI: 10.1074/jbc.M113.496968

(67) Vojnic, E.; Mourão, A.; Seizl, M.; Simon, B.; Wenzeck, L.; Larivière, L.; Baumli, S.; Baumgart, K.; Meisterernst, M.; Sattler, M.; et al. Structure and VP16 binding of the Mediator Med25 activator interaction domain. *Nat Struct Mol Biol* **2011**, *18*, 404-409. DOI: 10.1038/nsmb.1997

(68) Towse, C.-L.; Hopping, G.; Vulovic, I.; Daggett, V. Nature versus design: the conformational propensities of d-amino acids and the importance of side chain chirality. *Protein Engineering, Design and Selection* **2014**, *27*, 447-455. DOI: 10.1093/protein/gzu037

(69) Lopes, J. L. S.; Miles, A. J.; Whitmore, L.; Wallace, B. A. Distinct circular dichroism spectroscopic signatures of polyproline II and unordered secondary structures: Applications in secondary structure analyses. *Protein Science* **2014**, *23*, 1765-1772. DOI: 10.1002/pro.2558

(70) Crespo, L.; Sanclimens, G.; Montaner, B.; Pérez-Tomás, R.; Royo, M.; Pons, M.; Albericio, F.; Giralt, E. Peptide Dendrimers Based on Polyproline Helices. *Journal of the American Chemical Society* **2002**, *124*, 8876-8883. DOI: 10.1021/ja020364m

(71) Shi, Z.; Olson, C. A.; Rose, G. D.; Baldwin, R. L.; Kallenbach, N. R. Polyproline II structure in a sequence of seven alanine residues. *Proceedings of the National Academy of Sciences* **2002**, *99*, 9190-9195. DOI: 10.1073/pnas.112193999

(72) Furuta, M.; Fujisawa, T.; Urago, H.; Eguchi, T.; Shingae, T.; Takahashi, S.; Blanch, E. W.; Unno, M. Raman optical activity of tetra-alanine in the poly(<scp>l</scp>-proline) II type peptide conformation. *Physical Chemistry Chemical Physics* **2017**, *19*, 2078-2086. DOI: 10.1039/c6cp07828a

(73) Roy, O.; Dumonteil, G.; Faure, S.; Jouffret, L.; Kriznik, A.; Taillefumier, C. Homogeneous and Robust Polyproline Type I Helices from Peptoids with Nonaromatic α-Chiral Side Chains. *Journal of the American Chemical Society* **2017**, *139*, 13533-13540. DOI: 10.1021/jacs.7b07475

(74) Wang, D.; Chen, K.; Kulp, J. L.; Arora, P. S. Evaluation of Biologically Relevant Short α-Helices Stabilized by a Main-Chain Hydrogen-Bond Surrogate. *Journal of the American Chemical Society* **2006**, *128*, 9248-9256. DOI: 10.1021/ja062710w

(75) Merritt, H. I.; Sawyer, N.; Watkins, A. M.; Arora, P. S. Anchor Residues Govern Binding and Folding of an Intrinsically Disordered Domain. *ACS Chemical Biology* **2022**, *17*, 2723–2727. DOI: 10.1021/acschembio.2c00619

(76) Farrera-Sinfreu, J.; Giralt, E.; Royo, M.; Albericio, F. Cell-Penetrating Proline-Rich Peptidomimetics. Humana Press, 2007; pp 241-267.

(77) Franz, J.; Lelle, M.; Peneva, K.; Bonn, M.; Weidner, T. SAP(E) – A cell-penetrating polyproline helix at lipid interfaces. *Biochimica et Biophysica Acta (BBA) - Biomembranes* **2016**, *1858*, 2028-2034. DOI: https://doi.org/10.1016/j.bbamem.2016.05.021

(78) Lee, C. W.; Ferreon, J. C.; Ferreon, A. C.; Arai, M.; Wright, P. E. Graded enhancement of p53 binding to CREB-binding protein (CBP) by multisite

phosphorylation. *Proc Natl Acad Sci U S A* **2010**, *107*, 19290-19295. DOI: 10.1073/pnas.1013078107

(79) Joy, S. T.; Henley, M. J.; De Salle, S. N.; Beyersdorf, M. S.; Vock, I. W.; Huldin, A. J. L.; Mapp, A. K. A Dual-Site Inhibitor of CBP/p300 KIX is a Selective and Effective Modulator of Myb. *Journal of the American Chemical Society* **2021**, *143*, 15056-15062. DOI: 10.1021/jacs.1c04432

(80) Buhrlage, S. J.; Bates, C. A.; Rowe, S. P.; Minter, A. R.; Brennan, B. B.; Majmudar, C. Y.; Wemmer, D. E.; Al-Hashimi, H.; Mapp, A. K. Amphipathic Small Molecules Mimic the Binding Mode and Function of Endogenous Transcription Factors. *ACS Chemical Biology* **2009**, *4*, 335-344. DOI: 10.1021/cb900028j

(81) Breen, M. E.; Joy, S. T.; Baruti, O. J.; Beyersdorf, M. S.; Henley, M. J.; De Salle, S. N.; Ycas, P. D.; Croskey, A.; Cierpicki, T.; Pomerantz, W. C. K.; et al. Garcinolic Acid Distinguishes Between GACKIX Domains and Modulates Interaction Networks. *ChemBioChem* **2023**, *24*. DOI: 10.1002/cbic.202300439

(82) Block, K. M.; Wang, H.; Szabó, L. Z.; Polaske, N. W.; Henchey, L. K.; Dubey, R.; Kushal, S.; László, C. F.; Makhoul, J.; Song, Z.; et al. Direct Inhibition of Hypoxia-Inducible Transcription Factor Complex with Designed Dimeric Epidithiodiketopiperazine. *Journal of the American Chemical Society* **2009**, *131*, 18078-18088. DOI: 10.1021/ja807601b

(83) Garlick, J. M.; Sturlis, S. M.; Bruno, P. A.; Yates, J. A.; Peiffer, A. L.; Liu, Y.; Goo, L.; Bao, L.; De Salle, S. N.; Tamayo-Castillo, G.; et al. Norstictic Acid Is a Selective Allosteric Transcriptional Regulator. *Journal of the American Chemical Society* **2021**, *143*, 9297-9302. DOI: 10.1021/jacs.1c03258

(84) Sarabia, F.; Martín-Gálvez, F.; Chammaa, S.; Martín-Ortiz, L.; Sánchez-Ruiz, A. Chiral Sulfur Ylides for the Synthesis of Bengamide E and Analogues. *The Journal of Organic Chemistry* **2010**, *75*, 5526-5532. DOI: 10.1021/jo100696w

(85) Wu, Z.; Belanger, G.; Brennan, B. B.; Lum, J. K.; Minter, A. R.; Rowe, S. P.; Plachetka, A.; Majmudar, C. Y.; Mapp, A. K. Targeting the Transcriptional Machinery with Unique Artificial Transcriptional Activators. *Journal of the American Chemical Society* **2003**, *125*, 12390-12391. DOI: 10.1021/ja036685v

(86) Pattelli, O. N.; Valdivia, E. M.; Beyersdorf, M. S.; Regan, C. S.; Rivas, M.; Hebert, K. A.; Merajver, S. D.; Cierpicki, T.; Mapp, A. K. A Lipopeptidomimetic of Transcriptional Activation Domains Selectively Disrupts Med25 Protein-Protein Interactions. *Angewandte Chemie International Edition* **2024**. DOI: 10.1002/anie.202400781

(87) Shao, H.; Oltion, K.; Wu, T.; Gestwicki, J. E. Differential scanning fluorimetry (DSF) screen to identify inhibitors of Hsp60 protein-protein interactions. *Org Biomol Chem* **2020**, *18*, 4157-4163. DOI: 10.1039/d0ob00928h

(88) Wu, T.; Yu, J.; Gale-Day, Z.; Woo, A.; Suresh, A.; Hornsby, M.; Gestwicki, J. E. Three Essential Resources to Improve Differential Scanning Fluorimetry (DSF) Experiments. Cold Spring Harbor Laboratory: 2020.

(89) Delaglio, F.; Grzesiek, S.; Vuister, G. W.; Zhu, G.; Pfeifer, J.; Bax, A. NMRPipe: a multidimensional spectral processing system based on UNIX pipes. *J Biomol NMR* **1995**, *6*, 277-293. DOI: 10.1007/bf00197809

(90) Lee, W.; Tonelli, M.; Markley, J. L. NMRFAM-SPARKY: enhanced software for biomolecular NMR spectroscopy. *Bioinformatics* **2015**, *31*, 1325-1327. DOI: 10.1093/bioinformatics/btu830

(91) Liu, M.; Liu, Y.; Deng, L.; Wang, D.; He, X.; Zhou, L.; Wicha, M. S.; Bai, F.; Liu, S. Transcriptional profiles of different states of cancer stem cells in triple-negative breast cancer. *Mol Cancer* **2018**, *17*, 65. DOI: 10.1186/s12943-018-0809-x

(92) Aw Yong, K. M.; Ulintz, P. J.; Caceres, S.; Cheng, X.; Bao, L.; Wu, Z.; Jiagge, E. M.; Merajver, S. D. Heterogeneity at the invasion front of triple negative breast cancer cells. *Sci Rep* **2020**, *10*, 5781. DOI: 10.1038/s41598-020-62516-8

Chapter 3 Lipopeptidomimetics Display Modifiable Target Selectivity

3.1 Abstract

Diverse approaches have been utilized for the identification of inhibitors for coactivator protein–protein interactions (PPIs) for transcriptional modulation. Certain methodologies have made progress towards addressing the systemic challenges in this pursuit; however, these avenues are not applicable in some of the most complex scenarios. Additionally, such strategies, such as rationally designed and natural product inhibitors, may be limited in their applicability across multiple complexes, either due to the high specificity in their design or their structural complexity, which in turns restricts the modifiability and derivatization of the activity endowing scaffolds. Here, we propose that lipopeptidomimetics have the potential of surpassing these limitations as coactivator inhibitors, by demonstrating that they are modifiable scaffolds with tunable selectivity resulting from modifications on their peptide sequence.

In fact, a single amino acid modification to the sequence of LPPM-8 led to changes in the selectivity patterns of the molecule.

We show that LPPM-D2A allosterically inhibits the CBP KIX PPI with sub-micromolar affinity, demonstrates selectivity for this coactivator in a variety of contexts, and engages with the allosteric network of the protein. We provide evidence for the validity of the selectivity switch through various biophysical and biochemical assessments and determine that this selectivity change does not occur as a result of an overall increase in the promiscuity of the LPPM. The data from this chapter reinforces the potential of LPPMs as an important and generalizable strategy in inhibitor design for coactivator PPIs.

3.2 Introduction

3.2.1 The case for a generalizable strategy for coactivator PPI inhibitor design

In medicinal chemistry, an approach that is commonly used to target protein families with shared structural or functional characteristics, is the utilization of privileged scaffolds. This term refers to the strategy of deriving high affinity ligands from core structures with the capability of binding to more than one protein within the family.[1] This scaffold-based design has evolved into an integral component of multiple lead generation platforms for diverse categories of targets.[2] (Figure 3.1). For instance, multiple scaffolds have been incorporated in the structures of kinase inhibitors, including purine, for cyclin dependent kinase (CDK) inhibitors, as well as imidazole, benzimidazoles, azaindoles, quinolones, among others.[2] This strategy has also been used in the development of more complicated therapeutics, such as in the case of multi-target kinase inhibitors. Approved molecules that act as dual EGFR/HER2 inhibitors, such as lapatinib, neratinib, and afatinib, all share a core scaffold in their structures, and display differences in the affinity and activity, deriving from differences in the chemical groups surrounding this core

structure.[3-5] These examples illustrate that core scaffolds have been harnessed to target various proteins within a protein family in a selective manner.

Olomucine   Roscovitine   Puralanol A
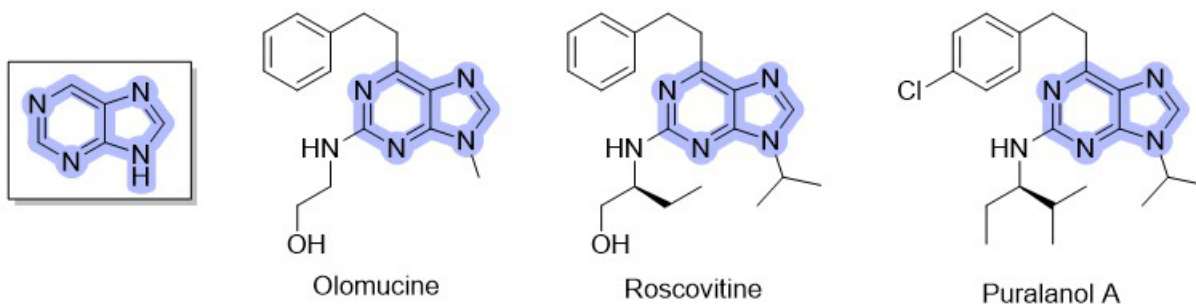
Purine-based CDK inhibitors

Lapatinib

Afatinib

Neratinib
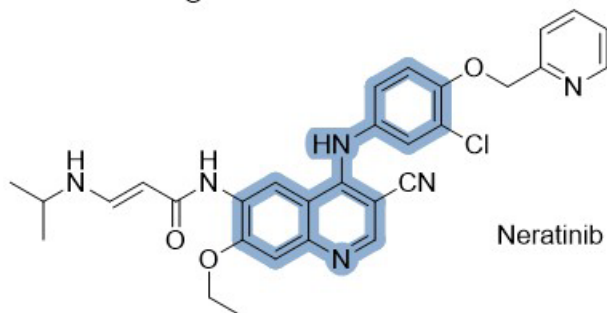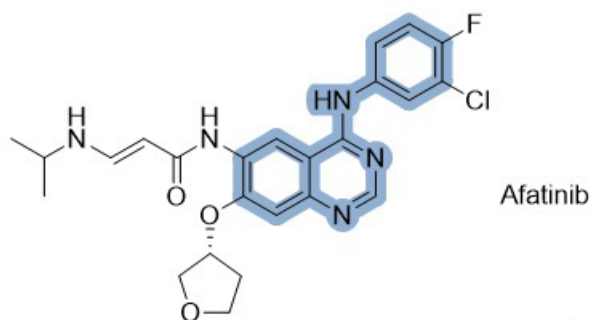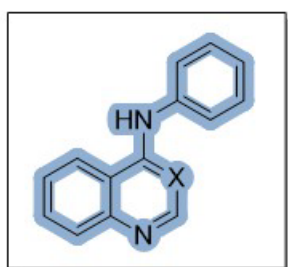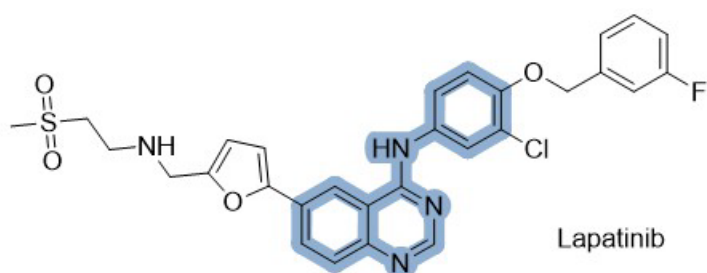
EGFR/HER2 inhibitors

Figure 3.1. Privileged scaffolds in different classes of kinase inhibitors, CDK (top) and dual-targeting EGFR/HER2(bottom). Adapted from Zhao & Dietrich, 2015.[2]

A parallel framing to that of privileged scaffolds has been proposed in the development of inhibitors for protein–protein interactions (PPIs). Studies have suggested that in these cases, hot spot residues on the proteins themselves, which are amino acids that account for the majority of the overall free energy of binding, can be considered 'privileged', just as certain moieties on synthetic privileged scaffolds.[6, 7] The consideration of these hot spot residues in the development of inhibitors is exemplified by MDM2•p53 blocking molecules, where spiro-oxindole and 6-chloroindole-based molecules were used to inhibit the indole-binding site of W23 on p53.[8, 9] The accumulation of data on the types of molecules that are apt candidates for inhibiting increasingly complex PPIs, has led to the suggestion that the selection of a particular PPI inhibitor scaffold must be led by the characteristics of the protein target itself.[10]

In general, comparable scaffolds to those of kinase inhibitors or of hot spot-containing PPI inhibitors have not been identified for the more complex types of PPIs. This includes those between coactivators and activators, the majority of which are driven by the accumulation of moderate interactions, rather than hotspot drivers. The identification of a coactivator PPI-targeting structure with characteristics that meet those of privileged scaffolds is a long-term goal in the field that would require a large allocation of resources for screening and characterization. However, an analysis of the motifs of identified inhibitors and the features important for their activity against coactivator PPIs, can provide a basis for progress towards this goal. A milestone in the pursuit of generalizable coactivator PPI inhibitor scaffold would be a molecule that has tunable target selectivity, and a method for changing the selectivity through alterations of the

scaffold in a predictable way. Such a tool would facilitate the widespread targeting of undruggable proteins in a more streamlined manner.

3.2.2 The CBP/p300 KIX domain as a target for validation of the LPPM approach

CREB binding protein (CBP) and p300 are paralog proteins that have been termed master coactivators of transcription, given their widespread involvement in cell processes essential for maintaining homeostasis.[11] Through multidomain structures, CPB/p300 functions as a transcriptional coactivator and histone acetyl transferase, thereby playing critical roles in transcriptional initiation.[12] In its capacity as an interaction hub, CBP/p300 interacts with activator proteins using the KIX, TAZ1, IBiD and TAZ2 domains.[13] This expansive protein network, when dysregulated, contributes to the development of neurodegenerative disease and multiple types of cancer.[14, 15] The kinase inducible-domain interacting (KIX) domain, is known as one of the most important molecular recognition sites for PPIs in transcriptional regulation, in part due to its engagement with a variety of activators, as shown in Figure 3.2.[16] The KIX domain has a structure comprised of three alpha helices, which make up two binding surfaces which are connected to each other through a well-characterized allosteric network in the core of the protein domain.[17, 18]
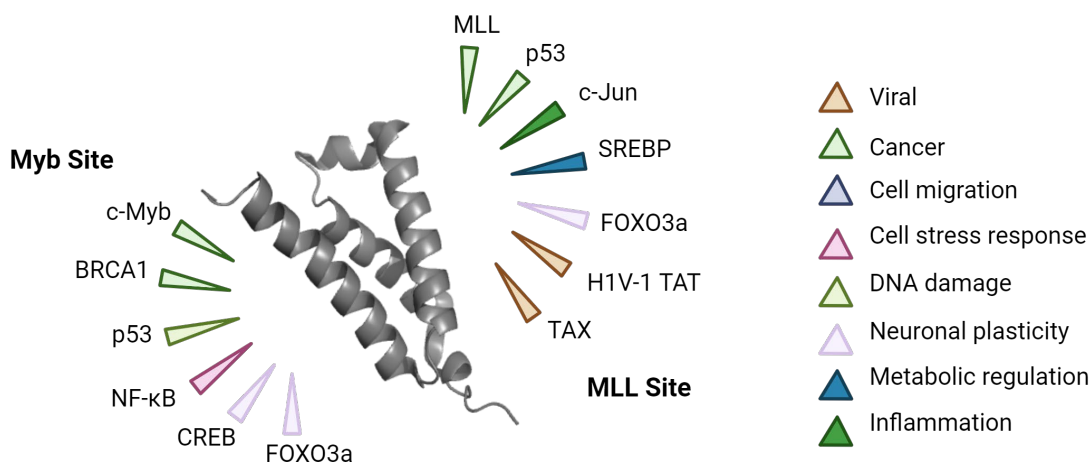
Figure 3.2. PPI network at the two binding sites of CBP/p300 KIX and dependent pathways. PDB 2AGH. Figure created with BioRender.com.

Research efforts have been directed towards dissecting the mechanisms for binding recognition of KIX. For instance, studies into the allosteric network of the KIX domain have identified that the activator c-Myb is known to engage using a folding-after-binding mechanism, and it binds with altered binding constants when the TAD of MLL is engaging KIX.[19, 20] Computational analysis of the formation of ternary complexes with ligand pairs and KIX, has uncovered that allostery in this domain occurs through the selection of lowly-populated configurations, with each subsequent ligand having a preference for a particular subset of these microstates.[21] Furthermore, the relationship between the mechanisms of binding partner recognition and the conformational plasticity of KIX has been characterized.[22-24] These studies provide a detailed understanding of not only the dynamics and mechanisms underlying the complexity of its function, but given the breath of this characterization, they also inform on challenges of targeting this protein and similar coactivators with PPI inhibitors.

Along this vein, diverse strategies have been utilized to develop inhibitors of the PPIs of KIX. These include the rational design of structurally constrained

peptidomimetics, fragment-based screening and tethering for the development of covalent inhibitors, natural product library screening, and dual-site peptide-based inhibitors.[20, 24-32] Similar to the mechanistic investigations of KIX, these studies offer a landscape of the multiple ways to achieve the inhibition of KIX PPIs, and insight into how this inhibition can affect one or more characteristics its activity. For example, studies with small molecules have reported on the effects on cooperativity in the allosteric network of KIX upon binding of a covalent molecule.[20] Other studies illustrate the selectivity and potency advantages offered by molecules that target the two binding sites of KIX.[26, 27] Lastly, the amenability of natural product scaffolds as inhibitors also demonstrates the potential of inhibition non-canonical sites of KIX, as in the case of garcinolic acid. Other examples highlight the selectivity drawbacks of less complex natural product scaffolds, as is the case of Sekikaic and Lobaric acid, for example.[25, 33] The accumulation of evidence on effective this ABD a good candidate to use as a secondary target for the validation of novel inhibitor approaches. In this chapter, it will also be used to assess the sequence-based target modifiability and selectivity switch of lipopeptidomimetic scaffolds.
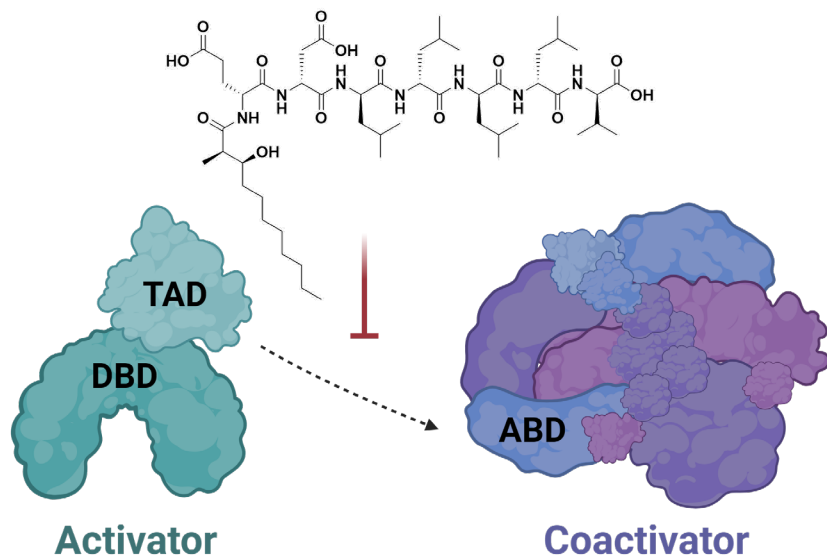
Figure 3.3 LPPM-8 as an inhibitor of coactivator•activator PPIs. Figure created with BioRender.com.

3.3 Results and Discussion

3.3.1 Switching the coactivator target of LPPMs to target CBP KIX PPIs specifically

The alanine scan of LPPM-8 (Library B) was tested against the complex formed between CBP KIX and the TAD of MLL (2840-2858) to assess how the change at every residue would affect the selectivity of the resulting analog for either Med25 AcID or CBP KIX. An analogous competitive fluorescence polarization binding screen to the previously used for Med25 to measure IC_{50} values was employed, and these were used to obtain the corresponding K_i values, using the binding affinity of the CBP KIX•MLL complex and published calculation methods.[34] The resulting K_i values are summarized on Figure 3.4 below. LPPM-8 has between a 5 and 8 fold preference to inhibit Med25•ATF6α over CBP KIX•MLL (See Figure 3.4 and Figure 2.14).
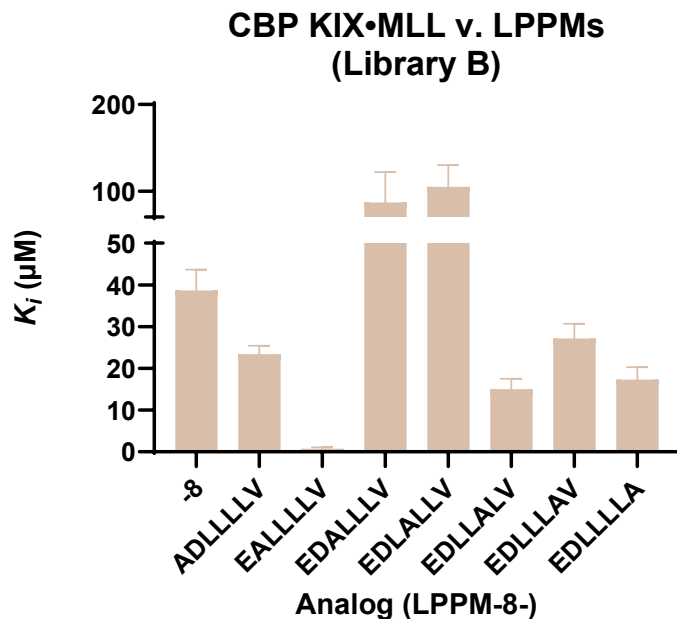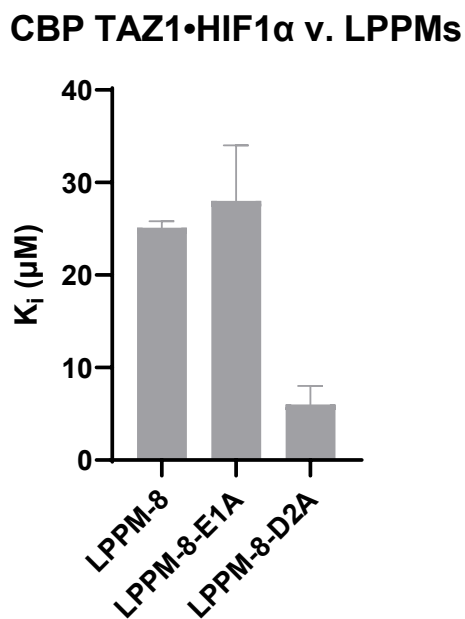
Figure 3.4. Inhibition constants of CBP KIX•MLL by alanine scan of LPPM-8 as determined by competitive fluorescence polarization assays. Apparent IC_{50} values were determined through titration of compound for CBP KIX•MLL in experimental triplicate with the indicated error (SD). The IC_{50} values were converted to K_i values using the apparent K_d value based on the direct binding CBP KIX•MLL. Data shown is the average of three independent experiments with the indicated error (SD).

The contribution of each residue of LPPM-8 to its selectivity for a particular coactivator appears to be variable across the sequence, as summarized on Figure 3.5 below, which presents the calculation of fold changes of the K_i against CBP KIX / Med25. LPPM analogs E1 and L3 show comparable K_i values for both CBP KIX / Med25, as the fold changes calculated are within 0.75 and 1.25 units, suggesting that modification of the original residue at those sites for alanine residues leads to a loss of the selectivity of LPPM-8 for Med25. Residues closer to the C-terminus of the peptide sequence (L4-V7) do not exhibit the same decrease in their selectivity for Med25, as they maintain a >2 fold change preference for Med25. L5 is the analog with the most similar selectivity for Med25 as LPPM-8, with a fold change of between 4-10. Strikingly, this analysis showed that analog D2A, has a preference >6 fold for inhibiting CBP KIX•MLL over Med25, suggesting that modifications to the peptide sequence of LPPM-8 may not only lead to a decrease in

the selectivity for Med25, but also, that these changes may in fact redirect their selectivity towards a completely separate complex. What follows is the characterization of the switch in the selectivity of LPPM-8-D2A for CBP KIX PPIs.
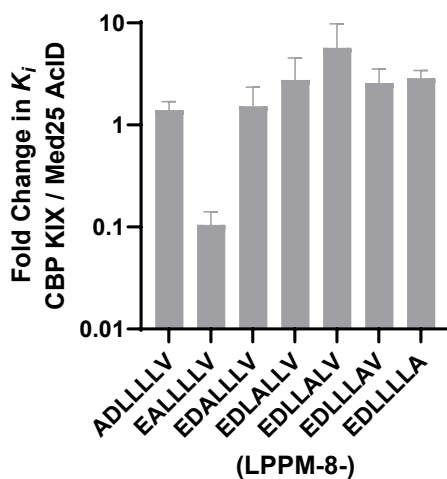
Figure 3.5. Fold-changes in the K_i of LPPMs in Library B for inhibition of CBP KIX / Med25 AcID PPIs. K_i values used to compute the fold change are represented in data from Figures and X . Data shown is the average calculation of three independent experiments for each Ki, with the indicated error (SD).

To validate the observed trends above, and to further assess the possibility that D2A exhibited characteristics as a potential CBP KIX inhibitor, measurements of the T_m of CBP KIX in the presence of LPPM-8-D2A were conducted using differential scanning fluorimetry. As presented on Figure 3.6 below, incubation of CBP KIX with equivalents between 0.25 and 1X of LPPM-8-D2A, leads to progressive changes on the shape of the melting curve of KIX (Figure 3.6-A), which corresponds to decreases in the T_m of the protein (Figure 3.6-B). Concentration equivalents of LPPM-8-D2A were tested up to 10X [KIX], and the relationship between these values and the resulting KIX T_m was plotted and fit with a sigmoidal curve (Figure 3.6-C), in accordance with published methods. It can be observed that concentration equivalents as low as 0.5X of LPPM-8-D2A, are sufficient to induce a change in the T_m of CBP KIX of >10 °C. Milder ΔT_m values are observed at the concentrations of LPPM-8-D2A above 2 equivalents. The first derivative curves of the T_m

93

of CBP KIX incubated with >5 equivalents of compound are included in Appendix Figure

C.3.
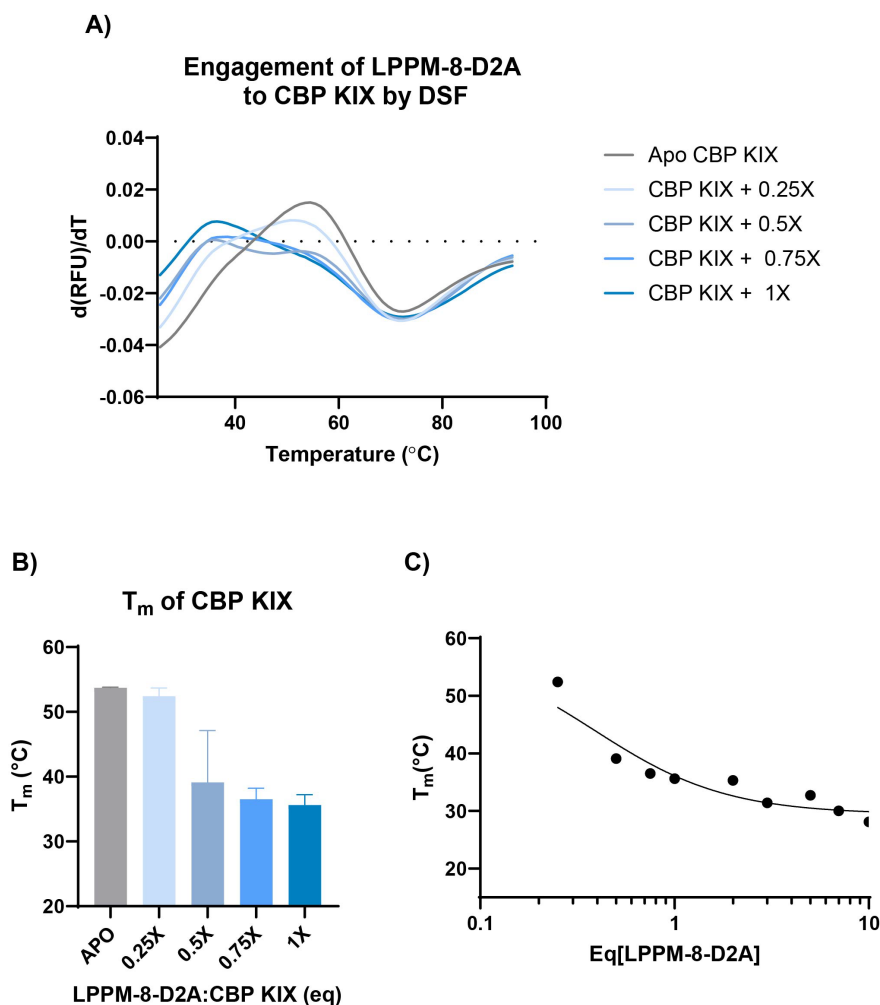
Figure 3.6. Characterization of the engagement of CBP KIX by LPPM-8-D2A as determined by DSF. A) First derivative of the melting temperature curve of CBP KIX incubated with titrations of LPPM-8-D2A between 0 − 1X equivalents. Measurements were conducted in technical triplicates, and data depicted corresponds to the representation of biological triplicates. B) Melting temperature of CBP KIX derived from data in A, using DSFWorld.[35] C) Sigmoidal fitting between the Tm of CBP KIX and equivalents of LPPM-8-D2A tested. R^2 = 0.9.

By comparison, no changes are observed in the T_m of CBPKIX when equivalents

ranging between 0.25X and 1X of LPPM-8, LPPM-8-E1A, or LPPM-8-L4A are incubated

with the protein (Figure 3.7). These results highlight the unique effect on the T_m of CBP

KIX induced by LPPM-8-D2A, which based on these studies, appears to be intrinsic to

the sequence of the analog. An important observation in these results is that removal of

a charged residue in the peptide sequence is not the only factor that leads to the changes in the activity observed in LPPM-8-D2A, as the E1A analog does not exhibit the same engagement of KIX in these experiments. An assessment of the effect on the secondary structure of the KIX domain in the presence of LPPM-8-D2A with CD was performed (Appendix Figure C.7). The resulting measurement, shows a larger change in the intensity of the spectra by comparison to the expected curve, potentially as a feature of binding.
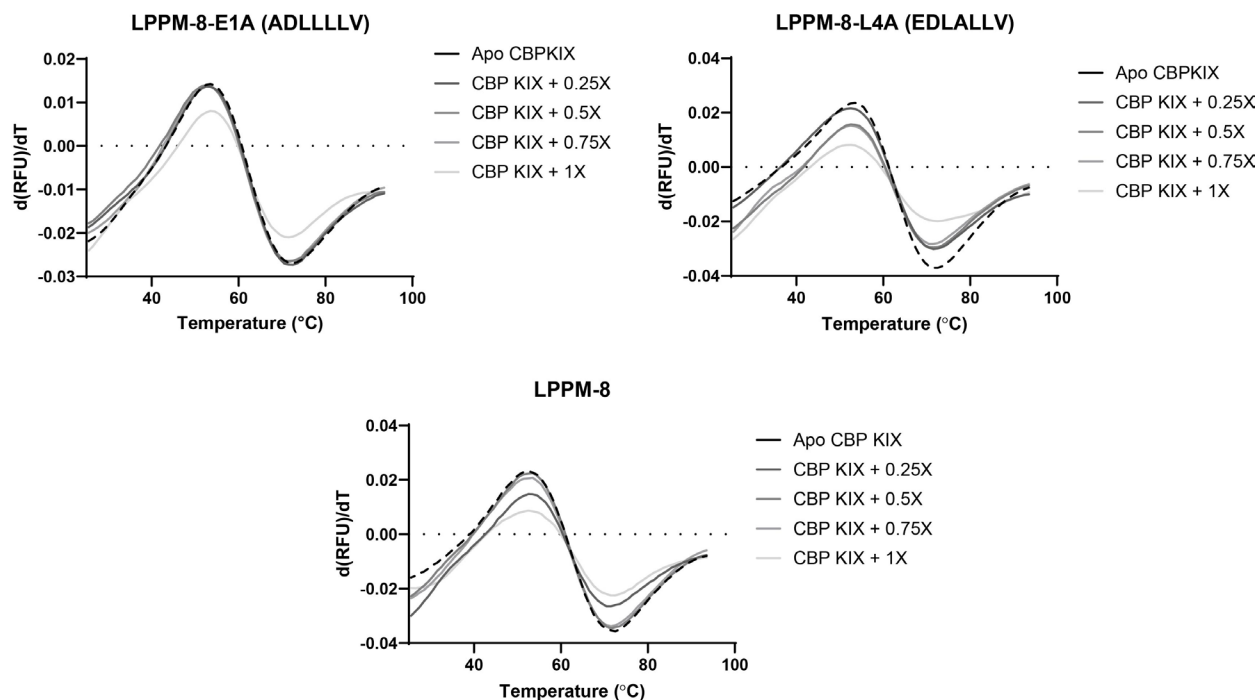
Figure 3.7. First derivative of the melting curve of CBP KIX incubated with titrations of LPPMs obtained by DSF. Data was acquired in technical triplicates and is representative of biological duplicates.

An initial question that arose from the observations above, is whether the decrease of electrostatic repulsion in the peptide sequence may be responsible for the apparent changes in the behavior in solution of these analogs. An additional question is, if the removal of a negative charge is specific to the location of the adjacent acidic residues. To assess whether analogs with one fewer negative charge show differences in their characteristics in solution, specifically in their propensity for aggregation, detergent

screens in a competitive binding assay format against CBP KIX•MLL were conducted. These assays were performed using the detergent NP40, the K_i values of the charge analogs were measured across detergent concentrations of 0.001, 0.01 and 0.1%. The resulting K_i values are presented in Figure 3.8 below. The K_i of analog LPPM-8-E1A increases 3-fold between the lowest and highest [NP40], whereas there is ~2- fold variability in the K_is of LPPM-8-D2A over the same concentrations of detergent. This suggests that the removal of the charges at each of these locations has a different effect on the propensity of aggregation of the LPPM, and that each of the residues distinctly contribute to solvation effects. These results demonstrate that LPPM-8-D2A does not exhibit the same characteristics of aggregation as LPPM-8 and LPPM-8-E1A as determined by detergent screens commonly used in the field.
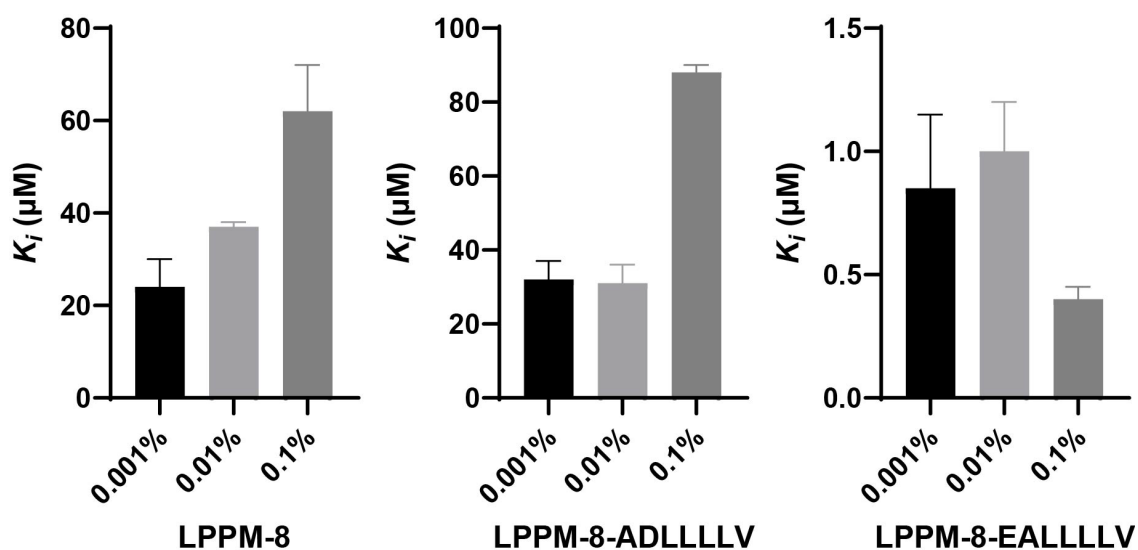
Figure 3.8. Inhibition of CBP KIX•MLL by LPPM-8, LPPM-8-E1A and LPPM-8-D2A with different NP40 concentrations as determined by competitive fluorescence polarization assays. Apparent IC_{50} values were determined through titration of compound for CBP KIX•MLL PPI performed in experimental triplicate with the indicated error (SD). The IC_{50} values were converted to Ki values using the apparent Kd value based on the direct binding of CBP KIX•MLL PPI using a Ki calculator. Data shown is the average of two independent experiments with the indicated error (SD).

The KIX domain is one of multiple ABDs of the coactivator CBP/p300. The TAZ1 ABD, is a domain known to bind to the TADs of hypoxia-inducible factors (HIF), a PPI that

promotes the expression of proliferative genes in hypoxic cancer cells.[36] To assess the selectivity of the analog LPPM-8-D2A for KIX among other CBP ABDs, we tested a selection of LPPMs against the PPI of CBP TAZ1 with the TAD of HIF1α. The results are presented in Figure 3.9 below. As observable by the comparison in the Ki values of the tested LPPMs against the complex of CBP TAZ1•HIF1α, the D2A analog is unique in its high affinity to inhibit this PPI, in comparison to the Med25-targeting LPPM-8, and the charge analog E1A. This *Ki* is 2-fold higher than the measured *Ki* for CBP KIX•MLL, suggesting a degree of selectivity within the domains of CBP.

CBP TAZ1•HIF1α v. LPPMs

Figure 3.9. Inhibition constants of CBP TAZ1•HIF1α by certain alanine analogs of LPPM-8 as determined by competitive fluorescence polarization assays. Apparent IC_{50} values were determined through titration of compound for CBP TAZ1•HIF1α in experimental triplicate with the indicated error (SD). The IC_{50} values were converted to K_i values using the apparent K_d value based on the direct binding CBP TAZ1•HIF1α. Data shown is the average of three independent experiments with the indicated error (SD).

Ultimately, the data from this section indicates that among the LPPMs tested against CBP KIX•MLL, D2A is a unique analog in its display of inhibitory activity of the complex, in its engagement with the domain, that has lower aggregation properties than

the E1A analog, and is selective for KIX over other CBP ABDs. Next, we assessed the structural features in LPPM-8-D2A that are important for engaging with CBP KIX.

3.3.2 The features on LPPM-8-D2A contribute to its inhibitory activity for CBP KIX

In previous experiments targeting Med25 AcID, it was demonstrated that LPPMs with bacteria-derived lipids, ranging in length between C_3 and C_8 had a decreased affinity to inhibit Med25 PPIs (not shown). We assessed the same relationship in the KIX-targeting LPPM-8-D2A by using two synthetic lipids: (2R, 3S) 3-hydroxy-2-methyl pentanoate, and (2S, 3R) 3-hydroxy-2-methyl pentanoate. These lipids were named MV5 and MV11, respectively. These were coupled to the peptide sequence that was characterized to bind to CBP KIX, EALLLLV, and tested against the CBP KIX•MLL PPI in a competitive FP assay format. As observed on Figure 3.10 below, the shorter lipids lose the affinity for inhibiting KIX PPIs, with a measured IC_{50} >300 µM. Similarly, these molecules do not change the T_m of CBP KIX above 2°C when assessed using DSF. Comparatively, at the concentrations tested, LPPM-8-D2A induced a change in the T_m of KIX >10°C. Only MV11-D2A at 5 equivalents [KIX] led to what is considered a significant effect with this assay. This data demonstrates that the mid-chain fatty acid on LPPM-8-D2A is necessary to effectively target KIX PPIs, in a similar way as observed in Med25. Additionally, based on these results, it is clear that the length of the lipid tail is crucial for the activity of these molecules *in vitro.*
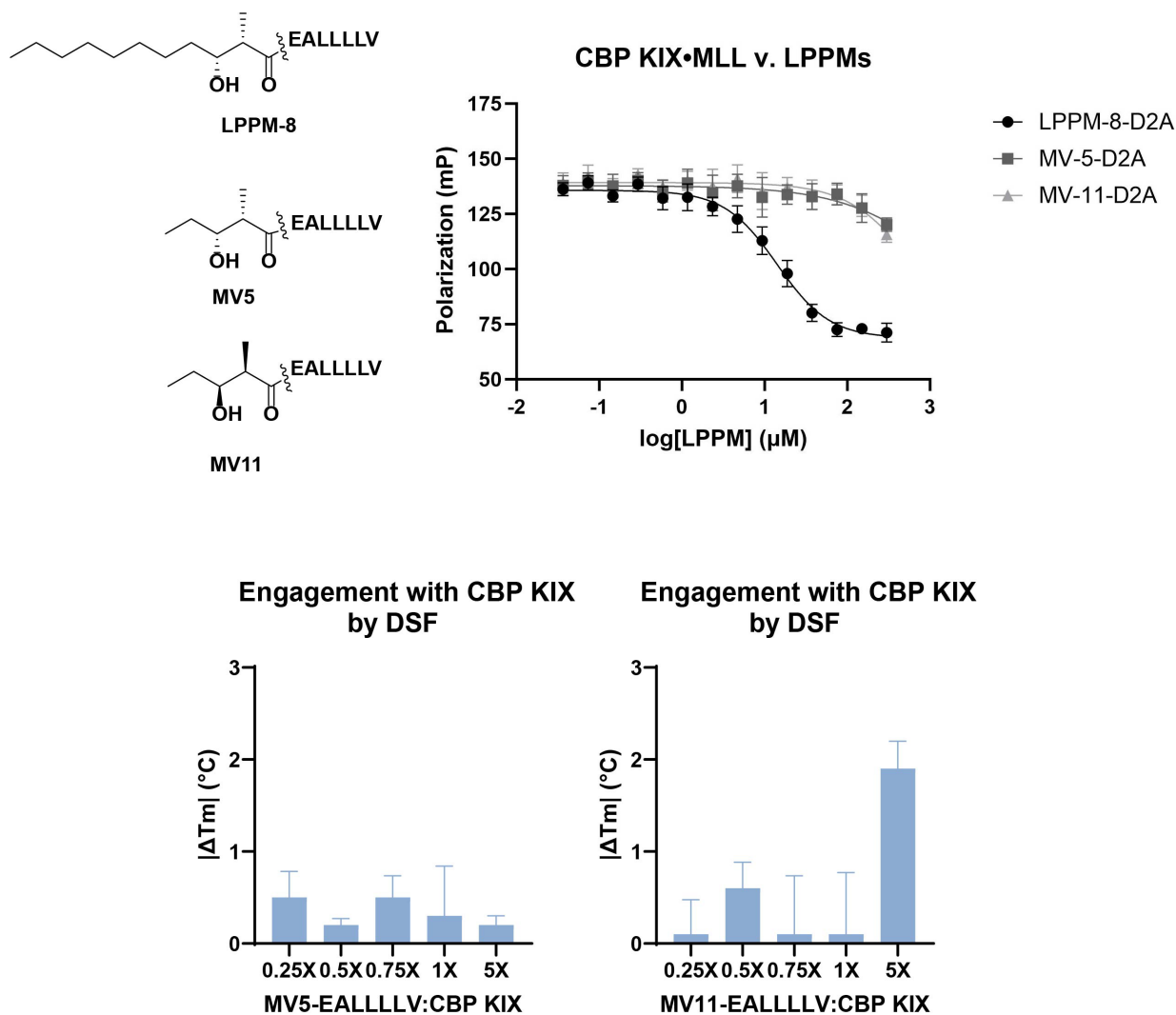
Figure 3.10. Characterization of the activity of short acyl groups (MV5 and MV11) coupled to EALLLLV (D2A) against CBP KIX PPIs. Top) Inhibition of CBP KIX•MLL as determined by competitive fluorescence polarization assays Apparent IC_{50} values were determined through titration of compound for CBP KIX•MLL in experimental triplicate. The IC_{50} values are >highest concentration of compound tested and are therefore reported as >300 µM. Data shown is the average of two independent experiments with the indicated error (SD). Bottom) Change in the melting temperature of CBP KIX when incubated with MV5 and MV11 as determined by DSF. First derivative of the melting curve of these data found in Appendix figure C. 8. Data is representative of three experimental triplicates and biological duplicates. Values shown obtained using DSFworld.

To test the sequence specificity of the modification at the Asp residue resulting in the change of the selectivity of LPPM-8, additional DSF experiments with CBP KIX were performed using selected analogs. Specifically, LPPM-8-E1P and LPPM-8-D2P from library C, or the proline scan of the parent sequence, were incubated with KIX at the

concentrations that LPPM-8-D2A yielded a change in the T_m of the protein. As presented

on Figure 3.11 below, neither one of the analogs tested led to significant changes in the

T_m of CBP KIX. It can be concluded from this data that the removal of the negative charge

at position 2 of the peptide sequence us not sufficient for inhibitory activity against CBP

KIX. As determined by DSF, a modification at that site to a proline side chain does not

equal the effects observed when that residue is modified to an alanine. To determine the

permissibility of modifications at that site that lead to the selectivity switch, a thorough

screen of amino acids with different properties would have to be conducted. Preliminarily,

from the comparison of the DSF results between the D2A and D2P, a conclusion is that

structure-breaking side chains, such as proline, are not among the modifications that lead

to this selectivity switch. This data supports a general assumption of this work, that the

inhibitory activity of the LPPMs, is sequence specific.
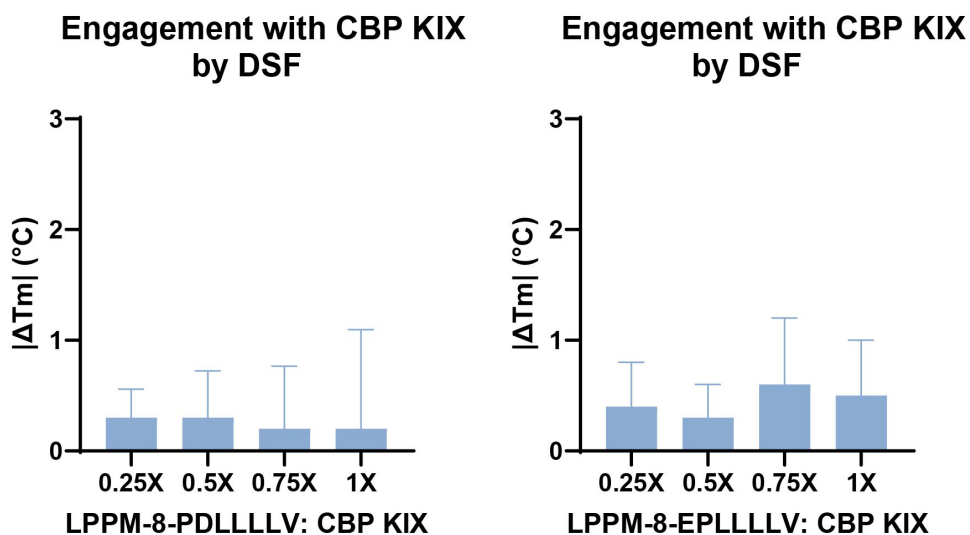
Figure 3.11. Change in the melting temperature of CBP KIX when incubated with LPPM-8-E1P and LPPM-8-D2P as determined by DSF. Data is representative of three experimental triplicates and biological duplicates. Calculations of the T_m shown were obtained using DSFworld. First derivative of the melting curve of these data found in Appendix figure C.9.

3.3.3 LPPM-8-D2A is selective for CBP KIX within the GACKIX family of domains

The GACKIX super family is a group of protein domains that share the same fold to that of the CBP KIX domain, which is characterized by 3 α-helices and 2 short 3_{10}-helices.[37] Additional members in the GACKIX family are the fungal and plant Mediator subunits Gal11/Med15, as well as the mammalian ARC105 (Figure 3.12). Sequence alignment analysis of these domains has identified important conserved residues at the hydrophobic core of KIX, which serve to stabilize the structure of the domain. These include W591, Y/F640 and Y649. R600 is another conserved residue that is engaged in a cation-π interaction with the aromatic ring at position 640. If R600 undergoes post-translational methylation, disruptions to the interaction of CBP KIX with pKID can occur. Following the categorization of these domains as part of the same protein fold family, transcriptional activators that bind to the ARC105 and Gal11/Med15 in their respective organisms were identified, further cementing their function as transcriptional coactivators, analogous to CBP KIX.
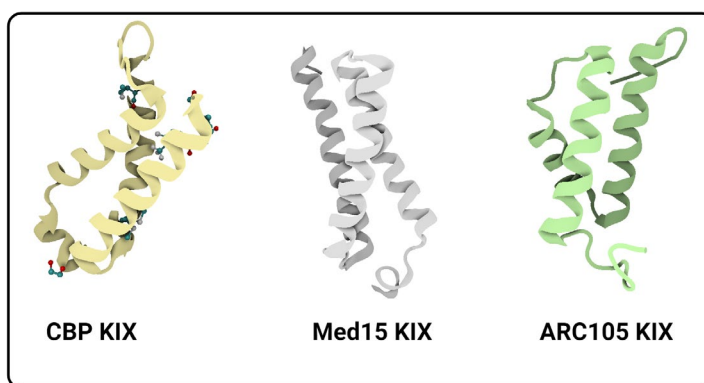
Figure 3.12 Structures of GACKIX domains. PDB entries: 2AGH, 2K0N, and 2GUT. Figure created with BioRender.com.

Considering the structural similarities of these proteins, an important aspect of KIX-targeting inhibitors is selectivity for one domain over the others in the GACKIX family.

This assessment was performed, for example, in the characterization of natural product garcinolic acid and of the dual-site inhibitor MybLL-tide.[25, 26] Specifically, the selectivity of these molecules for CBP KIX was determined by testing these molecules against a panel of KIX domains consisting of *S. cerevisiae* Med15, *C. glabrata* Med15, and human ARC105. In these cases, it was found that the selectivity of each of these molecules was significant, contributing to their further characterization in biological settings. Here, we analogously assess the selectivity of certain LPPMs between CBP KIX and ARC105, given that these are the only domains with the potential to be found simultaneously in mammalian systems.

We identified the sterol-regulatory element binding protein 1 (SREBP1) TAD as a binding partner to ARC105 in the literature, an interaction that is involved in the activator of pathways related to cholesterol and lipid homeostasis.[38, 39] The direct binding assay of ARC105 and a construct of SREBP1a, consisting of the 18-42 residues, led to an affinity constant of 4.7 ± 0.5 μM. A competitive binding assay was then performed to identify the potential inhibitory activity of LPPM-8-D2A against the PPI between the ARC105•SREBP1a complex, for comparison with its K_i for CBP KIX. As presented on Figure 3.13 below, neither of the compounds tested displayed the potential for inhibiting this PPI, demonstrating their selectivity for CBP KIX over the ARC105 KIX domain. The ARC105 KIX domain, although it shares in several of its structural and conserved residues to those of CBP KIX, is also known to have a few key different characteristics in its sequence. For instance, at its surface, residues Y658 and K662 on CBP KIX, are I64 and D68 on ARC105, a divergence in sequence conservation that has been related to the selectivity of CREB and Myb for CBP KIX over ARC105.[38] Furthermore, based on

structural studies, the binding site of SREBP1 on ARC105 has been proposed to be distinct from the binding sites of Myb, CREB and MLL on CBP KIX. This intrinsic mechanism of sequence-based selectivity of activator binding between ARC105 and CBP may also be the basis for the low affinity of LPPM-8-D2A for inhibiting the ARC105•SREBP1a PPI.
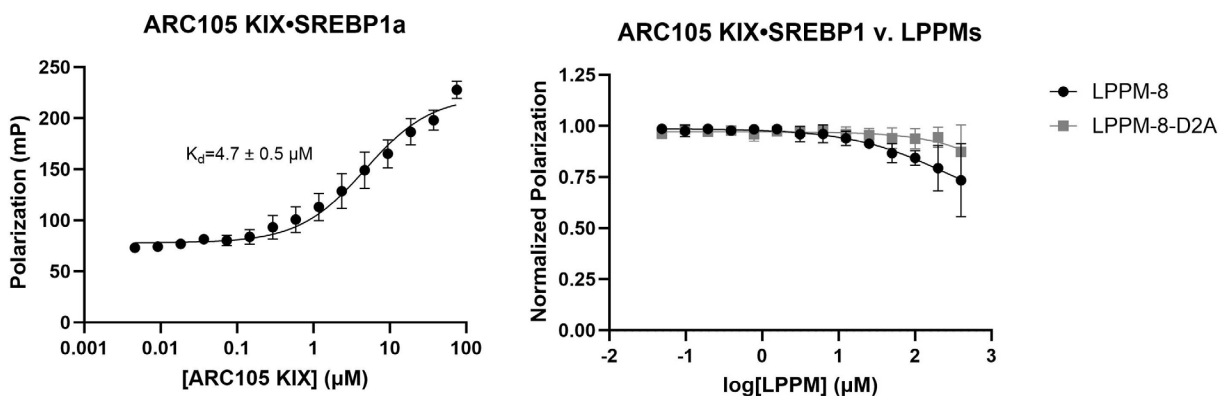
Figure 3.13. Assessment of selectivity of LPPM-8-D2A for ARC105 KIX. Left) Direct binding of ARC105 KIX•SREBP1. Right) Inhibition of ARC105 KIX•SREBP1 by LPPM-8, LPPM-8-D2A as determined by competitive fluorescence polarization assays Apparent IC_{50} values were determined through titration of compound for ARC105 KIX•SREBP1 in experimental triplicate. The IC_{50} values are >highest concentration of compound tested and are therefore reported as >400 µM. Data shown is the average of two independent experiments with the indicated error (SD).

As an additional assessment of any potential interactions between LPPM-8-D2A and ARC105, a series of DSF experiments were performed to identify whether there is a measurable engagement of the protein domain by the LPPM. We were interested in engagement that may be reflected on changes of the T_m of the protein, or on differences in the rates of melting, parameters that can be observed on the first-derivative curves of the relative fluorescence measured during this assay. Figure 3.14 below shows these measurements, specifically with incubation of ARC105 with either LPPM-8, LPPM-8-E1A,

D2A, or L4A. As observed, only the D2A analog induces measurable changes in the first derivative T_m curve of ARC105.
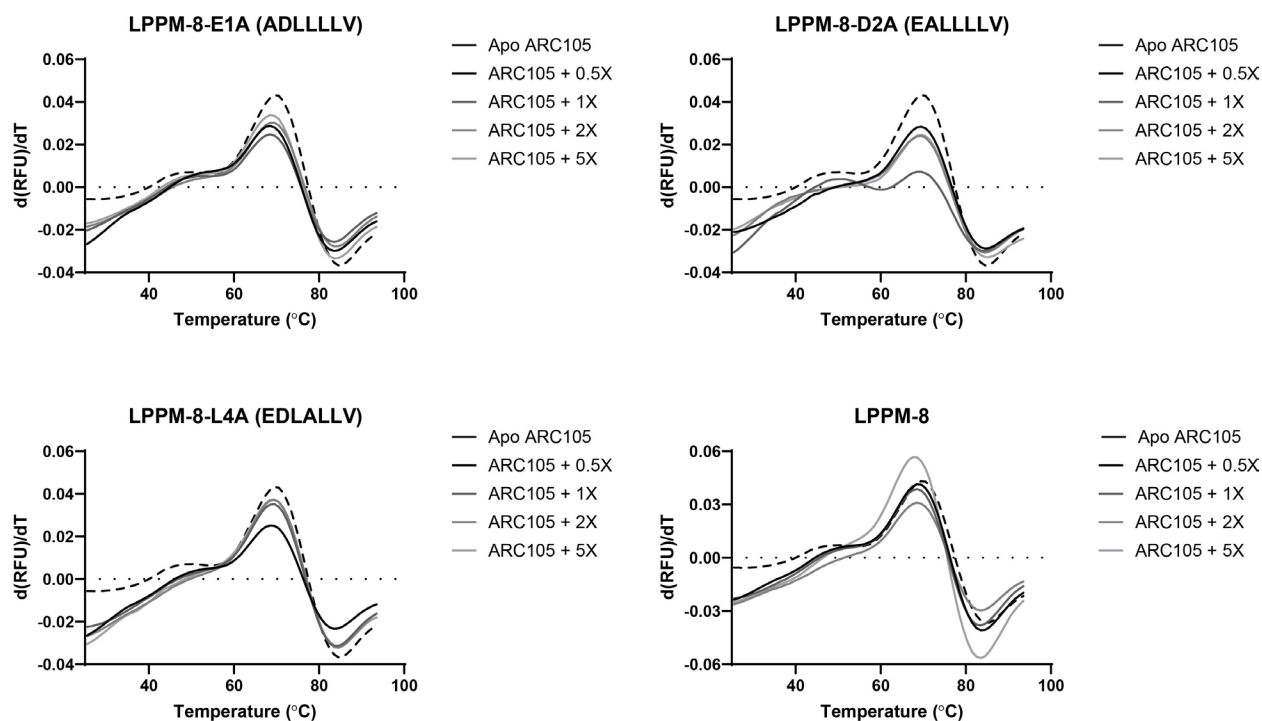
Figure 3.14. First derivative of the melting curve of ARC105 KIX incubated with titrations of LPPMs obtained by DSF. Data was acquired in technical triplicates and is representative of experiments performed in biological duplicates.

The downward shift in the maximum of the curve at increasing concentrations of the analog corresponds to a decrease in the rate of unfolding of the protein domain. However, due to lateral shifts in this maximum not being observed across the titration measurements of this molecule, no changes in the T_m were calculated by the published methods. These observations suggest that while there may be binding events between LPPM-8-D2A and ARC105, interpreted from the changes in the melting curve of ARC105, these are either not strong or specific enough to induce changes in the T_m of the protein. However, considering that D2A is the analog with the most pronounced display of effects on the melting curve of ARC105, it can be deduced that the particular amino acid sequence on this analog, that is the change from an Asp to an Ala, is conducive to

inducing these changes on ARC105 unfolding. This hypothesis is consistent with the lack of inhibitory activity observed on the fluorescence polarization binding assays. Taken together, given that there is no inhibition of ARC105 KIX PPIs, and no changes on the T_m of ARC105 are measured in the presence of LPPM-8-D2A, it can be concluded that LPPM-D2A does not interact with ARC105 KIX as it does with CBP KIX, thereby showcasing selectivity for the CBP KIX domain over other similarly folded domains of the family.

3.3.4 LPPM is an allosteric inhibitor of CBP KIX PPIs

The two binding sites of the KIX domain of CBP are connected through a well-defined allosteric network. This allostery is characterized by cooperative binding at the two TAD-binding sites, with increased affinity for the TADs of CREB-pKID and Myb, when KIX is precomplexed with MLL. [17, 18, 40] Further work done with molecular dynamic simulations and small molecule co-chaperones, has identified that the loop regions of the KIX domain contribute considerably to the allosteric character exhibited by the protein when in ternary complex form. [21, 30] Thus, given our characterization of the inhibition of the CBP KIX•MLL PPI with LPPM-8-D2A, we sought out to determine whether this molecule exhibited inhibition of the PPIs of the allosteric site of KIX. Using a competitive FP-assay format, the inhibitory constant of LPPM-8-D2A against CBP KIX•Myb and CBP KIX•pKID was determined. The control LPPM-8-E1A was used in these experiments to account for the sequence-specificity of the charge modification in the D2A analog. The results of these assessments are presented in Figure 3.15 below.
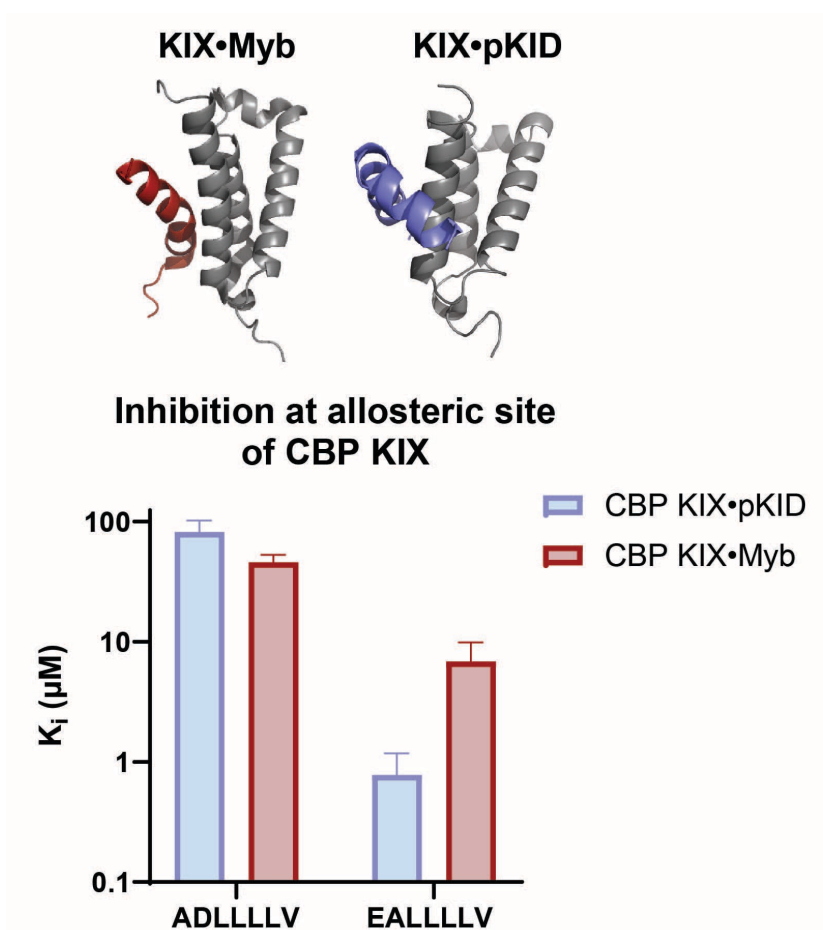
Figure 3.15 Assessment of the allosteric inhibition of CBP KIX PPIs by LPPM-8-D2A.Top) Unique binding modes of Myb/pKID to CBP KIX.[21] PDB 2AGH. Bottom) The inhibition of CBP KIX•Myb/pKID by LPPM-8-E1A, LPPM-8-D2A as determined by competitive fluorescence polarization assays. Apparent IC_{50} values were determined through titration of compound for CBP KIX•Myb/pKID in experimental triplicate. Data shown is the average of three independent experiments with the indicated error (SD).

As exhibited by the *Ki* values of LPPM-8-D2A and LPPM-8-E1A against KIX•Myb/pKID, it is evident that the D2A analog inhibits the PPIs that take place on the secondary binding site of the protein, whereas the E1A analog does not. This suggests that the D2A analog may bind to the MLL site in a way that engages the allosteric network of KIX. However, competition FP experiments performed with the complex between CBP KIX•Myb at 25% bound, did not point to an enhancement in the affinity of Myb to CBP KIX in the presence of LPPM-8-D2A. (Appendix Figure C.4) These results, especially the value of the affinity of inhibition of the pKID PPI, point to the ability to use CREB-

dysregulated models for biological assessments of the activity of this molecule in the future. Further, a particular observation on these results is that there is a 10-fold preference for the inhibition of the CBP KIX•pKID PPI over that of CBP•KIX Myb. Considering the differences in the binding modes of these TADs to KIX, as illustrated on Figure 3.15, a conclusion that can be derived is that the D2A analog may bind in a unique form with the KIX domain, this being the basis for the selectivity of inhibiting this PPI over that of Myb.

Given the results above, the next step in the characterization of the activity of LPPM-8-D2A, was to define the binding site on CBP KIX. To this end, ^1H ^{15}N HSQC spectroscopy was performed with titrations of the LPPM-8-D2A molecule. As illustrated on Figure 3.16, most of the chemical shift perturbations (CSPs) on KIX (75 µM) in the presence of 1.1 equivalents of this analog are located along the α1 helix. At 2 equivalents of LPPM-8-D2A, residues with CSPs >2 standard deviations are present on both of the 3_{10}-helices. At the concentrations of LPPM measured, there are no significant perturbations of the residues at the MLL binding surface (F612, Y631), rather, residues adjacent to this binding site were perturbed (V604, V08, I611, D622, also see Figure 3.17). CSP shifts at these residues have been previously observed in the binding of other inhibitors to KIX, and correlate with what has been described as an allosteric small molecule binding site on the protein domain.[25, 41] Considering the single-digit µM inhibition of both MLL and pKID interactions by LPPM-8-D2A, and its binding outside the interaction area of these TADs, it can be concluded that this molecule acts mainly as an allosteric inhibitor of KIX PPIs.
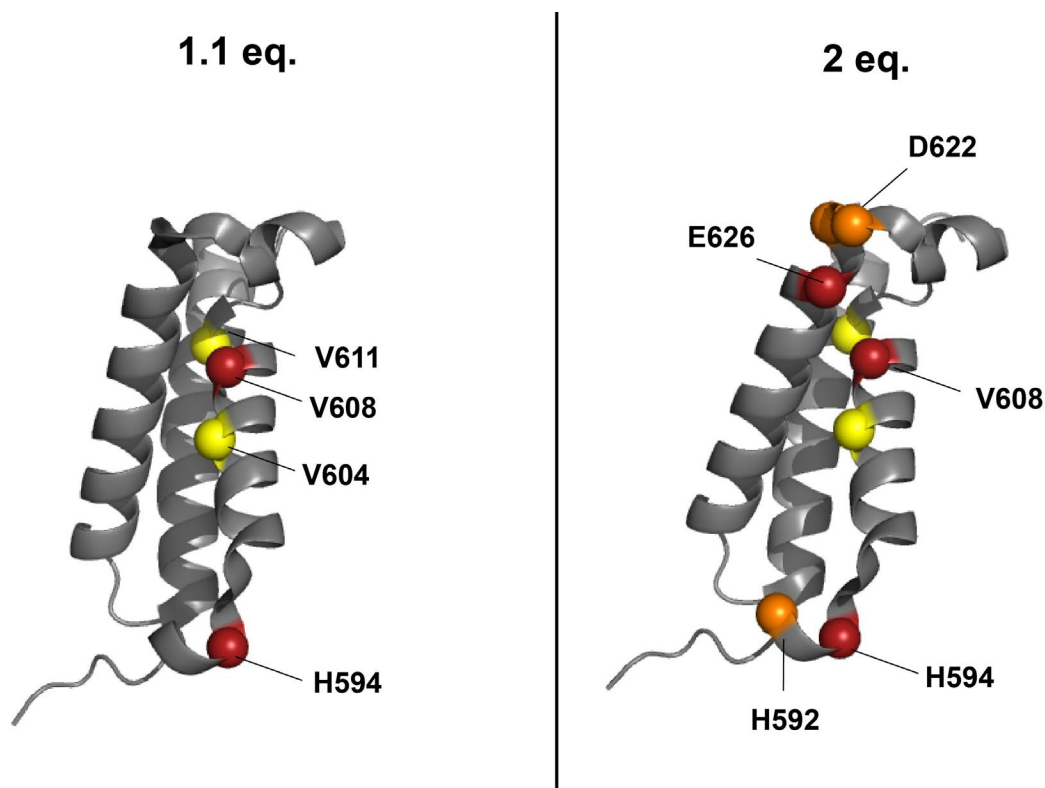
Figure 3.16 ^{1}H, ^{15}N-HSQC CSPs induced by binding of 1.1 eq (left) and 2 eq. (right) of LPPM-8-D2A mapped onto CBP KIX (PDB ID 2AGH). Yellow = 1-2 standard deviations of the average CSP, orange = 2-3 standard deviations, red ≥ 3 standard deviations. All perturbed residues above 1 standard deviation) found in Appendix Figures C.10-C.13

Interestingly, titration of analog LPPM-8-E1A, which inhibits the CBP KIX•MLL PPI with 30-fold lower affinity than LPPM-8-D2A (Figure 3.4), induces CSPs on KIX with a slightly different pattern. For instance, both analogs lead to changes at residues on the α1 helix (R624, V608, V694, I611) but only D1A also leads to perturbation of residue Y658 at both 1.1 and 2 equivalents (Appendix Figures C.14-18). This residue is part of the Myb/ pKID binding surface and the allosteric network between the two TAD binding sites on KIX. However, since this analog inhibits these PPIs with a K_i > 50 μM, the perturbation of Y658 may be due to non-specific binding. Given that LPPM-E1A/D2A only differ in the location of both a negative charge and an alanine on their sequence, it is possible that

this leads to the difference in the engagement of the residues at the 3-$_{10}$ helices of KIX, which contains some acidic residues. Overall, LPPM-8-D2A interacts with KIX and inhibits its PPIs through a different mechanism than how LPPM-8 inhibits Med25 PPIs (See Chapter 2). These results highlight the versatility and potential of this scaffold to be derivatized into inhibitors of structurally and mechanistically diverse coactivator ABDs.
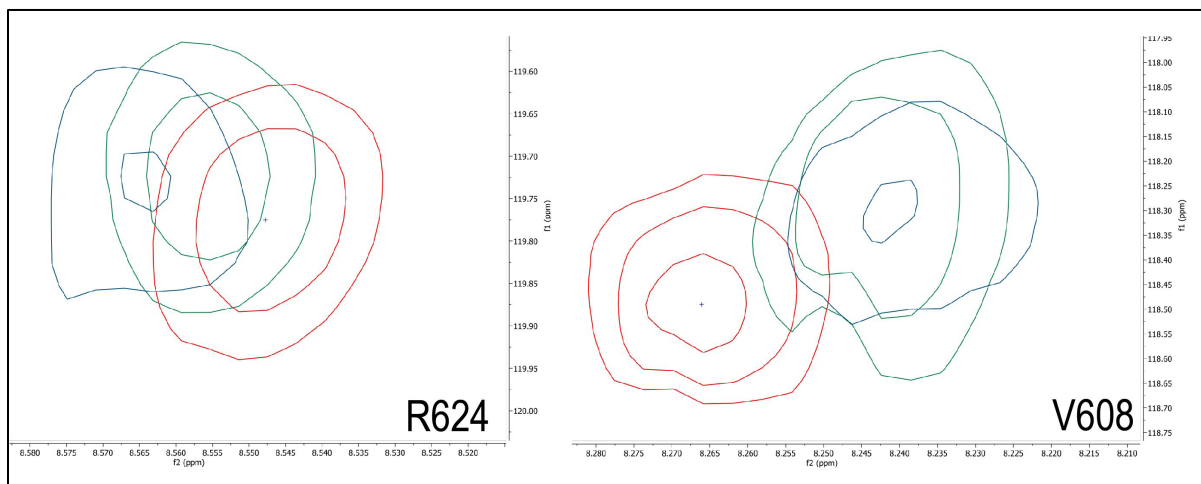
Figure 3.17 Overlay of ^{1}H, ^{15}N-HSQC CSPs of free CBP KIX (red), 1.1 eq LPPM-8-D2A (green) and 2 eq. of LPPM-8-D2A (blue) for KIX residues R624 and V608.

3.4 Conclusions and Future Directions

There are multiple structural and dynamic challenges in the targeting of coactivator PPIs. Historically, diverse approaches have been utilized in the discovery of small molecules and design of peptide-based probes to inhibit these PPIs. Often, promising scaffolds are either very specific in their design for a particular target or are non-selective across a group of coactivators. A current need in the field is a generalizable strategy to develop PPI inhibitors that can be derived from a core scaffold and that yields selective analogs for different coactivator proteins. The first step in this process is the identification of a modifiable inhibitor of coactivator PPIs with tunable target selectivity.

109

In this chapter, we report on the biochemical and biophysical characterization of the selectivity switch of the target coactivator of lipopeptidomimetic molecules. LPPM-8-D2A, displays a change in its selectivity for CBP KIX over Med25 AcID. We define this switch to be specific to the modification of the amino acid at location 2 from an aspartic acid to an alanine and determine that the same form of modification at another location within the peptide sequence does not lead to the same form of selectivity switch. We demonstrate that LPPM-8-D2A has a degree of selectivity for CBP KIX among other ABDs in CBP, and among the GACKIX family of protein domains, even though this sequence can still be optimized further for selectivity. We observe the allosteric inhibition of KIX PPIs in both *in-vitro* and structural characterizations. These studies also corroborate that in the design of lipopeptidomimetics to target coactivator proteins, the length, and properties of the lipid in the molecule that improve the affinity of a peptide for a particular coactivator are consistent across targets. That is, a mid-chain fatty acid is required to achieve an inhibitory activity in the low-micromolar range. Future work in the characterization of LPPM-8-D2A as an inhibitor of CBP KIX PPIs includes the assessment of its activity in cellular models of dysregulated CBP function.

From these results, we conclude that the design of lipopeptidomimetics is an approach to yield selective and modifiable molecules with potent affinities for coactivator PPIs. We propose that leveraging this strategy in combination with robust methods for molecule diversification, screening platforms and affinity maturation, has the potential to generate inhibitors for a variety of challenging coactivator targets. This work features the potential of lipidation as an underexplored avenue in this field for enhancing the inhibitory activity of a peptide, and it also highlights the open questions of the role of lipids in

transcription. An additional direction from the results of this work, is the dissection of the role of lipids at different stages of transcription, as a way to better define the mechanisms through which lipidation improves the affinity and selectivity of TAD-like peptides.

3.5 Materials and Methods

Protein Expression and Purification

CBP KIX

CBP KIX (586-672) was expressed as previously described with minor modifications.[25] Plasmid was transformed via heat-shock into competent E. coli BL21 (DE3) cells. The cells were then plated on LB agar plates with selection antibiotic. A 5 mL overnight culture was prepared from plated colonies in LB, and it was used to inoculate a 1-L TB culture supplemented with 0.1 mg/mL of ampicillin.^{13}C,^{15}N-labeled CBP KIX was similarly expressed. Plasmid was transformed via heat-shock into competent E. coli BL21 (DE3) cells. The cells were then plated on LB agar plates with selection antibiotic. A 50 mL overnight culture was prepared from plated colonies in LB, and it was used on inoculate a 1L culture of M9 minimal media supplemented with 0.1 mg/mL of ampicillin, 1 g/L ^{15}NH$_4$Cl, 2 g/L ^{13}C-D-glucose, and 0.5% ^{13}C,^{15}N-labeled Bioexpress media (all labeled components were purchased from Cambridge Isotopes). Before inoculation, the overnight culture was pelleted, and media exchanged into the same M9 minimal media.

Protein purification was performed according to previously described methods using an AKTA Pure FPLC.[42, 43] Cell pellets were resuspended in ~35 mL lysis buffer (10 mM phosphate, 300 mM NaCl, 10 mM imidazole, pH 7.2), 40 µL β-mercaptoethanol, and a cOmplete protease inhibitor tablet (Roche). Cells were lysed by sonication and insoluble cellular material was pelleted by centrifugation at 9500 rpm for 20 min at 4ºC. The lysate

filtered and loaded onto an AKTA Pure FPLC equipped with a 5 mL Ni HisTrap HP column (GE Healthcare) pre-equilibrated with wash buffer (10 mM phosphate, 300 mM NaCl, 10 mM imidazole, pH 7.2). CBP KIX was then purified using a gradient of 10–600 mM imidazole (other buffer components were constant), and fractions containing CBP KIX were pooled and subjected to secondary purification using a HiTrap SP HP cation exchange column (GE Healthcare) using buffer (50 mM sodium phosphate, 1 mM dithiothreitol (DTT), pH 7.2) with gradient of 0-1 M NaCl. Previous to column loading, a secondary cOmplete protease inhibitor tablet (Roche) was dissolved into the pooled fractions. Upon elution, fractions containing pure protein were dialyzed into storage buffer (10 mM sodium phosphate, 100 mM NaCl, 10% glycerol, pH 6.8) or NMR buffer (20 mM sodium phosphate, 150 mM NaCl, pH 6.5) overnight at 4ºC. Concentration was determined via ultraviolet/visible (UV/Vis) spectroscopy on a NanoDrop instrument at 280 nm using an extinction coefficient of 12,950 $M^{-1}cm^{-1}$. Aliquots were flash frozen in liquid N2 and stored at –80 ºC until further use. Protein identity was confirmed by mass spectrometry (Agilent 6545 LC/Q-TOF) and purity was assessed via sodium dodecyl sulphate–polyacrylamide gel electrophoresis (SDS-PAGE) on a 4-20% tris-glycine (Biorad) gel stained using Quick Coomassie (Anatrace).

ARC105 KIX

ARC105 KIX (1-78) from plasmid pET-15B His6-ARC105(1-78) was expressed as previously described with minor modifications.[44] Plasmid was transformed via heat-shock into competent E. coli BL21 (DE3) cells. The cells were then plated on LB agar plates with selection antibiotic. A 10 mL overnight culture was prepared from plated colonies in LB, and it was used to inoculate a 1-L TB culture supplemented with 0.1 mg/mL of

ampicillin. The culture was grown at 37ºC (250 rpm) until an OD_{600} of 0.6.-0.8 was reached. The culture was cooled to 21ºC for 1 hour, and expression was induced with addition of isopropyl β-D-1-thiogalactopyranoside (IPTG, final concentration 0.1 mM). Cultures were grown overnight at 21ºC (250 rpm), and the next morning the cells were pelleted by centrifugation at 6000 rpm at 4 ºC for 30 minutes.

Pellets were flash frozen in liquid N_2 and stored at -80ºC until lysis. Cell pellets were resuspended in ~35 mL lysis buffer (10 mM phosphate, 300 mM NaCl, 10 mM imidazole, pH 7.2), 40 µL β-mercaptoethanol, and a cOmplete protease inhibitor tablet (Roche). Cells were lysed by sonication and insoluble cellular material was pelleted by centrifugation at 9500 rpm for 20 min at 4ºC. The lysate was filtered and loaded onto an AKTA Pure FPLC equipped with a 5 mL Ni HisTrap HP column (GE Healthcare) pre-equilibrated with wash buffer (10 mM phosphate, 300 mM NaCl, 10 mM imidazole, pH 7.2). Arc105 KIX was then purified using a gradient of 10–600 mM imidazole (other buffer components were constant), and fractions containing Arc105 KIX were pooled and subjected to secondary purification using a HiTrap SP HP cation exchange column (GE Healthcare) using buffer (50 mM sodium phosphate, 1 mM dithiothreitol (DTT), pH 7.2) with gradient of 0-1 M NaCl. Previous to column loading, a secondary cOmplete protease inhibitor tablet (Roche) was dissolved into the pooled fractions. Upon elution, fractions containing pure protein were dialyzed into storage buffer (10 mM sodium phosphate, 100 mM NaCl, 10% glycerol, pH 6.8) overnight at 4ºC. Concentration was determined via ultraviolet/visible (UV/Vis) spectroscopy on a NanoDrop instrument at 280 nm using an extinction coefficient of 6,990 $M^{-1}cm^{-1}$. Aliquots were flash frozen in liquid N_2 and stored at –80ºC until further use. Protein identity was confirmed by mass spectrometry (Agilent

6545 LC/Q-TOF) and purity was assessed via sodium dodecyl sulphate–polyacrylamide gel electrophoresis (SDS-PAGE) on a 4-20% tris-glycine (Biorad) gel stained using Quick Coomassie (Anatrace).

CBP TAZ1

The expression plasmid for CBP TAZ1(324-423) was generously provided by Prof. Paramjit Arora.[26, 45] Protein was expressed in BL21 DE3 E. coli. Cells were grown in LB containing 0.1 mg/mL ampicillin and 1 mM $ZnCl_2$ to an optical density (OD 600 nm) of 0.8 (37°C, 250 rpm), cooled to 22°C and induced with 100 µM IPTC for 5 hours. Cells were harvested by centrifugation (20 min, 6500xg) and stored at -80°C. Cell pellets were lysed by sonication in lysis buffer (50 mM Tris, 150mM NaCl, pH 6.3) containing cOmplete protease inhibitor (Roche, 11873580001). The GST tagged protein was affinity purified using a GSTrap column (GE Healthcare). After initial binding of the protein to the column, elution was conducted using a buffer containing 10 mM reduced glutathione. An additional round of purification was completed using ion-exchange chromatography on a Source S column (GE Healthcare) in phosphate buffer (50 mM, 1 mM DTT, pH 7.2) by eluting with a NaCl gradient from 0 to 1M. Purified protein was buffer-exchanged by dialysis (overnight, 4°C) into 10 mM Tris, 100 mM NaH2PO4, 10% glycerol, 1mM DTT, 100 µM ZnCl2, pH 6.8. Purity was determined by Coomassie stained polyacrylamide gel. Protein concentration was determined by UV-Vis spectroscopy using an extinction coefficient, $\varepsilon=$ 49,110 $M^{-1}cm^{-1}$. Purified protein samples (>90% pure) were aliquoted and stored at -80°C.

Solid phase synthesis and purification of activator peptides

Activator peptides were synthesized using rink amide resin (CEM) using standard Fmoc solid-phase peptide synthesis protocols as previously described.[25, 26, 46]. The

peptides were cleaved with 95% trifluoroacetic acid (TFA, Sigma Aldrich), 2.5% triisopropylsilane (TIPS, Sigma Aldrich), and 2.5% H_2O solution for two hours, and subsequently precipitated with chilled diethyl ether. The products were purified to homogeneity using reverse-phase HPLC on a C18 column with a 10-40% solvent B gradient (A: 0.1% TFA in water, B: acetonitrile) and stored at -20°C as DMSO stock solutions. The identity of each peptide was confirmed by LC-MS (Agilent 6545 LC/Q-TOF). FITC-labeled peptides were quantified on a NanoDrop instrument at 495 nm using extinction coefficient 72,000 $M^{-1}cm^{-1}$. Acetylated IBiD was quantified at 280 nm using extinction coefficient 1,490 $M^{-1}cm^{-1}$.

Solid phase synthesis and purification of LPPMs

Peptide portion of LPPMs were synthesized using either rink amide resin (CEM) or Fmoc-D-Val-Tentagel S TRT resin (Rapp Polymere) and standard Fmoc solid-phase peptide synthesis protocols as previously described.[46] LPPM-2-LPPM-5 were acetylated at the N-terminus using a cocktail of acetic anhydride and triethylamine (TEA, Fisher Scientific) in DCM for 30 min. Analogs LPPM-6 and LPPM-7 were coupled with undecanoic acid (5 equiv.) using 1:1:1 ratio of 0.5 M HBTU in DMF, 0.49 M HOBT in DMF, and 1.0 M DPIEA in DMF for 15 hr. Analogs LPPM-8 and LPPM-9 were coupled to pure (2S, 3R)-2-methyl-3hydroxyundecanoic acid (5 equiv.) using 1:1:1 ratio 0.5 M HBTU in DMF, 0.49 M HOBT in DMF, and 1.0 M DIPEA in DMF for 16 hr. Analog LPPM-10 was coupled to pure (2R, 3S)-2-methyl-3-hydroxyundecanoic acid (2 equiv.) using 1:1:1 ratio 0.5 M HBTU in DMF, 0.49 M HOBT in DMF, and 1.0 M DIPEA in DMF for 16 hr.

The peptides were cleaved with 95% trifluoroacetic acid (TFA, Sigma Aldrich), 2.5% triisopropylsilane (TIPS, Sigma Aldrich), and 2.5% H_2O solution for two hours, and

subsequently precipitated with chilled diethyl ether. The products were purified to homogeneity using reverse-phase HPLC on a C_{18} column with a 10-100% solvent B gradient (A: 0.1% TFA in water, B: acetonitrile) and stored at -20°C as DMSO stock solutions. The identity of each peptide was confirmed by LC-MS (Agilent 6545 LC/Q-TOF).

Direct binding assays

Dissociation constants (K_d) for fluorescein-labeled activator peptide tracers with respective coactivator ABDs were determined using fluorescence polarization as previously described.[25, 34, 35] For each experiment, 20 nM tracer was incubated with varying concentrations of protein in binding buffer (10 mM $NaPO_4$, 100 mM NaCl, 10% glycerol, 0.001% NP-40, pH 6.8) and incubated in a black 384 well low volume plate (Corning) for 30 minutes. Fluorescence polarization was detected using a BioTek plate reader equipped with the FI-FP module (485 nm/520 nm) and the dissociation constant was calculated using by fitting the formula below to the observed polarization values as a function of protein concentration. Data was analyzed using GraphPad Prism 10.

$$y = c + (b - c) \times \frac{(Kd + a + x) - \sqrt{(Kd + a + x)^2 - 4ax}}{2a}$$

Competition binding assays

Inhibition values (K_i, IC_{50}) for LPPMs were determined using a competitive fluorescence polarization assay format, as previously described.[26, 46, 47] Assays were run in experimental triplicate with a final sample volume of 20 µL, in a low volume, black, 384-well plate (Corning) and read using a plate reader (BioTek) equipped with the FI-FP module (485/520 nm). Each experiment used a final tracer concentration of 20 nM of FITC-labelled peptide and a concentration of protein equivalent to 3x the K_d in binding

buffer (10 mM NaPO$_4$, 100 mM NaCl, 10% glycerol, 0.001% NP-40, pH 6.8). Protein and tracer were precomplexed and incubated in the presence of serially diluted LPPM (50 nM to 400 µM) for 30 minutes. Polarization values were fit to a non-linear regression using the built-in equation "log(inhibitor) vs. response – variable slope (four parameters)" (shown below) in Prism 10 to derive IC$_{50}$ values. The IC$_{50}$ values were converted to K$_i$ values using the apparent K$_d$ value calculated from the direct binding experiments of each coactivator ABD•FITC-TAD complex using a K$_i$ calculator.[25] Reported K$_i$ values are the average of three biological replicates with the indicated error representing the standard deviation of the triplicates.

$$y = Bottom + (Top - Bottom)/(1 + 10^{(LogIC50-X)*HillSlope})$$

Differential Scanning Fluorimetry

Experiments were performed in technical triplicate of 20 µL sample volumes, as preciously described.[35, 46, 48] Assay buffer used was 25 mM sodium phosphate, 125 mM sodium chloride, 0.001% Triton X-100, and pH 7.8. To determine T$_m$, 8 µM protein in the presence of 5X SYPRO orange dye (1:1000 dilution in buffer of purchased 5000X stock in DMSO; Invitrogen) was incubated alone or with ligands at the indicated equivalents of compound at RT for 30 minutes. An Applied Biosystems StepOnePlus qPCR instrument was used to obtain melting curves by excitation at 488 nm and emission measured at 602 nm over a temperature gradient of 25–95°C with a 1 °C/min increase. Raw fluorescence data was imported into the online data analysis program, DSFworld, and Tm was calculated by determining the maximum of the first derivative (dRFU).[35, 49] For data visualization, raw fluorescence units and dRFU was plotted as a function of temperature using GraphPad Prism software. Change in melting temperature (ΔT$_m$) of each ligand was calculated as the difference between the Tm of the protein and the Tm of the protein

+ ligand. Reported values are the averages of biological duplicates and their indicated error representing the standard deviation of the duplicates.

NMR Spectroscopy

NMR assignments of CBP KIX (586-672) were determined from previous studies using ^{15}N-labeled protein.[34, 50, 51] Constant time ^{1}H,^{15}N-HSQC experiments were performed using 75 µM ^{13}C,^{15}N-labeled CBP KIX in NMR buffer (20 mM sodium phosphate pH 6.5, 150 mM NaCl, 3 mM DTT, 10% D2O, and 2% DMSO) on a Bruker 600 MHz instrument equipped with a cryoprobe. Data processing and visualization was performed using Mestrenova. Ligand-protein complexes were assessed at titration points of 0.2, 0.5, 0.8, 1.1, 2, and 3 equivalents of compound, relative to protein concentration. Control spectra were obtained with CBP KIX, DTT, D$_2$O and DMSO only. Chemical shift perturbations ($\Delta\delta$) were calculated from the proton ($\Delta\delta$H) and carbon ($\Delta\delta$C) chemical shifts by:

$$\Delta\delta = \sqrt{(abs(\Delta\delta_H)^2) + (abs(\Delta\delta_N)^2)}$$

3.6 References

References

(1) Evans, B. E.; Rittle, K. E.; Bock, M. G.; DiPardo, R. M.; Freidinger, R. M.; Whitter, W. L.; Lundell, G. F.; Veber, D. F.; Anderson, P. S.; Chang, R. S.; et al. Methods for drug discovery: development of potent, selective, orally effective cholecystokinin antagonists. *J Med Chem* **1988**, *31*, 2235-2246. DOI: 10.1021/jm00120a002

(2) Zhao, H.; Dietrich, J. Privileged scaffolds in lead generation. *Expert Opin Drug Discov* **2015**, *10*, 781-790. DOI: 10.1517/17460441.2015.1041496

(3) Bartlett, P. A.; Entzeroth, M.; Royal Society of, C. *Exploiting chemical diversity for drug discovery*; Royal Society of Chemistry Cambridge, UK, 2006.

(4) Veselý, J.; Havlicek, L.; Strnad, M.; Blow, J. J.; Donella-Deana, A.; Pinna, L.; Letham, D. S.; Kato, J.; Detivaud, L.; Leclerc, S.; et al. Inhibition of cyclin-dependent kinases by purine analogues. *Eur J Biochem* **1994**, *224*, 771-786. DOI: 10.1111/j.1432-1033.1994.00771.x

(5) An, J.; Totrov, M.; Abagyan, R. Pocketome via comprehensive identification and classification of ligand binding envelopes. *Mol Cell Proteomics* **2005**, *4*, 752-761. DOI: 10.1074/mcp.M400159-MCP200

(6) Clackson, T.; Wells, J. A. A hot spot of binding energy in a hormone-receptor interface. *Science* **1995**, *267*, 383-386. DOI: 10.1126/science.7529940

(7) Kozakov, D.; Hall, D. R.; Chuang, G. Y.; Cencic, R.; Brenke, R.; Grove, L. E.; Beglov, D.; Pelletier, J.; Whitty, A.; Vajda, S. Structural conservation of druggable hot spots in protein-protein interfaces. *Proc Natl Acad Sci U S A* **2011**, *108*, 13528-13533. DOI: 10.1073/pnas.1101835108

(8) Ding, K.; Lu, Y.; Nikolovska-Coleska, Z.; Qiu, S.; Ding, Y.; Gao, W.; Stuckey, J.; Krajewski, K.; Roller, P. P.; Tomita, Y.; et al. Structure-based design of potent non-peptide MDM2 inhibitors. *J Am Chem Soc* **2005**, *127*, 10130-10131. DOI: 10.1021/ja051147z

(9) Popowicz, G. M.; Czarna, A.; Wolf, S.; Wang, K.; Wang, W.; Dömling, A.; Holak, T. A. Structures of low molecular weight inhibitors bound to MDMX and MDM2 reveal new approaches for p53-MDMX/MDM2 antagonist drug discovery. *Cell Cycle* **2010**, *9*, 1104-1111. DOI: 10.4161/cc.9.6.10956

(10) Ran, X.; Gestwicki, J. E. Inhibitors of protein-protein interactions (PPIs): an analysis of scaffold choices and buried surface area. *Curr Opin Chem Biol* **2018**, *44*, 75-86. DOI: 10.1016/j.cbpa.2018.06.004

(11) Breen, M. E.; Mapp, A. K. Modulating the masters: chemical tools to dissect CBP and p300 function. *Current Opinion in Chemical Biology* **2018**, *45*, 195–203. DOI: https://doi.org/10.1016/j.cbpa.2018.06.005

(12) Weinert, B. T.; Narita, T.; Satpathy, S.; Srinivasan, B.; Hansen, B. K.; Schölz, C.; Hamilton, W. B.; Zucconi, B. E.; Wang, W. W.; Liu, W. R.; et al. Time-Resolved Analysis Reveals Rapid Dynamics and Broad Scope of the CBP/p300 Acetylome. *Cell* **2018**, *174*, 231-244.e212. DOI: 10.1016/j.cell.2018.04.033

(13) Song, C. Z.; Keller, K.; Chen, Y.; Murata, K.; Stamatoyannopoulos, G. Transcription coactivator CBP has direct DNA binding activity and stimulates transcription factor DNA binding through small domains. *Biochem Biophys Res Commun* **2002**, *296*, 118–124. DOI: 10.1016/s0006-291x(02)00842-2

(14) Iyer, N. G.; Özdag, H.; Caldas, C. p300/CBP and cancer. *Oncogene* **2004**, *23*, 4225-4231. DOI: 10.1038/sj.onc.1207118

(15) Chen, Q.; Yang, B.; Liu, X.; Zhang, X. D.; Zhang, L.; Liu, T. Histone acetyltransferases CBP/p300 in tumorigenesis and CBP/p300 inhibitors as promising novel anticancer agents. *Theranostics* **2022**, *12*, 4935-4948. DOI: 10.7150/thno.73223

(16) Thakur, J. K.; Yadav, A.; Yadav, G. Molecular recognition by the KIX domain and its role in gene regulation. *Nucleic Acids Res* **2014**, *42*, 2112-2125. DOI: 10.1093/nar/gkt1147

(17) Brüschweiler, S.; Schanda, P.; Kloiber, K.; Brutscher, B.; Kontaxis, G.; Konrat, R.; Tollinger, M. Direct Observation of the Dynamic Process Underlying Allosteric Signal Transmission. *Journal of the American Chemical Society* **2009**, *131*, 3063-3068. DOI: 10.1021/ja809947w

(18) Brüschweiler, S.; Konrat, R.; Tollinger, M. Allosteric Communication in the KIX Domain Proceeds through Dynamic Repacking of the Hydrophobic Core. *ACS Chemical Biology* **2013**, *8*, 1600-1610. DOI: 10.1021/cb4002188

(19) Gianni, S.; Morrone, A.; Giri, R.; Brunori, M. A folding-after-binding mechanism describes the recognition between the transactivation domain of c-Myb and the KIX domain of the CREB-binding protein. *Biochem Biophys Res Commun* **2012**, *428*, 205-209. DOI: 10.1016/j.bbrc.2012.09.112

(20) Wang, N.; Lodge, J. M.; Fierke, C. A.; Mapp, A. K. Dissecting allosteric effects of activator–coactivator complexes using a covalent small molecule ligand. *Proceedings of the National Academy of Sciences* **2014**, *111*, 12061-12066. DOI: 10.1073/pnas.1406033111

(21) Peiffer, A. L.; Garlick, J. M.; Joy, S. T.; Mapp, A. K.; Brooks, C. L., 3rd. Allostery in the dynamic coactivator domain KIX occurs through minor conformational micro-states. *PLoS Comput Biol* **2022**, *18*, e1009977. DOI: 10.1371/journal.pcbi.1009977

(22) Boehr, D. D.; Nussinov, R.; Wright, P. E. The role of dynamic conformational ensembles in biomolecular recognition. *Nature Chemical Biology* **2009**, *5*, 789-796. DOI: 10.1038/nchembio.232

(23) Singh, G. P.; Ganapathi, M.; Dash, D. Role of intrinsic disorder in transient interactions of hub proteins. *Proteins* **2007**, *66*, 761-765. DOI: 10.1002/prot.21281

(24) Wang, N.; Majmudar, C. Y.; Pomerantz, W. C.; Gagnon, J. K.; Sadowsky, J. D.; Meagher, J. L.; Johnson, T. K.; Stuckey, J. A.; Brooks, C. L., III; Wells, J. A.; et al. Ordering a Dynamic Protein Via a Small-Molecule Stabilizer. *Journal of the American Chemical Society* **2013**, *135*, 3363-3366. DOI: 10.1021/ja3122334

(25) Breen, M. E.; Joy, S. T.; Baruti, O. J.; Beyersdorf, M. S.; Henley, M. J.; De Salle, S. N.; Ycas, P. D.; Croskey, A.; Cierpicki, T.; Pomerantz, W. C. K.; et al. Garcinolic Acid Distinguishes Between GACKIX Domains and Modulates Interaction Networks. *ChemBioChem* **2023**, *24*. DOI: 10.1002/cbic.202300439

(26) Joy, S. T.; Henley, M. J.; De Salle, S. N.; Beyersdorf, M. S.; Vock, I. W.; Huldin, A. J. L.; Mapp, A. K. A Dual-Site Inhibitor of CBP/p300 KIX is a Selective and Effective

Modulator of Myb. *Journal of the American Chemical Society* **2021**, *143*, 15056-15062. DOI: 10.1021/jacs.1c04432

(27) Liu, Y.; Joy, S. T.; Henley, M. J.; Croskey, A.; Yates, J. A.; Merajver, S. D.; Mapp, A. K. Inhibition of CREB Binding and Function with a Dual-Targeting Ligand. *Biochemistry* **2024**, *63*, 1-8. DOI: 10.1021/acs.biochem.3c00469

(28) Ramaswamy, K.; Forbes, L.; Minuesa, G.; Gindin, T.; Brown, F.; Kharas, M. G.; Krivtsov, A. V.; Armstrong, S. A.; Still, E.; de Stanchina, E.; et al. Peptidomimetic blockade of MYB in acute myeloid leukemia. *Nature Communications* **2018**, *9*, 110. DOI: 10.1038/s41467-017-02618-6

(29) Sato, N.; Suetaka, S.; Hayashi, Y.; Arai, M. Rational peptide design for inhibition of the KIX-MLL interaction. *Sci Rep* **2023**, *13*, 6330. DOI: 10.1038/s41598-023-32848-2

(30) Lodge, J. M.; Majmudar, C. Y.; Clayton, J.; Mapp, A. K. Covalent Chemical Cochaperones of the p300/CBP GACKIX Domain. *Chembiochem* **2018**, *19*, 1907-1912. DOI: 10.1002/cbic.201800173

(31) Modell, A. E.; Marrone, F., III; Panigrahi, N. R.; Zhang, Y.; Arora, P. S. Peptide Tethering: Pocket-Directed Fragment Screening for Peptidomimetic Inhibitor Discovery. *Journal of the American Chemical Society* **2022**, *144*, 1198–1204. DOI: 10.1021/jacs.1c09666

(32) Suetaka, S.; Oka, Y.; Kunihara, T.; Hayashi, Y.; Arai, M. Rational design of a helical peptide inhibitor targeting c-Myb–KIX interaction. *Scientific Reports* **2022**, *12*, 816. DOI: 10.1038/s41598-021-04497-w

(33) Majmudar, C. Y.; Højfeldt, J. W.; Arevang, C. J.; Pomerantz, W. C.; Gagnon, J. K.; Schultz, P. J.; Cesa, L. C.; Doss, C. H.; Rowe, S. P.; Vásquez, V.; et al. Sekikaic acid and lobaric acid target a dynamic interface of the coactivator CBP/p300. *Angew Chem Int Ed Engl* **2012**, *51*, 11258-11262. DOI: 10.1002/anie.201206815

(34) Nikolovska-Coleska, Z.; Wang, R.; Fang, X.; Pan, H.; Tomita, Y.; Li, P.; Roller, P. P.; Krajewski, K.; Saito, N. G.; Stuckey, J. A.; et al. Development and optimization of a binding assay for the XIAP BIR3 domain using fluorescence polarization. *Anal Biochem* **2004**, *332*, 261-273. DOI: 10.1016/j.ab.2004.05.055

(35) Wu, T.; Yu, J.; Gale-Day, Z.; Woo, A.; Suresh, A.; Hornsby, M.; Gestwicki, J. E. Three Essential Resources to Improve Differential Scanning Fluorimetry (DSF) Experiments. Cold Spring Harbor Laboratory: 2020.

(36) Zhang, Y.; Wang, S.; Hu, H.; Li, X. A systematic study of HIF1A cofactors in hypoxic cancer cells. *Scientific Reports* **2022**, *12*, 18962. DOI: 10.1038/s41598-022-23060-9

(37) Novatchkova, M.; Eisenhaber, F. Linking transcriptional mediators via the GACKIX domain super family. *Curr Biol* **2004**, *14*, R54-55. DOI: 10.1016/j.cub.2003.12.042

(38) Yang, F.; Vought, B. W.; Satterlee, J. S.; Walker, A. K.; Jim Sun, Z. Y.; Watts, J. L.; DeBeaumont, R.; Mako Saito, R.; Hyberts, S. G.; Yang, S.; et al. An ARC/Mediator subunit required for SREBP control of cholesterol and lipid homeostasis. *Nature* **2006**, *442*, 700-704. DOI: 10.1038/nature04942

(39) Oliner, J. D.; Andresen, J. M.; Hansen, S. K.; Zhou, S.; Tjian, R. SREBP transcriptional activity is mediated through an interaction with the CREB-binding protein. *Genes Dev* **1996**, *10*, 2903-2911. DOI: 10.1101/gad.10.22.2903

(40) Goto, N. K.; Zor, T.; Martinez-Yamout, M.; Dyson, H. J.; Wright, P. E. Cooperativity in transcription factor binding to the coactivator CREB-binding protein (CBP). The mixed

lineage leukemia protein (MLL) activation domain binds to an allosteric site on the KIX domain. *J Biol Chem* **2002**, *277*, 43168-43174. DOI: 10.1074/jbc.M207660200

(41) Gee, C. T.; Arntson, K. E.; Koleski, E. J.; Staebell, R. L.; Pomerantz, W. C. K. Dual Labeling of the CBP/p300 KIX Domain for 19F NMR Leads to Identification of a New Small-Molecule Binding Site. *ChemBioChem* **2018**, *19*, 963-969. DOI: 10.1002/cbic.201700686

(42) Block, K. M.; Wang, H.; Szabó, L. Z.; Polaske, N. W.; Henchey, L. K.; Dubey, R.; Kushal, S.; László, C. F.; Makhoul, J.; Song, Z.; et al. Direct Inhibition of Hypoxia-Inducible Transcription Factor Complex with Designed Dimeric Epidithiodiketopiperazine. *Journal of the American Chemical Society* **2009**, *131*, 18078-18088. DOI: 10.1021/ja807601b

(43) Garlick, J. M.; Sturlis, S. M.; Bruno, P. A.; Yates, J. A.; Peiffer, A. L.; Liu, Y.; Goo, L.; Bao, L.; De Salle, S. N.; Tamayo-Castillo, G.; et al. Norstictic Acid Is a Selective Allosteric Transcriptional Regulator. *Journal of the American Chemical Society* **2021**, *143*, 9297-9302. DOI: 10.1021/jacs.1c03258

(44) Wu, Z.; Belanger, G.; Brennan, B. B.; Lum, J. K.; Minter, A. R.; Rowe, S. P.; Plachetka, A.; Majmudar, C. Y.; Mapp, A. K. Targeting the Transcriptional Machinery with Unique Artificial Transcriptional Activators. *Journal of the American Chemical Society* **2003**, *125*, 12390-12391. DOI: 10.1021/ja036685v

(45) Majmudar, C. Y.; Højfeldt, J. W.; Arevang, C. J.; Pomerantz, W. C.; Gagnon, J. K.; Schultz, P. J.; Cesa, L. C.; Doss, C. H.; Rowe, S. P.; Vásquez, V.; et al. Sekikaic Acid and Lobaric Acid Target a Dynamic Interface of the Coactivator CBP/p300. *Angewandte Chemie International Edition* **2012**, *51*, 11258-11262. DOI: 10.1002/anie.201206815

(46) Pattelli, O. N.; Valdivia, E. M.; Beyersdorf, M. S.; Regan, C. S.; Rivas, M.; Hebert, K. A.; Merajver, S. D.; Cierpicki, T.; Mapp, A. K. A Lipopeptidomimetic of Transcriptional Activation Domains Selectively Disrupts Med25 Protein-Protein Interactions. *Angewandte Chemie International Edition* **2024**. DOI: 10.1002/anie.202400781

(47) Henderson, A. R.; Henley, M. J.; Foster, N. J.; Peiffer, A. L.; Beyersdorf, M. S.; Stanford, K. D.; Sturlis, S. M.; Linhares, B. M.; Hill, Z. B.; Wells, J. A.; et al. Conservation of coactivator engagement mechanism enables small-molecule allosteric modulators. *Proc Natl Acad Sci U S A* **2018**, *115*, 8960-8965. DOI: 10.1073/pnas.1806202115

(48) Shao, H.; Oltion, K.; Wu, T.; Gestwicki, J. E. Differential scanning fluorimetry (DSF) screen to identify inhibitors of Hsp60 protein-protein interactions. *Org Biomol Chem* **2020**, *18*, 4157-4163. DOI: 10.1039/d0ob00928h

(49) Sarabia, F.; Martín-Gálvez, F.; Chammaa, S.; Martín-Ortiz, L.; Sánchez-Ruiz, A. Chiral Sulfur Ylides for the Synthesis of Bengamide E and Analogues. *The Journal of Organic Chemistry* **2010**, *75*, 5526-5532. DOI: 10.1021/jo100696w

(50) Delaglio, F.; Grzesiek, S.; Vuister, G. W.; Zhu, G.; Pfeifer, J.; Bax, A. NMRPipe: a multidimensional spectral processing system based on UNIX pipes. *J Biomol NMR* **1995**, *6*, 277-293. DOI: 10.1007/bf00197809

(51) Lee, W.; Tonelli, M.; Markley, J. L. NMRFAM-SPARKY: enhanced software for biomolecular NMR spectroscopy. *Bioinformatics* **2015**, *31*, 1325-1327. DOI: 10.1093/bioinformatics/btu830

Chapter 4 Conclusions and Outlook

4.1 Summary

Coactivators are important interaction hubs within transcription and play a central role in activating gene programs to respond to extracellular cues and maintain homeostasis.[1] Dysregulation in their PPI network has been implicated in various cancers and neurological disorders, although the direct contribution to disease development is not always clearly understood.[2-4] Inhibitor development for these PPIs is a strategy to dissect the function of coactivators in dysregulated systems.[2] Historically, this has been challenging due to the large surface interfaces, the dynamic nature, and the recognition mechanisms of these systems.[5-8] These factors limit the structural information available for rational-design or structure-based approaches, especially for complex targets. While sequences within activator interaction surfaces have inherent ABD-recognition capabilities, as short peptides, they lack potency and selectivity.[9-15] We propose that peptides with TAD-like characteristics have potential as the basis for the development of inhibitor platforms when modified with activity-endowing groups, such as lipids.[16, 17] We test this strategy by developing lipopeptidomimetics (LPPMs) against the PPIs of two coactivators, Med25 AcID and CBP KIX, defining the molecular recognition characteristics for each case and determining the selectivity of respective LPPMs for each target. From these results, we propose that LPPMs are tunable scaffolds with the potential to become a generalizable strategy to inhibit coactivator PPIs.

4.2 Conclusions

This dissertation focused on characterizing LPPMs as selective inhibitors for coactivator PPIs. Chapter one surveyed the features of these proteins that complicate inhibitor development, ranging from their shallow structural topology to dynamic substructures and permissibility in interaction sequenes.[18-20] This introductory chapter also identified the minimal binding sequences of activator TADs as a basis for the developing peptide-based inhibitors, considering their use as synthetic activators of transcription when conjugated to DNA-binding sequences.[10, 12, 21-23] However, these short peptides are unsuitable as coactivator PPI inhibitors when unconstrained or unmodified.[24, 25] Thus, the chapter concluded with the proposal of lipid-conjugation to the N-terminus of TAD-like peptides to enhance the molecule's affinity and selectivity for coactivators *in-vitro*, and increase its stability and permeability in cells.

Chapter two demonstrated the strategy's viability by employing a peptide that mimics TAD composition against the PPIs of Med25.[18, 23, 26, 27] We found that the incorporation of a medium-chain, branched fatty acid to a heptameric peptide, LPPM-8, increases its activity >20 fold, and makes it a selective molecule for Med25 PPIs. Correlating the structure, protein interaction, and inhibitory activity across analog libraries, we uncovered contributions from lipid structure, peptide residues, and the molecule's C-terminal moiety to LPPM-8's effectiveness. We identified the binding mode of LPPM-8 using ^1H ^{13}C HSQC spectroscopy and identify the binding site as the H2 face of the Activator Interacting Domain (AcID) of Med25, categorizing LPPM-8 primarily as an orthosteric inhibitor. Upon verification of the biological activity of this molecule in cells, we then set out to identify whether this strategy could apply to other coactivator PPIs.

In chapter three, with the ultimate goal of defining whether this strategy has potential as a generalizable approach to develop coactivator PPI inhibitors, we tested our libraries of analogs against the complex of CBP KIX•MLL. We identify that changes to LPPMs within the peptide sequence result in the modification of the selectivity of these molecules for a different coactivator target. Specifically, the D2A change of the sequence EDLLLLV, leads to a 10-fold selectivity switch towards the inhibition of CBP KIX•MLL over that of Med25 PPIs. This switch was validated by assessing the selectivity of this LPPM across CBP ABD domains, and ARC105, another member of the GACKIX family of proteins. We corroborate that appending a mid-chain fatty acid to the 7-mer is necessary for the inhibition of KIX PPIs with high affinity, aligning with characteristics of Med25-targeting LPPMs. We also mapped LPPM-8-D2A's binding site on KIX, illuminating engagement with the domain's allosteric network.

4.3 Future Directions

Findings presented in this dissertation illuminate the LPPM strategy's potential as a powerful tool for enhancing the activity of peptide-based inhibitors, particularly for targets like coactivators with dynamic substructures, extensive binding surfaces, and intricate mechanisms of molecular recognition. Going forward, research can leverage these findings, moving from a proof-of concept phase to a systematic approach for inhibitor design. This section outlines potential paths for establishing this strategy as a streamlined platform for discovering novel LPPMs against diverse targets.

4.3.1 Further assessment of the binding and activity for KIX of LPPM-8-D2A

The immediate next step in the assessment of the selectivity switch of LPPM-8-D2A as an inhibitor of CBP KIX PPIs, is the verification of its activity in a biological setting, specifically, in disease models of dysregulated KIX PPIs. Given the *in-vitro* characterization of the inhibition of the PPI network of KIX presented in chapter three, a promising context to test the effect of LPPM-8-D2A in endogenous CBP, are models of dysregulation in the PPIs between CBP and the Cyclic-AMP response element binding protein (CREB). CREB has been defined as a proto-oncogene in different tumor types, given its involvement in the activation of gene programs related to cell differentiation, proliferation and survival in nerve cells.[28, 29] Upon the phosphorylation of the kinase inducible domain (KID) of CREB, the domain interacts with KIX and kick starts gene expression.[30]

Considering the affinity of LPPM-8-D2A for inhibiting the CBP KIX•pKID interaction is about 1 µM, models where this interaction is dysregulated are an optimal context for biological assessment of LPPM activity. As determined by the tool DepMap, an online consortium for defining a cancer dependency map,[31] gliomas and rhabdomyosarcomas are examples of these. The specific questions to be answered in this context, include: is there engagement of full-length CBP by the LPPM in the context of the full proteome? Is transcription of CBP•CREB-dependent genes affected by the treatment of LPPM-8-D2A? Is there interference of the intracellular complex formed between CBP KIX and CREB pKID? Answering these questions would provide a better framework for the translation of activity of LPPMs in cellular systems from *in-vitro* characterization campaigns. Furthermore, it would provide support to the case for the use of LPPMs as a strategy to develop bioactive, selective, and potent inhibitors.

Furthermore, complementing our current findings with a binding model using a molecular dynamics framework, based on the invitro and structural data presented in chapter three, could better inform on the specific role in binding of the LPPM features that we know are necessary in high affinity inhibitors. Put together, these data may provide a pathway into future targets to test this strategy with. Additionally, given our current basis of the aspects that are consistent in the activity of LPPMs across targets, the data obtained from this future direction may aid in the optimization of specific questions to pursue in the characterization of future LPPMs.

4.3.2 Optimizing high-throughput LPPM synthesis and screening

A direction to enhance the breadth of the LPPM approach, is the capitalization of high-throughput library development as part of the screening methodology. Given the two-fragment modality of the lipopeptidomimetics, that is, the lipid and the peptide, there are several ways in which the high-throughput diversification of these two fragments could be prioritized. For instance, this could take the form of incorporating a screening step where a form of combinatorial peptide library or selection platform is utilized to identify high-affinity binders pre-emptive to the lipidation step.[32-34] Considering the recent advances in screening for peptide-based PPI inhibitors, at this stage one could also integrate peptide modification strategies such as cyclization or stapling, depending on the specific protein targets.[35, 36] Taken together, an example of these options may be the screening of macrocyclic peptides using an mRNA display platform. Once a peptide with a good starting affinity is identified, relative to an identified benchmark, the lipidation step would follow. A diverse selection of lipids would then be used to modify the identified hits from

the library/evolution step. Given the limited record on the function of lipids within transcription, there is a wide variety of lipid structures that could be screened at this stage.
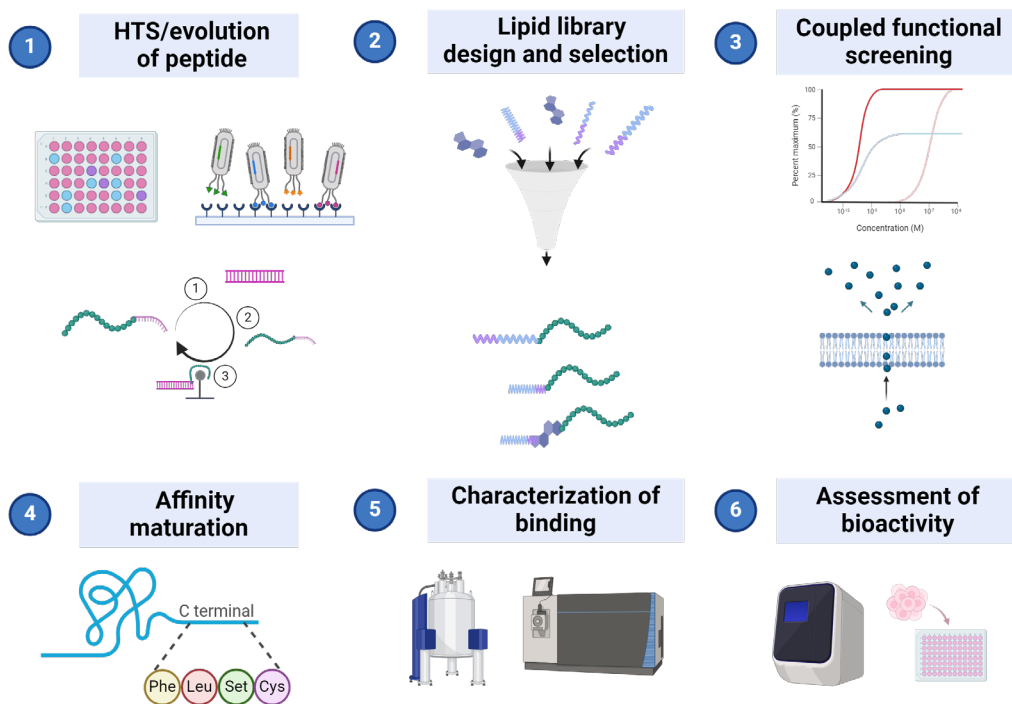
Figure 4.1. Potential workflow for robust development and screening of LPPMs for novel targets. Figure created with BioRender.com.

Based on our data, we predict that this form of peptide production and screening could drastically increase the quality of hits identified for a particular target, and the resulting activity of the molecules could continue to be improved following lipidation and additional affinity maturation strategies. Evidence that supports this strategy comes from a recent example of a synthetic, stapled lipopeptide that binds to the spike protein of COVID-19 to prevent infection.[37] Depending on the goal for utilizing the LPPM strategy, screening platforms that account for additional molecular and biological properties can be incorporated during the initial selection and testing of the LPPMs. One that is particularly novel in the field, and that is particularly suited for this type of molecules given the lipid

portion of the LPPMs, is to screen for membrane permeability in conjunction with screening for activity.[38] There is a wide range of forms the optimization of this strategy can take place, but the target and the goal can direct the design of such adaptation of this workflow. Ultimately, the limited utilization of lipidated peptides for targeting challenging proteins, in conjunction with the data presented in this dissertation and the possibilities to increase the robustness in screening, together provide an insight into the potential of this strategy for the development of potent PPI inhibitors.

4.3.3 Application of the LPPM strategy beyond coactivator complexes

Outside of coactivator•activator PPIs in transcriptional activation, other components of the transcriptional machinery interact with similar mechanisms and structural features that resemble those of the proteins characterized in this dissertation. For instance, certain domains of general transcription factors (GTFs), can act as coactivators by binding to activators in a distinct context from enhancer-located transcriptional activation models. For example, domains within TFIID and TFIIH engage in PPIs with TADs of activators to initiate gene expression, oftentimes a mechanism that is also dysregulated in different forms of disease and isn't well understood.[39, 40] In some cases, these PPIs also have therapeutic relevance and occur over broad, dynamic surfaces. The PPIs between GTFs and activators may then be defined as targets to inhibit using LPPMs.
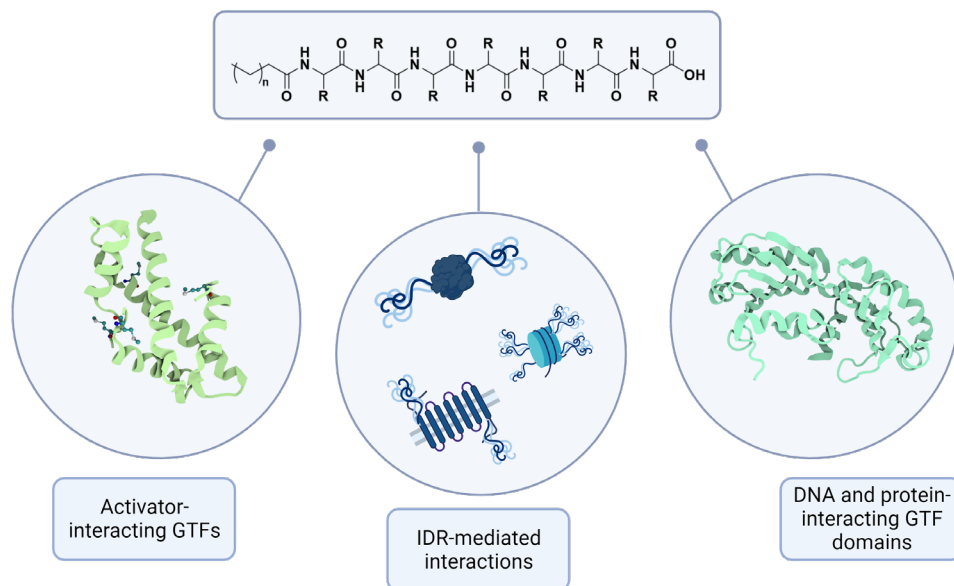
Figure 4.2. Potential applications of the LPPM inhibitor development approach beyond coactivator•activator PPIs. Figure created with BioRender.com.

Other families of proteins sharing characteristics with coactivators, including dynamic and intrinsically disordered regions found in nuclear and extracellular receptors, and proteins involved in genome maintenance and epigenetic regulation, also could be viable LPPM targets.[18] In these systems, it is also well understood that the dynamic regions within them are important in their function, and targeting them using the LPPM approach by incorporating the design strategies outlined in 4.3.2, could provide a powerful source of inhibitors of their function.

4.4 References

References

(1) Ptashne, M.; Gann, A. Transcriptional activation by recruitment. *Nature* **1997**, *386*, 569–577. DOI: 10.1038/386569a0

(2) Darnell, J. E., Jr. Transcription factors as targets for cancer therapy. *Nat Rev Cancer* **2002**, *2*, 740–749. DOI: 10.1038/nrc906

(3) Lee, Tong I.; Young, Richard A. Transcriptional Regulation and Its Misregulation in Disease. *Cell* **2013**, *152*, 1237–1251. DOI: https://doi.org/10.1016/j.cell.2013.02.014

(4) Bradner, J. E.; Hnisz, D.; Young, R. A. Transcriptional Addiction in Cancer. *Cell* **2017**, *168*, 629–643. DOI: 10.1016/j.cell.2016.12.013

(5) Bushweller, J. H. Targeting transcription factors in cancer - from undruggable to reality. *Nat Rev Cancer* **2019**, *19*, 611–624. DOI: 10.1038/s41568-019-0196-7

(6) Chen, A.; Koehler, A. N. Transcription Factor Inhibition: Lessons Learned and Emerging Targets. *Trends Mol Med* **2020**, *26*, 508–518. DOI: 10.1016/j.molmed.2020.01.004

(7) Dunker, A. K.; Uversky, V. N. Drugs for 'protein clouds': targeting intrinsically disordered transcription factors. *Curr Opin Pharmacol* **2010**, *10*, 782–788. DOI: 10.1016/j.coph.2010.09.005

(8) Ran, X.; Gestwicki, J. E. Inhibitors of protein-protein interactions (PPIs): an analysis of scaffold choices and buried surface area. *Curr Opin Chem Biol* **2018**, *44*, 75-86. DOI: 10.1016/j.cbpa.2018.06.004

(9) Buhrlage, S. J.; Bates, C. A.; Rowe, S. P.; Minter, A. R.; Brennan, B. B.; Majmudar, C. Y.; Wemmer, D. E.; Al-Hashimi, H.; Mapp, A. K. Amphipathic Small Molecules Mimic the Binding Mode and Function of Endogenous Transcription Factors. *ACS Chemical Biology* **2009**, *4*, 335-344. DOI: 10.1021/cb900028j

(10) Ma, J.; Ptashne, M. A new class of yeast transcriptional activators. *Cell* **1987**, *51*, 113–119. DOI: 10.1016/0092-8674(87)90015-8

(11) Mapp, A. K.; Ansari, A. Z. A TAD further: exogenous control of gene activation. *ACS Chem Biol* **2007**, *2*, 62-75. DOI: 10.1021/cb600463w

(12) Mapp, A. K.; Ansari, A. Z.; Ptashne, M.; Dervan, P. B. Activation of gene expression by small molecule transcription factors. *Proc Natl Acad Sci U S A* **2000**, *97*, 3930–3935. DOI: 10.1073/pnas.97.8.3930

(13) Nyanguile, O.; Uesugi, M.; Austin, D. J.; Verdine, G. L. A nonnatural transcriptional coactivator. *Proc Natl Acad Sci U S A* **1997**, *94*, 13402–13406. DOI: 10.1073/pnas.94.25.13402

(14) Piskacek, M.; Vasku, A.; Hajek, R.; Knight, A. Shared structural features of the 9aaTAD family in complex with CBP. *Mol Biosyst* **2015**, *11*, 844-851. DOI: 10.1039/c4mb00672k

(15) Piskacek, S.; Gregor, M.; Nemethova, M.; Grabner, M.; Kovarik, P.; Piskacek, M. Nine-amino-acid transactivation domain: establishment and prediction utilities. *Genomics* **2007**, *89*, 756-768. DOI: 10.1016/j.ygeno.2007.02.003

(16) Zhang, L.; Bulaj, G. Converting peptides into drug leads by lipidation. *Curr Med Chem* **2012**, *19*, 1602–1618. DOI: 10.2174/092986712799945003

(17) Kowalczyk, R.; Harris, P. W. R.; Williams, G. M.; Yang, S. H.; Brimble, M. A. Peptide Lipidation - A Synthetic Strategy to Afford Peptide Based Therapeutics. *Adv Exp Med Biol* **2017**, *1030*, 185–227. DOI: 10.1007/978-3-319-66095-0_9

(18) Holehouse, A. S.; Kragelund, B. B. The molecular basis for cellular function of intrinsically disordered protein regions. *Nature Reviews Molecular Cell Biology* **2023**. DOI: 10.1038/s41580-023-00673-0

(19) Arkin, M. R.; Tang, Y.; Wells, J. A. Small-molecule inhibitors of protein-protein interactions: progressing toward the reality. *Chem Biol* **2014**, *21*, 1102–1114. DOI: 10.1016/j.chembiol.2014.09.001

(20) Mouchiroud, L.; Eichner, L. J.; Shaw, R. J.; Auwerx, J. Transcriptional coregulators: fine-tuning metabolism. *Cell Metab* **2014**, *20*, 26–40. DOI: 10.1016/j.cmet.2014.03.027

(21) Piskacek, M.; Havelka, M.; Rezacova, M.; Knight, A. The 9aaTAD Transactivation Domains: From Gal4 to p53. *PLoS One* **2016**, *11*, e0162842. DOI: 10.1371/journal.pone.0162842

(22) Piskacek, S.; Gregor, M.; Nemethova, M.; Grabner, M.; Kovarik, P.; Piskacek, M. Nine-amino-acid transactivation domain: Establishment and prediction utilities. *Genomics* **2007**, *89*, 756–768. DOI: https://doi.org/10.1016/j.ygeno.2007.02.003

(23) Ravarani, C. N.; Erkina, T. Y.; De Baets, G.; Dudman, D. C.; Erkine, A. M.; Babu, M. M. High-throughput discovery of functional disordered regions: investigation of transactivation domains. *Mol Syst Biol* **2018**, *14*, e8190. DOI: 10.15252/msb.20188190

(24) Ramaswamy, K.; Forbes, L.; Minuesa, G.; Gindin, T.; Brown, F.; Kharas, M. G.; Krivtsov, A. V.; Armstrong, S. A.; Still, E.; de Stanchina, E.; et al. Peptidomimetic blockade of MYB in acute myeloid leukemia. *Nature Communications* **2018**, *9*, 110. DOI: 10.1038/s41467-017-02618-6

(25) Rowe, S. P.; Mapp, A. K. Assessing the permissiveness of transcriptional activator binding sites. *Biopolymers* **2008**, *89*, 578-581. DOI: 10.1002/bip.20946

(26) Sigler, P. B. Acid blobs and negative noodles. *Nature* **1988**, *333*, 210–212. DOI: 10.1038/333210a0

(27) Henderson, A. R.; Henley, M. J.; Foster, N. J.; Peiffer, A. L.; Beyersdorf, M. S.; Stanford, K. D.; Sturlis, S. M.; Linhares, B. M.; Hill, Z. B.; Wells, J. A.; et al. Conservation of coactivator engagement mechanism enables small-molecule allosteric modulators. *Proceedings of the National Academy of Sciences* **2018**, *115*, 8960-8965. DOI: 10.1073/pnas.1806202115

(28) Xiao, X.; Li, B. X.; Mitton, B.; Ikeda, A.; Sakamoto, K. M. Targeting CREB for cancer therapy: friend or foe. *Curr Cancer Drug Targets* **2010**, *10*, 384–391. DOI: 10.2174/156800910791208535

(29) Sapio, L.; Salzillo, A.; Ragone, A.; Illiano, M.; Spina, A.; Naviglio, S. Targeting CREB in Cancer Therapy: A Key Candidate or One of Many? An Update. *Cancers* **2020**, *12*, 3166. DOI: 10.3390/cancers12113166

(30) Dahal, L.; Kwan, T. O. C.; Shammas, S. L.; Clarke, J. pKID Binds to KIX via an Unstructured Transition State with Nonnative Interactions. *Biophys J* **2017**, *113*, 2713–2722. DOI: 10.1016/j.bpj.2017.10.016

(31) Tsherniak, A.; Vazquez, F.; Montgomery, P. G.; Weir, B. A.; Kryukov, G.; Cowley, G. S.; Gill, S.; Harrington, W. F.; Pantel, S.; Krill-Burger, J. M.; et al. Defining a Cancer Dependency Map. *Cell* **2017**, *170*, 564–576.e516. DOI: 10.1016/j.cell.2017.06.010

(32) Todaro, B.; Ottalagana, E.; Luin, S.; Santi, M. Targeting Peptides: The New Generation of Targeted Drug Delivery Systems. *Pharmaceutics* **2023**, *15*. DOI: 10.3390/pharmaceutics15061648

(33) Bozovičar, K.; Bratkovič, T. Evolving a Peptide: Library Platforms and Diversification Strategies. *Int J Mol Sci* **2019**, *21*. DOI: 10.3390/ijms21010215

(34) Monti, A.; Vitagliano, L.; Caporale, A.; Ruvo, M.; Doti, N. Targeting Protein-Protein Interfaces with Peptides: The Contribution of Chemical Combinatorial Peptide Library Approaches. *Int J Mol Sci* **2023**, *24*. DOI: 10.3390/ijms24097842

(35) Peacock, H.; Suga, H. Discovery of De Novo Macrocyclic Peptides by Messenger RNA Display. *Trends in Pharmacological Sciences* **2021**, *42*, 385–397. DOI: 10.1016/j.tips.2021.02.004

(36) Moiola, M.; Memeo, M. G.; Quadrelli, P. Stapled Peptides-A Useful Improvement for Peptide-Based Drugs. *Molecules* **2019**, *24*. DOI: 10.3390/molecules24203654

(37) Bird, G. H.; Patten, J. J.; Zavadoski, W.; Barucci, N.; Godes, M.; Moyer, B. M.; Owen, C. D.; DaSilva-Jardine, P.; Neuberg, D. S.; Bowen, R. A.; et al. A stapled lipopeptide platform for preventing and treating highly pathogenic viruses of pandemic potential. *Nature Communications* **2024**, *15*, 274. DOI: 10.1038/s41467-023-44361-1

(38) Hu, J.; Chan, A. I.; Adaligil, E.; Kekessie, I.; Takahashi, M.; Song, A.; Cunningham, C. N.; Paegel, B. M. Liposomal Permeation Assay for Droplet-Scale Pharmacokinetic Screening. *Journal of Medicinal Chemistry* **2023**, *66*, 6288-6296. DOI: 10.1021/acs.jmedchem.3c00138

(39) Talukdar, P. D.; Chatterji, U. Transcriptional co-activators: emerging roles in signaling pathways and potential therapeutic targets for diseases. *Signal Transduct Target Ther* **2023**, *8*, 427. DOI: 10.1038/s41392-023-01651-w

(40) Xu, Y.; Milazzo, J. P.; Somerville, T. D. D.; Tarumoto, Y.; Huang, Y. H.; Ostrander, E. L.; Wilkinson, J. E.; Challen, G. A.; Vakoc, C. R. A TFIID-SAGA Perturbation that Targets MYB and Suppresses Acute Myeloid Leukemia. *Cancer Cell* **2018**, *33*, 13-28.e18. DOI: 10.1016/j.ccell.2017.12.002

Appendix A: Characterization of synthesized peptides
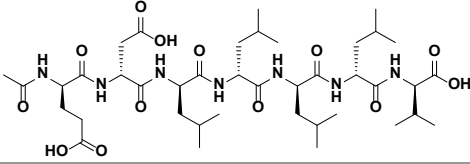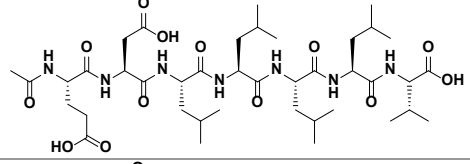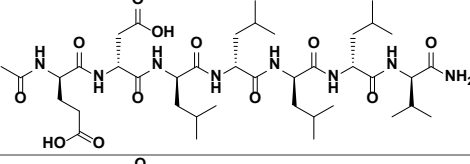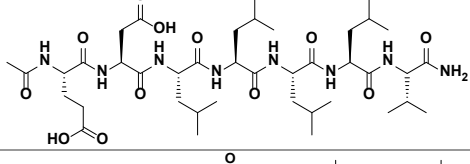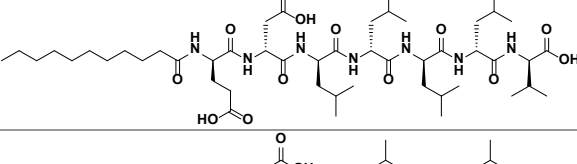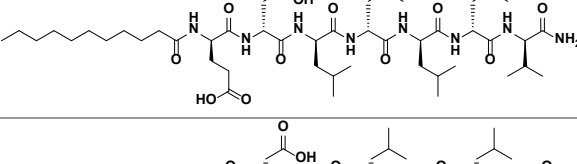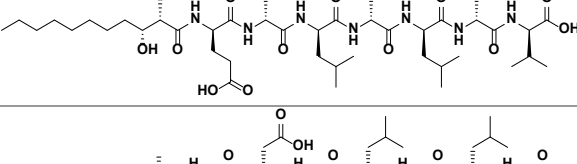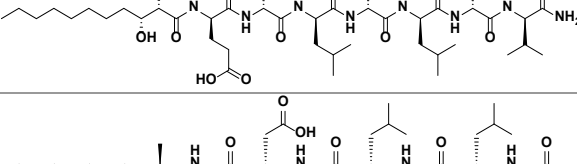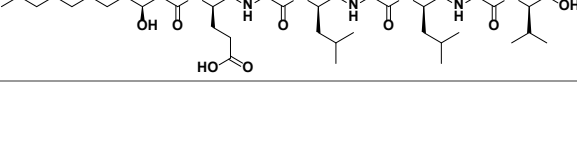
Appendix Table A.1 Sequences of activator peptides used in this study.

Peptide	Sequence (N'-C')
ATF6α (38-75)	FITC-βAla-FTDTDELQLEAANETYENNFDNLDFDLDLMPWESDIWD
ETV1 (38-68)	FITC-βAla-DLAHDSEELFQDLSQLQETWLAEAQVPDNDEQ
ETV4 (45-76)	FITC-βAla-LPPLDSEDLFQDLSHFQETWLAEAQVPDSDEQ
ETV5 (38-68)	FITC-βAla-DLAHDSEELFQDLSQLQEAWLAEAQVPDDEQ
MLL (2840-2858)	FITC-βAla-DCGNILPSDIMDFVLKNTP
Myb (219-316)	FITC-βAla-KEKRIKELELLLMSTENELKGQQVLP
ACTR (1041-1088)	FITC-βAla-PSNLEGQSDERALLDQLHTLLSNTDATGLEEIDRALGIPELVNQGQAL
pKID (105-133)	FITC-(AEEAc)-TDSQKRREILSRRPS(PO$_4$)YRKILNDLSSDAPG
IBiD (2063-2111)	Ac-SPSALQDLLRTLKSPSSPQQQQQVLNILKSNPQLMAAFIKQRTAKYVAN
SREBP1a (18-42)	FITC- βAla-APCDLDAALLTDIEDMLNLINNQDSD
HIF1α (786-823)	FITC- βAla-SMDESGLPQLTSYDCEVNAPIQGSRNLLQGEELLRALDQVN
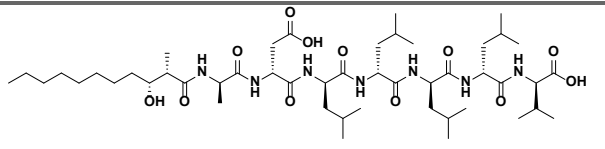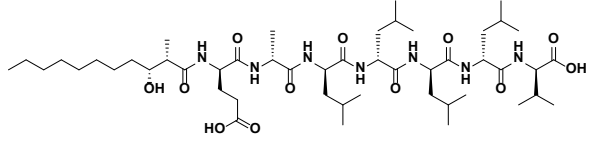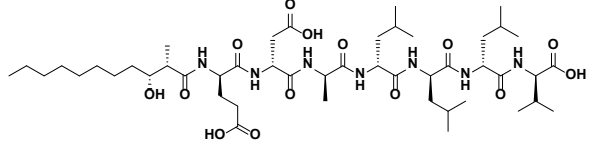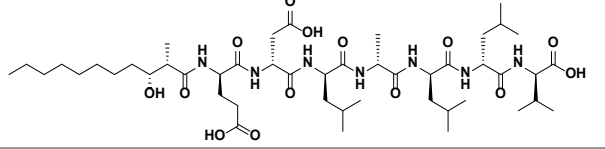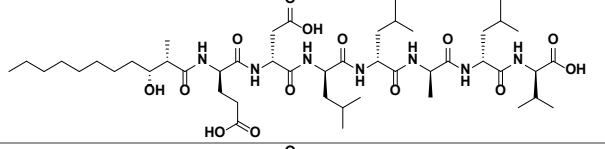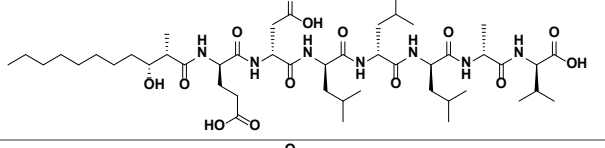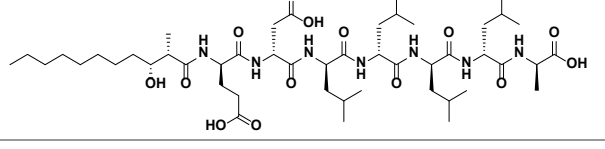
Appendix Table A.2 Summary of masses of activator peptides used in this study.

Peptide	Expected Mass (M+1)	Observed Mass (M+1)
FITC-ATF6α (38-75)	5045.0405	5045.0478
FITC-ETV1 (38-69)	4173.7598	4173.7637
FITC-ETV4 (45-76)	4159.7846	4159.7915
FITC-ETV5 (38-68)	4029.7063	4029.7150
FITC-MLL (2840-2858)	2551.0935	2551.1160
FITC-Myb (219-316)	3526.81	3526.8126
FITC-ACTR (1041-1088)	5616.6928	5615.7288
FITC-pKID (105-133)	3972.8839	3972.8951
Ac-IBiD (2063-2111)	5493.9855	5493.0173
SREBP1a (18-42)	3291.3570	3291.3792
HIF1α(786-823)	4962.2423	4962.7561
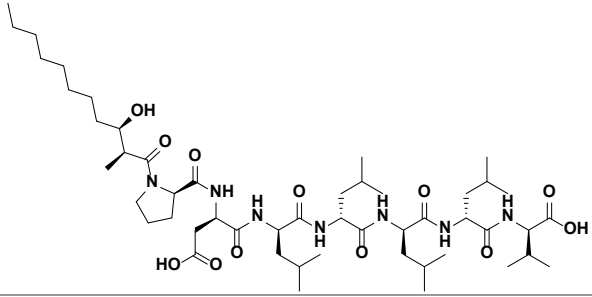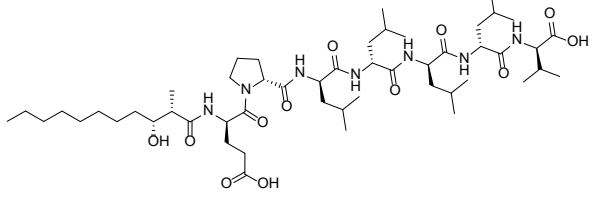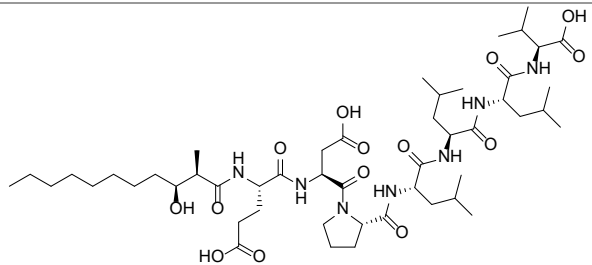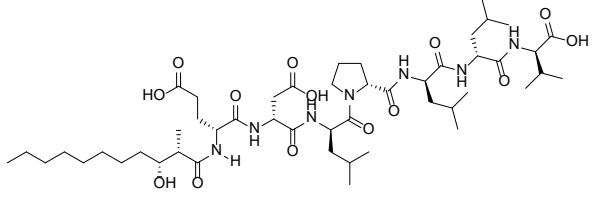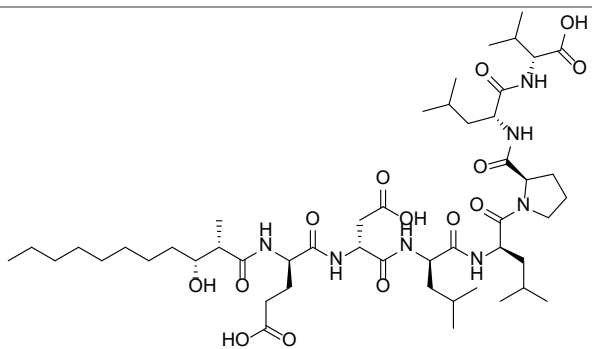
Appendix Table A.3. Summary of lipopeptidomimetic structures and masses used in this study (Library A).
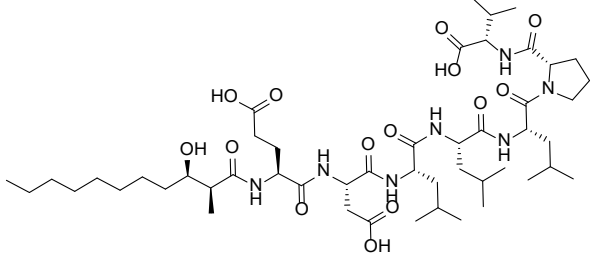
Peptide	Structure	Expected Mass (M+1)	Observed Mass (M+1)
LPPM-2		855.4953	855.5003
LPPM-3		855.4953	855.5003
LPPM-4		854.5113	854.5168
LPPM-5		854.5113	854.5168
LPPM-6		981.6362	981.6399
LPPM-7		980.6522	980.6559
LPPM-8		1011.6468	1011.6532
LPPM-9		1010.6627	1010.6680
LPPM-10		1011.6468	1011.6524

Appendix Table A.4. Summary of lipopeptidomimetic structures and masses used in this study (Library B).

Peptide	Structure	Expected Mass (M+1)	Observed Mass (M+1)
LPPM-8 ADLLLLV		953.6413	953.6489
LPPM-8 EALLLLV		967.6569	967.6699
LPPM-8 EDALLLV		969.5998	969.6021
LPPM-8 EDLALLV		969.5998	969.6045
LPPM-8 EDLLALV		969.5998	969.6080
LPPM-8 EDLLLAV		969.5998	969.6097
LPPM-8 EDLLLLA		983.6155	983.6205

Appendix Table A.5. Summary of lipopeptidomimetic structures and masses used in this study (Library C).

Peptide	Structure	Expected Mass (M+1)	Observed Mass (M+1)
LPPM-8 PDLLLLV		979.6569	979.6516
LPPM-8 EPLLLLV		993.6726	993.6751
LPPM-8 EDPLLLV		995.6155	995.6191
LPPM-8 EDLPLLV		995.6155	995.6172
LPPM-8 EDLLPLV		995.6155	995.6168

| LPPM-8 EDLLLPV | | 995.6155 | 995.6168 |

Analytical Traces of Peptides Used in this Study
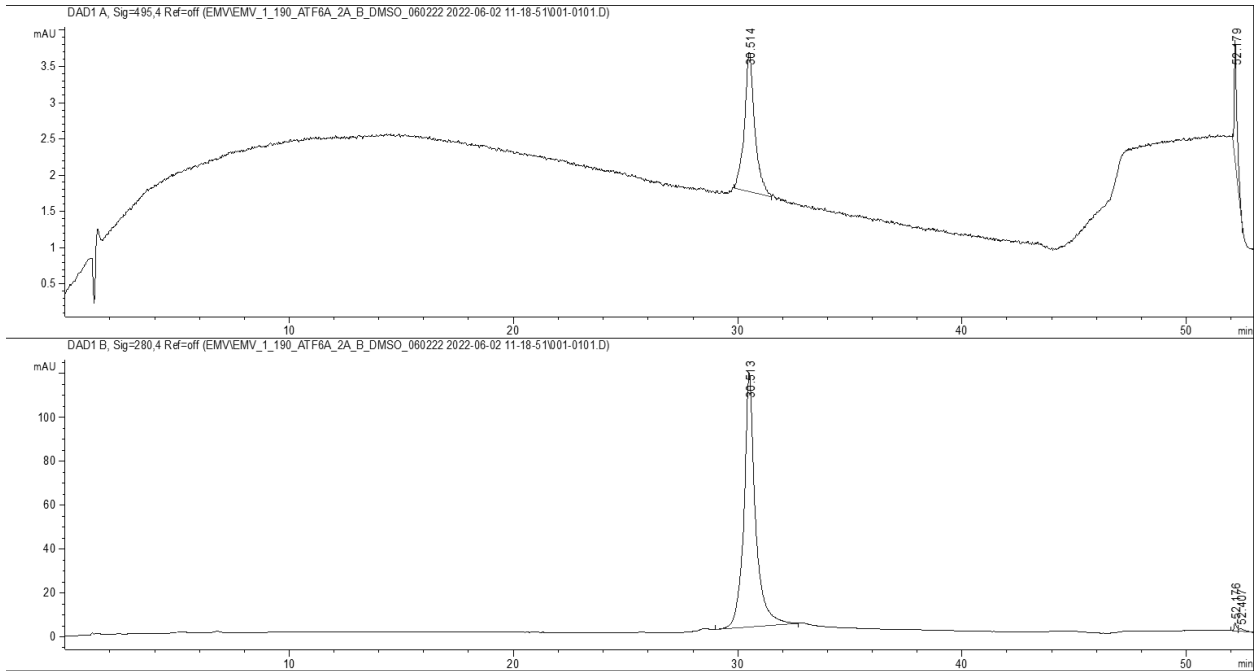
Appendix Figure A.1 Analytical HPLC trace of FITC-ATF6α (38-75) monitored at 495 nm (top) and 280 nm (bottom).
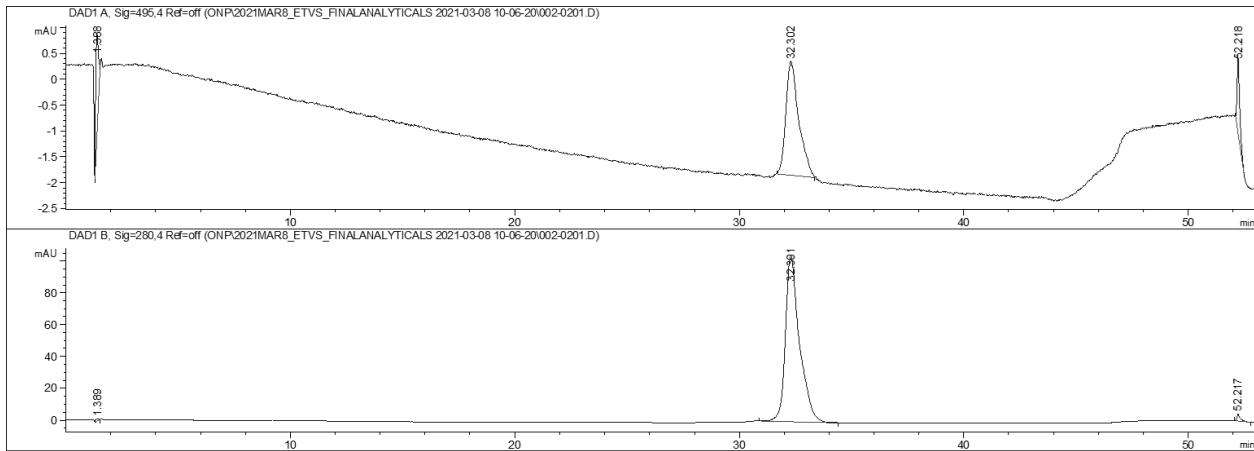
Appendix Figure A.2 Analytical HPLC trace of FITC-ETV1 (38-69) monitored at 495 nm (top) and 280 nm (bottom).
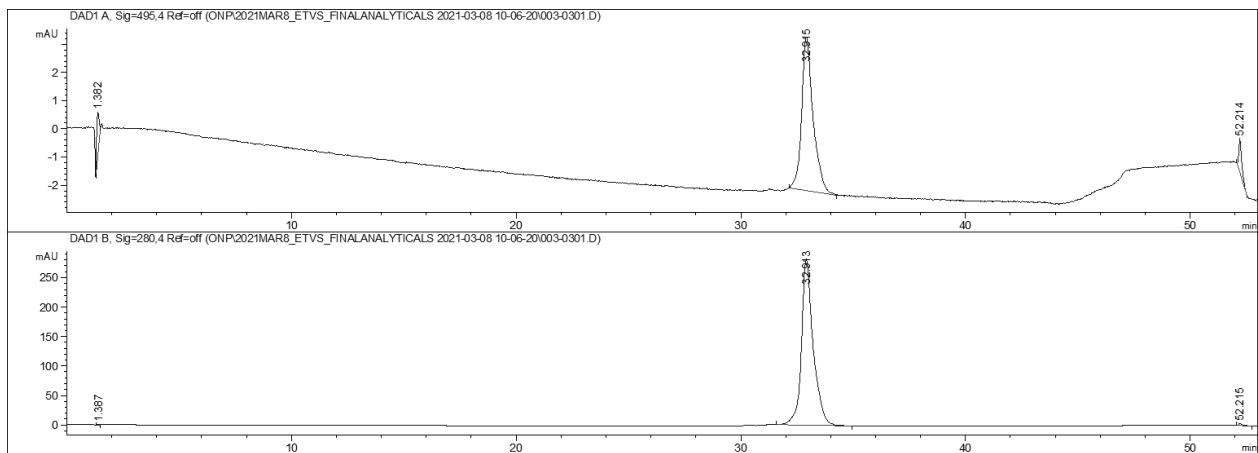
Appendix Figure A.3 Analytical HPLC trace of FITC-ETV4 (45-76) monitored at 495 nm (top) and 280 nm (bottom).
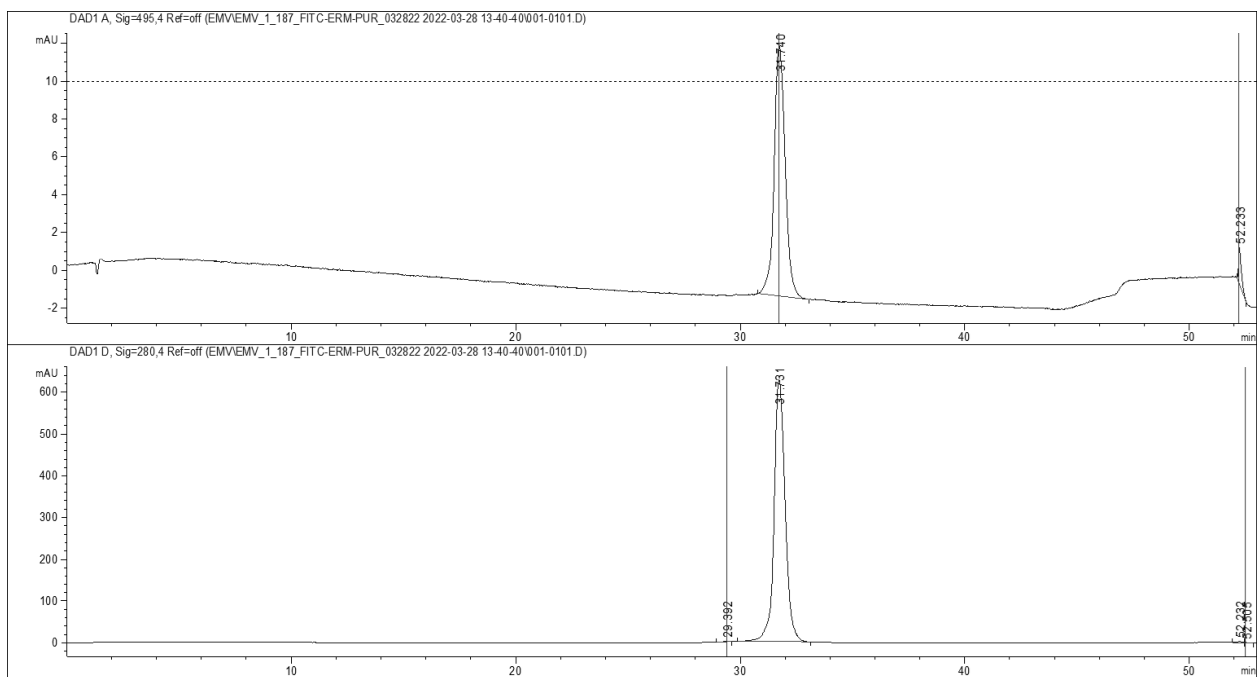
Appendix Figure A.4 Analytical HPLC trace of FITC-ETV5 (38-68) monitored at 495 nm (top) and 280 nm (bottom).
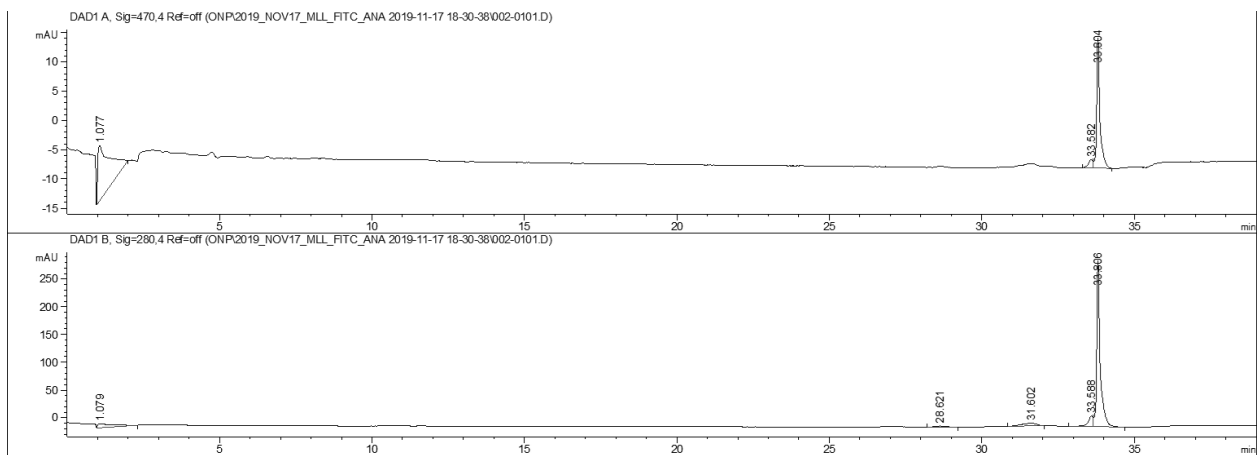
Appendix Figure A.5 Analytical HPLC trace of FITC-MLL (2840-2858) monitored at 495 nm (top) and 280 nm (bottom).
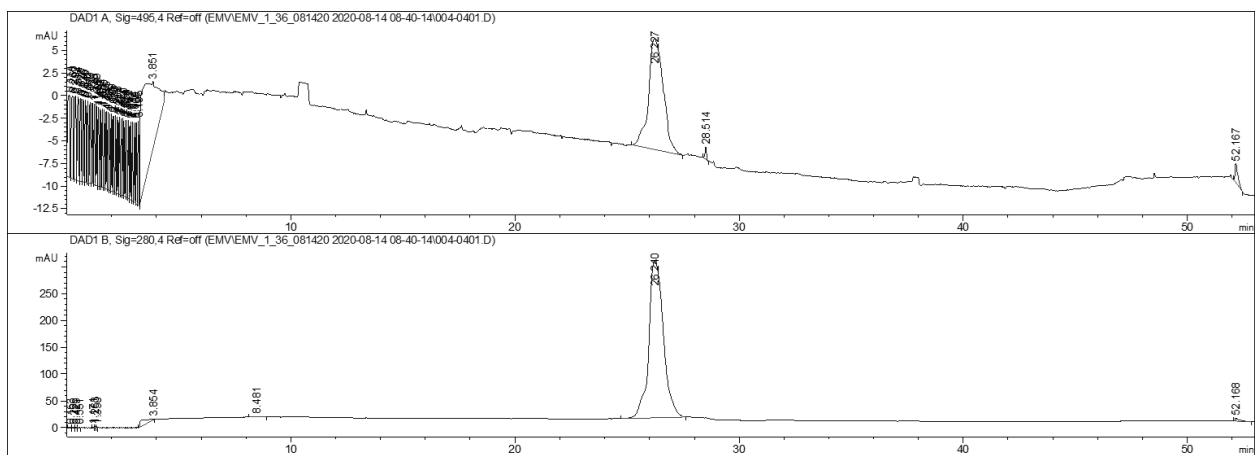
Appendix Figure A.6 Analytical HPLC trace of FITC-Myb (219-316) monitored at 495 nm (top) and 280 nm (bottom).
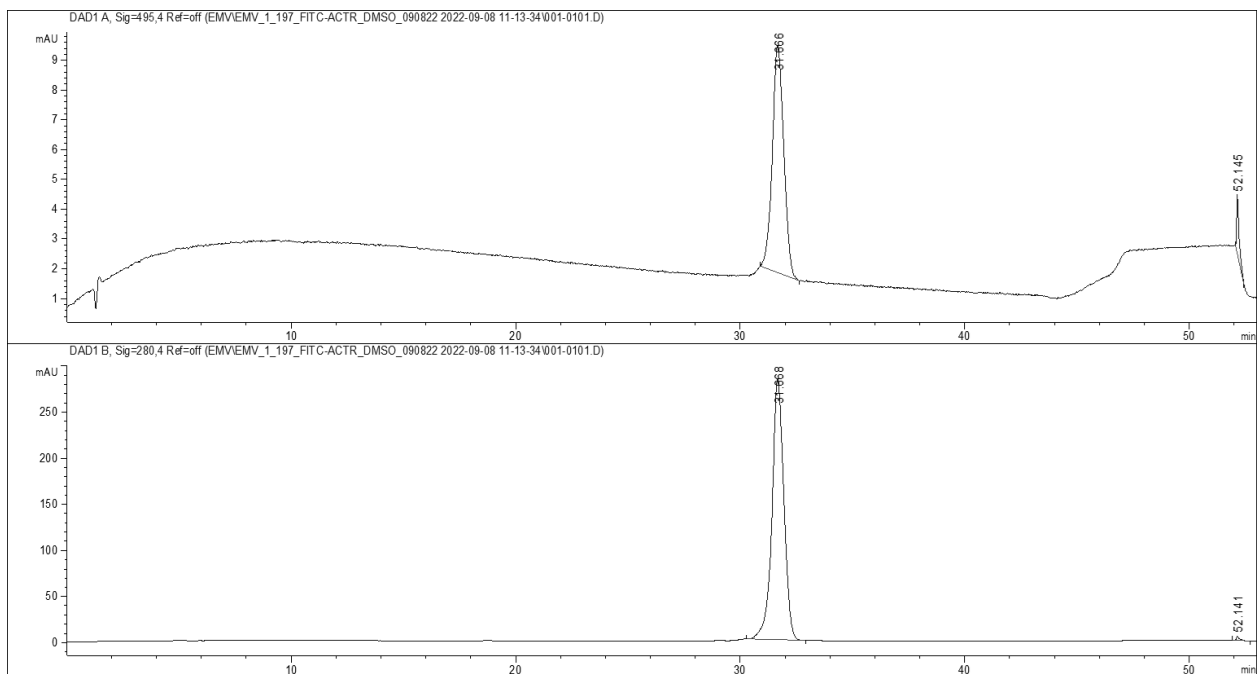
Appendix Figure A.7 Analytical HPLC trace of FITC-ACTR (1041-1088) monitored at 495 nm (top) and 280 nm (bottom).
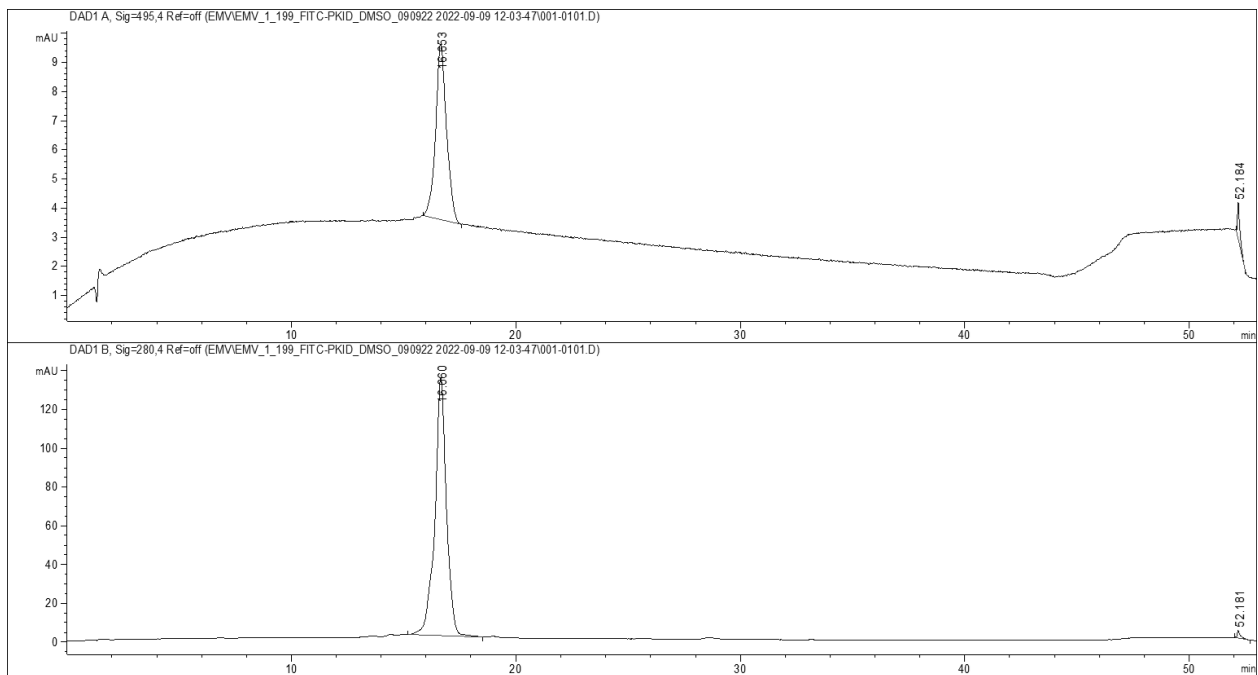
Appendix Figure A.8 Analytical HPLC trace of FITC-pKID (105-133) monitored at 280 nm (top) and 495 nm (bottom).
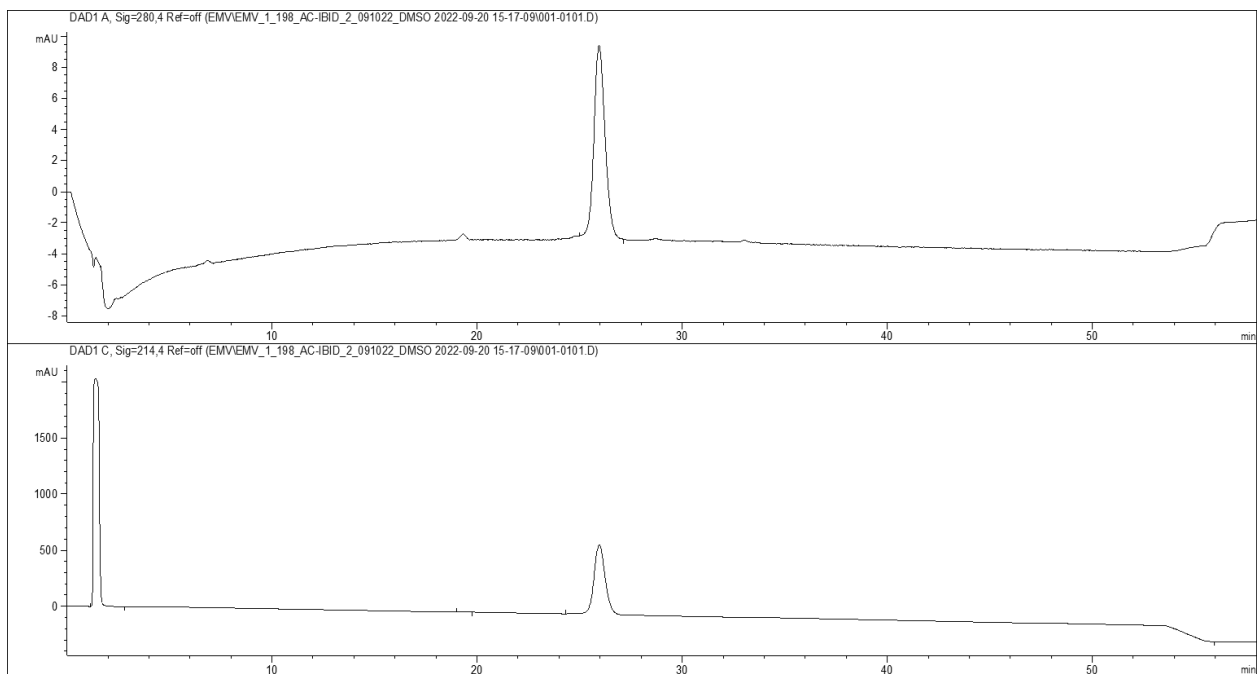
Appendix Figure A.9 Analytical HPLC trace of Ac-IBiD (2063-2111) monitored at 280 nm (top) and 214 nm (bottom). Peak before 5 min. in 214 nm trace corresponds to solvent peak, DMSO, that was used to dissolve sample.
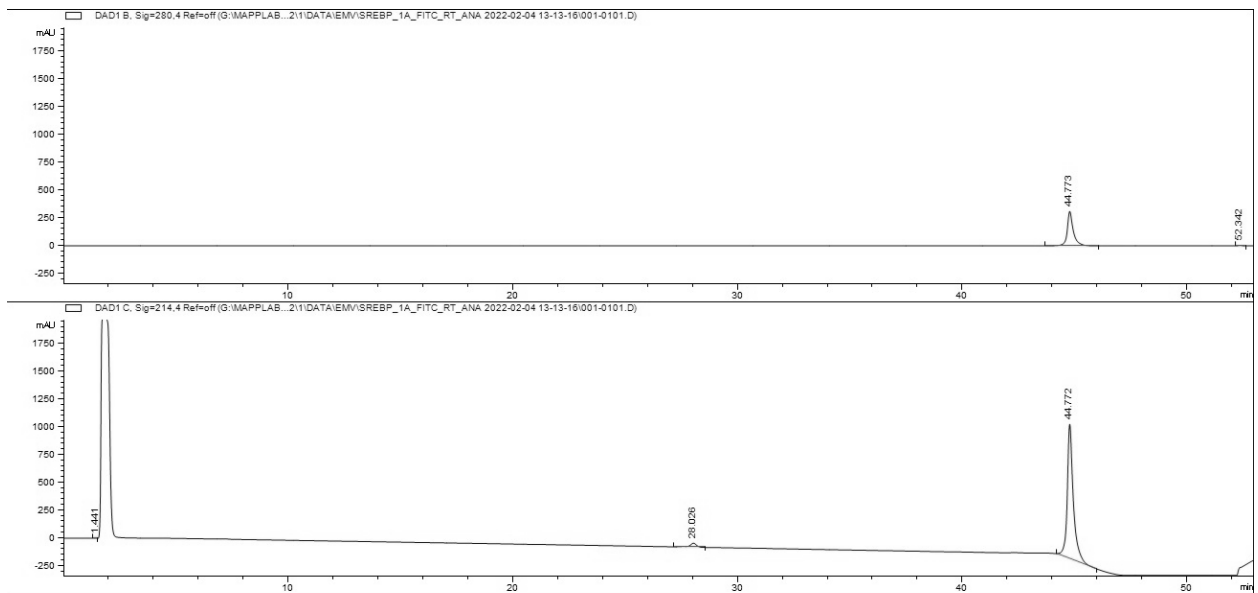
Appendix Figure A.10 Analytical HPLC trace of SREBP1a (18-42) monitored at 280 nm (top) and 214 nm (bottom). Peak before 5 min. in 214 nm trace corresponds to solvent peak, DMSO, that was used to dissolve sample
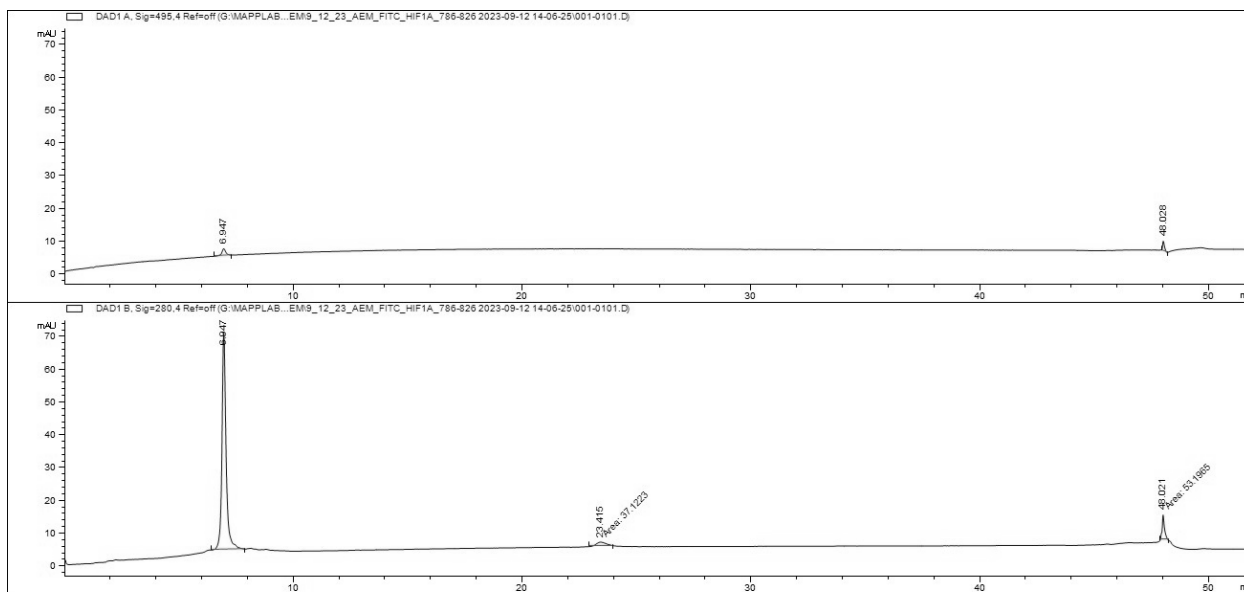
Appendix Figure A.11 Analytical HPLC trace of HIF1α (786-823) monitored at 495 nm (top) and 280 nm (bottom).

Activator Peptide Mass Spectrometry
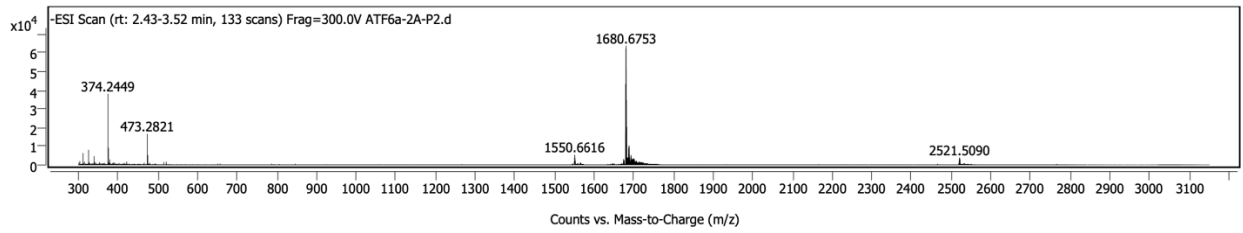
Appendix Figure A.12 MS of FITC-ATF6α (38-75) MS
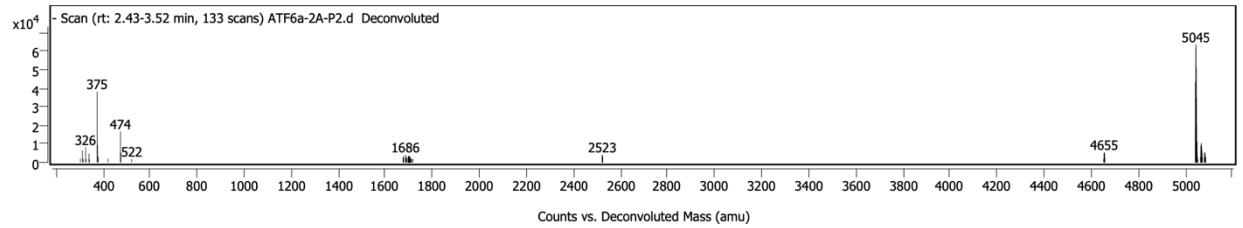
Appendix Figure A.13 Deconvoluted MS of FITC-ATF6α (38-75)
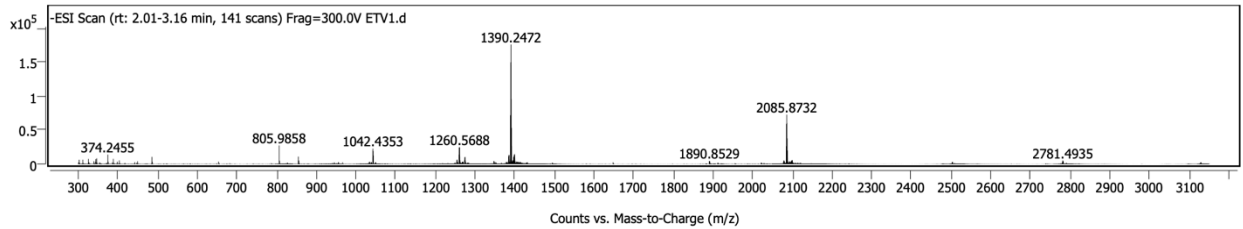
Appendix Figure A.14 MS of FITC-ETV1 (38-69) MS
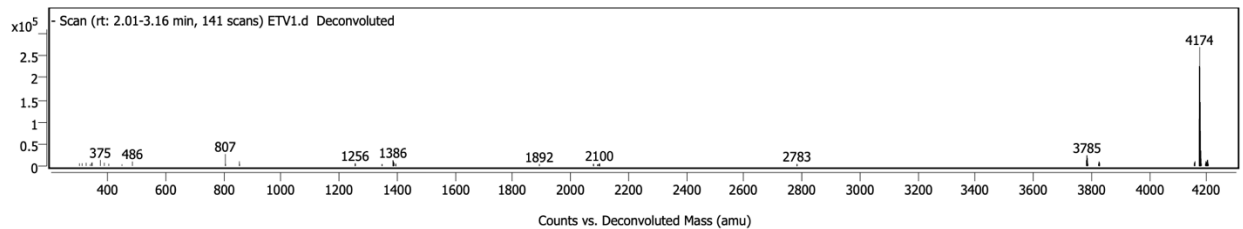
Appendix Figure A.15 Deconvoluted MS of FITC-ETV1 (38-69)
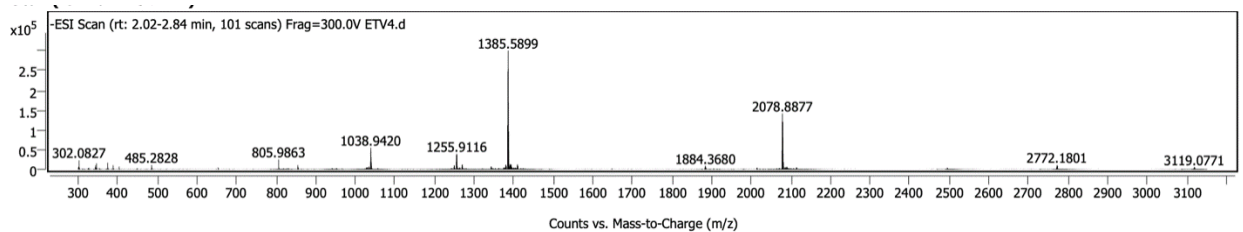
Appendix Figure A.16 MS of FITC-ETV4 (45-76)
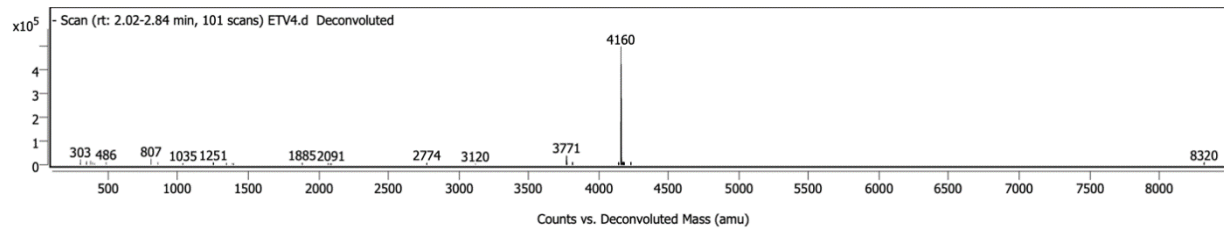
Appendix Figure A.17 Deconvoluted MS of FITC-ETV4 (45-76)
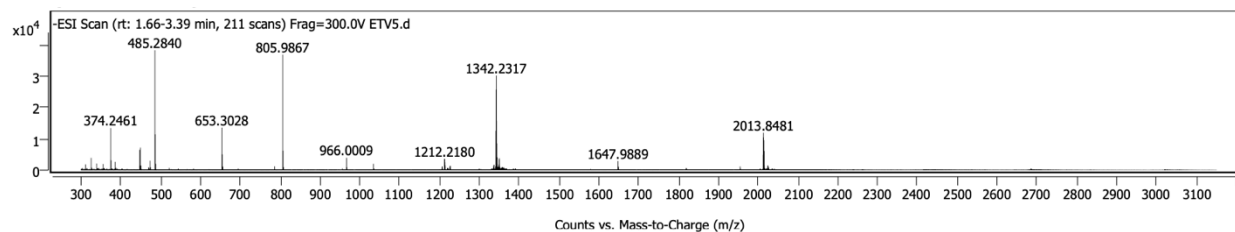
Appendix Figure A.18 MS of FITC-ETV5 (38-68)
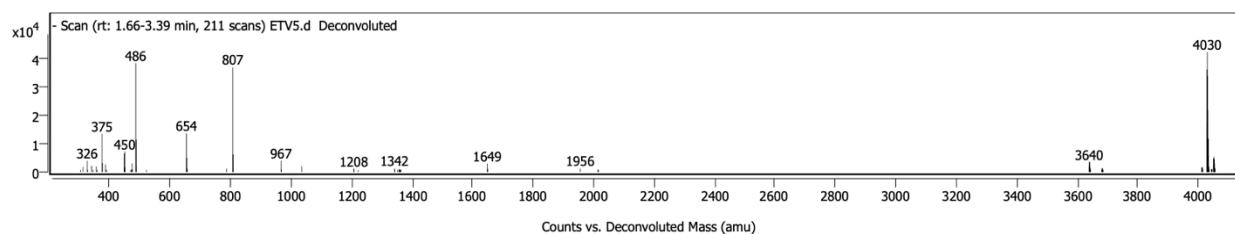
Appendix Figure A.19 Deconvoluted MS of FITC-ETV5 (38-68)
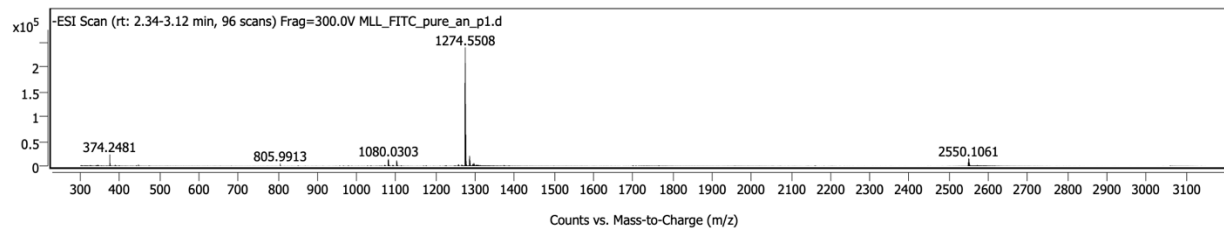
Appendix Figure A.20 MS of FITC-MLL (2840-2858)
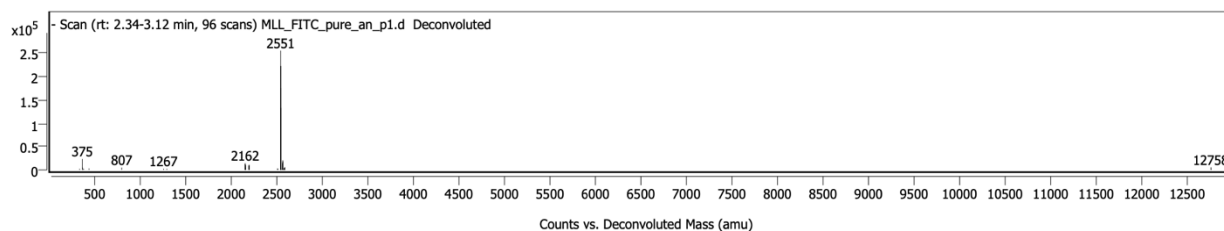
Appendix Figure A.21 Deconvoluted MS of FITC-MLL (2840-2858)
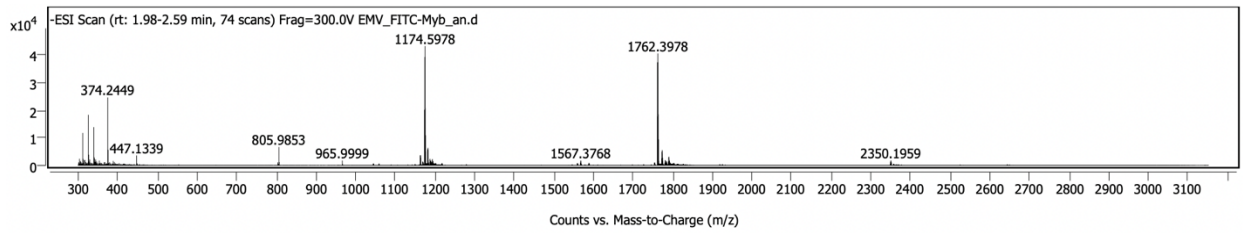
Appendix Figure A.22 MS of FITC-Myb (219-316)
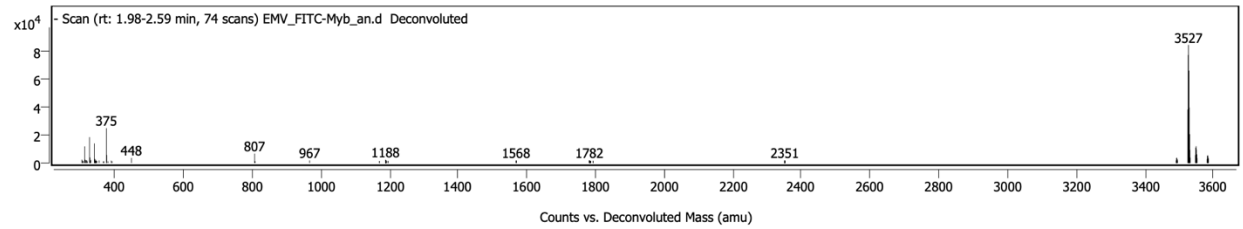
Appendix Figure A.23 Deconvoluted MS of FITC-Myb (219-316)
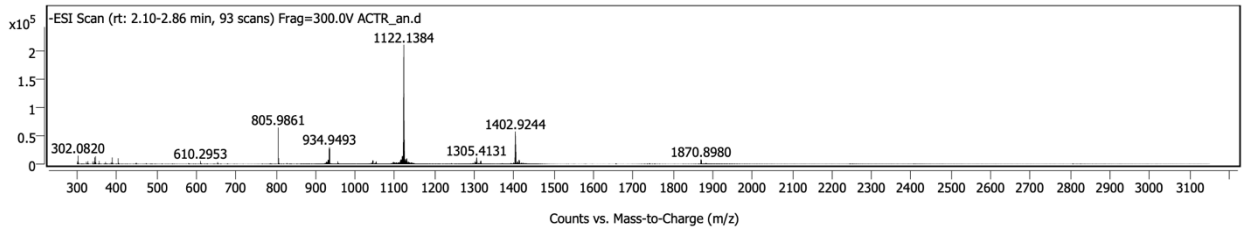
Appendix Figure A.24 MS of FITC-ACTR (1041-1088)
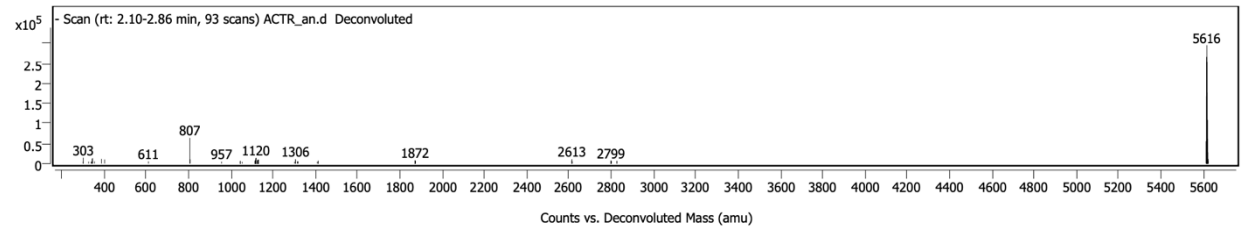
Appendix Figure A.25 Deconvolution of FITC-ACTR (1041-1088) Deconvolution
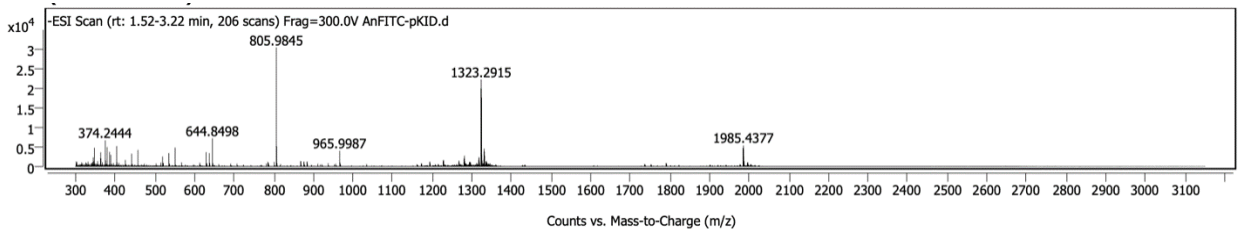
Appendix Figure A.26 MS of FITC-pKID (105-133)
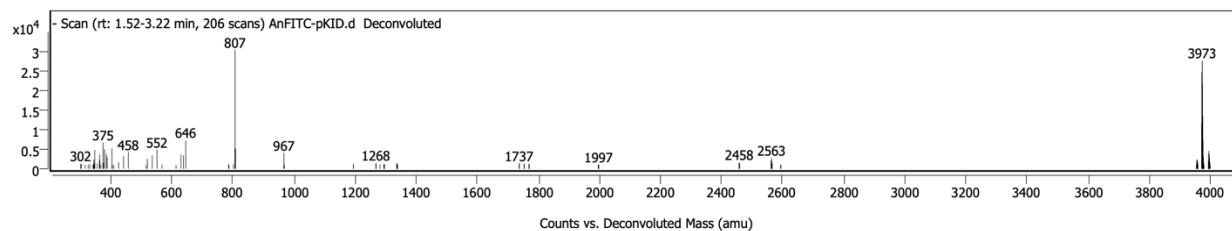
Appendix Figure A.27 Deconvolution of FITC-pKID (105-133)
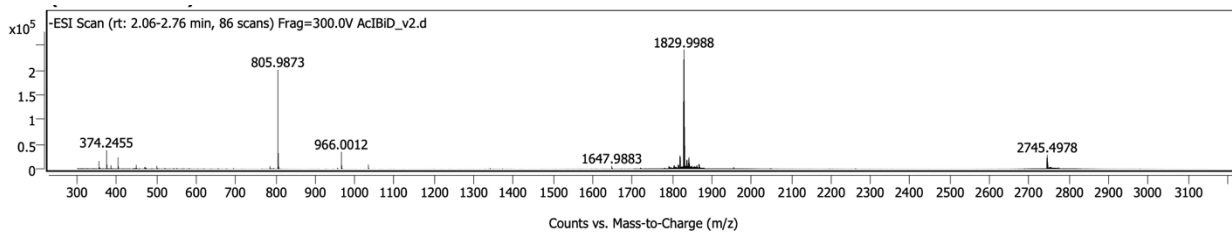
Appendix Figure A.28 MS of Ac-IBiD (2063-2111)
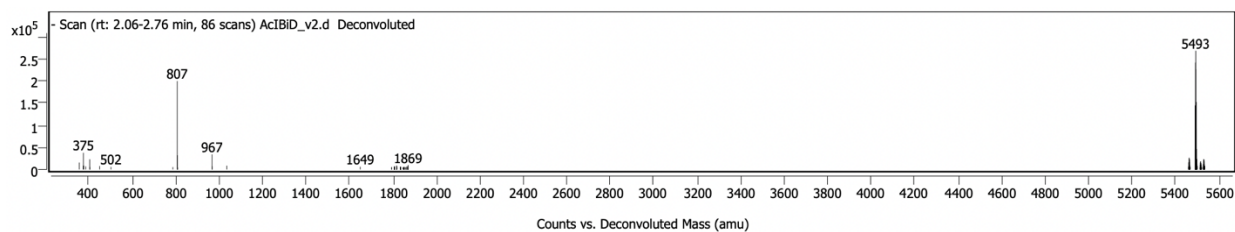
Appendix Figure A.29 Deconvolution of Ac-IBiD (2063-2111)
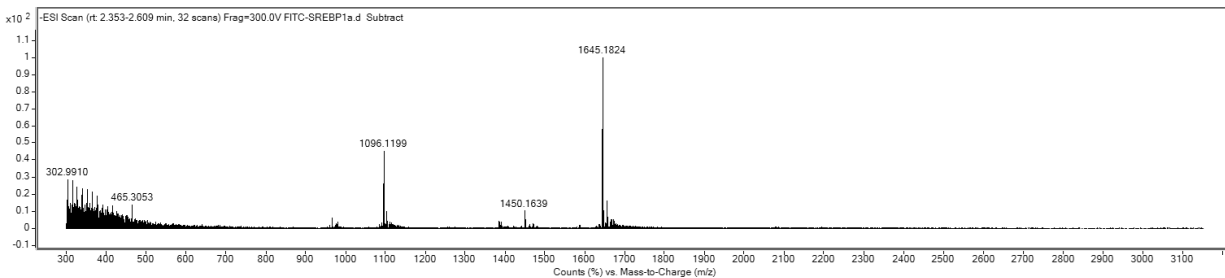
Appendix Figure A.30 MS of FITC-SREBP1a (18-42)
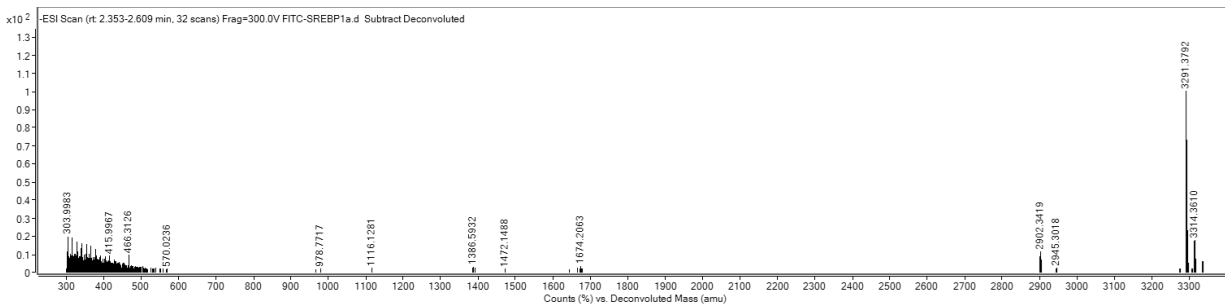
Appendix Figure A.31 Deconvolution of FITC-SREBP1a (18-42)
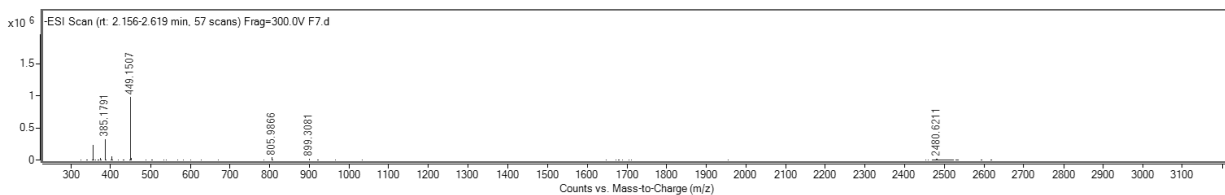
Appendix Figure A.32 MS of FITC-HIF1α (786-823)
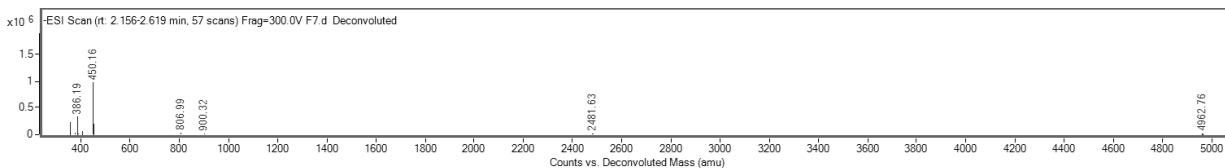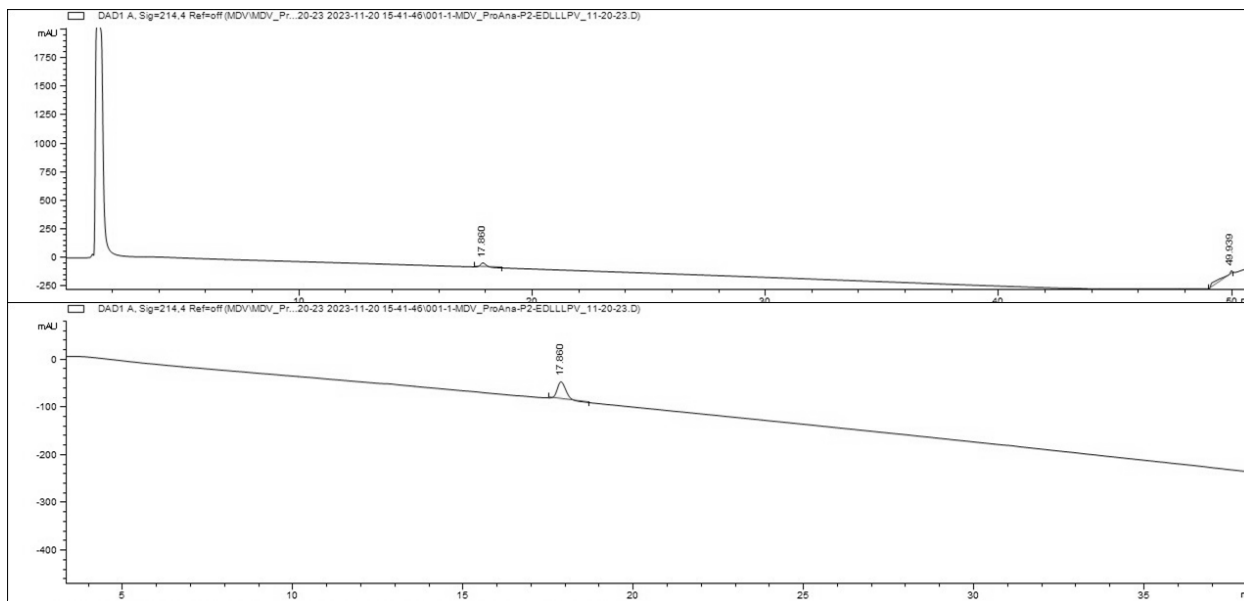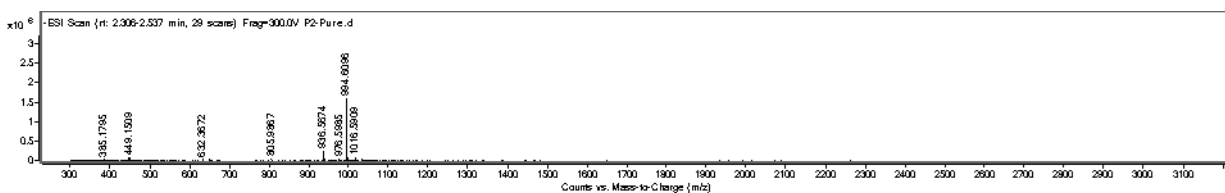

Appendix Figure A.33 Deconvolution of FITC-HIF1α (786-823)
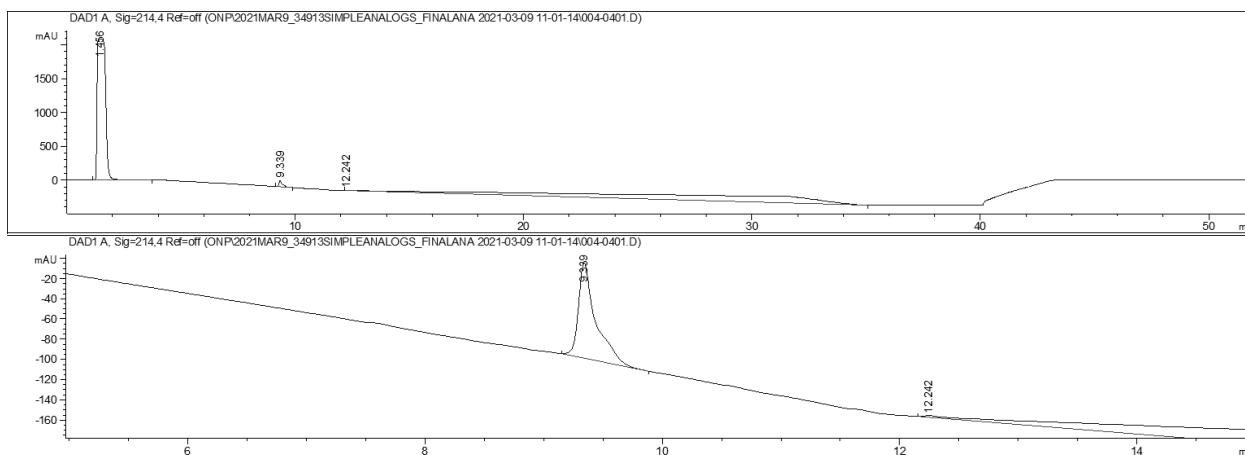
Appendix Figure A.34 Analytical trace of LPPM-2. Zoomed in analytical trace. Peak before 5 min. corresponds to solvent peak, DMSO, that was used to dissolve sample. Purity > 97% at 214 nm.
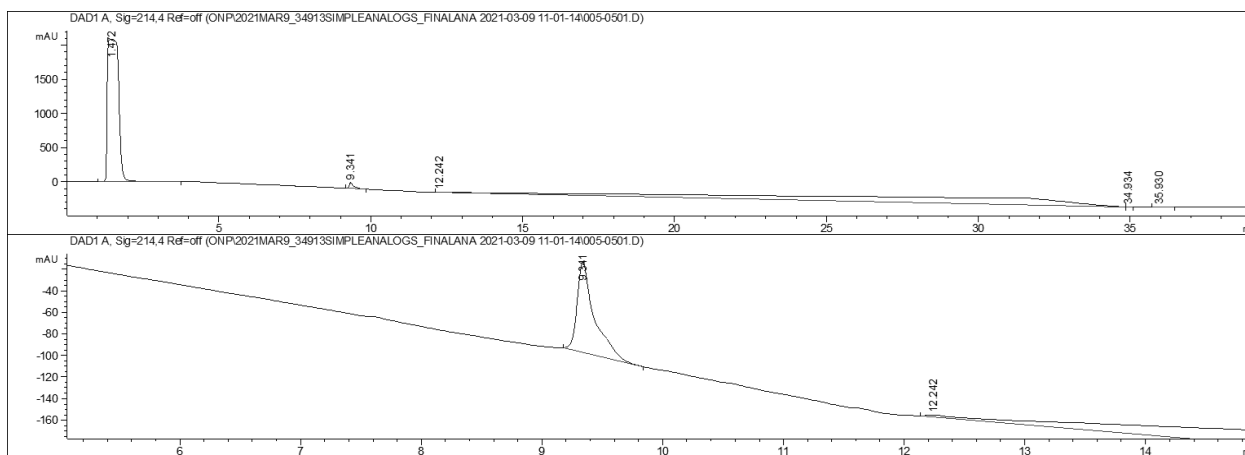
Appendix Figure A.35 Analytical trace of LPPM-3**.** Zoomed in analytical trace. Peak before 5 min. corresponds to solvent peak, DMSO, that was used to dissolve sample. Purity > 97% at 214 nm.
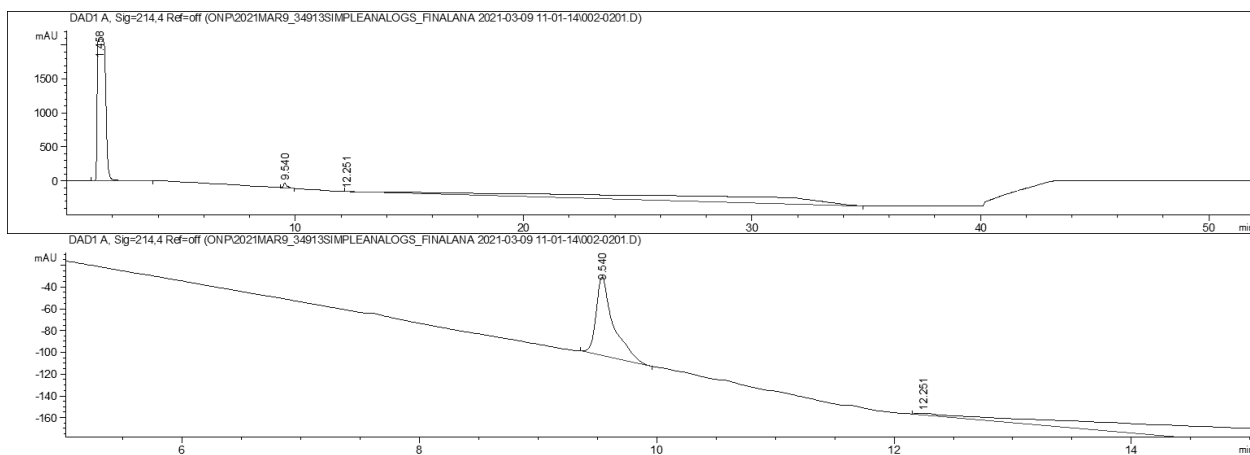
Appendix Figure A.36 Analytical trace of LPPM-4. Zoomed in analytical trace. Peak before 5 min. corresponds to solvent peak, DMSO, that was used to dissolve sample. Purity > 97% at 214 nm.
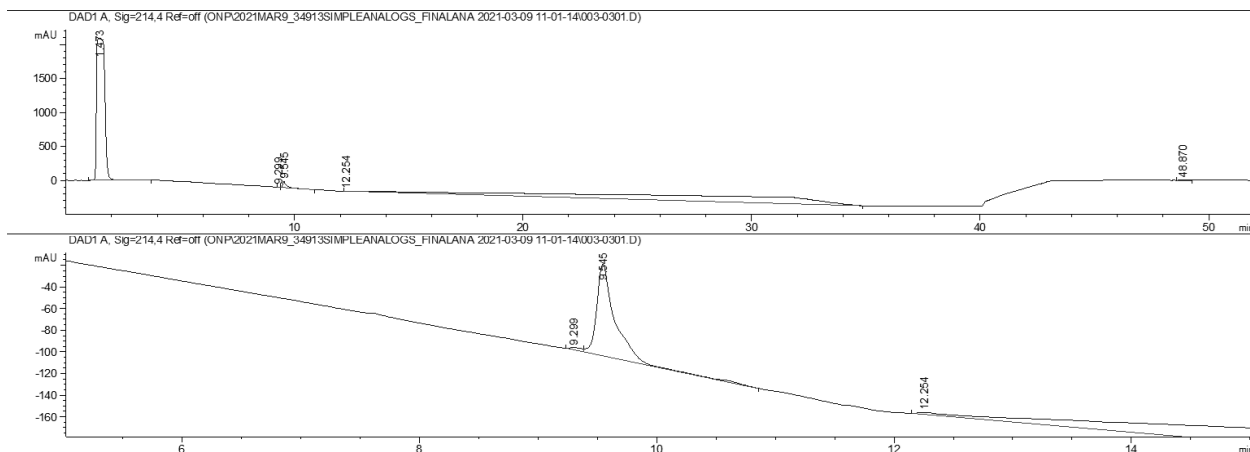
Appendix Figure A.37 Analytical trace of LPPM-5. Zoomed in analytical trace. Peak before 5 min. corresponds to solvent peak, DMSO, that was used to dissolve sample. Purity > 97% at 214 nm.
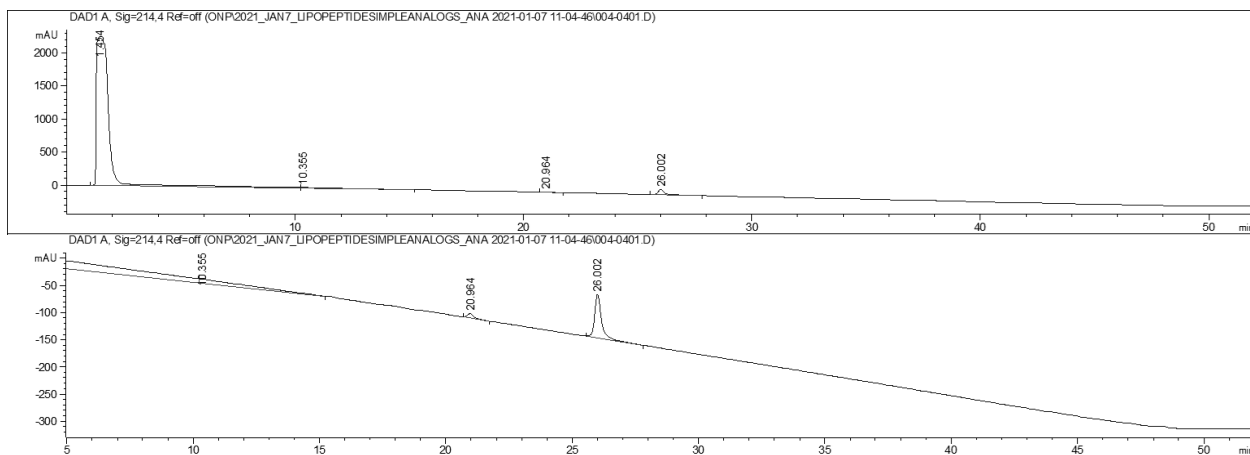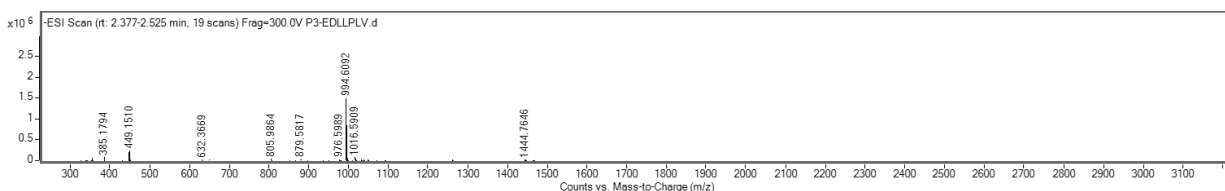

Appendix Figure A.38 Analytical trace of LPPM-6. Zoomed in analytical trace. Peak before 5 min. corresponds to solvent peak, DMSO, that was used to dissolve sample. Purity > 90% at 214 nm.
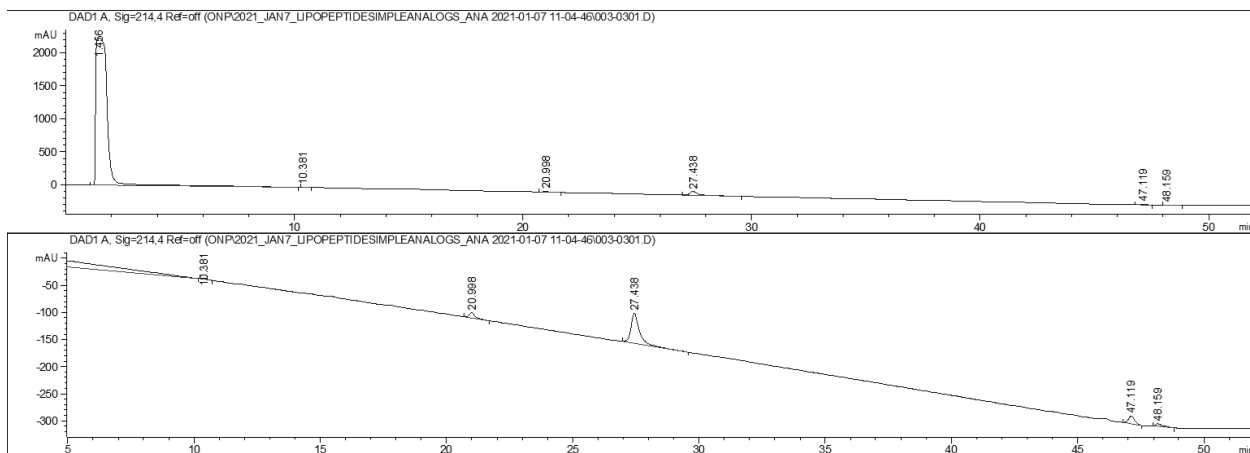
Appendix Figure A.39 Analytical trace of LPPM-7. Zoomed in analytical trace. Peak before 5 min. corresponds to solvent peak, DMSO, that was used to dissolve sample. Purity > 90% at 214 nm.
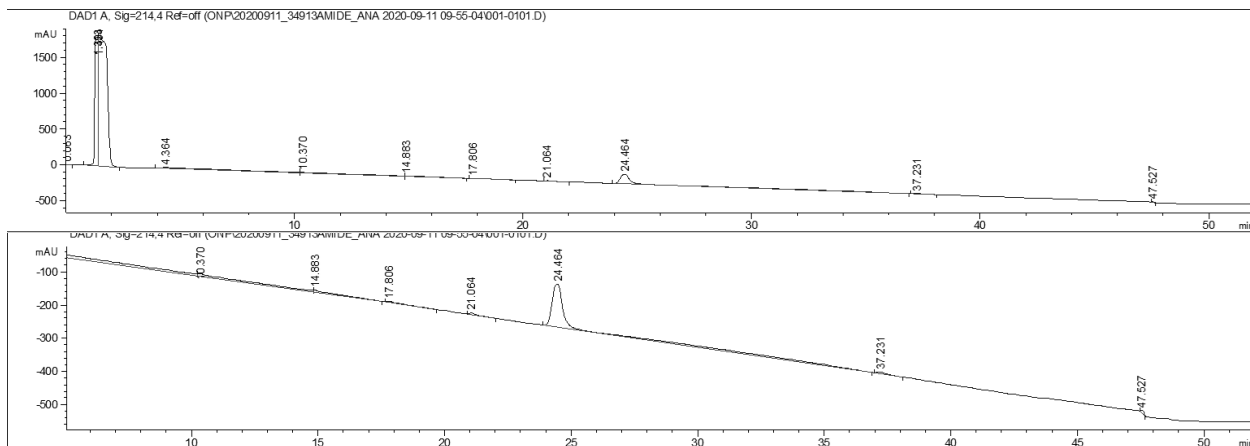
Appendix Figure A.40 Analytical trace of LPPM-8. Zoomed in analytical trace. Peak before 5 min. corresponds to solvent peak, DMSO, that was used to dissolve sample. Purity > 97% at 214 nm.

153
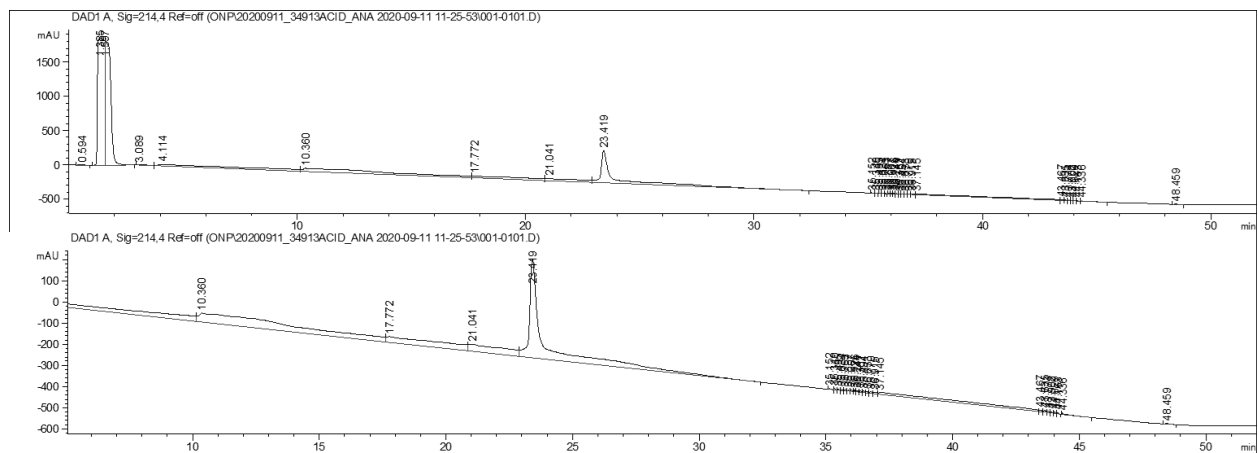
Appendix Figure A.41 Analytical trace of LPPM-9. Zoomed in analytical trace. Peak before 5 min. corresponds to solvent peak, DMSO, that was used to dissolve sample. Purity > 97% at 214 nm.
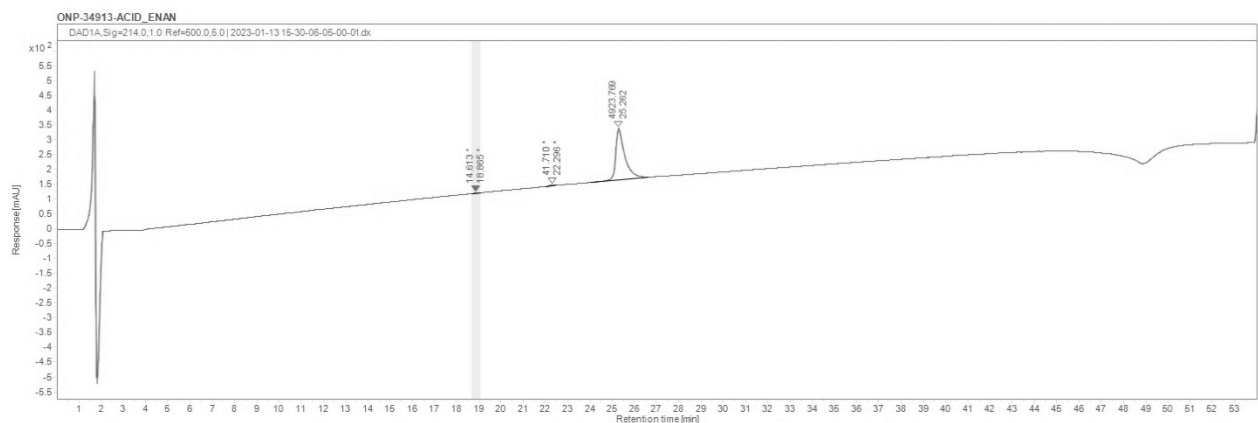
Appendix Figure A.42 Analytical trace of LPPM-10. Zoomed in analytical trace. Peak before 5 min. corresponds to solvent peak, DMSO, that was used to dissolve sample. Purity > 97% at 214 nm.
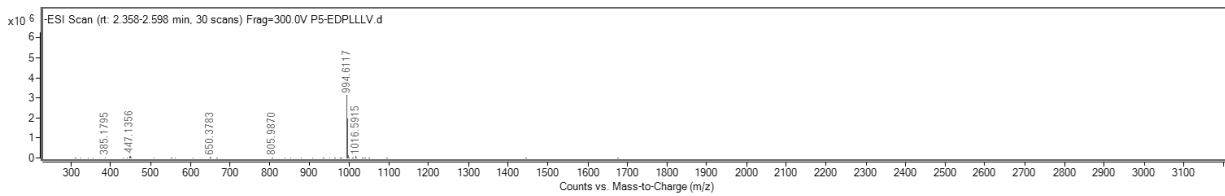
Appendix Figure A.43 MS of LPPM-2
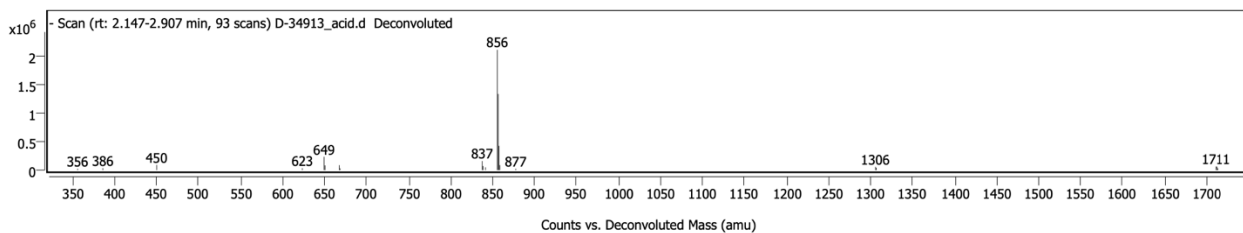
Appendix Figure A.44 Deconvolution of LPPM-2
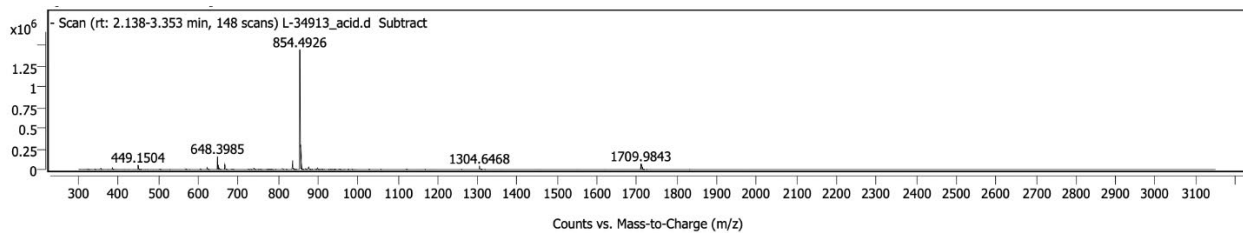
Appendix Figure A.45 MS of LPPM-3
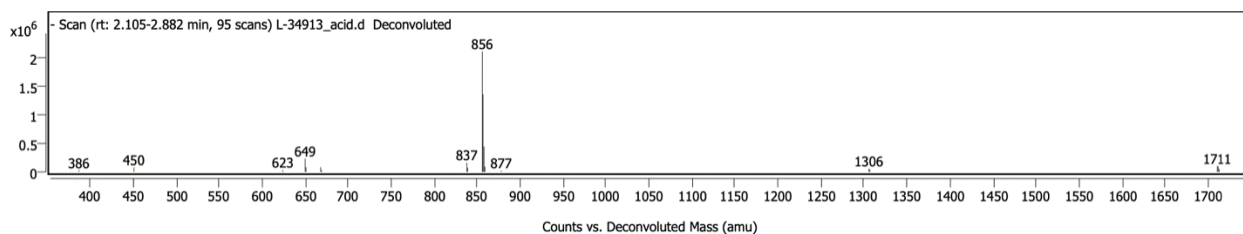
Appendix Figure A.46 Deconvolution of LPPM-3
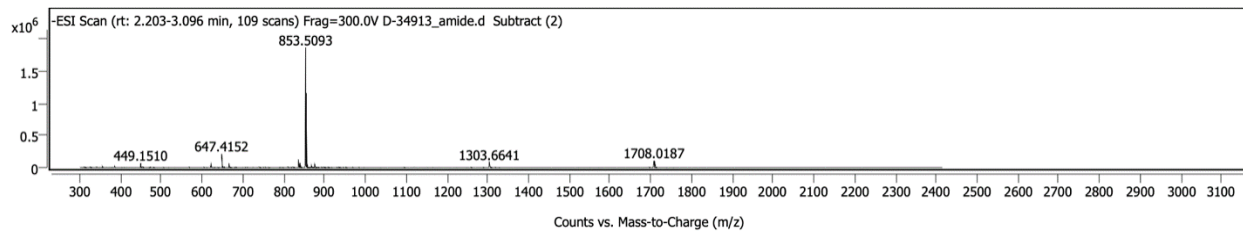
Appendix Figure A.47 MS of LPPM-4
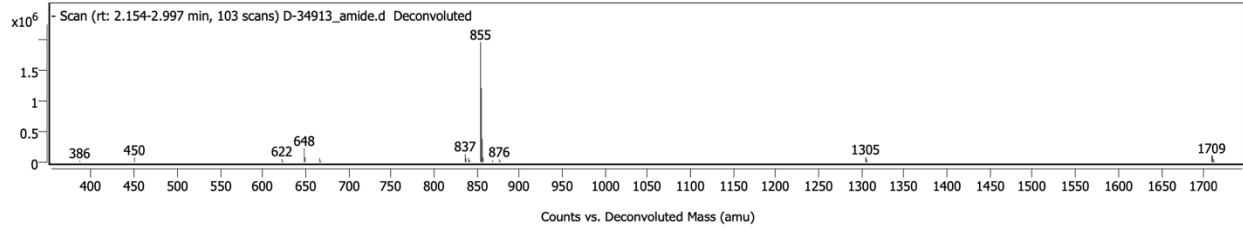
Appendix Figure A.48 Deconvolution of LPPM-4
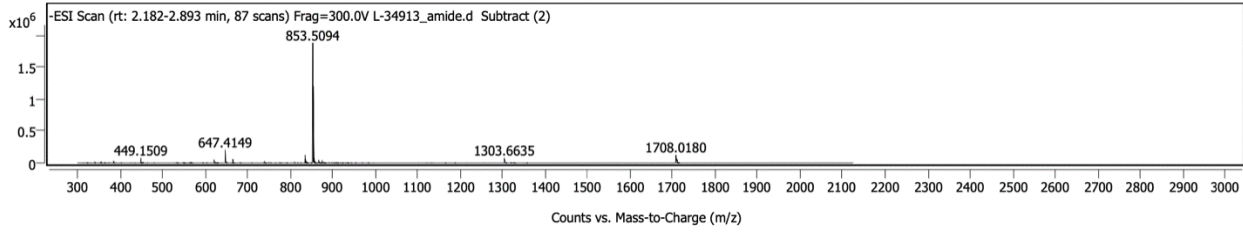
Appendix Figure A.49 MS of LPPM-5
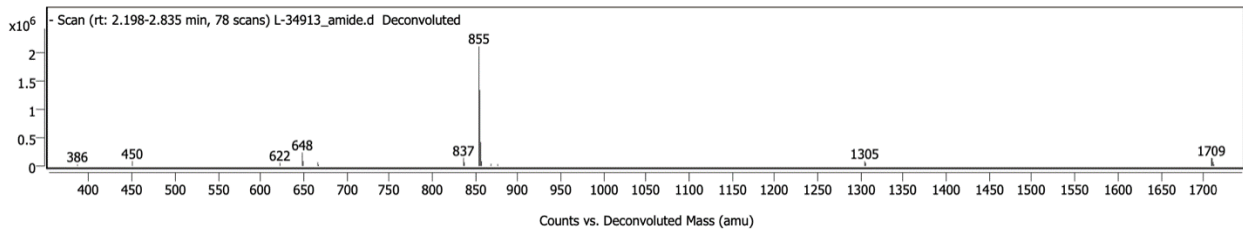
Appendix Figure A.50 Deconvolution of LPPM-5
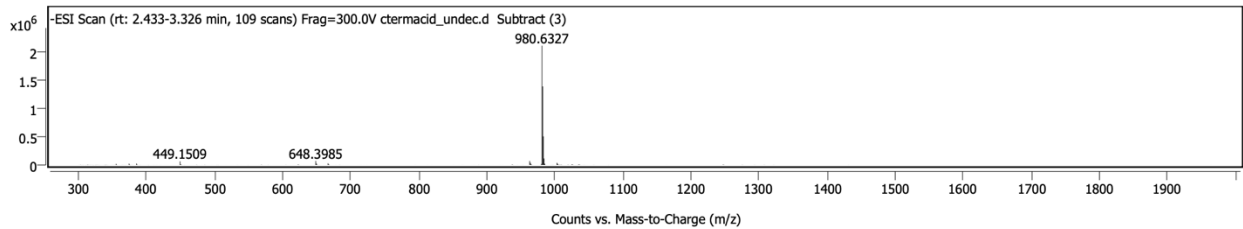
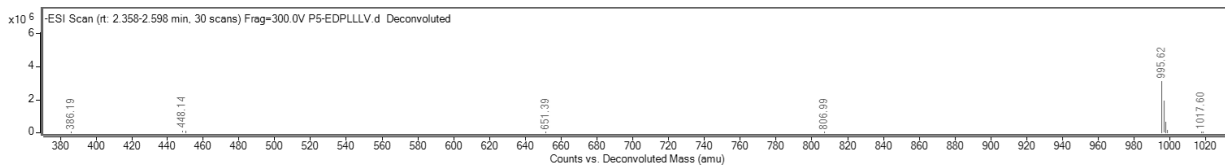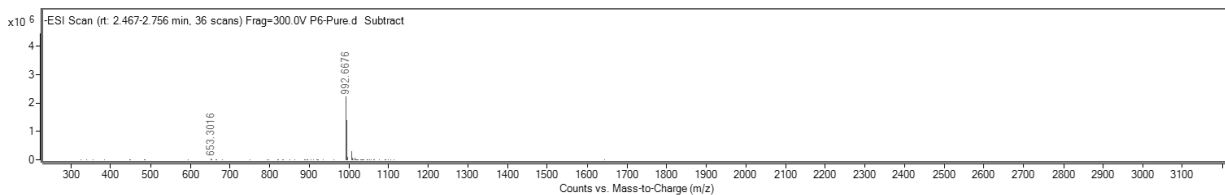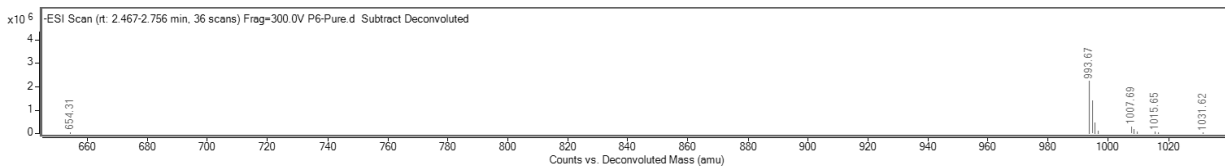Appendix Figure A.51 MS of LPPM-6
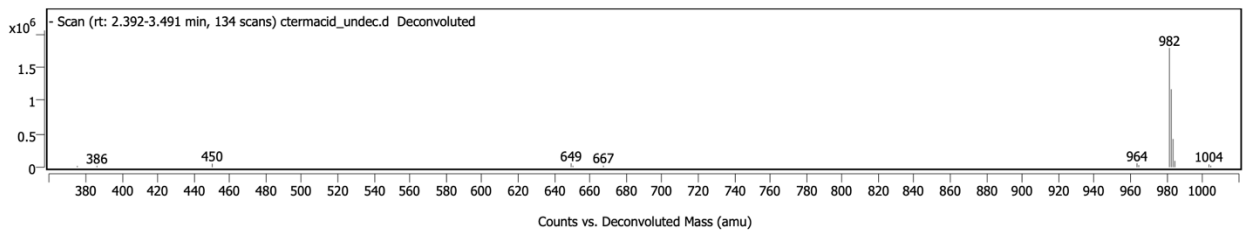
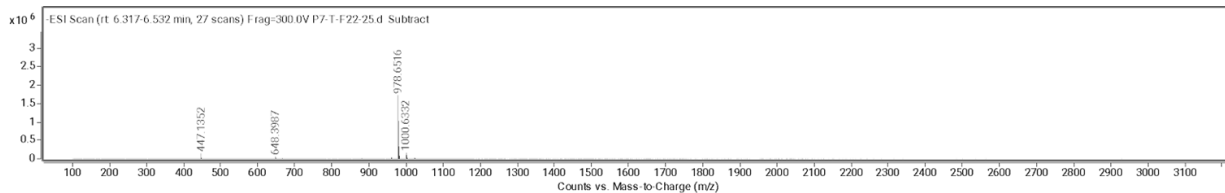Appendix Figure A.52 Deconvolution of LPPM-6
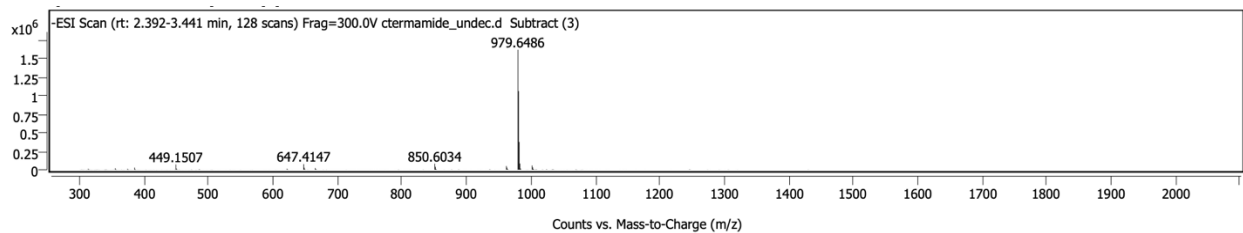
Appendix Figure A.53 MS of LPPM-7
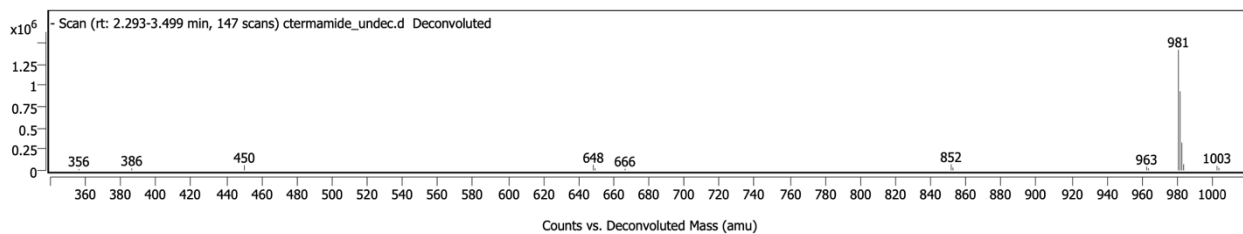
Appendix Figure A.54 Deconvolution of LPPM-7
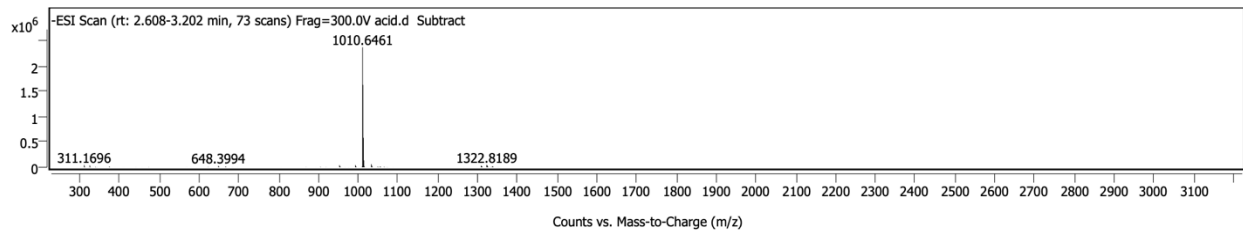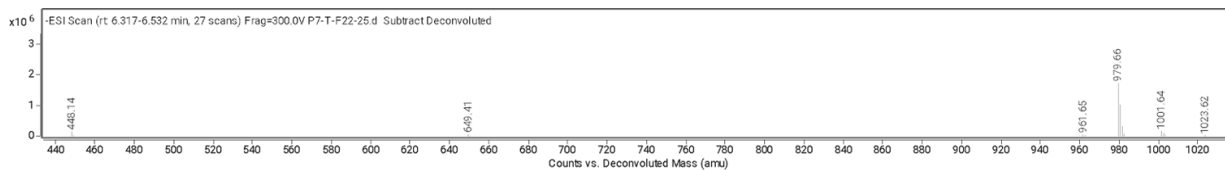

Appendix Figure A.55 MS of LPPM-8
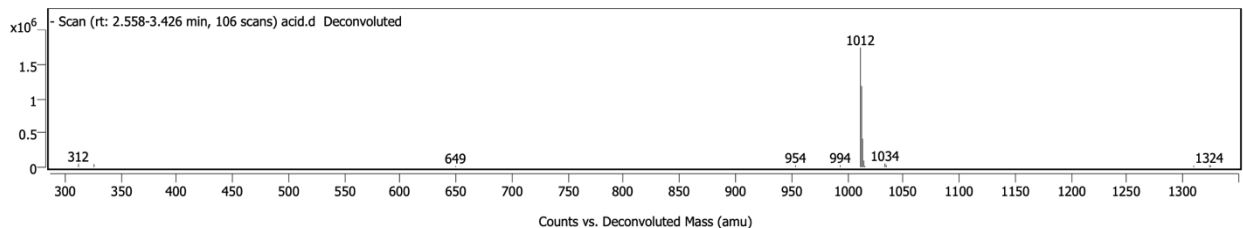
Appendix Figure A.56 Deconvolution of LPPM-8
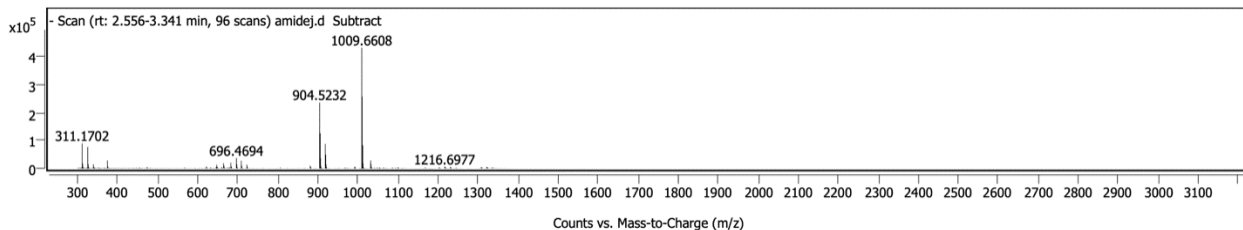
Appendix Figure A.57 MS of LPPM-9

157
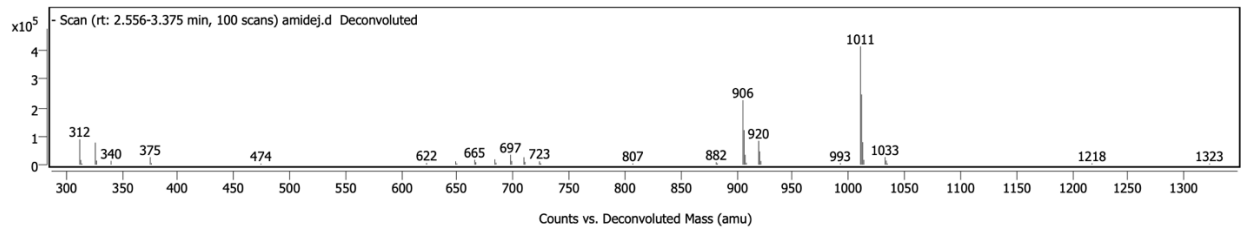
Appendix Figure A.58 Deconvolution of LPPM-9
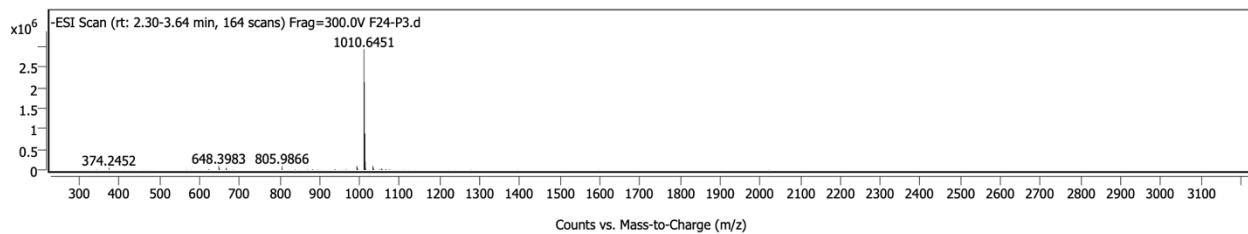
Appendix Figure A.59 MS of LPPM-10
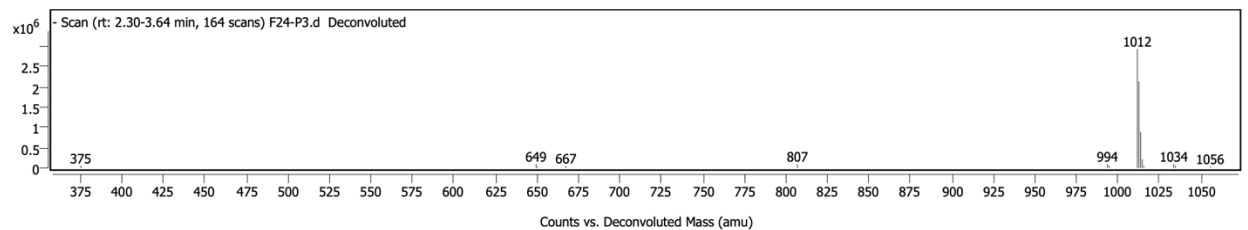
Appendix Figure A.60 Deconvolution of LPPM-10

Appendix Figure A.61 Analytical trace of LPPM-8-ADLLLLV. Zoomed in analytical trace. Peak before 5 min. corresponds to solvent peak, DMSO. Purity >99% at 214 nm.

Appendix Figure A.62 Analytical trace of LPPM-8-EALLLLV. Zoomed in analytical trace. Peak before 5 min. corresponds to solvent peak, DMSO. Purity >99% at 214 nm.

Appendix Figure A.63 Analytical trace of LPPM-8-EDALLLV. Purity >91% at 214 nm.

160
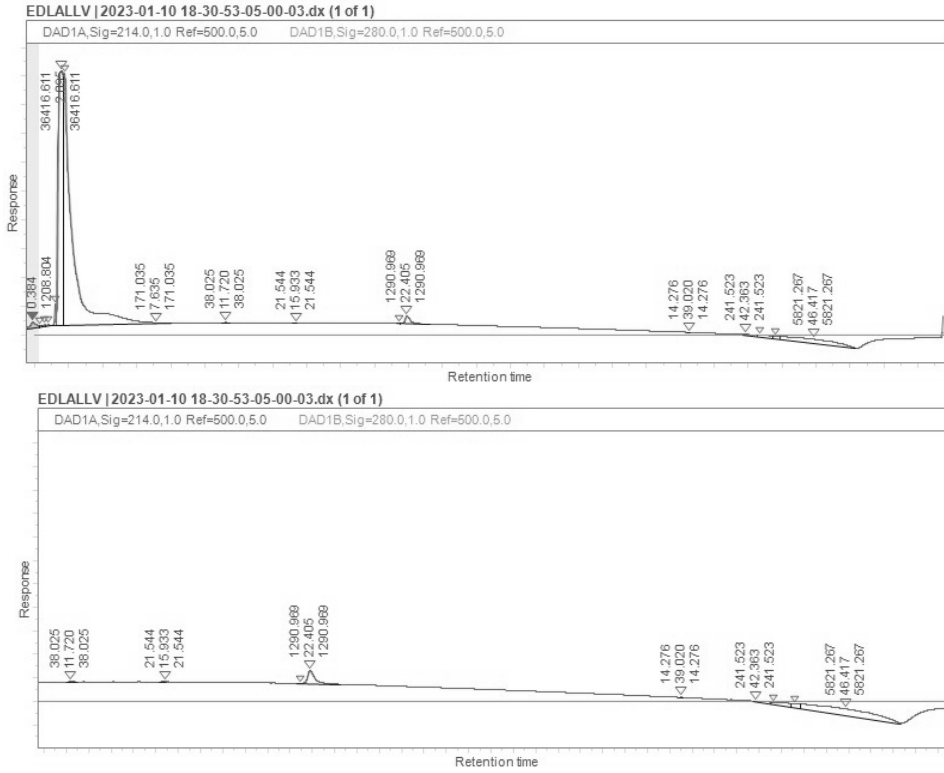
Appendix Figure A.64 Analytical trace of LPPM-8-EDLALLV. Zoomed in analytical trace. Peak before 5 min. corresponds to solvent peak, DMSO. Purity >99% at 214 nm
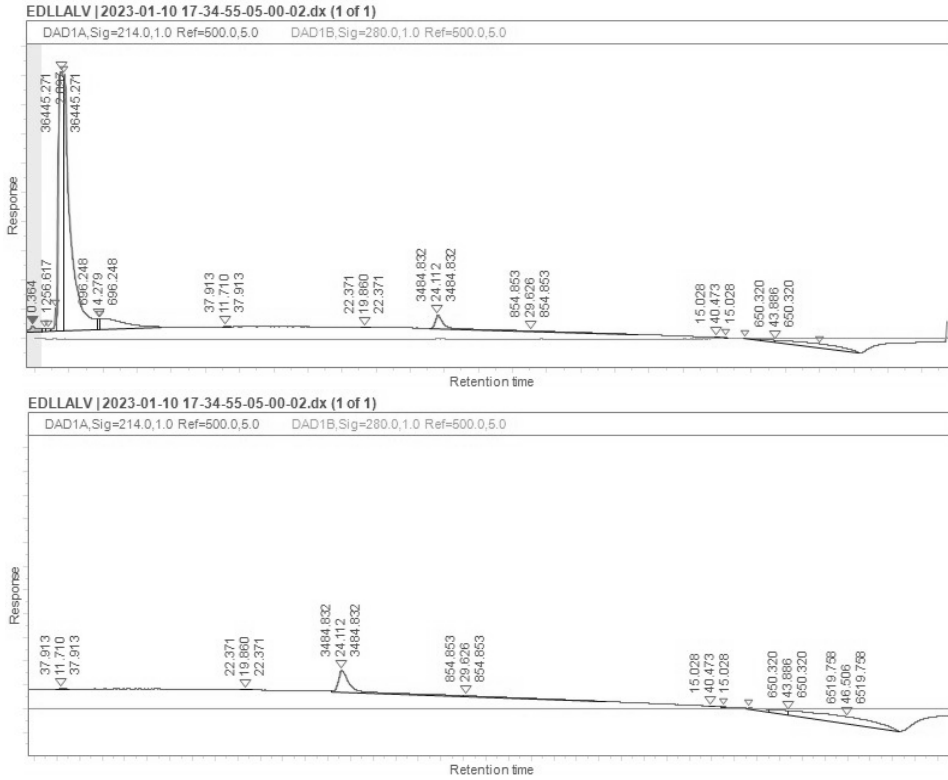
Appendix Figure A.65 Analytical trace of LPPM-8-EDLLALV. Zoomed in analytical trace. Peak before 5 min. corresponds to solvent peak, DMSO. Purity >99% at 214 nm.
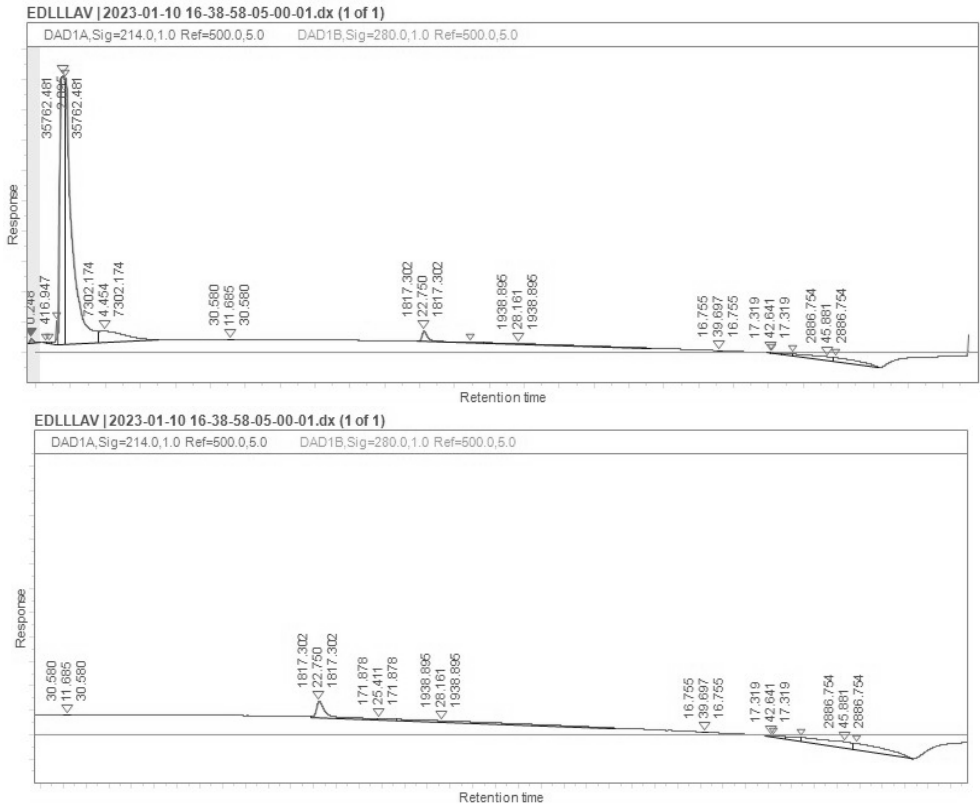
Appendix Figure A.66 Analytical trace of LPPM-8-EDLLLAV. Zoomed in analytical trace. Peak before 5 min. corresponds to solvent peak, DMSO. Purity >99% at 214 nm.
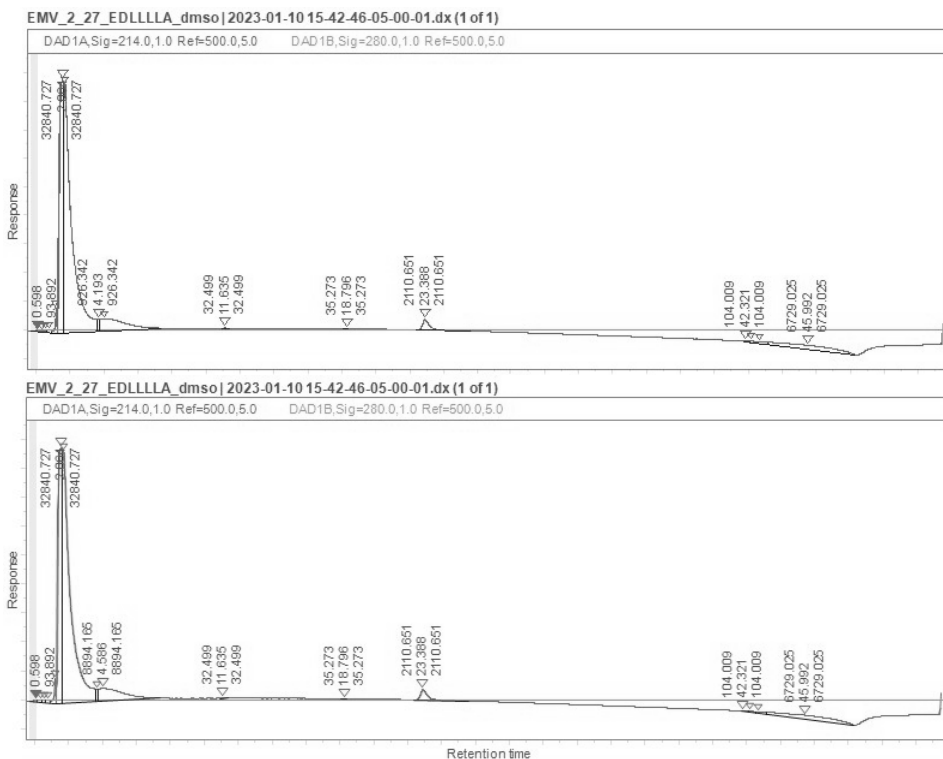
Appendix Figure A.67 Analytical trace of LPPM-8-EDLLLLA. Zoomed in analytical trace. Peak before 5 min. corresponds to solvent peak, DMSO. Purity >99% at 214 nm.

High Resolution Mass Spectrometry of Lipopeptidomimetics – Library B
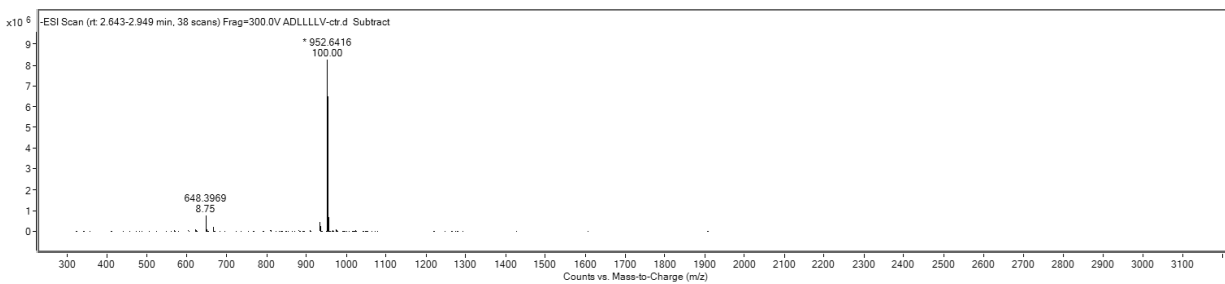
Appendix Figure A.68 MS of LPPM-8-ADLLLLV
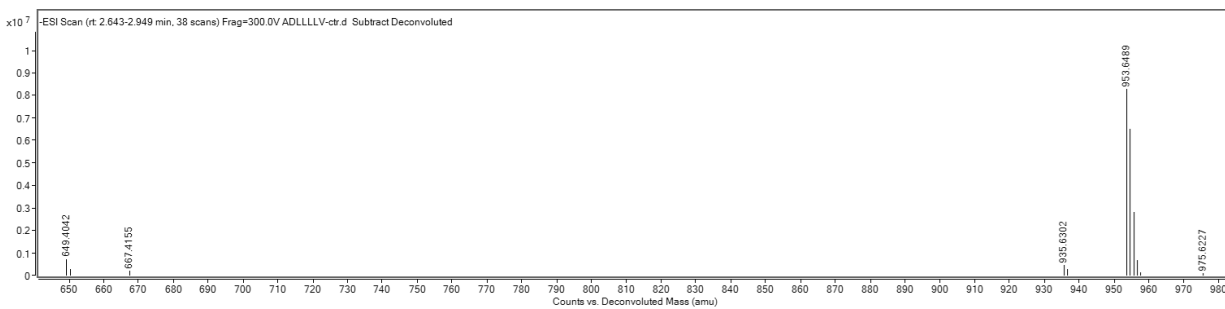
Appendix Figure A.69 Deconvolution of LPPM-8-ADLLLLV
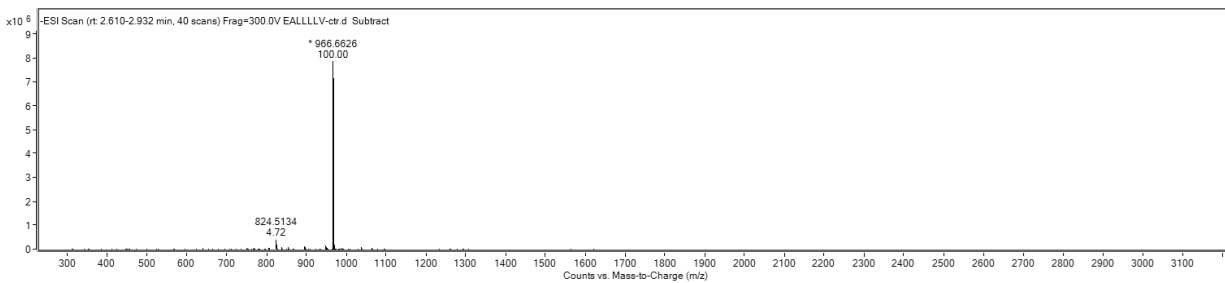
Appendix Figure A.70 MS of LPPM-8-EALLLLV
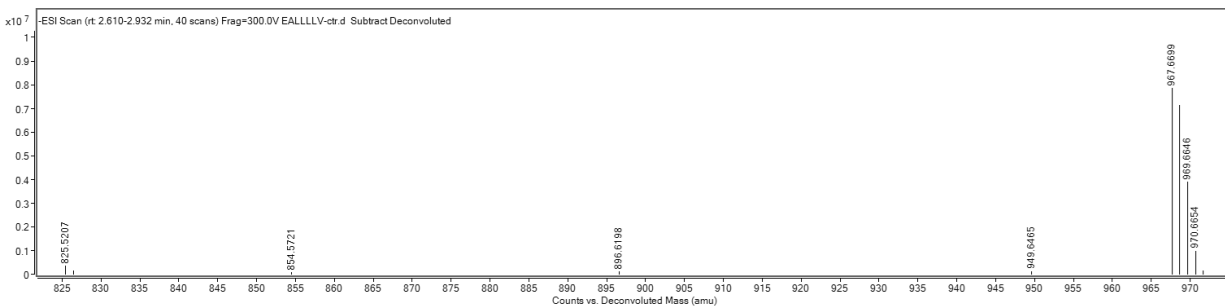
Appendix Figure A.71 Deconvolution of LPPM-8-EALLLLV
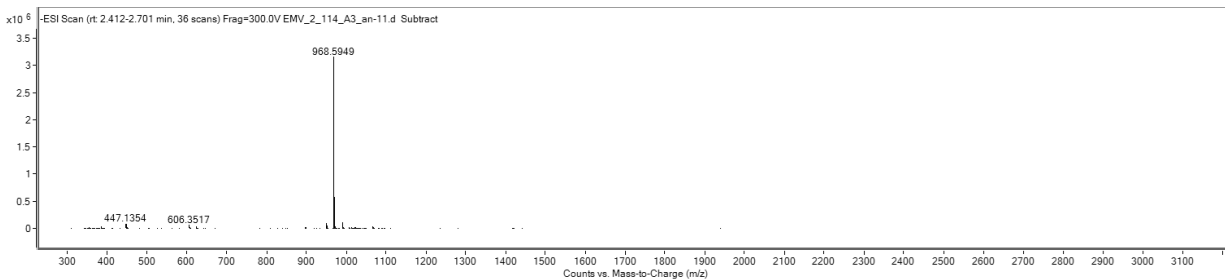
Appendix Figure A.72 MS of LPPM-8-EDALLLV
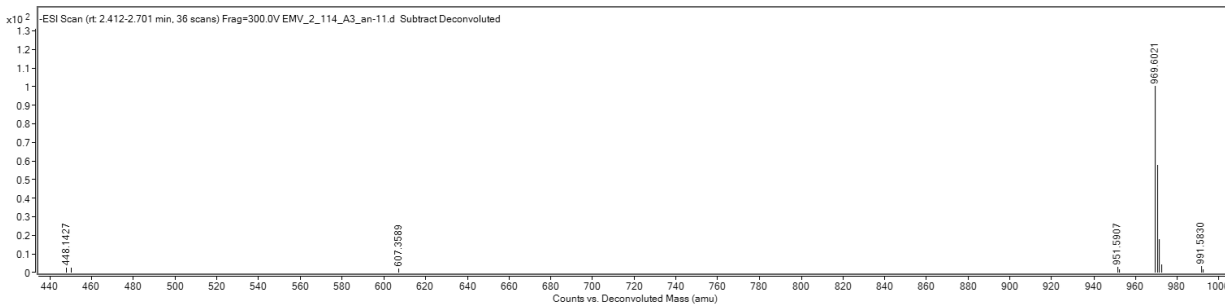
Appendix Figure A.73 Deconvolution of LPPM-8-EDALLLV
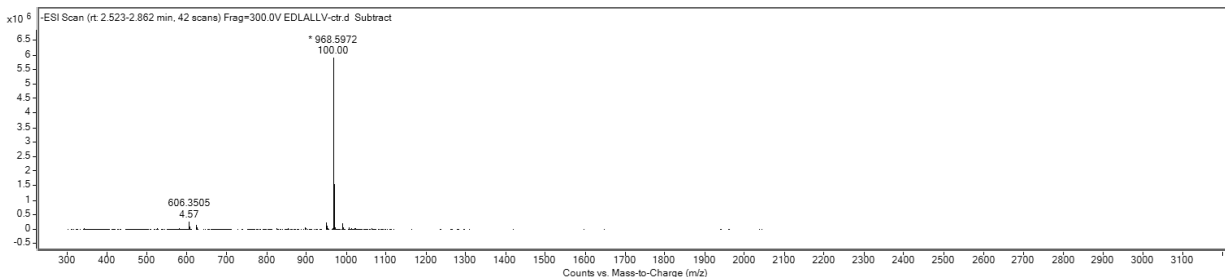
Appendix Figure A.74 MS of LPPM-8-EDLALLV
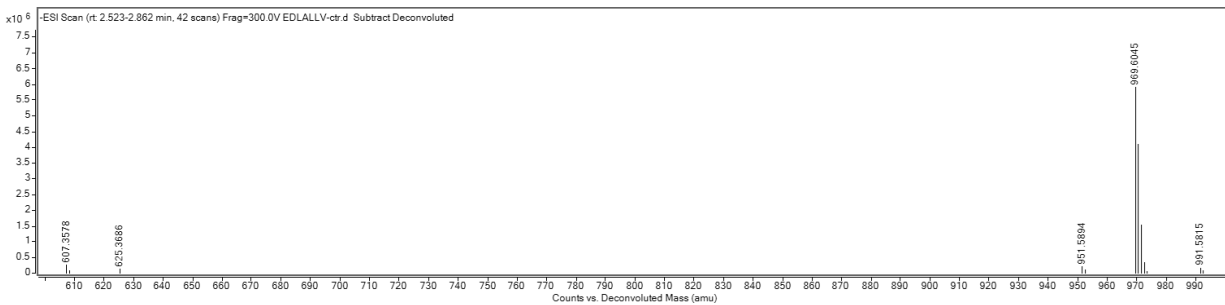
Appendix Figure A.75 Deconvolution of LPPM-8-EDLALLV

166
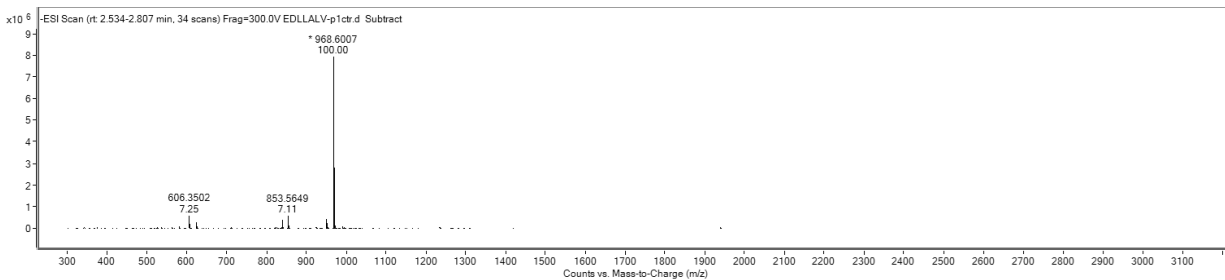
Appendix Figure A.76 MS of LPPM-8-EDLLALV
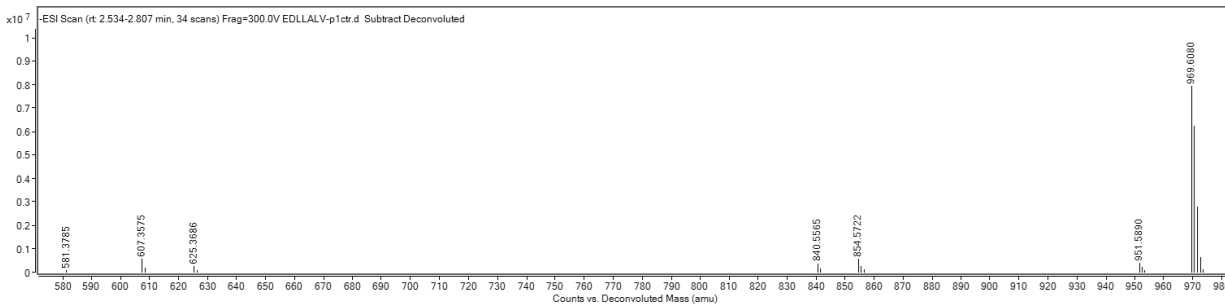
Appendix Figure A.77 Deconvolution of LPPM-8-EDLLALV
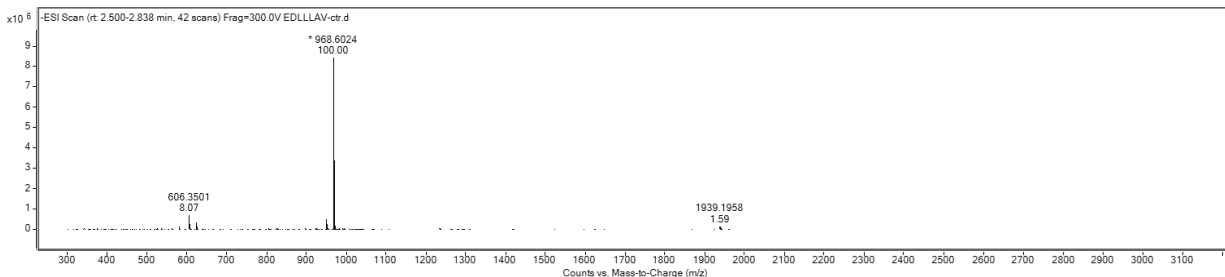
Appendix Figure A.78 MS of LPPM-8-EDLLLAV
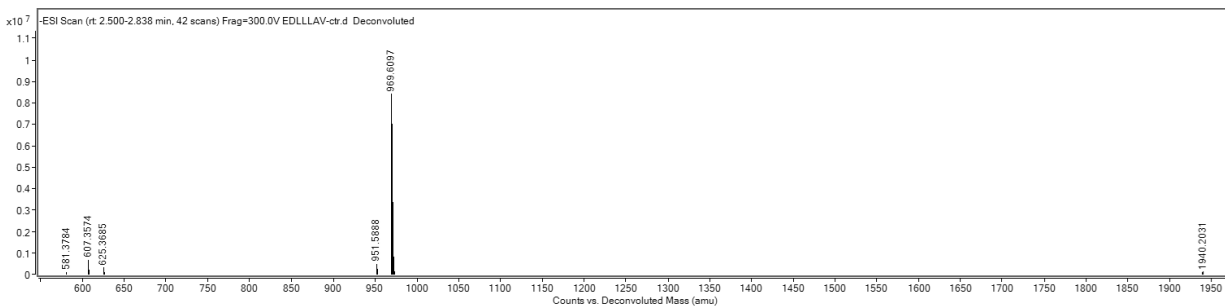
Appendix Figure A.79 Deconvolution of LPPM-8-EDLLLAV
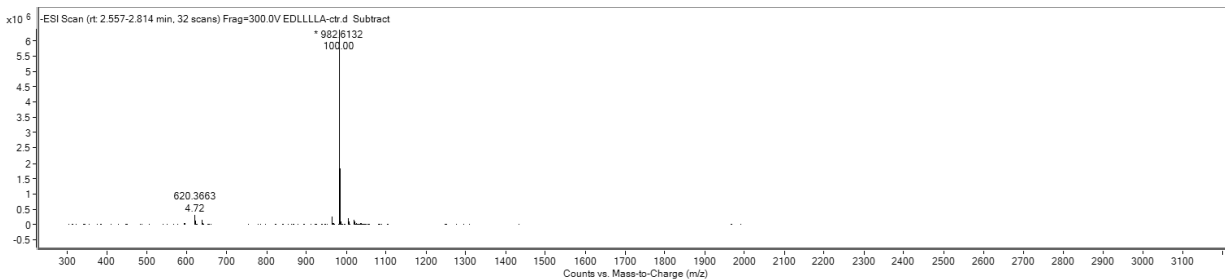
Appendix Figure A.80 MS of LPPM-8-EDLLLLA
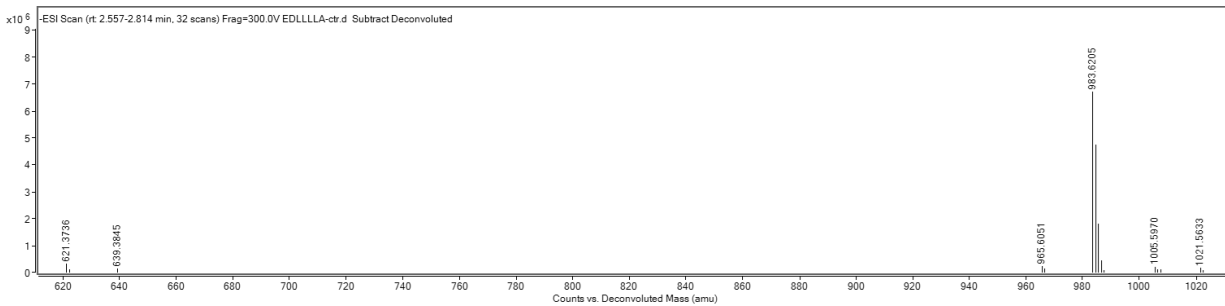
Appendix Figure A.81 Deconvolution of LPPM-8-EDLLLLA

Appendix Figure A.82 Analytical trace of LPPM-8-EPLLLLV**.** Zoomed in analytical trace. Peak before 5 min. corresponds to solvent peak, DMSO. Purity >99% at 214 nm.
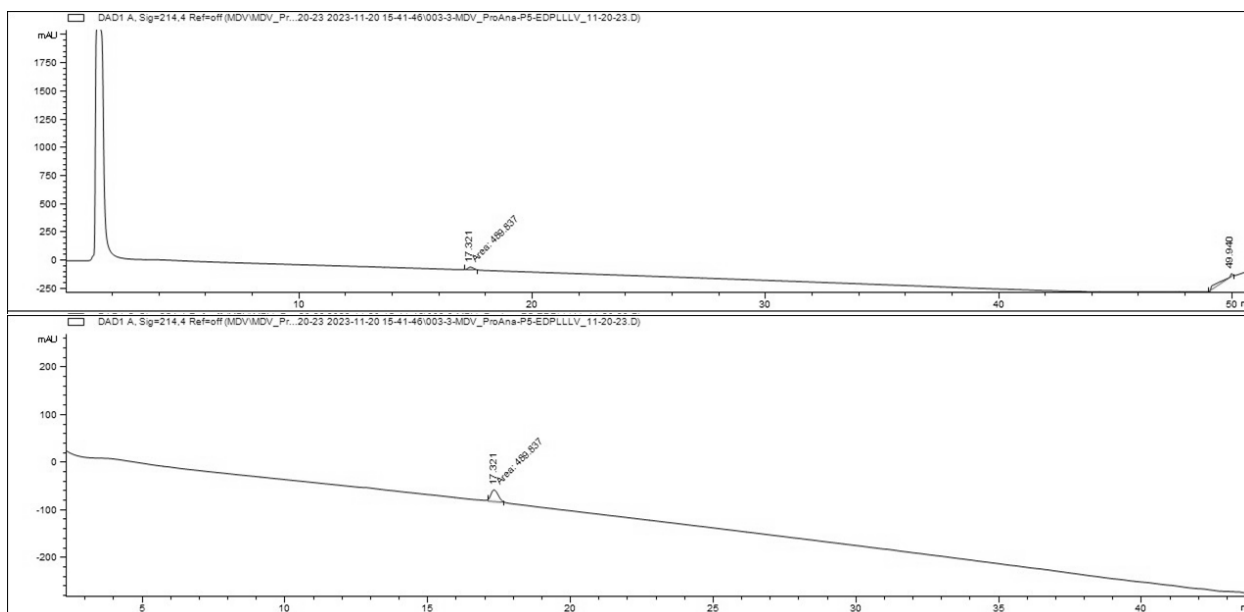
Appendix Figure A.83 Analytical trace of LPPM-8-EDPLLLV**.** Zoomed in analytical trace. Peak before 5 min. corresponds to solvent peak, DMSO. Purity >99% at 214 nm.
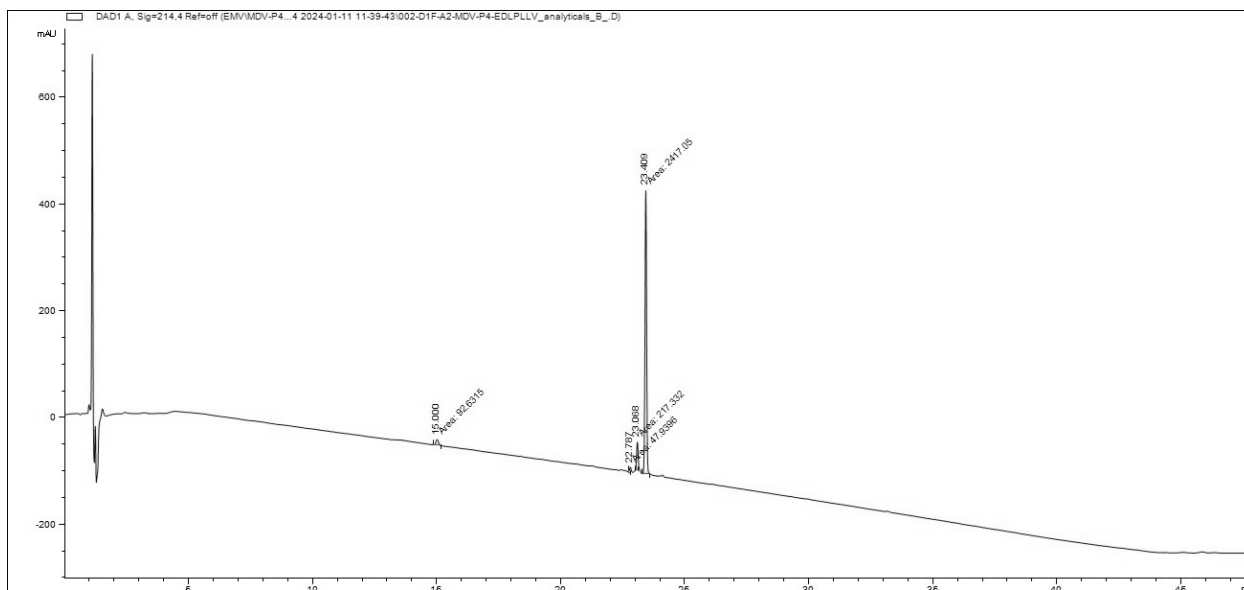
Appendix Figure A.84 Analytical trace of LPPM-8-EDLPLLV. Peak before 5 min. corresponds to solvent peak, DMSO. Purity % at 214 nm.
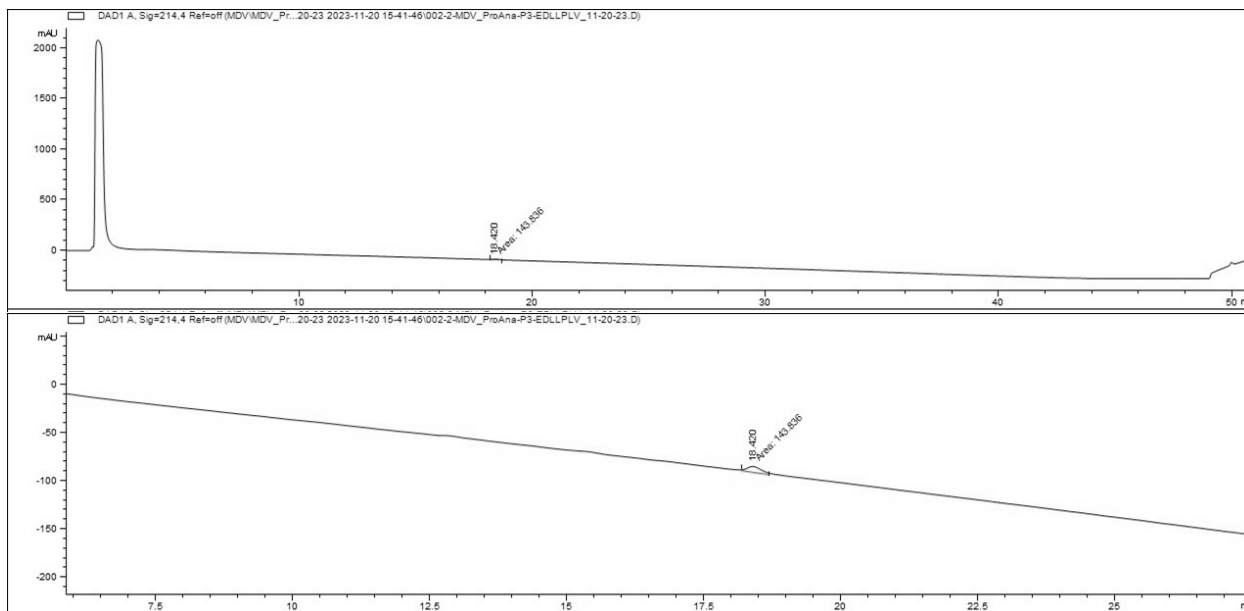
Appendix Figure A.85 Analytical trace of LPPM-8-EDLLPLV. Zoomed in analytical trace. Peak before 5 min. corresponds to solvent peak, DMSO. Purity >99% at 214 nm.

Appendix Figure A.86 Analytical trace of LPPM-8-EDLLLPV. Zoomed in analytical trace. Peak before 5 min. corresponds to solvent peak, DMSO. Purity >99% at 214 nm

Appendix Figure A.87 MS of LPPM-8-EDLLLPV
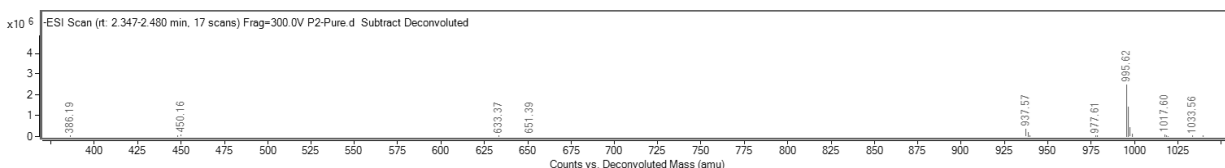
Appendix Figure A.88 Deconvolution of LPPM-8-EDLLLPV

Appendix Figure A.89 MS of LPPM-8-EDLLPLV
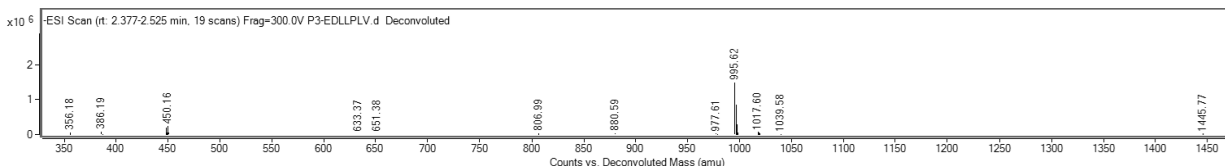
Appendix Figure A.90 Deconvolution of LPPM-8-EDLLPLV
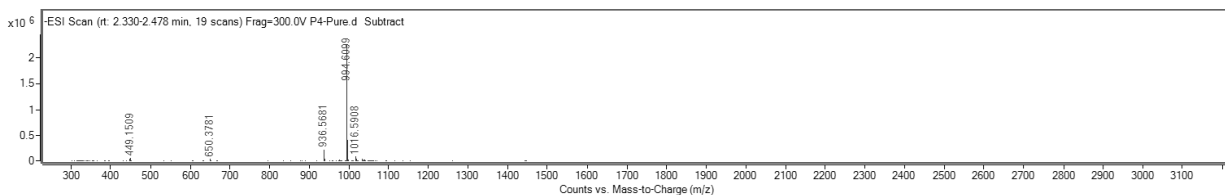
Appendix Figure A.91 MS of LPPM-8-EDLPLLV
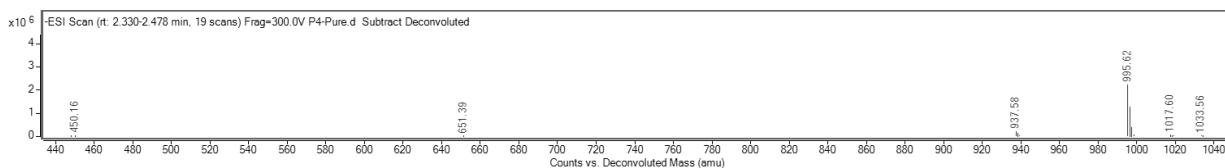
Appendix Figure A.92 Deconvolution of LPPM-8-EDLPLLV

Appendix Figure A.93 MS of LPPM-8-EDPLLLV

Appendix Figure A.94 Deconvolution of LPPM-8-EDPLLLV

Appendix Figure A.95 MS of LPPM-8-EPLLLLV

Appendix Figure A.96 Deconvolution of LPPM-8-EPLLLLV

Appendix Figure A.97 MS of LPPM-8-PDLLLLV

Appendix Figure A.98 Deconvolution of LPPM-8-PDLLLLV

.

Appendix B: Supplemental Data for Chapter 2: A lipopeptidomimetic of TADs selectively disrupts Med25 PPIs
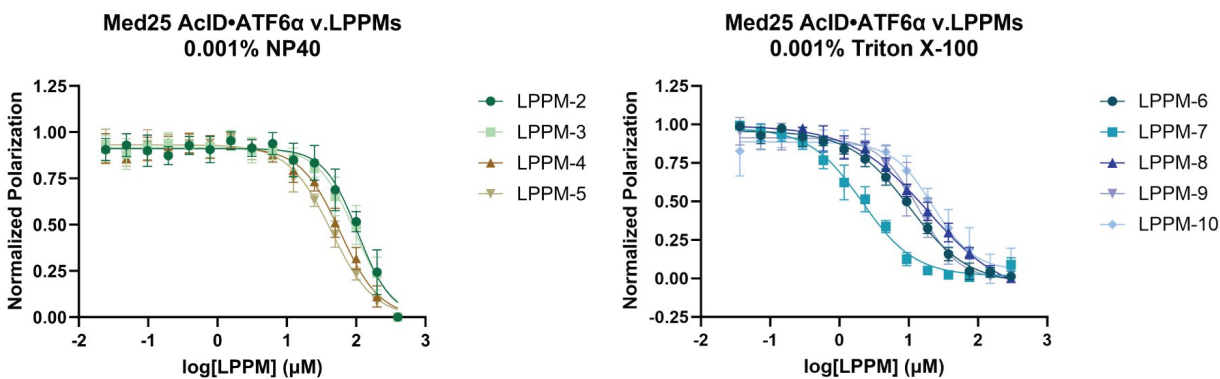
Appendix Figure B.1 Inhibition binding curves of Med25 AcID•ATF6α by LPPM library A as determined by competitive fluorescence polarization assays. Apparent IC_{50} values were determined through titration of compound for Med25 AcID•ATF6α in experimental triplicate with the indicated error (SD). Data shown is the average of three independent experiments with the indicated error (SD). Experiments on the left conducted by O.Pattelli.
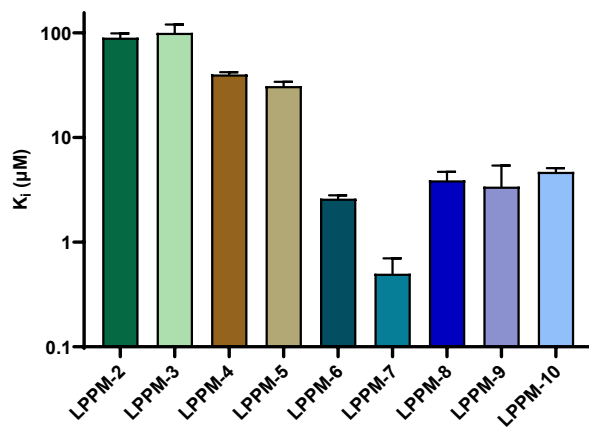

Appendix Figure B.2 Inhibition of Med25 AcID•ATF6α by lipopeptidomimetics as determined by competitive fluorescence polarization assays. Apparent IC_{50} values were determined through titration of compound for Med25 AcID•ATF6α in experimental triplicate with the indicated error (SD). The IC_{50} values were converted to K_i values using the apparent K_d value based on the direct binding of Med25 AcID•ATF6α. Data shown is the average of three independent experiments with the indicated error (SD).
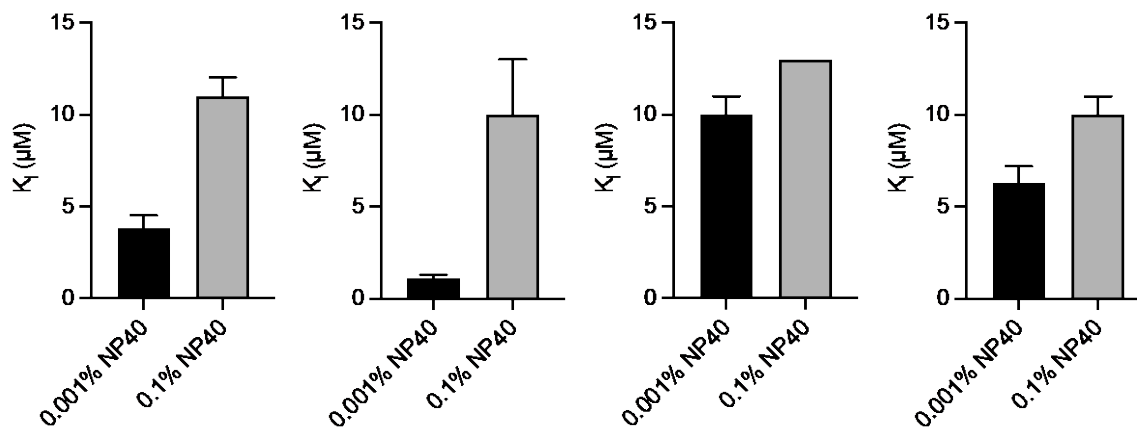
Appendix Figure B.3 Inhibition of Med25 AcID•ATF6α by LPPM-6 (left), LPPM-7 (left middle), LPPM-8 (right middle), and LPPM-9 (right) with different NP40 concentrations as determined by competitive fluorescence polarization assays. Apparent IC_{50} values were determined through titration of compound for Med25 AcID•ATF6α PPI performed in triplicate with the indicated error (SD). The IC_{50} values were converted to K_i values using the apparent K_d value based on the direct binding of Med25 AcID•ATF6α PPI using a K_i calculator. Data shown is the average of two independent experiments with indicated error (SD). Experiments conducted by O.Pattelli.
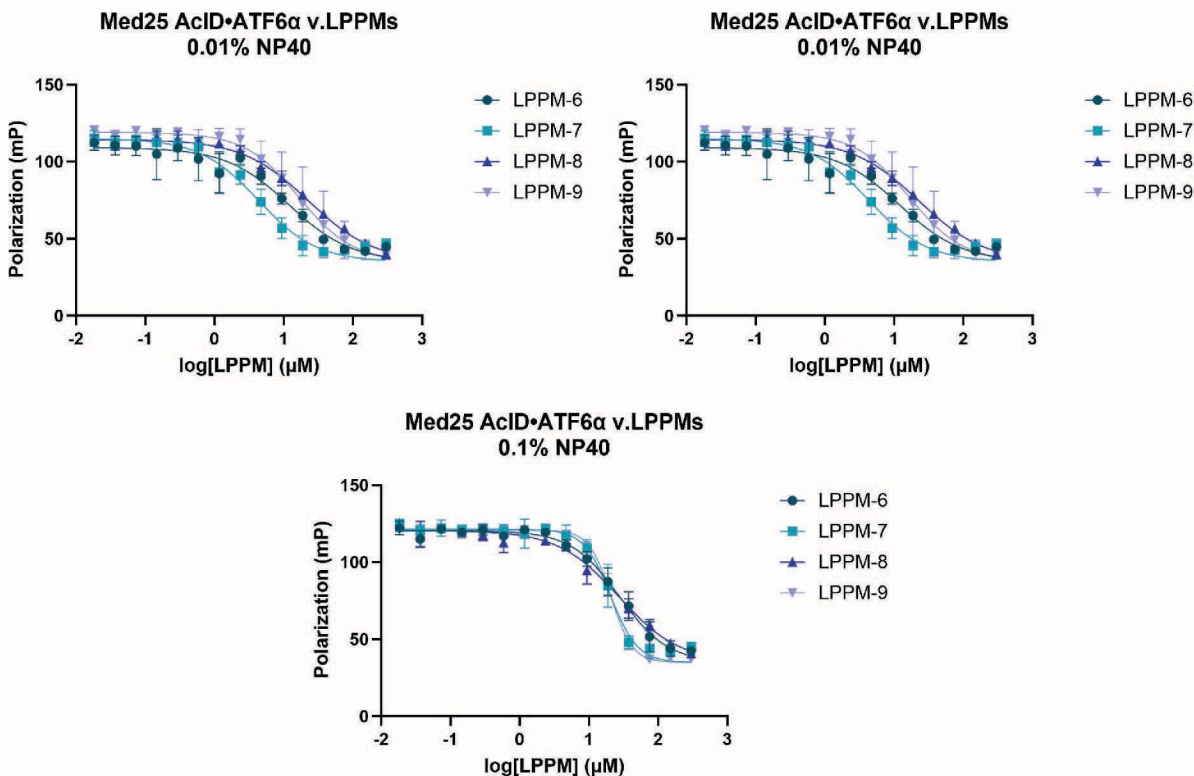
Appendix Figure B.41 Inhibition binding curves of Med25 AcID•ATF6α by LPPM-6,LPPM-7, LPPM-8, and LPPM-9 with different NP40 concentrations (0.001%, 0.01%, 0.1%) as determined by competitive fluorescence polarization assays. Apparent IC_{50} values were determined through titration of compound for Med25 AcID•ATF6α PPI performed in experimental triplicate with the indicated error (SD). Data shown is the average of two independent experiments with the indicated error (SD).
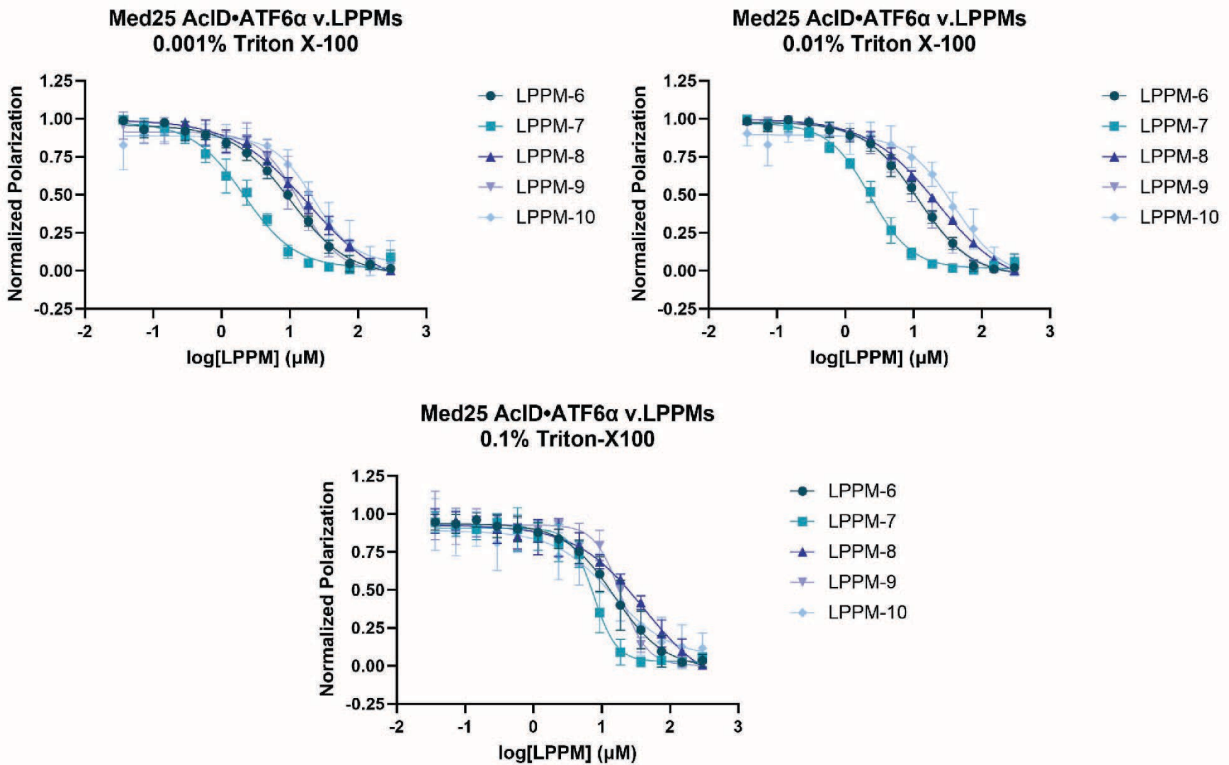
Appendix Figure B.52 Inhibition binding curves of Med25 AcID•ATF6α by LPPM-6,LPPM-7, LPPM-8, LPPM-9 and LPPM-10 with different Triton X-100 concentrations (0.001%, 0.01%, 0.1%) as determined by competitive fluorescence polarization assays. Apparent IC_{50} values were determined through titration of compound for Med25 AcID•ATF6α PPI performed in experimental triplicate with the indicated error (SD). Data shown is the average of three independent experiments with the indicated error (SD).
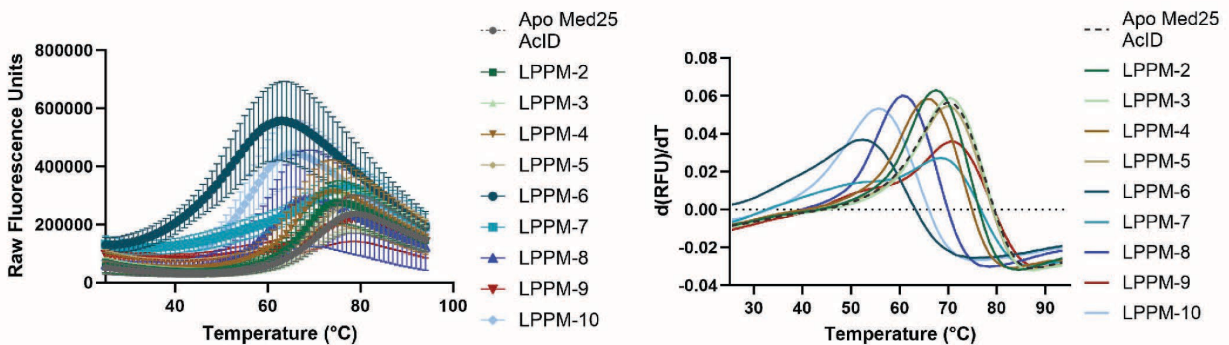
Appendix Figure B.6 DSF data for LPPMs 2-10. Raw fluorescence units (left) and first derivative (right) traces of Med25 AcID with 5 equiv. of each respective LPPM. Melting temperature was determined from raw fluorescence data using DSFworld. Data was obtained in technical triplicates with the indicated error (SD) and is representative of experiments performed in biological triplicates.
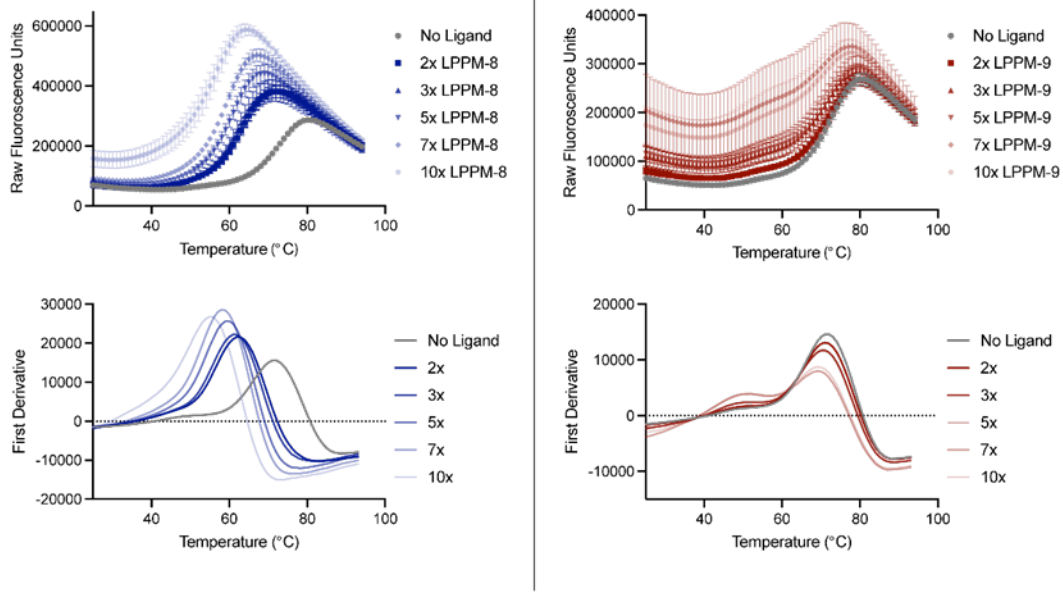
Appendix Figure B.7. Raw DSF data for LPPM-8 and LPPM-9. Left. Raw fluorescence units (top) and first derivative (bottom) traces of Med25 AcID 2, 3, 5, 7, and 10 equiv. of LPPM-8. Right. Raw fluorescence units (top) and first derivative (bottom) traces of Med25 AcID 2, 3, 5, 7, and 10 equiv. of LPPM-9. Melting temperature was determined from raw fluorescence data using DSFworld. Data was obtained in technical triplicates with the indicated error (SD) and is representative of experiments performed in biological duplicates.
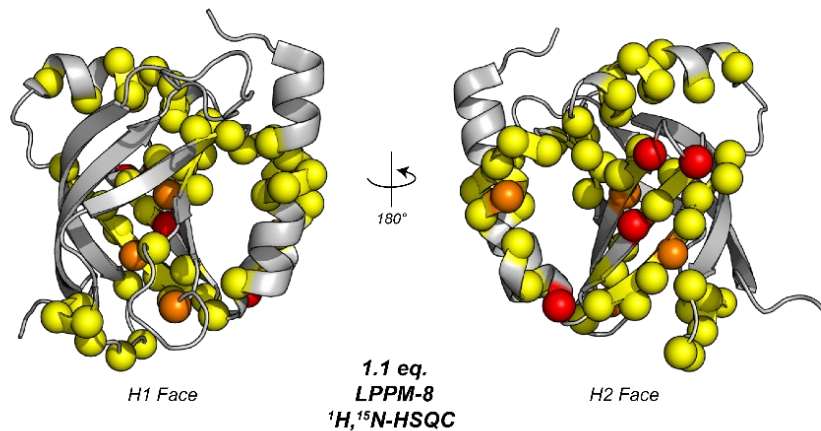
Appendix Figure B.8 All ^{1}H, ^{15}N-HSQC perturbations of 1.1 equiv. of LPPM-8 mapped onto Med25 AcID (PDB ID 2XNF). All residues with CSPs above the signal-to-noise (S/N) ratio (≥ 0.02 ppm) are shown, including several residues with weaker shift patterns (yellow residues). Yellow = 0.02 ppm – 0.085 ppm, orange = 0.0851 ppm – 0.14 ppm, red ≥ 0.141 ppm.
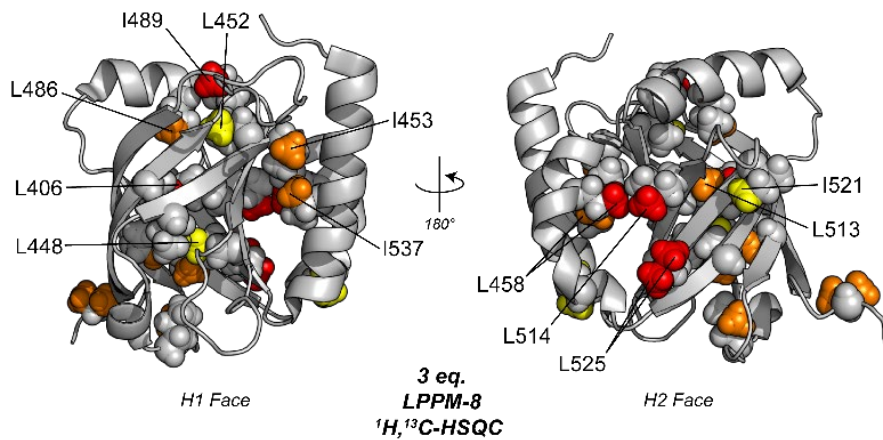
Appendix Figure B.9 Chemical shifts perturbations from saturated concentrations of LPPM-8 (3 equiv.) mapped onto Med25 AcID (PDB ID 2XNF).^{1}H,^{13}C-HSQC spectra with high concentrations of LPPM-8 showed increased chemical shift perturbations, though significant perturbations (orange and red residues) occurred primarily on the H2 face of AcID and flanking α-helices. Yellow = 0.02 ppm - 0.0249 ppm, orange = 0.025 ppm - 0.049 ppm, red ≥ 0.0.0491 ppm.
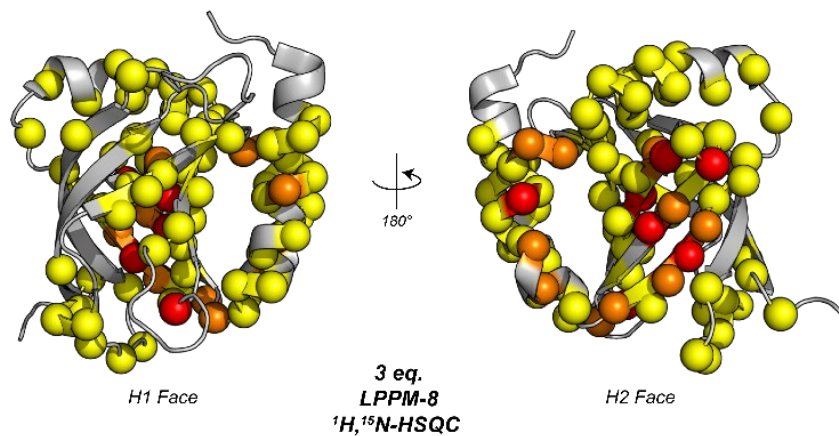
Appendix Figure B.10 Chemical shifts perturbations from saturated concentrations of LPPM-8 (3 equiv.) mapped onto Med25 AcID (PDB ID 2XNF). ^{1}H, ^{15}N-HSQC spectra revealed several significant changes to the H2 face, with only minor shifts affecting the H1 face (yellow residues). Yellow = 0.02 ppm - 0.085 ppm, orange = 0.0851 ppm - 0.14 ppm, red ≥ 0.141 ppm.
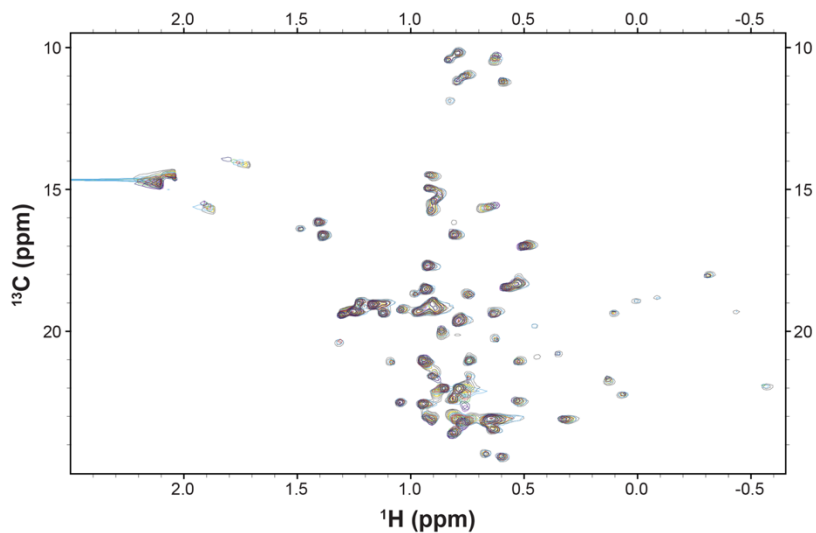
Appendix Figure B.11 ^{1}H,^{13}C-HSQC spectra of LPPM-8 and all residues CSPs. ^{1}H, ^{13}C-HSQC CSPs of Med25 residues with 1.1 equiv. of LPPM-8.
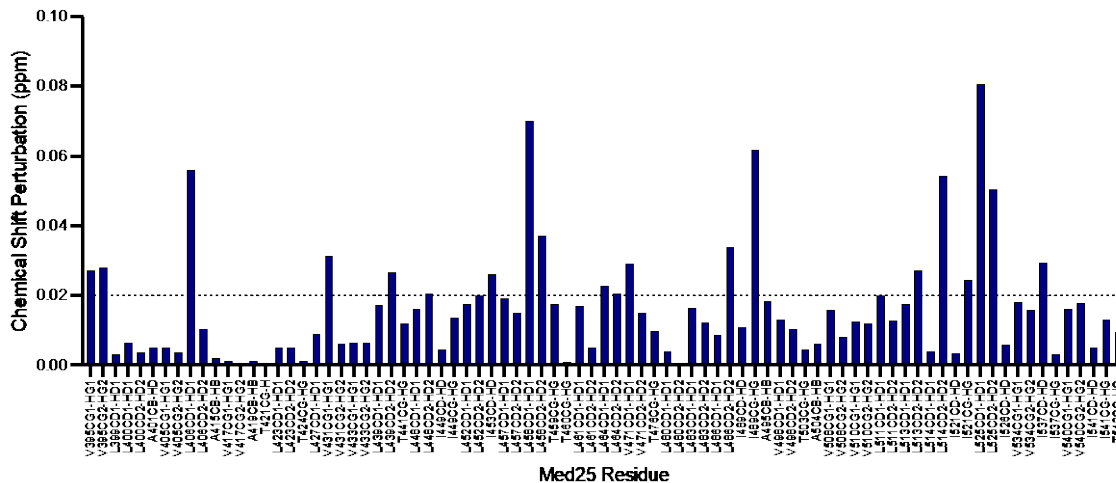
Appendix Figure B.12 ^{1}H,^{13}C-HSQC spectra of LPPM-8 and all Med25 residues CSPs. ^{1}H, ^{13}C HSQC CSPs of Med25 residues with 3 equiv. of LPPM-8. Dashed line indicates the level of 3 standard deviations above the average chemical shift perturbation.
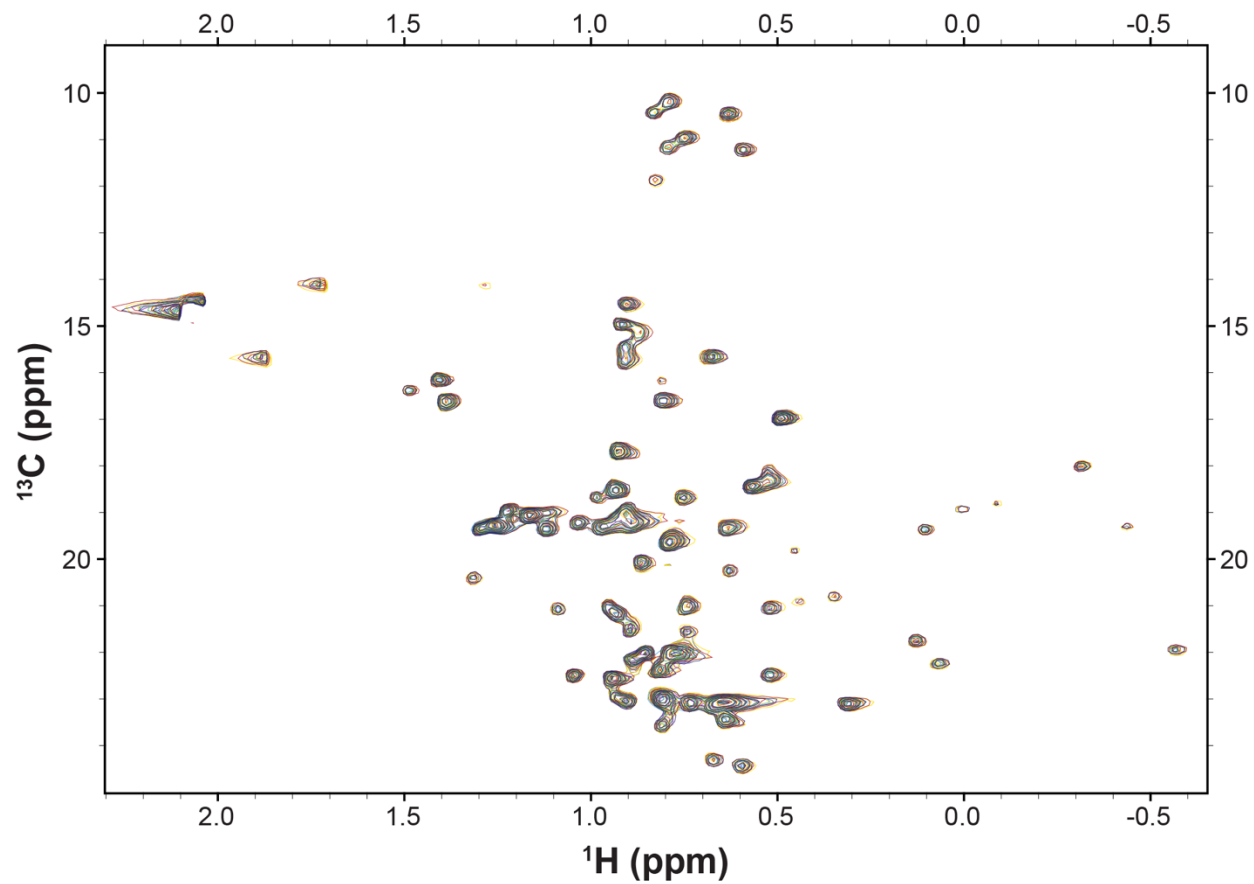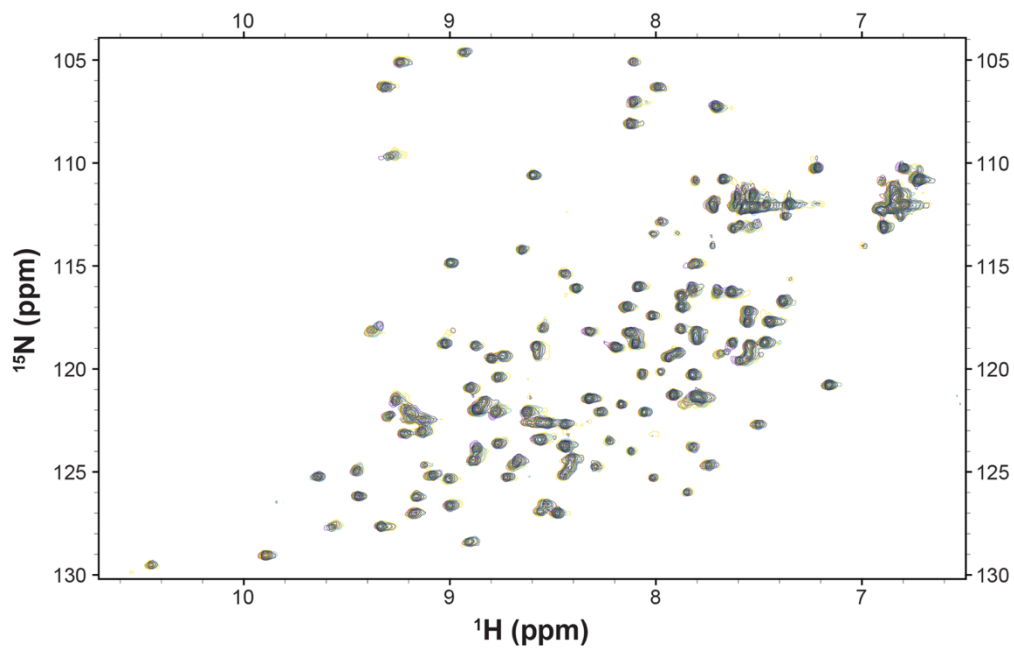
Appendix Figure B.13 ^{1}H, ^{13}C-HSQC spectra of LPPM-9 and all residue CSPs. Top. Overlay of ^{1}H, ^{13}C-HSQC spectra of Med25 with titration of LPPM-9. Spectra shown are free Med25 (dark grey), 0.2 equiv. of LPPM-9 (yellow), 0.5 equiv. LPPM-9 (light blue), 0.8 equiv. LPPM-9 (red), 1.1 equiv. LPPM-9 (green), 2 equiv. LPPM-9 (dark blue), 3 equiv. LPPM-9 (purple).
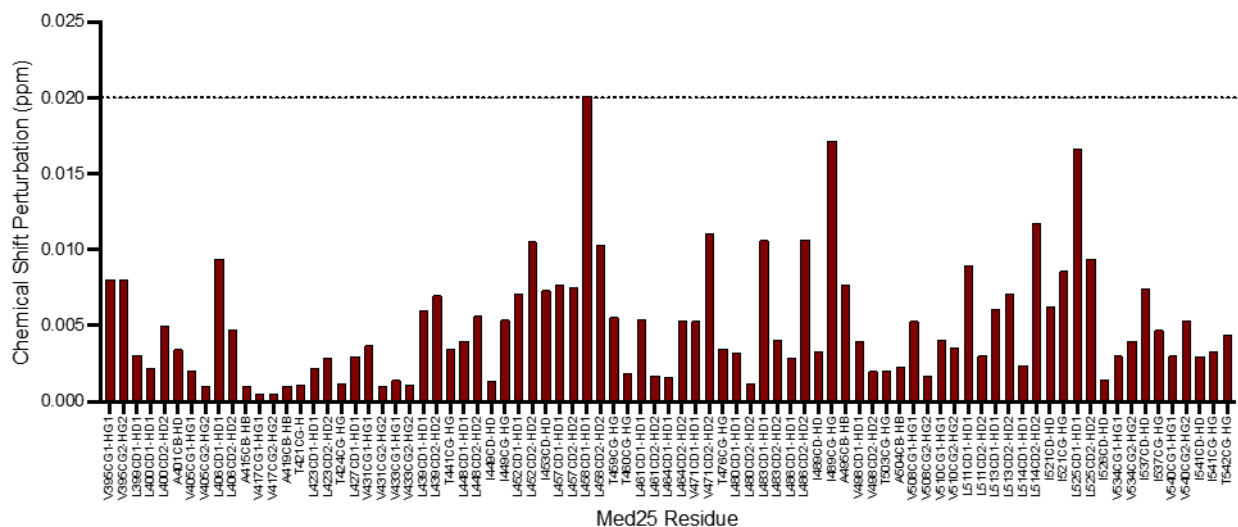
Appendix Figure B.14 ^{1}H,^{13}C-HSQC spectra of LPPM-9 and all residue CSPs. ^{1}H, ^{13}C-HSQC CSPs of Med25 residues with 3 equiv. of LPPM-9. Dashed line indicates the level of 3 standard deviations above the average chemical shift perturbation.
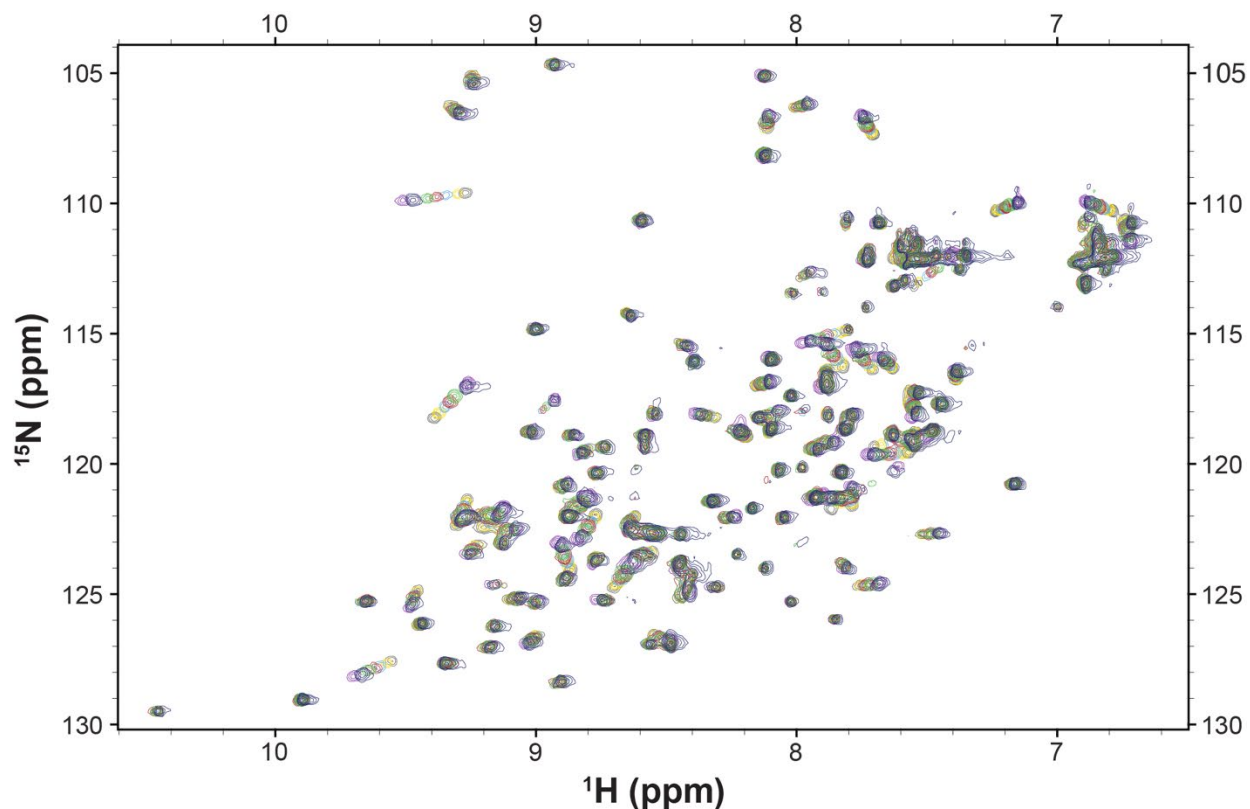
Appendix Figure B.15. Overlay of ^{1}H, ^{15}N-HSQC spectra of Med25 with titration of LPPM-8. Spectra shown are free Med25 (dark grey), 0.2 equiv. of LPPM-8 (yellow), 0.5 equiv. LPPM-8 (light blue), 0.8 equiv. LPPM-8 (red), 1.1 equiv. LPPM-8 (green), 2 equiv. LPPM-8 (dark blue), 3 equiv. LPPM-8 (purple).
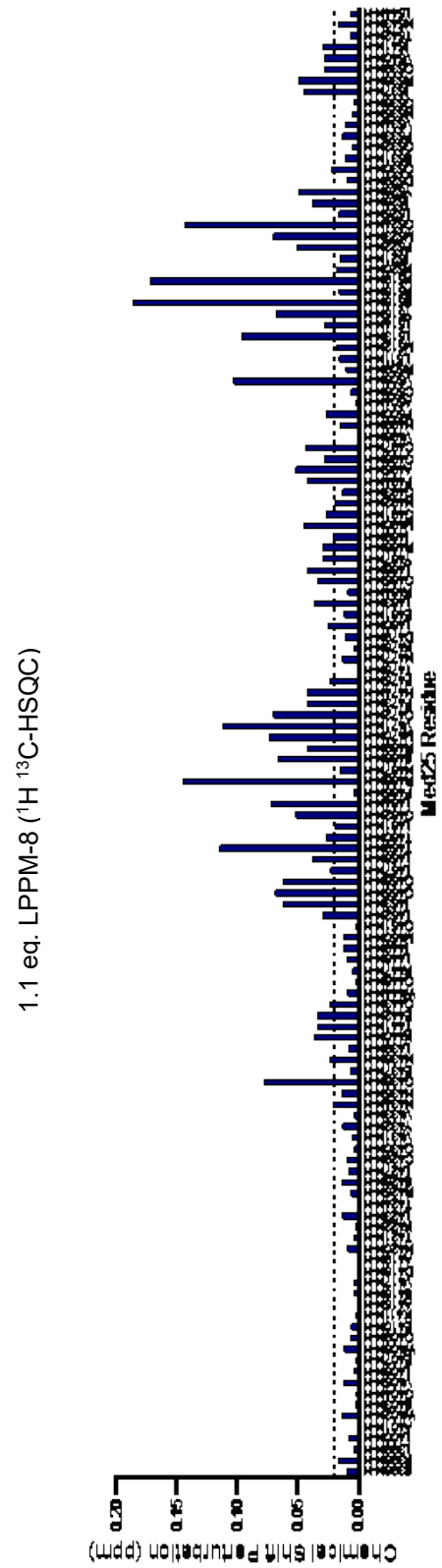
Appendix Figure B.16 ^{1}H,^{15}N-HSQC CSPs of Med25 residues with 1.1 equiv. of LPPM-8. Dashed line indicates the level of 3 standard deviations above the average chemical shift perturbation.
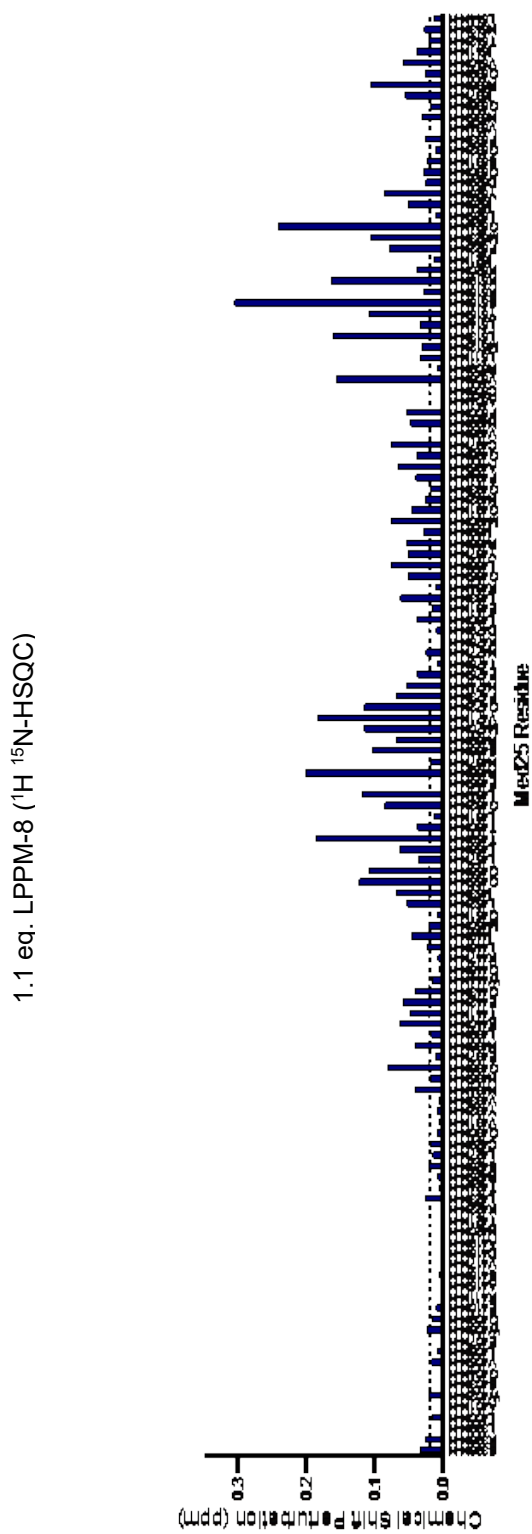
Appendix Figure B.17 ^{1}H, ^{15}N-HSQC CSPs of Med25 residues with 3 equiv. of LPPM-8. Dashed line indicates the level of 3 standard deviations above the average chemical shift perturbation

Appendix Figure B.18 Overlay of ^{1}H, ^{15}N-HSQC spectra of Med25 with titration of LPPM-9. Spectra shown are free Med25 (dark grey), 0.2 equiv. of LPPM-9 (yellow), 0.5 equiv. LPPM-9 (light blue), 0.8 equiv. LPPM-9 (red), 1.1 equiv. LPPM-9 (green), 2 equiv. LPPM-9 (dark blue), 3 equiv. LPPM-9 (purple).
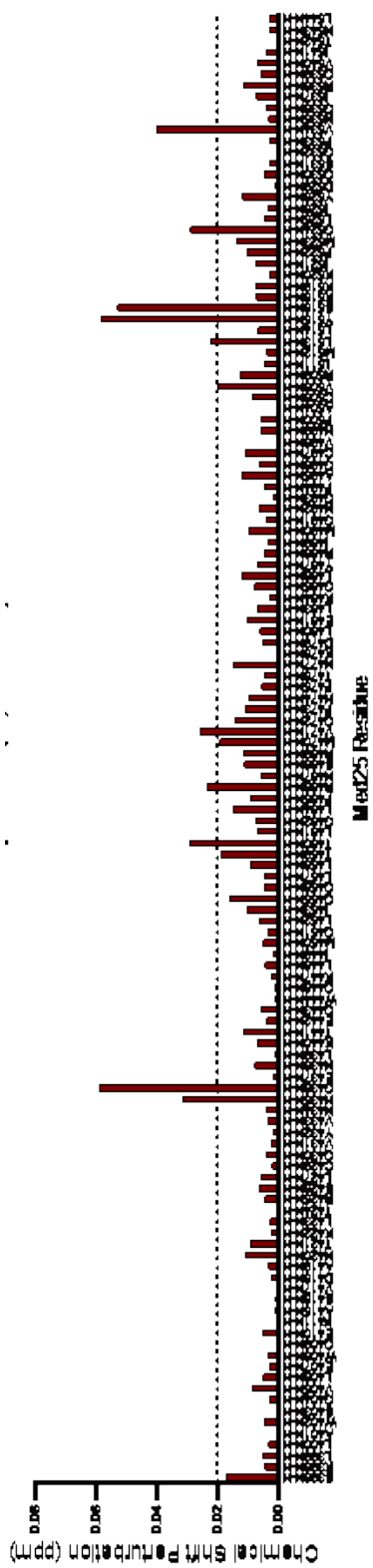
Appendix Figure B.19 ^{1}H, ^{15}N-HSQC CSPs of Med25 residues with 1.1 equiv. of LPPM-9. Dashed line indicates the level of 3 standard deviations above the average chemical shift perturbation.
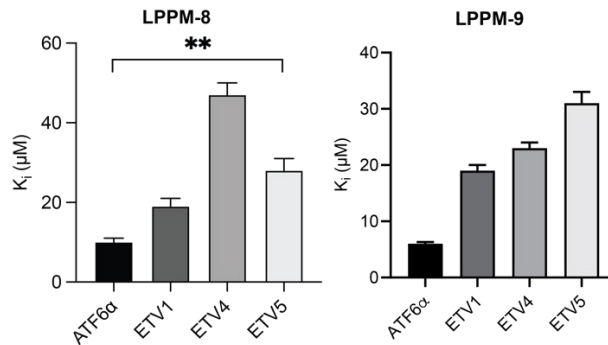
Appendix Figure B.20 Inhibition of Med25 AcID•ETV1, ETV4 and ETV5 by lipopeptidomimetics LPPM-8 and LPPM-9 as determined by competitive fluorescence polarization assays. Apparent IC_{50} values were determined through titration of compound for Med25 AcID•ETV1/ETV4/ETV5 in experimental triplicate with the indicated error (SD). The IC_{50} values were converted to K_i values using the apparent K_d value based on the direct binding of Med25 AcID• ETV1/ETV4/ETV5. Experiments conducted by O.Pattelli.
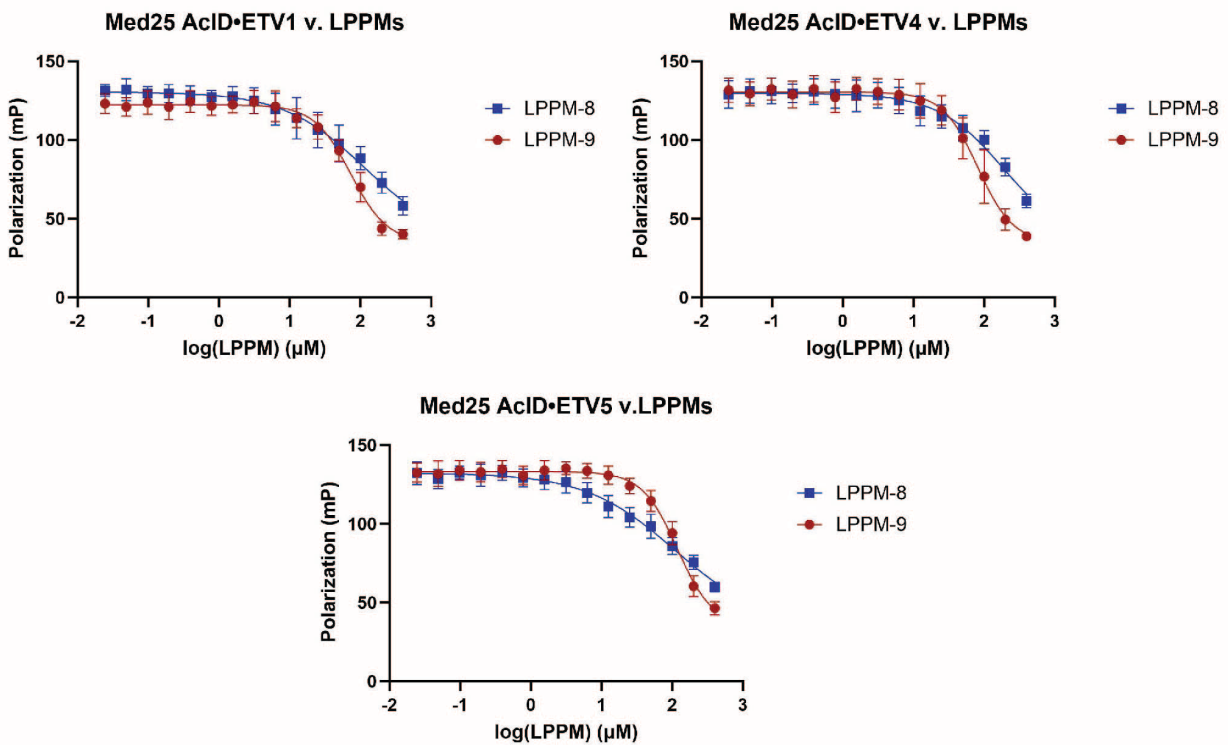
Appendix Figure B.21 Inhibition binding curves of Med25 AcID•ETV1, ETV4 and ETV5 by lipopeptidomimetics as determined by competitive fluorescence polarization assays. Apparent IC_{50} values were determined through titration of compound for Med25 AcID• ETV1/ETV4/ETV5 in experimental triplicate with the indicated error (SD). Data shown is the average of three biological replicates with the indicated error (SD). Experiments conducted by O.Pattelli.

186
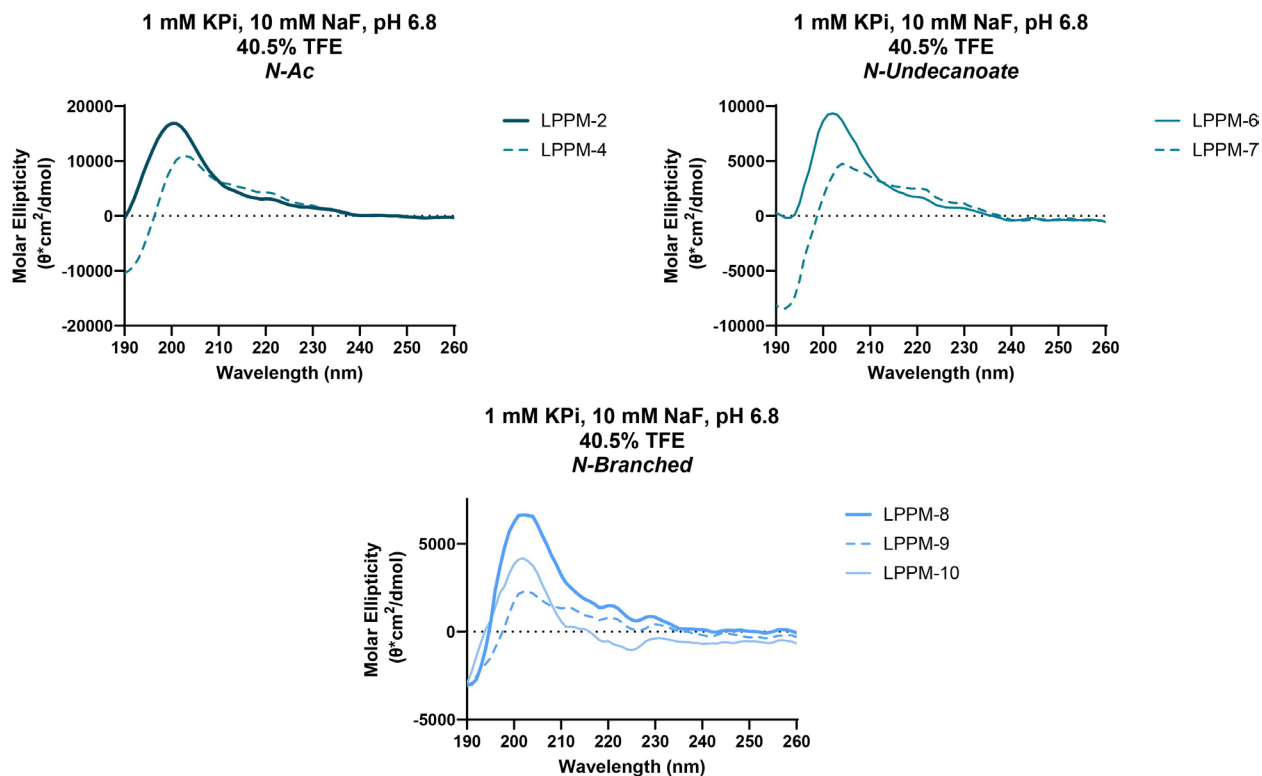
Appendix Figure B.22 Circular dichroism spectra for *D*-amino acid LPPMs at minimal salt concentrations. The molar ellipticity of each sample was determined from the mean residue CD corrected for the number of amino acids and the concentration of sample using the Jasco Spectra Manager Software v.2.5. CD spectra were obtained in 40% TFE/potassium phosphate buffer as indicated. Data was obtained from 5 acquisitions.
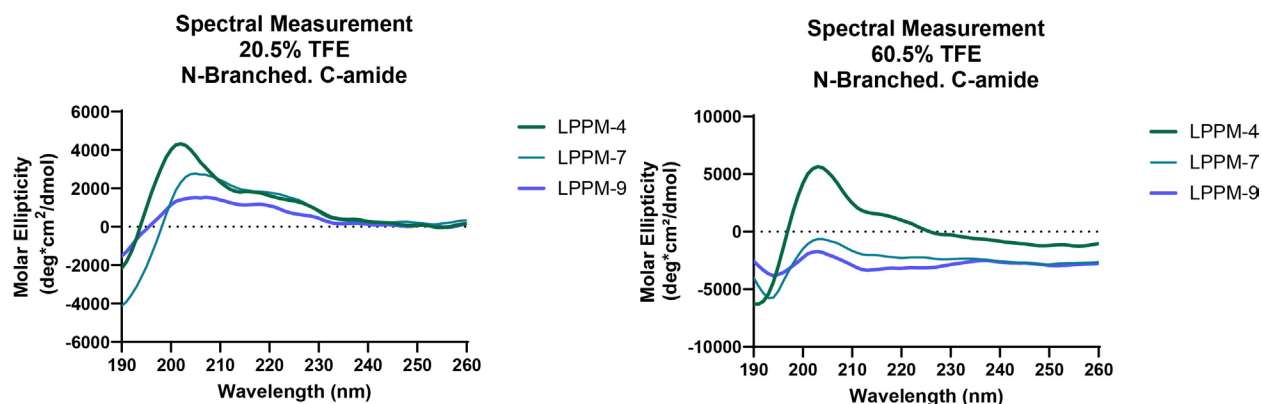

Appendix Figure B.23 Circular dichroism spectra of C-terminal -NH$_2$ LPPMs at increasing TFE%. The molar ellipticity of each sample was determined from the mean residue CD corrected for the number of amino acids and the concentration of sample using the Jasco Spectra Manager Software v.2.5. Data was obtained from 5 acquisitions.
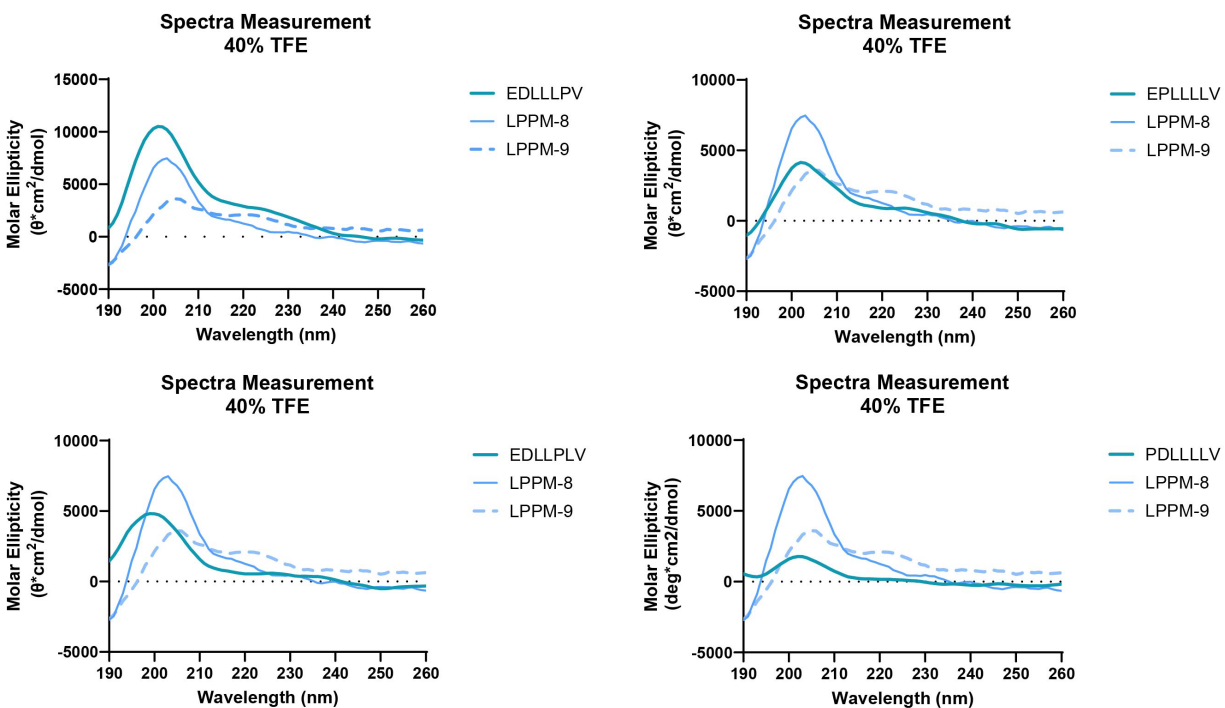
Appendix Figure B.24 Circular dichroism spectra for selected proline scan LPPM analogs. The molar ellipticity of each sample was determined from the mean residue CD corrected for the number of amino acids and the concentration of sample using the Jasco Spectra Manager Software v.2.5. CD spectra were obtained in 40% TFE/potassium phosphate buffer as indicated. Data was obtained from 5 acquisitions.
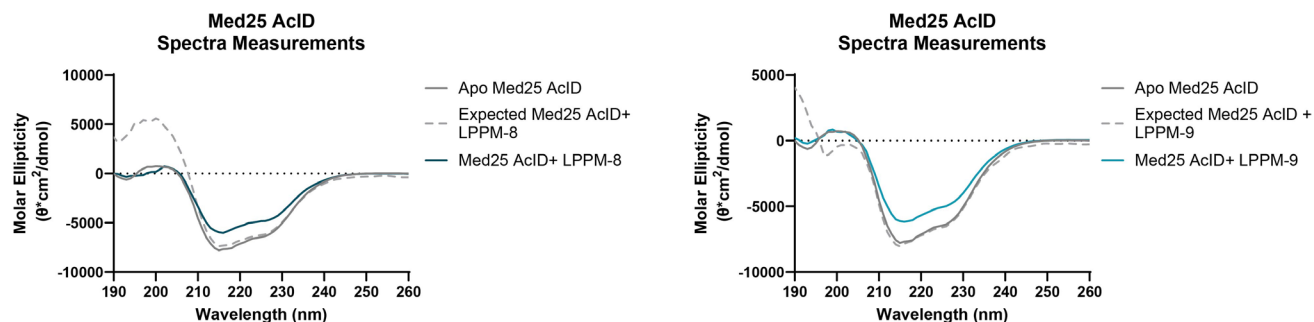
Appendix Figure B.25 Circular dichroism spectra of Med25 AcID incubated with 5 equivalents of LPPM-8 (left) and LPPM-9 (right). The molar ellipticity of each sample was determined from the mean residue CD corrected for the number of amino acids and the concentration of sample using the Jasco Spectra Manager Software v.2.5. CD spectra were obtained in **10% TFE/potassium phosphate buffer**. Data was obtained from 5 acquisitions
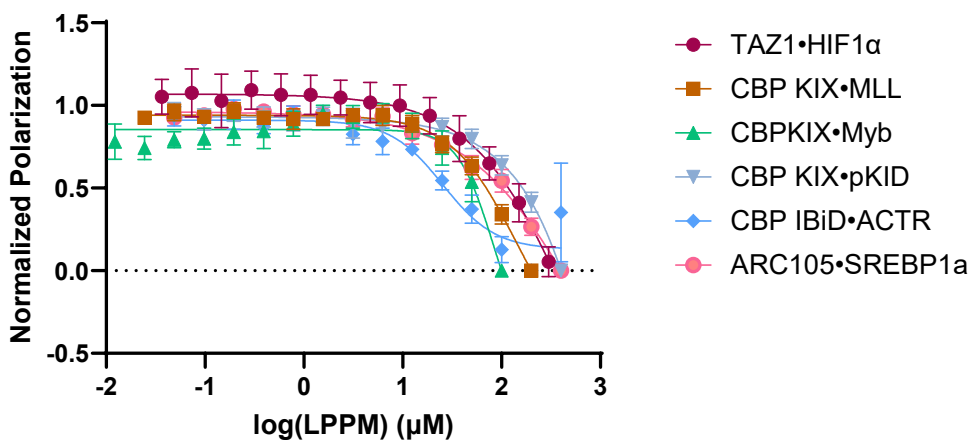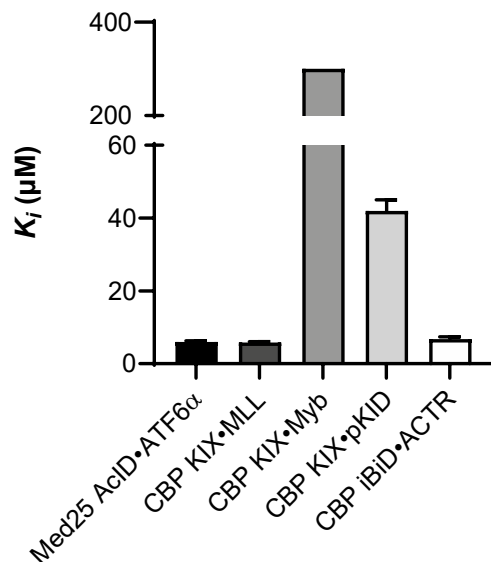
.
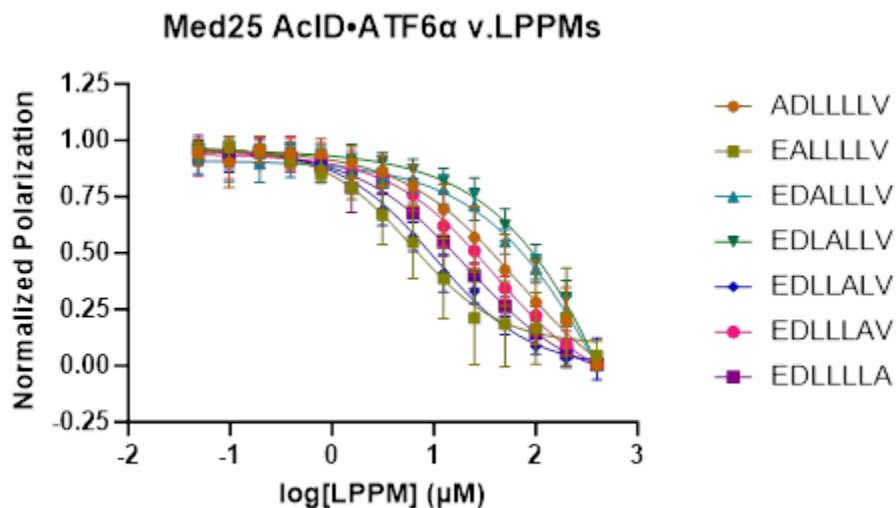
Appendix Figure B.26 Inhibition binding curves of Med25 AcID•ATF6α by alanine scan of LPPM-8 as determined by competitive fluorescence polarization assays. Apparent IC_{50} values were determined through titration of compound for Med25 AcID•ATF6α in experimental triplicate with the indicated error (SD). The IC_{50} values were converted to K_i values using the apparent K_d value based on the direct binding of Med25 AcID•ATF6α. Data shown is the average of three independent experiments with the indicated error (SD).
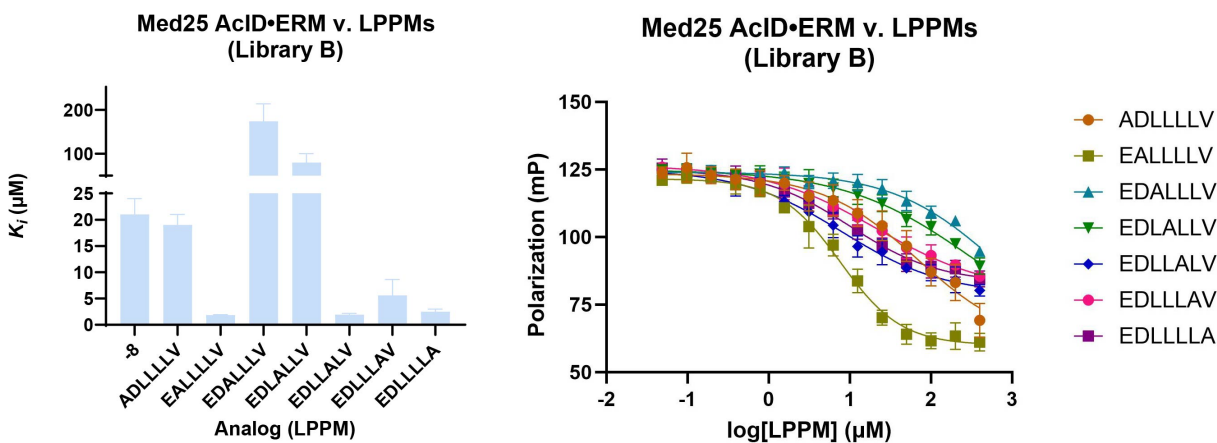
Appendix Figure B.27 Inhibition values and binding curves of Med25 AcID•ERM by alanine scan of LPPM-8 as determined by competitive fluorescence polarization assays. Apparent IC_{50} values were determined through titration of compound for Med25 AcID•ERM in experimental triplicate with the indicated error (SD). The IC_{50} values were converted to K_i values using the apparent K_d value based on the direct binding of Med25 AcID•ATF6α. Data shown is the average of two independent experiments with the indicated error (SD).
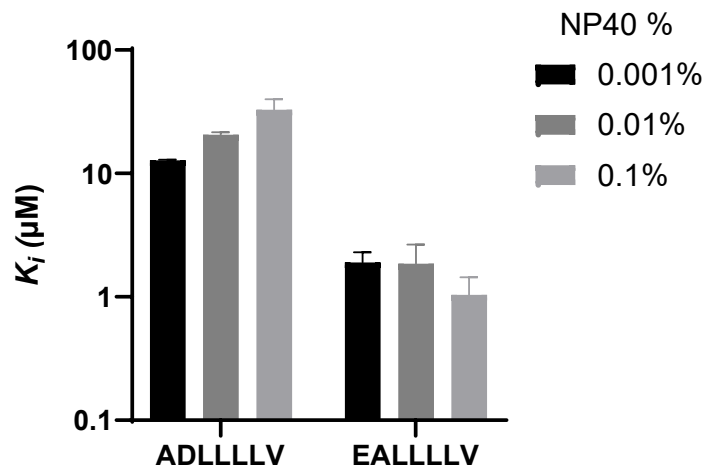
Appendix Figure B.28 Inhibition of Med25 AcID•ATF6α by LPPM-8 alanine charged analogs with different NP40 concentrations as determined by competitive fluorescence polarization assays. Apparent IC_{50} values were determined through titration of compound for Med25 AcID•ATF6α PPI performed in experimental triplicate with the indicated error (SD). The IC_{50} values were converted to Ki values using the apparent Kd value based on the direct binding of Med25 AcID•ATF6α PPI using a Ki calculator. Data shown is the average of two independent experiments with the indicated error (SD).


Appendix Figure B.29 Inhibition of CBP/ARC105 PPIs by lipopeptidomimetic LPPM-8 as determined by competitive fluorescence polarization assays. Apparent IC_{50} values were determined through titration of compound for CBP ABD•TADs in experimental triplicate with the indicated error (SD). The IC_{50} values were converted to K_i values using the apparent K_d value based on the direct binding of CBP ABD•TADs. Data shown is the average of two independent experiments with the indicated error (SD)

Appendix Figure B.30 Inhibition of CBP PPIs by lipopeptidomimetic LPPM-9 as determined by competitive fluorescence polarization assays. Apparent IC_{50} values were determined through titration of compound for CBP ABD•TADs in experimental triplicate with the indicated error (SD). The IC_{50} values were converted to K_i values using the apparent K_d value based on the direct binding of CBP ABD•TADs. Data shown is the average of two independent experiments with the indicated error (SD).
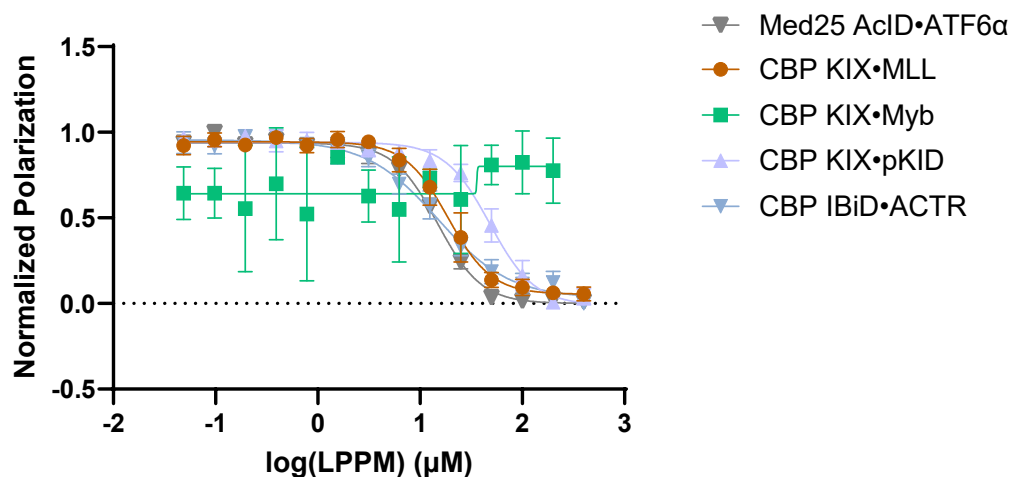
Appendix Figure B.31 Representative curves of the inhibition of CBP PPIs by lipopeptidomimetic LPPM-9 as determined by competitive fluorescence polarization assays. Apparent IC_{50} values were determined through titration of compound for CBP ABD•TADs in experimental triplicate with the indicated error (SD). Data shown is the representation of two independent experiments with the indicated error (SD).
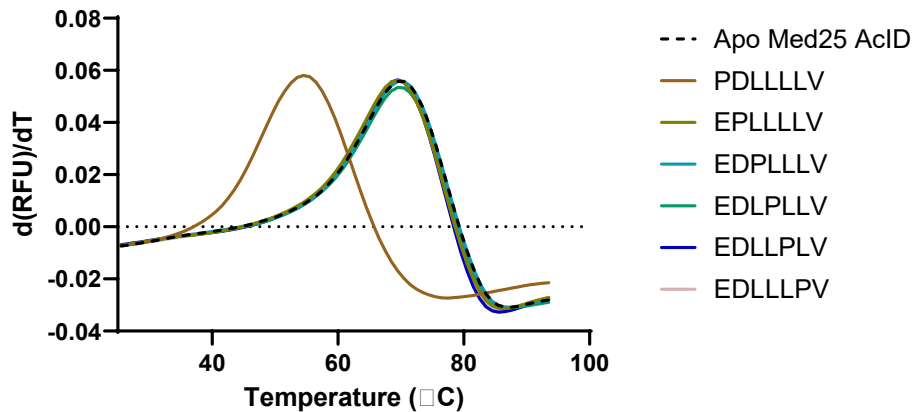
Appendix Figure B.32 . Engagement of LPPM library C with Med25 AcID. DSF data for Proline Scan of LPPM-8 (Library C). First derivative of the raw fluorescence units (RFU) traces of Med25 AcID with 5 equiv. of each respective LPPM.
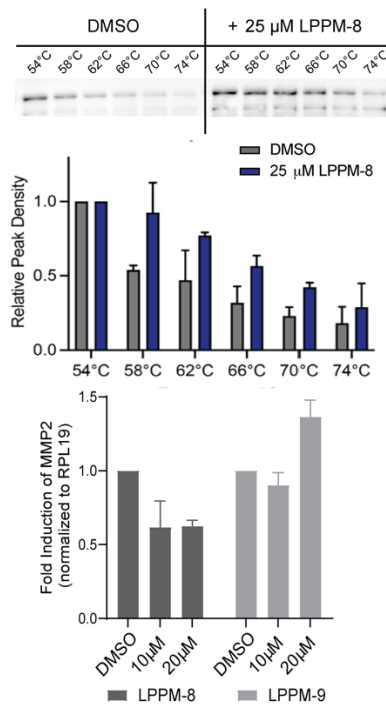
Appendix Figure B.33 LPPM-8 displays activity in a cellular context. Top. LPPM-8 stabilizes full length Med25 in VARI068 cell extracts. Cellular thermal shift assays (CETSA) were performed by dosing VARI068 nuclear extracts with 25 µM LPPM-8 or equivalent DMSO and subjecting the samples to increasing temperatures. Western blots using a Med25 antibody show an increased band intensity in LPPM-8-dosed samples compared to the DMSO treatment, indicating thermal shift stabilization and target engagement. Data in the bar graph is normalized to the DMSO control (grey) that is equal to 1. Data shown is representative of experiments performed in biological duplicates. Bottom. LPPM-8 inhibits a Med25-dependent gene in VARIO68 cells. Analysis and quantification of the transcript levels of the Med25•ETV5-

dependent gene MMP2 in the triple-negative breast cancer cell line VARI068 was performed using qPCR. Results indicate that treatment with LPPM-8 results in the decrease of MMP2 transcript levels. By comparison, increasing concentrations of LPPM-9 do not yield changes in MMP2 transcript levels. Values are normalized to the reference gene RPL19. Data shown is the average of three independent experiments each performed in technical triplicate with the indicated error (SD). Experiments conducted by O.Pattelli.
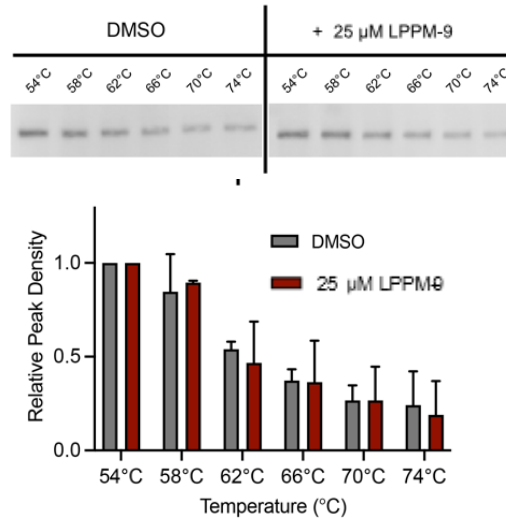

Appendix Figure B.34 Cellular thermal shift assays of LPPM-9 using VARI068 nuclear extracts. Experiments were conducted at 25 µM of lipopeptidomimetic compared to DMSO control (biological duplicates). Western blots show thermal stabilization for Med25 with LPPM-9. Band densities of LPPM-9, calculated using ImageJ, are similar to DMSO control. Error bars represent the standard deviation of the mean from biological duplicates. Experiments conducted by O. Pattelli.

# Appendix C: Supplemental Data for Chapter 3: Lipopeptidomimetics Display Modifiable Target Selectivity
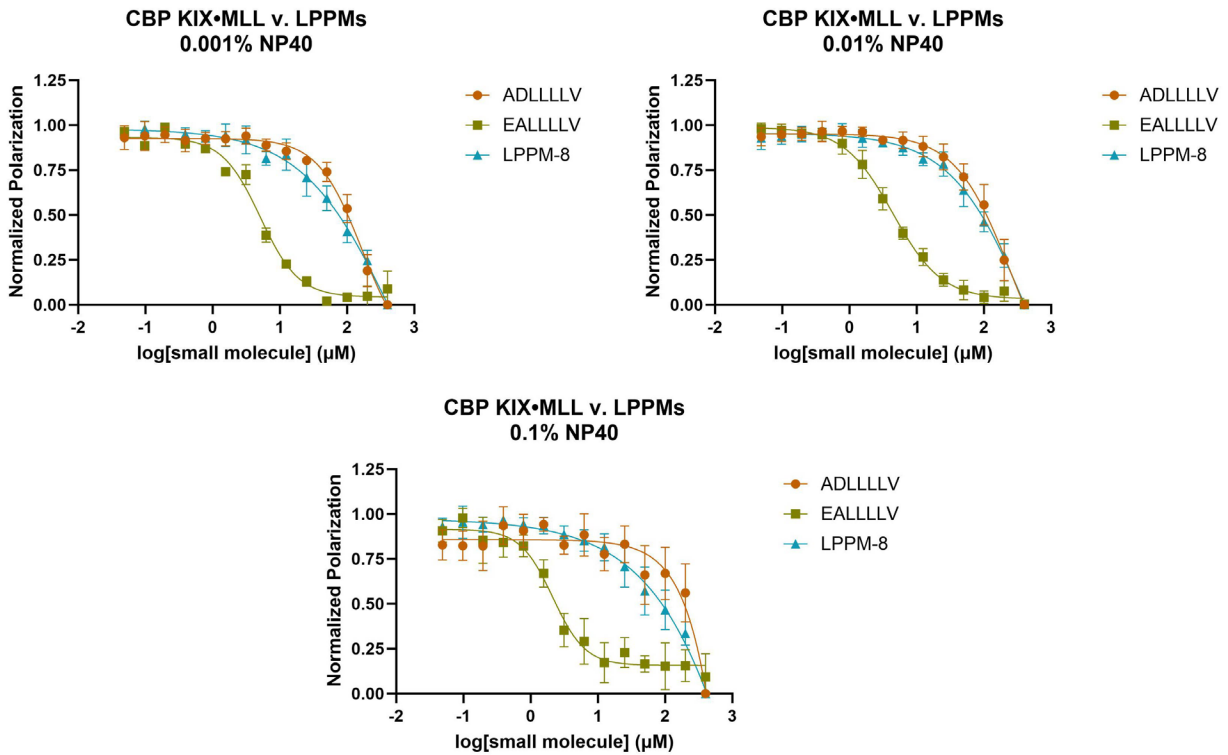
CBP KIX•MLL v. LPPMs
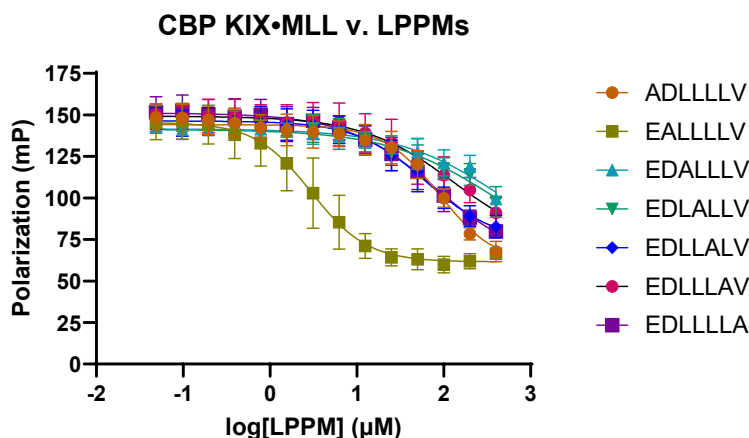
Appendix Figure C.1 Inhibition binding curves of CBP KIX•MLL (80% bound) by alanine scan of LPPM-8 as determined by competitive fluorescence polarization assays. Apparent IC_{50} values were determined through titration of compound for CBP KIX•MLL in experimental triplicate with the indicated error (SD). The IC_{50} values were converted to K_i values using the apparent K_d value based on the direct binding of CBP KIX•MLL. Data shown is the average of three independent experiments with the indicated error (SD).

CBP TAZ1•HIF1α v. LPPMs
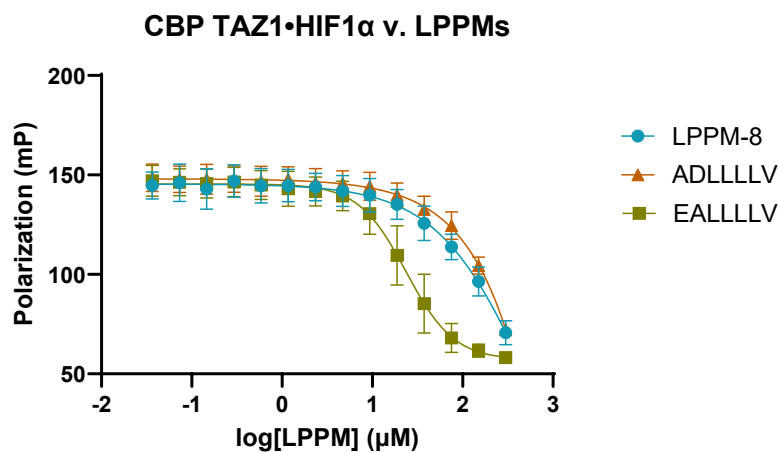
Appendix Figure C.2 Inhibition binding curves of CBP TAZ1•HIF1α by LPPM-8, LPPM-8-E1A and LPPM-8-D2A as determined by competitive fluorescence polarization assays. Apparent IC_{50} values were determined through titration of compound for CBP TAZ1•HIF1α in experimental triplicate with the indicated error (SD). The IC_{50} values were converted to K_i values using the apparent K_d value based on the direct binding of CBP TAZ1•HIF1α. Data shown is the average of three independent experiments with the indicated error (SD).

194
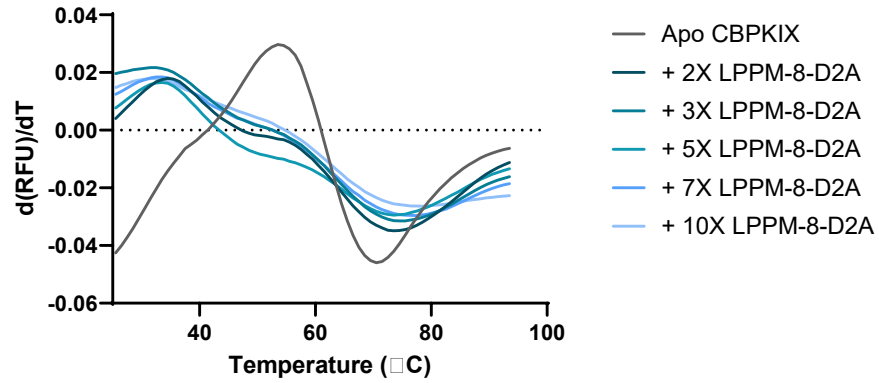
Appendix Figure C.3 Characterization of the engagement of CBP KIX by LPPM-8-D2A at higher LPPM equivalents as determined by DSF. First derivative of the melting temperature curve of CBP KIX incubated with titrations of LPPM-8-D2A between 2 – 10X equivalents. Measurements were conducted in technical triplicates, and data depicted corresponds to the representation of biological triplicates.
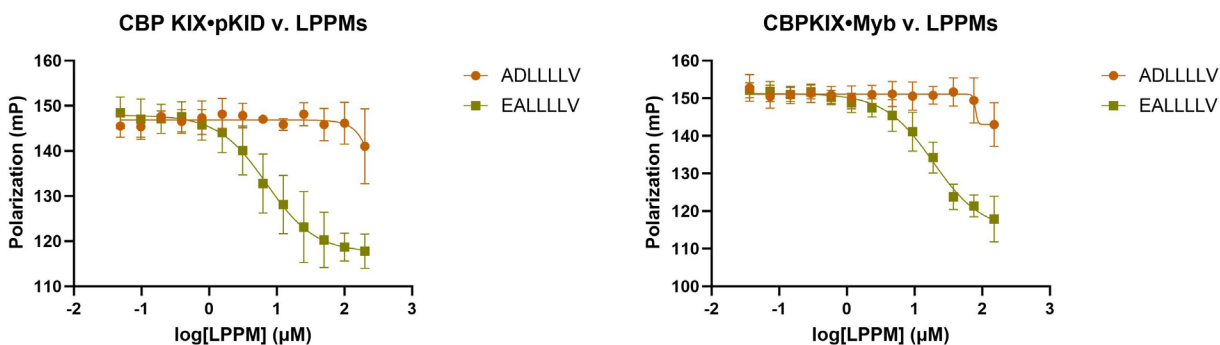

Appendix Figure C.4 Normalized inhibition binding curves of CBP KIX•MLL by LPPM-8, LPPM-8-E1A and LPPM-8-D2A with different NP40 concentrations (0.001%, 0.01%, 0.1%) as determined by competitive fluorescence polarization assays. Apparent IC_{50} values were determined through titration of compound for CBP KIX•MLL PPI performed in experimental triplicate with the indicated error (SD). Data shown is the average of two independent experiments with the indicated error (SD).

CBP KIX•Myb v. LPPMs
(25% Bound)
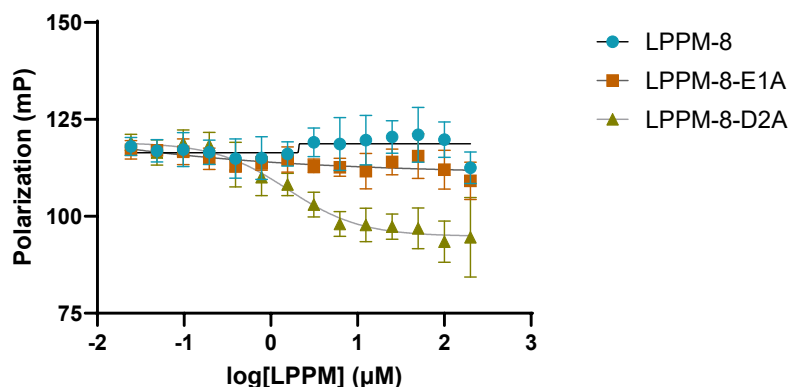
Appendix Figure C.5 Inhibition binding curves of CBP KIX•Myb (25% bound) by LPPM-8, LPPM-8-E1A and LPPM-8-D2A as determined by competitive fluorescence polarization assays. Apparent IC_{50} values were determined through titration of compound for CBP KIX•Myb in experimental triplicate with the indicated error (SD). The IC_{50} values were converted to K_i values using the apparent K_d value based on the direct binding of CBP KIX•Myb. Data shown is the average of three independent experiments with the indicated error (SD).


Appendix Figure C.6 Inhibition of PPIs at the allosteric site of CBP KIX. Inhibition binding curves of CBP KIX•pKID/Myb (80% bound) by LPPM-8-E1A and LPPM-8-D2A as determined by competitive fluorescence polarization assays. Apparent IC_{50} values were determined through titration of compound for CBP KIX• pKID/Myb in experimental triplicate with the indicated error (SD). The IC_{50} values were converted to K_i values using the apparent K_d value based on the direct binding of CBP KIX•pKID. Data shown is the average of three independent experiments (Myb) and two independent experiments (pKID) with the indicated error (SD).
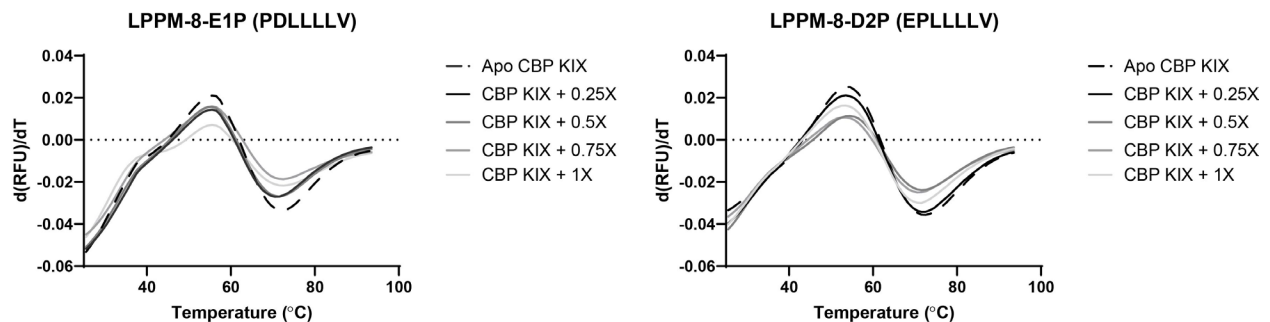
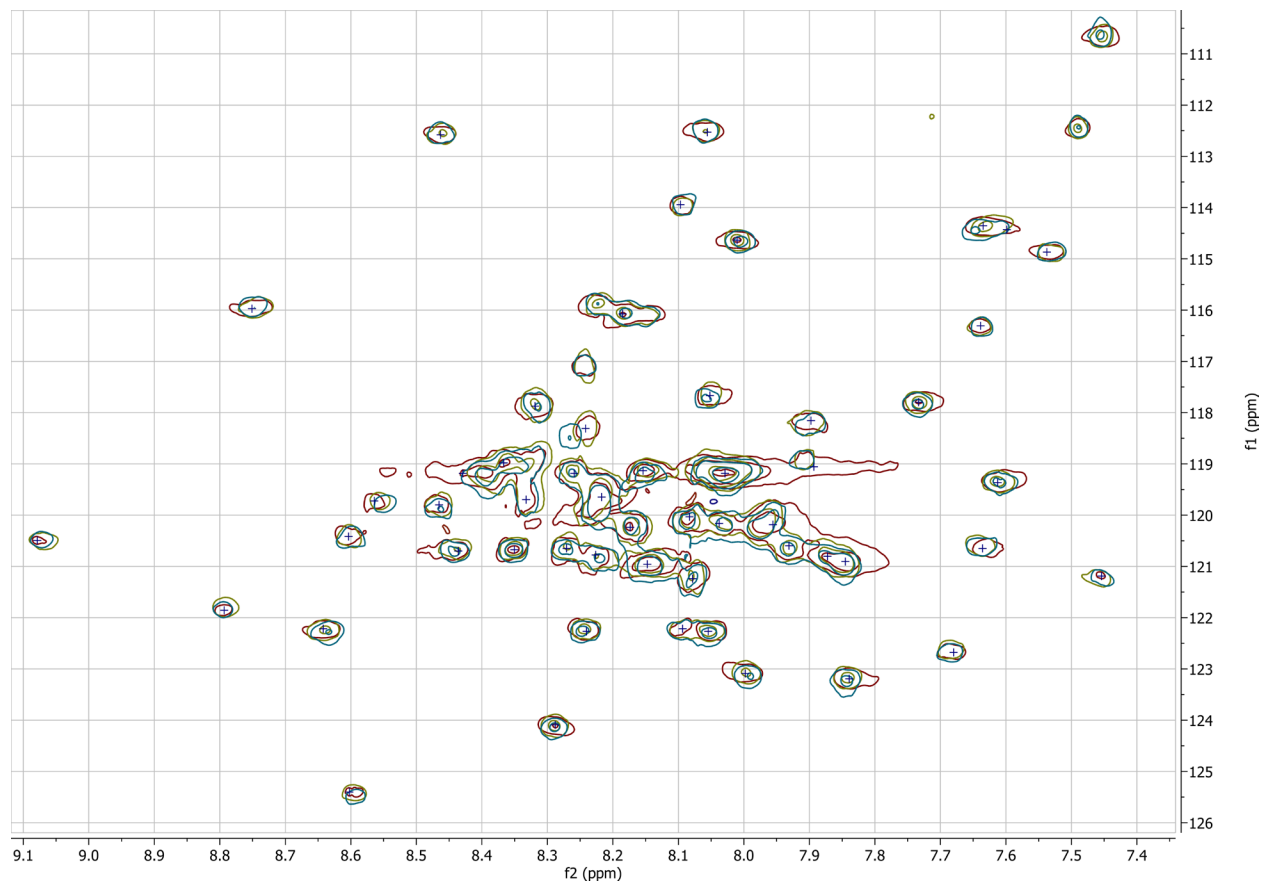**CBP KIX**
Spectra Measurements
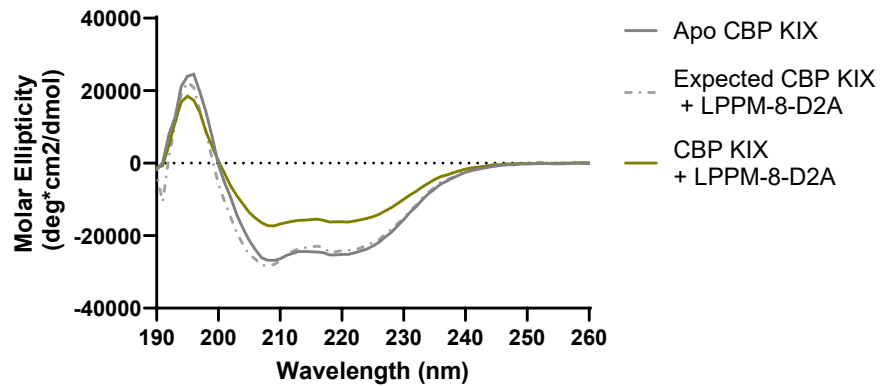
Appendix Figure C.7 Circular dichroism spectra of CBP KIX incubated with 5 equivalents of LPPM-8-D2A. The molar ellipticity of each sample was determined from the mean residue CD corrected for the number of amino acids and the concentration of sample using the Jasco Spectra Manager Software v.2.5. CD spectra were obtained in 10% TFE/potassium phosphate buffer. Data was obtained from 5 acquisitions.
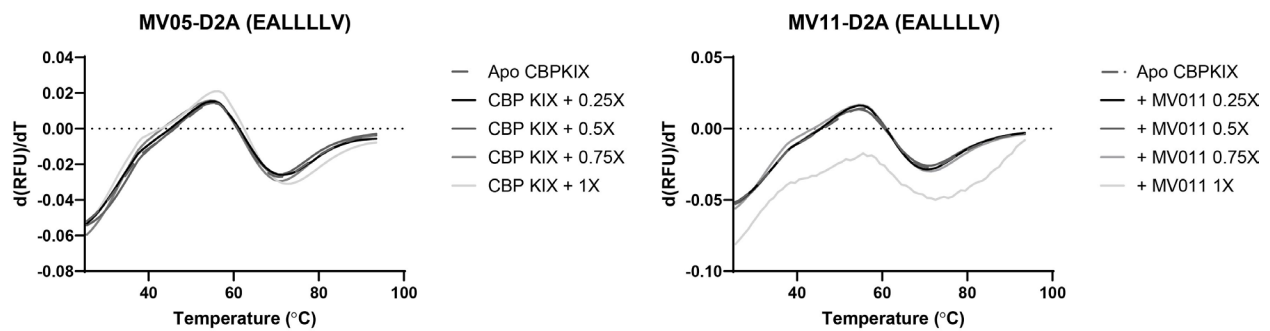
Appendix Figure C.8 First derivative of the melting curve of CBP KIX incubated with titrations of MV5, MV11 LPPMs obtained by DSF. Data was acquired in technical triplicates and is representative of biological duplicates.


Appendix Figure C.9 First derivative of the melting curve of CBP KIX incubated with titrations of LPPM-8-E1P/D2P obtained by DSF. Data was acquired in technical triplicates and is representative of biological duplicates.

Appendix Figure C.10 ^{1}H ^{15}N-HSQC NMR spectra of CBP KIX-LPPM-D2A complexes. Overlay of the HSQC spectra of ^{15}N-labeled CBP KIX with DMSO (blue), 1.1 equivalents of LPPM-D2A (green), and 2 equivalents (red). Aggregation observed at >2 equivalents.
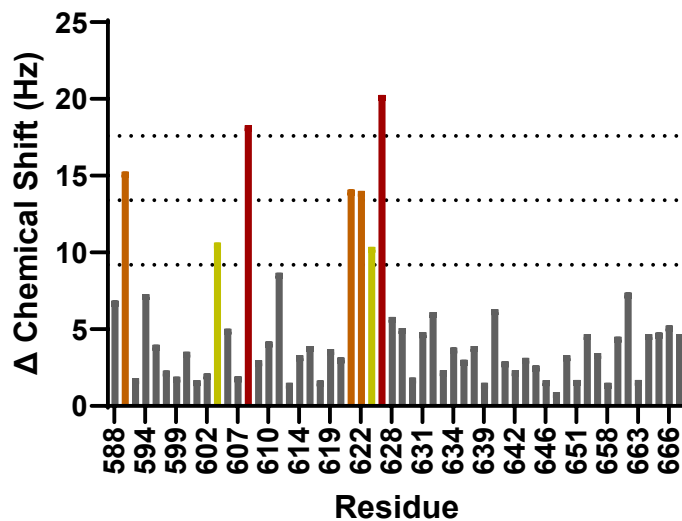
CBP KIX, LPPM-8-D2A (0.5 eq)
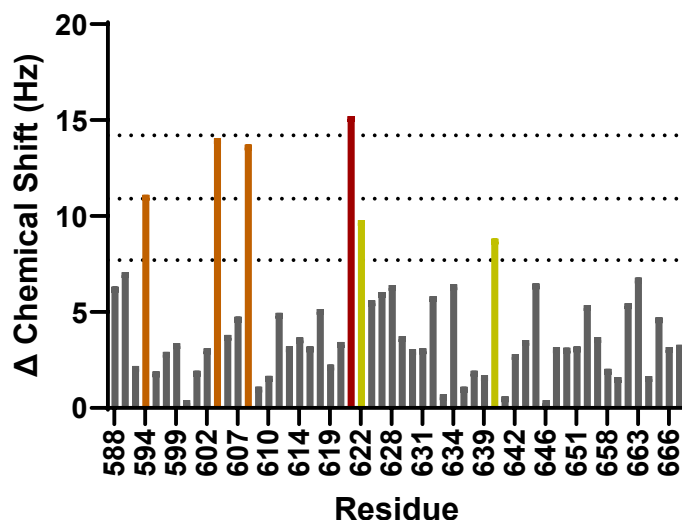
Appendix Figure C.11 ^{1}H ^{15}N-HSQC NMR chemical shift perturbations with ^{15}N CBP KIX after complexation with 0.5 eq LPPM-D2A. Residues that shift 1-2 (yellow), 2-3 (orange) and >3 standard deviations (red) were identified as being significantly perturbed as calculated by standard deviation of the mean chemical shift change of all assigned residues. Thresholds for 1,2,3 standard deviations are indicated by dashed lines.

CBP KIX, LPPM-8-D2A (1.1 eq)
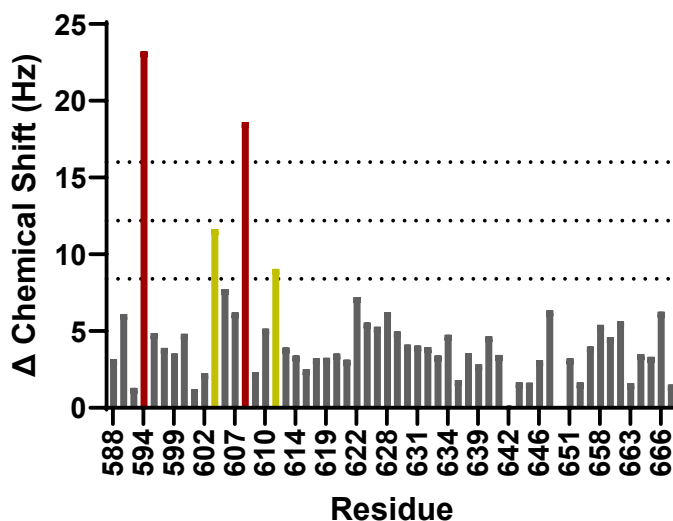
Appendix Figure C.12 ^{1}H ^{15}N-HSQC NMR chemical shift perturbations with ^{15}N CBP KIX after complexation with 1.1 eq LPPM-D2A. Residues that shift 1-2 (yellow), 2-3 (orange) and >3 standard deviations (red) were identified as being significantly perturbed as calculated by standard deviation of the mean chemical shift change of all assigned residues. Thresholds for 1,2,3 standard deviations are indicated by dashed lines.
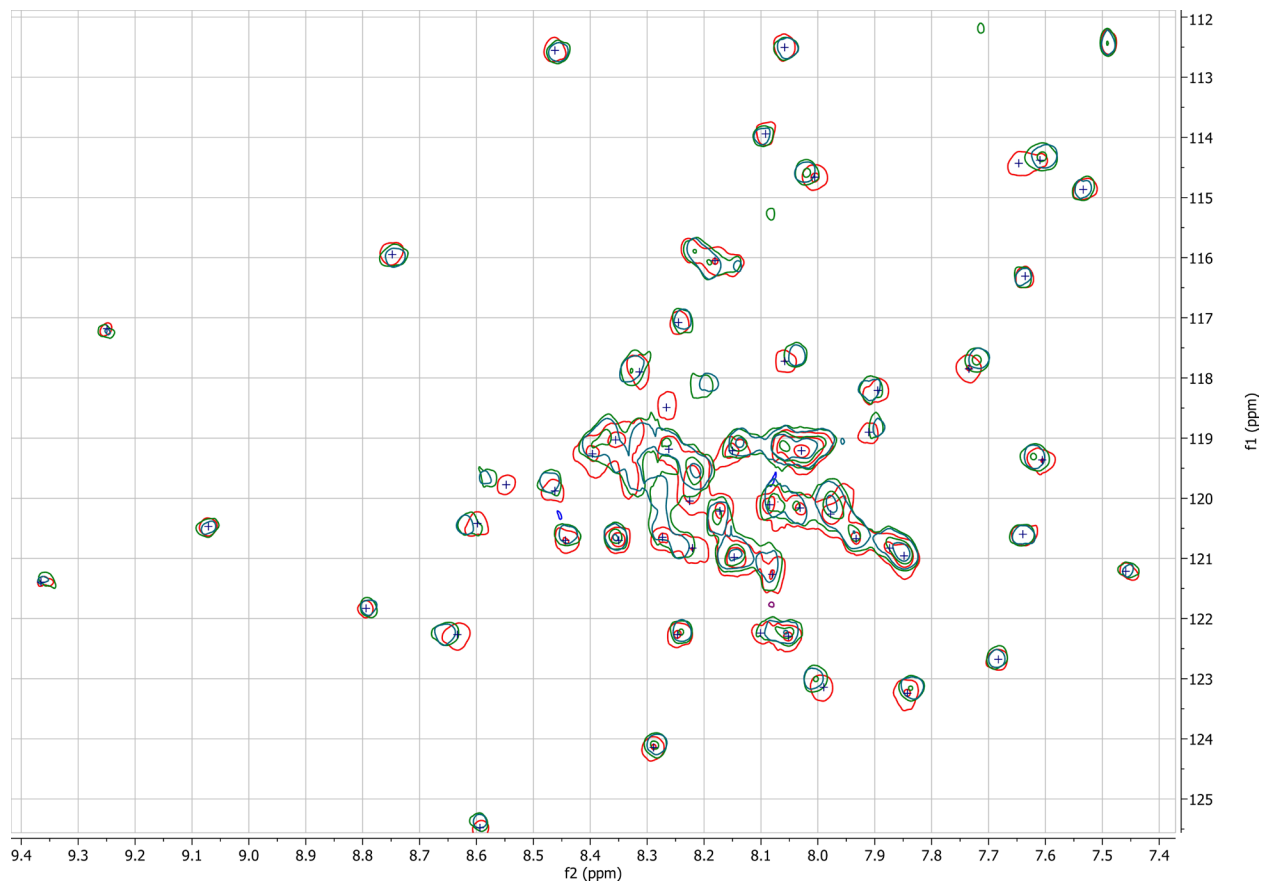
CBP KIX, LPPM-8-D2A (2 eq)

Appendix Figure C.13 ^{1}H ^{15}N-HSQC NMR chemical shift perturbations with ^{15}N CBP KIX after complexation with 2 eq LPPM-D2A. Residues that shift 1-2 (yellow), 2-3 (orange) and >3 standard deviations (red) were identified as being significantly perturbed as calculated by standard deviation of the mean chemical shift change of all assigned residues. Thresholds for 1,2,3 standard deviations are indicated by dashed lines.
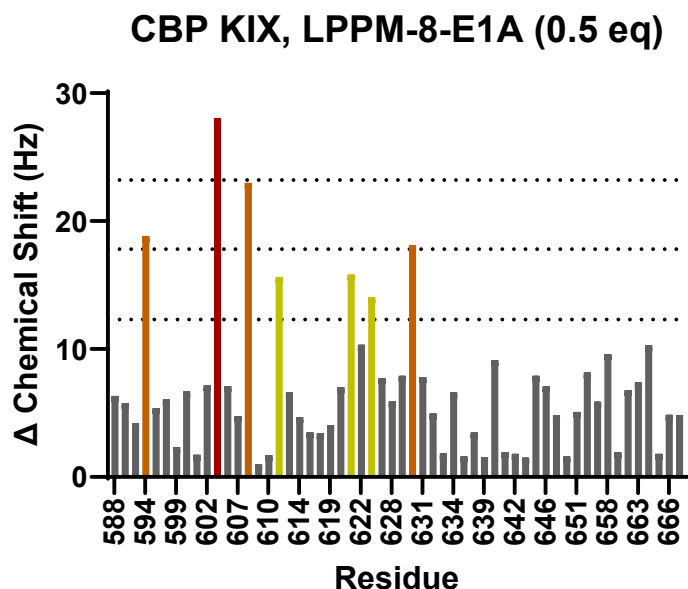
Appendix Figure C.14 ^{1}H ^{15}N-HSQC NMR spectra of CBP KIX-LPPM-E1A complexes. Overlay of the HSQC spectra of ^{15}N-labeled CBP KIX with DMSO (orange), 1.1 equivalents of LPPM-E1A (green), and 2 equivalents (blue). Aggregation observed at >2 equivalents.
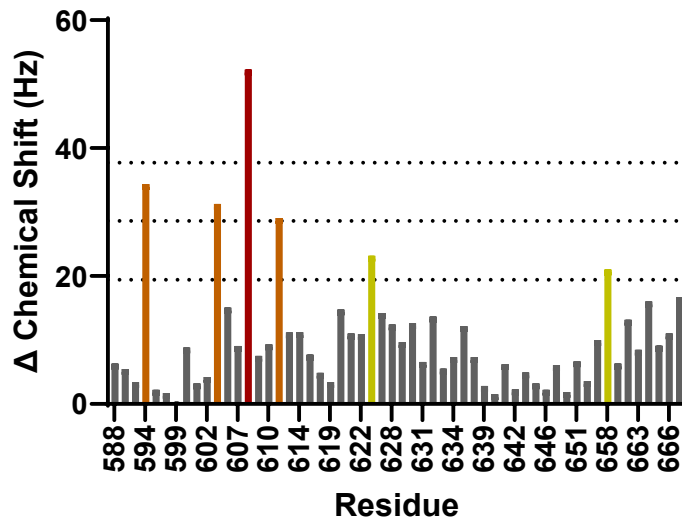
CBP KIX, LPPM-8-E1A (0.5 eq)

Appendix Figure C.15 ^{1}H ^{15}N-HSQC NMR chemical shift perturbations with ^{15}N CBP KIX after complexation with 0.5 eq LPPM-E1A. Residues that shift 1-2 (yellow), 2-3 (orange) and >3 standard deviations (red) were identified as being significantly perturbed as calculated by standard deviation of the mean chemical shift change of all assigned residues. Thresholds for 1,2,3 standard deviations are indicated by dashed lines.

CBP KIX, LPPM-8-E1A (1.1 eq)
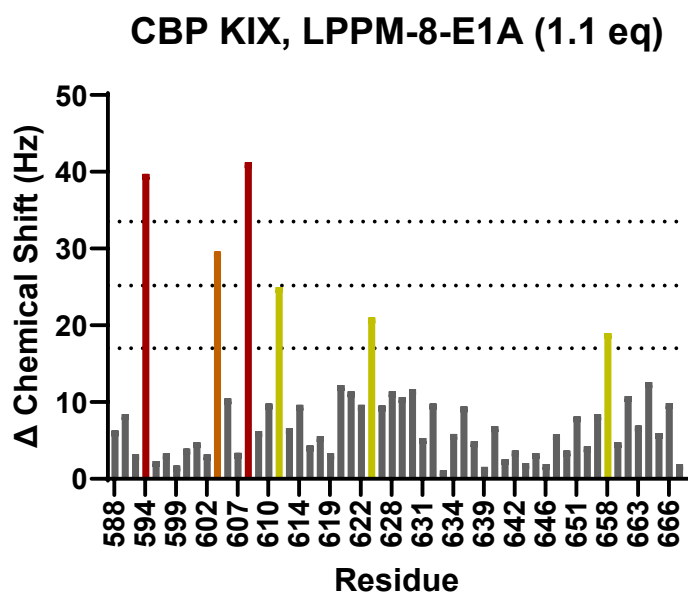
Appendix Figure C.16 ^{1}H ^{15}N-HSQC NMR chemical shift perturbations with ^{15}N CBP KIX after complexation with 1.1 eq LPPM-E1A. Residues that shift 1-2 (yellow), 2-3 (orange) and >3 standard deviations (red) were identified as being significantly perturbed as calculated by standard deviation of the mean chemical shift change of all assigned residues. Thresholds for 1,2,3 standard deviations are indicated by dashed lines.

CBP KIX, LPPM-8-E1A (2 eq)

Appendix Figure C.17 ^{1}H ^{15}N-HSQC NMR chemical shift perturbations with ^{15}N CBP KIX after complexation with 2 eq LPPM-E1A. Residues that shift 1-2 (yellow), 2-3 (orange) and >3 standard deviations (red) were identified as being significantly perturbed as calculated by standard deviation of the mean chemical shift change of all assigned residues. Thresholds for 1,2,3 standard deviations are indicated by dashed lines.
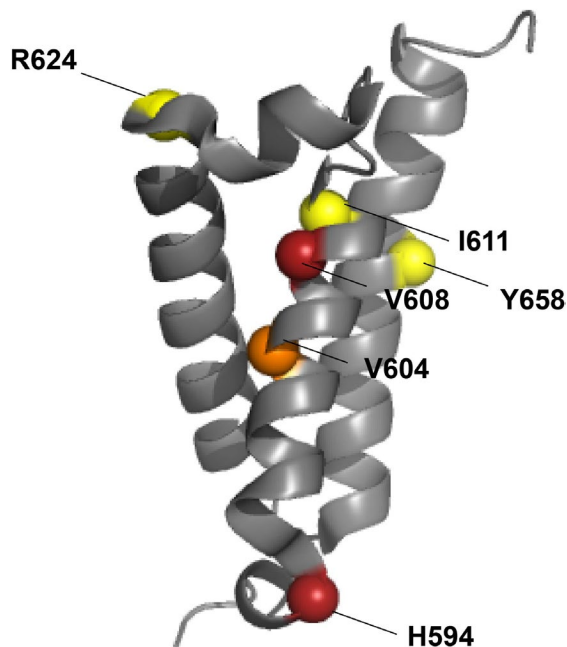
Appendix Figure C.18. ^{1}H, ^{15}N-HSQC CSPs induced by binding of 1.1 eq of LPPM-8-E1A mapped onto CBP KIX (PDB ID 2AGH). Yellow = 1-2 standard deviations of the average CSP, orange = 2-3 standard deviations, red ≥ 3 standard deviations. Representative bound MLL shown in black. The same residues are the only significantly perturbed at 2 eq. of LPPM-8-E1A.

## Appendix D: Assessment of the engagement of C-term NH$_2$ LPPMs to TADs

As described in Chapter 2, the C-terminal groups of LPPM-8 and LPPM-9 (Figure D.1) were crucial in their inhibitory activity against Med25 AcID PPIs. Activity characterization studies demonstrated that LPPM-9, did not significantly engage with Med25 *in-vitro* in DSF or structurally through ^{1}H ^{15}N and ^{1}H ^{13}C HSQC. Assessments of the selectivity of these molecules among a panel of other coactivator•activator complexes, also highlighted that LPPM-9 has a lower selectivity for Med25 than LPPM-8, despite having comparable K_i values against Med25 AcID•ATF6α. In a cellular context, there was also lack of engagement of Med25 with LPPM-9. Further, the structural characterization of analogs LPPM-8 and LPPM-9 with CD, determined that LPPM-8 has polyproline helical character, while LPPM-9 has a propensity towards forming an α-helix in the presence of TFE. This data put together, and the recognition that activator TADs preferentially bind as α-helical structures, led to the hypothesis that LPPM-9 may interact with the binding partner TAD, ATF6α rather than with the ABD of Med25. An initial effort to characterize the potential interactions between LPPM-9 and ATF6α was done using the acetylated construct of the ATF6α (38-75) TAD and 5 equivalents of LPPM-9 and DSF. The melting curve of the AcATF6α was not captured using this method, we later identified that this was probably as a result of this construct actually being present in an unfolded structure in solution (data not shown).
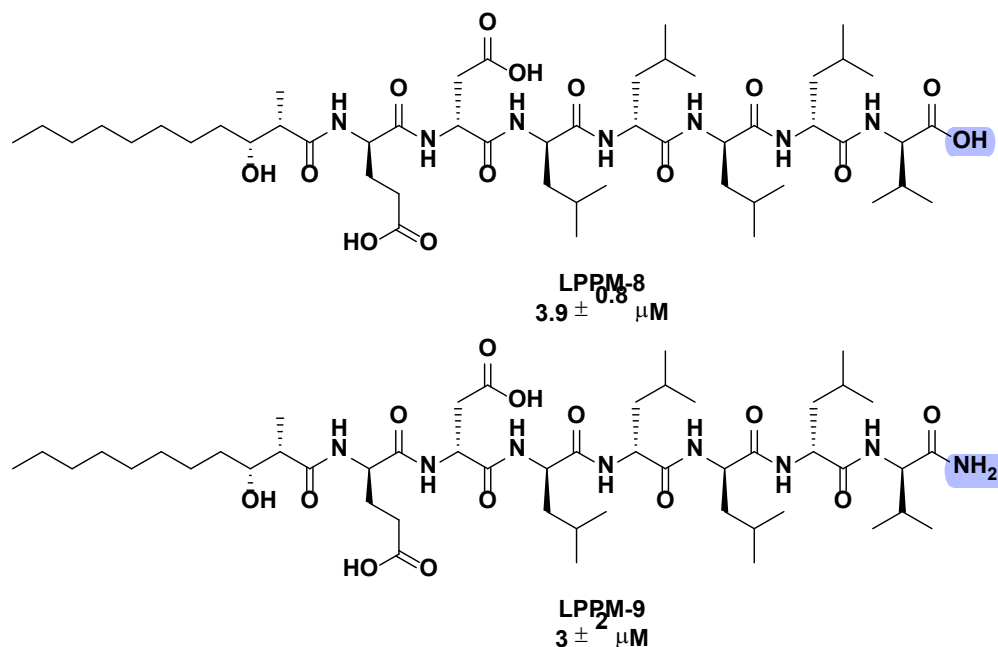
Appendix Figure D.1 Structures of lead analog LPPM-8 and the negative control LPPM-9.

Alternatively, we opted to perform CD spectral measurements of this same construct in the presence of 5 equivalents of either LPPM-9, LPPM-8 as a control, and varying concentrations of TFE (Figure D.2). The expected results were calculated based on the individual spectra of ATF6α and the LPPM analogs and are included in the graphs for each of the conditions tested. As observed by the change in the spectra of ATF6α over the increasing concentrations of TFE, it is clear that in the absence of this solvent, the peptide is unstructured in buffer solution, and across the concentrations tested, helicity was only measurable at 40% TFE. Additionally, at this condition, the expected and actual measurements of LPPM-9 and ATF6α are consistent, something not observed at 10% TFE for LPPM-9 and 0% TFE for LPPM-8. Considering the opposite signals emitted by the LPPMs and ATF6α due to their D and L amino acid content, and fact that only at a single TFE concentration the folded state of ATF6α is observed, it is challenging to determine engagement of LPPM-9 through this method. Instead, based on this data it can

be proposed that a more direct form of measurement of binding may be needed to determine if the interaction between LPPM-9 and ATF6α is taking place. A proposed avenue in this case is to utilize ^{1}H ^{13}C HSQC with labeled methyl residues of ATF6α and utilizing a larger construct that exhibits structure in solution in the absence of TFE.
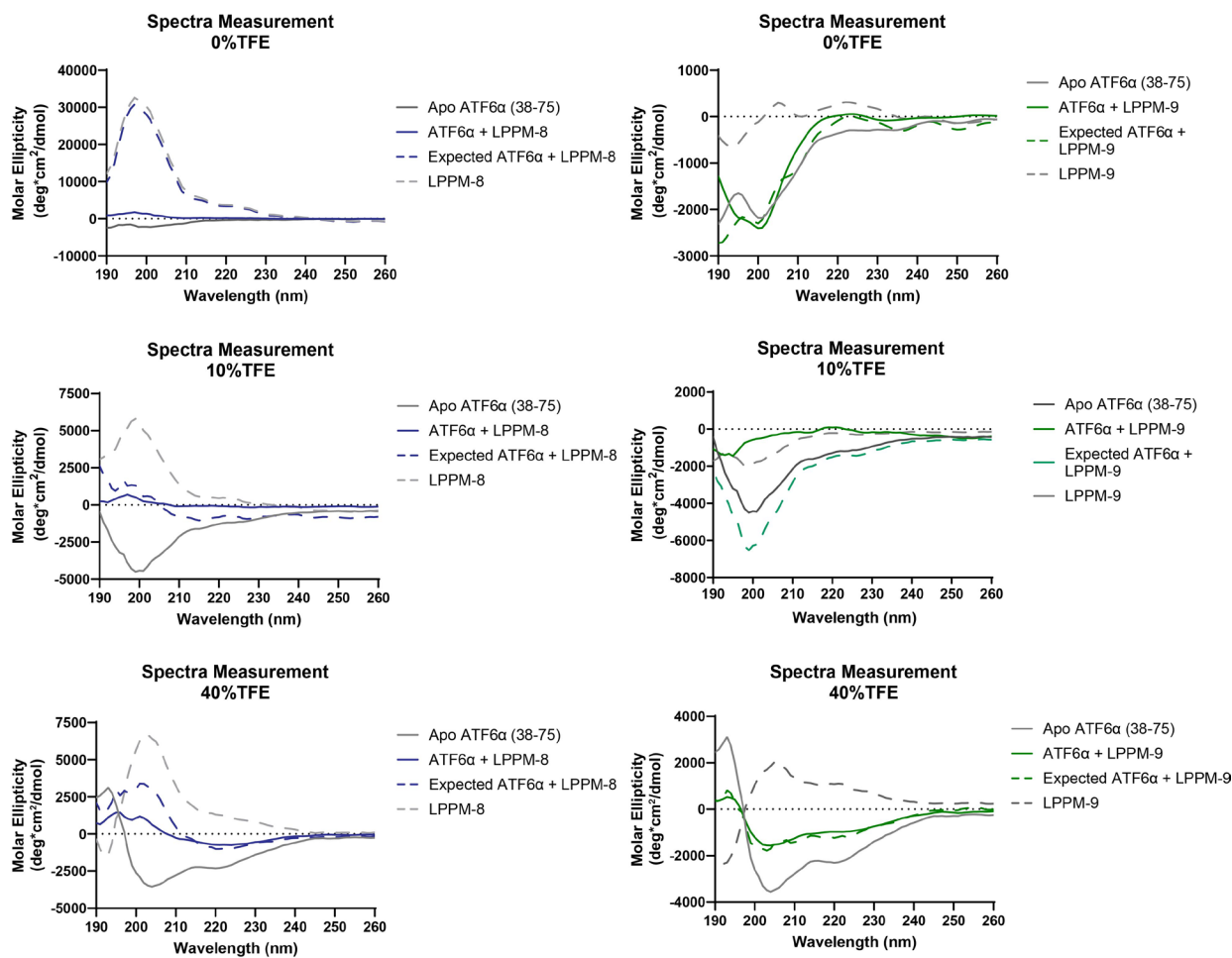
Appendix Figure D.2 Circular dichroism spectra of Ac-ATF6α incubated with 5 equivalents of LPPM-8 (left) or LPPM-9 (right) in the presence of 0% (top), 10% (middle) and 40% (bottom) TFE. The molar ellipticity of each sample was determined from the mean residue CD corrected for the number of amino acids and the concentration of sample using the Jasco Spectra Manager Software v.2.5. Data was obtained from 5 acquisitions.

Materials and Methods

All relevant materials and methods can be found in section 2.5.